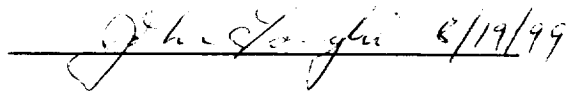


FINAL REPORT

NAGW-3407/NAG5-4558

**EXPERIMENTAL AND MODELING STUDIES
OF MASSIF ANORTHOSITES**


3/1/93 - 2/28/99

 8/19/99

John Longhi, P. I.

Lamont-Doherty Earth Observatory of Columbia University
Palisades, NY 10964

Phone: (914)-359-8659; FAX: (914)-365-8155
longhi@ldeo.columbia.edu

 Date: 8/19/99

Dr. John Mutter
Deputy Director
Lamont-Doherty Earth Observatory
Columbia University
P.O. Box 1000/Rt. 9W
Palisades, NY 10964
Phone: (914)-365-8525
FAX: (914)-365-2312
jcm@ldeo.columbia.edu

_____ Date: _____

Ms. Sonia Park
Projects Officer
Office of Contracts and Grants
Columbia University
1210 Amsterdam Ave.
New York, NY 10027
(212)-854-6851
(212)-8678-2628
scp10@columbia.edu

TABLE OF CONTENTS

INTRODUCTION	1
REPORT	1
REFERENCES	9
APPENDIX A. Journal Articles	12
APPENDIX B. Published Abstracts	12

INTRODUCTION

This termination report covers the latter part of a single research effort spanning several grant cycles. During this time there was a single title, "Experimental and Modeling Studies of Massif Anorthosites", but there were several contract numbers as the mode and location of NASA contract administration changed. Initially, the project was funded as an increment to the PI's other grant, "Early Differentiation of the Moon: Experimental and Modeling Studies", but subsequently it became an independent grant. Table 1 contains a brief summary of the dates and contract numbers.

**Table 1. Administrative Summary :
"Experimental and Modeling Studies of Massif Anorthosites"**

Dates	Contract No.	Comments
3/1/89 - 8/31/94	NAG 9-329	increment; final report submitted
3/1/93 - 2/28/97	NAGW-3407	independent contract no.; this report
6/1/97 - 2/28/99	NAG5-4558	independent contract no.; this report

Appendix A contains a list of the journal articles that cited support from this project after 3/31/93. Appendix B contains a list of the published abstracts supported by this project. Appendix C contains a set of reprints of the published papers and abstracts.

REPORT

The purpose of this project was to study the petrogenesis of Proterozoic (massif) anorthosites as possible analogs of lunar ferroan anorthosites (LFA). What the two groups of anorthosites have in common is intermediate Mg/Fe in mafic minerals indicating that their parent liquids were probably evolved from more primitive magmas, a relatively limited range in plagioclase composition suggesting suspension and accumulation, and separation from their mafic cumulates that is at least on the order of crustal thickness. To be sure there are many significant differences — plagioclase composition, tectonic setting, and areal extent — but what is more important than the obvious differences is the development of tangible models of large scale anorthosite petrogenesis against which the limited contextural information but extensive

mineral and chemical data base of lunar anorthosites can be compared. The incentive for developing terrestrial analogs has increased as diversity within the ferroan anorthosite suite has come to the fore [1,2] and as detailed geochemical models have suggested that ferroan anorthosites may not have crystallized directly from a homogeneous magma ocean [3]. This latter situation is ironic: although the concept of a magma ocean was originally developed to explain existence of lunar anorthosites [4], it is possible, now that there is independent indication of the existence of a magma ocean formed by a giant impact [e.g., 5], that lunar anorthosites may not have formed directly from a magma ocean, but rather from its aftermath. In any event, whether ferroan anorthosites were passively accreted to the bottom of a crust floating atop a magma ocean or whether ferroan anorthosites formed in plumes of plagioclase mushes detached from stagnant bodies of melt too dense to erupt on the surface, it seemed prudent to investigate terrestrial anorthosites in parallel with lunar anorthosites even though terrestrial anorthosites were obviously not exact analogs.

There were significant results in terms of emplacement and late stage evolution.

Emplacement

A key element in lending plausibility to a non- or post-magma ocean hypothesis is demonstrating the possibility of segregating plagioclase-rich suspensions or mushes from mafic cumulates on a scale of tens of kilometers. To this end we began this research by investigating two samples — one, an anorthositic dike, the other, a synthetic high-Al gabbro — that had been proposed as parental magmas of massif anorthosites in Labrador (Harp Lake). This work [6] demonstrated the dry liquidus of the anorthositic dike is too high ($> 1350^{\circ}\text{C}$) for a crustal melt or evolved liquid composition and that the liquidus plagioclase is far too anorthitic to match the zoned cores of plagioclase in the dike rock. Adding water would of course lower the liquidus, but would also make the liquidus plagioclase more calcic [7], thus increasing the mismatch with the rock. On the other hand, the high-Al gabbro composition (HLCA) has plagioclase and orthopyroxene with potentially parental compositions or near the liquidus at 10 - 12 kbar. In particular, the liquidus orthopyroxene at 12 kbar has Mg/Fe ratio and CaO and Al_2O_3 concentrations similar to those of aluminous megacrysts (bulk) with plagioclase exsolution lamellae [8], and in addition the plagioclase in this pressure range has a composition similar to that in the typical Harp Lake anorthosite. The implications of these results are that the aluminous opx megacrysts record transport from a lower crustal magma chamber to the upper crust where anorthosites are finally emplaced, whereas the presence of relatively sodic plagioclase (Ab/An partitioning is pressure-dependent) indicates that the plagioclase may have also been transported from lower to upper crust as a crystal-rich suspension [9].

We continued this work by quantifying the pressure-dependence of Ab/An partitioning for plagioclase-liquid and Al_2O_3 partitioning for orthopyroxene-liquid [9]. In particular, we reversed the concentrations of experimental orthopyroxenes at 6 and 11.5 kbar. We also

demonstrated that the high Al_2O_3 (incompatible) contents of opx megacrysts could not be the result of kinetic processes (rapid growth, failure of plagioclase to nucleate) because the megacrysts with the highest Al_2O_3 also have the highest Cr_2O_3 , yet either kinetic process would have led to a dramatic decrease in (compatible) Cr_2O_3 . These results were consistent with the general model that posits transport of suspension (or mushes) of 65 to 85 % plagioclase entrained in an evolved, high-Al basaltic composition from a ponded magma chamber at the base of the crust to a site of emplacement in the upper crust. At this point two formidable problems remained. One was the mode of transport from the lower to upper crust; the other was the petrogenesis of anorthosite massifs with average plagioclase composition considerably more sodic (e.g., An_{40-45}) than Harp Lake (An_{50-60}).

We began to address the first problem by reviewing the literature on the rheology of suspensions [9]. At high degrees of crystallinity, the crystals begin to form a rigid network or "granular-framework-controlled mass" [10] and not only does the effective viscosity of a suspension increase rapidly, but also movement is possible only by shearing and deformation of the crystalline matrix. Although there is ample evidence of deformation in many anorthosites in the form of granulation, bent twinning, and stress-induced twinning, there are also large tracts of less anorthositic rocks as well, e.g., leucogabbros in the Laramie Complex [11] and leuconorites in the Nain Complex [12] that show little or no evidence of deformation. So there appears to be an observation-based need for transporting at least some anorthositic magma as a rheological liquid. Theoretical considerations also militate against diapiric transport of a mass (i.e., a "solid") that cannot convect internally [13]. Under nearly static conditions the transition from liquid-state to solid-state rheology or the "critical melt fraction" may be described in terms of contiguity. Contiguity is the fraction of the surface area occupied by solid-solid contacts — in the present case, primarily plagioclase-plagioclase contacts — and contiguity values of 0.15 to 0.2 are cited as marking the critical transition [13]. A theoretical relation between contiguity, crystallinity, and wetting angle [14] predicts a critical melt fraction between 0.4 to 0.5 for wetting angles of 45° — the angle measured for potassic feldspar in granitic melt by [15] and which we confirmed for intermediate plagioclase in high-Al basaltic melt [16]. Some factors common in anorthositic rocks, a non-uniform distribution of crystal sizes and faceted crystal faces, may decrease contiguity [14]. Motion of a crystal-liquid mixture will decrease contiguity still further [14], so even a mass that begins to move with a deformable solid matrix may develop liquid-state rheology.

These considerations are at least permissive of diapiric transport of suspensions with 65 - 70 % entrained plagioclase — enough plagioclase to make leuconorites or leucogabbros (noritic and gabbroic anorthosites), but probably not enough for true anorthosites. Recent fieldwork at the Laramie Complex suggests a resolution to the problem. Unlike leucogabbros, which are typically layered and contain weakly deformed crystals, anorthosites occur in massive bodies and crystal deformation apparently increases with modal plagioclase [17]. These observations are

consistent with a second episode of plagioclase enrichment (the first having occurred in the ponded chamber at the base of the crust) following emplacement of a gabbroic anorthosite suspension (65-70 % plagioclase) in the upper crust: buoyant masses of plagioclase accumulate near the roof of the chamber, while gabbroic anorthosite accumulates on the floor, and buoyancy-driven self-deformation squeezes interstitial liquid out of the roof cumulates—the more deformation, the more plagioclase. Thus large masses of true anorthosite may be local phenomena developed after intrusions into the upper crust of liquid-state suspensions with 65-70% entrained plagioclase derived from lower crustal chambers.

This 3-stage model may have important implications for lunar anorthosites regardless of whether or not they formed from a magma ocean. Attention has been called to the fact that the compositional variation among lunar ferroan anorthosites cannot be explained by simple two component mixing of accumulated plagioclase and trapped interstitial liquid and that it is also difficult to imagine how simple filter-pressing could produce rocks with as much as 99% plagioclase on a large scale [18]. A resolution to these problems may be similar to the resolution of the problem of true terrestrial anorthosites, albeit on a larger scale. If lunar anorthosites do not form directly from a basaltic magma, but from a suspension (plagioclase entrained in a basaltic liquid) with noritic anorthosite composition, and the anorthosite deforms internally, squeezing out interstitial liquid, as it moves away from its parent, then it might prove possible to explain both modal and chemical variation. As a first step toward a more quantitative understanding of the dynamics of plagioclase mushes, we measured wetting angles using the terrestrial anorthosite from [6]. As mentioned above, a long duration experiment (350 hrs, 10 kbar, 1150 °C) was run just above the solidus, and 200 measurements made on SEM backscattered electron images yielded an average dihedral angle of 45° [16] — identical to the angle assumed in [15]. Because of its anisotropy and tendency to form faceted crystals, interpreting measured wetting angles for plagioclase in terms of contiguity and the flow of suspensions is a more formidable problem than for olivine or quartz. One observation that needs to be examined further is the apparent growth of megagrain from aggregates (see below) — this growth might first increase and then decrease contiguity.

The second formidable problem facing the polybaric model for terrestrial anorthosites is the petrogenesis of massifs with average plagioclase composition in the range of An₄₀₋₄₅. An evolved, but broadly basaltic magma (e.g. HLCA - above) is plausible parent magma for more calcic massifs, such as Harp Lake [8]. However, if the difference in average plagioclase composition were solely the result of the pressure effect on Ab-An partitioning, then the parent basalt of the more alkaline anorthosites would have ponded at the implausible depths of 50 to 70 km. One might suggest more extensive fractionation of the basaltic magma at depth. Perhaps, but not in the presence of plagioclase because Sr in the plagioclase from the more alkaline Norwegian anorthosites is 30 to 50 % higher than that in the more calcic Nain anorthosites; and Sr is highest in the most sodic plagioclase — that from the Labrieville Complex [19]. Perhaps,

the connection is a little more subtle: if similar basaltic magmas pond at different depths, then the magma that ponds at the deepest level would undergo the most extensive fractionation prior to reaching saturation with plagioclase — at which point anorthosite formation begins. Such a mechanism might account not only for more sodic plagioclase, but also generally higher levels of K, Ti, and P in associated rocks.

In order to address this problem, we have examined the liquidus equilibria of a primitive monzonite ("jotunite") from the Rogaland district of Norway [20]. This rock (TJ) is part of the chill margin of the Bjerkreim-Sokndal (B-S) layered intrusion which is itself part of the massif [21]. The composition of this rock has been proposed as that of the parent magma of the B-S intrusion [22] and of the associated swarm of dikes with composition ranging from monzonite to monzonite (mangerite) to quartz monzonite [23]. More importantly, compositions such as TJ have been suggested to have also been parental to the anorthosites at depth [24]. At 5 kbar the inferred crystallization sequence — plag → plag + ol → plag + ol + ilm → plag ± ol + ilm + opx — is identical to that observed in the most primitive cycles of the B-S intrusion, and the compositions of the olivine and plagioclase are similar to, albeit slightly more evolved than, the most primitive compositions observed in the intrusion [25]. Al_2O_3 concentrations in opx are also consistent with crystallization at $P \leq 5$ kbar. So the parent magma of the B-S intrusion was a slightly less evolved version of TJ. Plagioclase and orthopyroxene appear together on the liquidus of TJ from 10 to 13 kbar, where clinopyroxene joins them. So these pressures represent the logical choice for the genesis of TJ by melting or fractionation processes. This pressure range is also that predicted for the origin of the aluminous orthopyroxene megacrysts found within the anorthosites proper.

Later, we realized that, despite higher TiO_2 , P_2O_5 , and K_2O , TJ was cotectic with orthopyroxene and plagioclase at nearly the same pressures (~ 13 kb) as HLCA, and that at this pressure the composition of the opx was similar to the most aluminous megacrysts in the Norwegian (Rogaland) massif, while the plagioclase was similar to a great mass of that in the anorthositic rocks [21]. In an effort to understand this curious coincidence, we examined the liquidus relations of both compositions at the pressure where they are cotectic with pyroxene and plagioclase and found an even more perplexing situation [26]. Both of the bulk compositions project from the plagioclase component close to the plane of pyroxene compositions. Regions of composition space where liquidus curves cross the plane of their coexisting crystals are thermal maxima. Thus these 2 compositions lie close to the thermal maximum on the plag + opx + aug liquidus boundary where it crosses the plane of coexisting plagioclase and pyroxene compositions. Adjacent to the thermal maximum are thermal ridges on the plag + opx and plag + aug liquidus surfaces. Therefore, in this pressure range TJ and HLCA lie on the "thermal high-ground" of the liquidus surface — an unlikely situation for evolved liquids. Thus neither composition is likely to be reached by fractionation or even assimilation plus fractionation (AFC), because assimilation requires crystallization to provide the heat of melting and

crystallization will drive the liquid composition away from the thermal divide. At lower pressures the pyroxene + plagioclase thermal divide disappears [26], but both compositions move off the cotectic into the plagioclase liquidus volume, so AFC processes can produce compositions similar to HLCA and TJ only by assimilation into a more feldspathic liquid. Our work has shown that such liquids cannot be derived from melting the mantle or even fractionating mantle melts [26]. It thus appears that a variant of the lower crustal fusion hypothesis of [27] is most consistent with the data: Large ponded intrusions of basalt provide the heat for melting mafic granulitic material that necessarily lies close to or within the pyroxene+plagioclase thermal divide. Extensive partial melting produces liquids with the major element composition of high-Al basalt — such liquids are parental to anorthosites with more calcic plagioclase (e.g., Harp Lake); lower degrees of melting produce liquids with higher concentrations of K, Ti, P, and other incompatible elements — such liquids (primitive jotunites) are parental to anorthosites with more sodic plagioclase (e.g., portions of the Rogaland massifs). In all cases, however, there remains a need for mechanical enrichment of the parental liquids with plagioclase crystals in order to produce anorthositic rocks, because cotectic melts of the lower crust will have Al_2O_3 concentrations much lower than anorthosites. Of course, there is no evidence of water or major granite-forming events on the Moon, but formation of lunar anorthosites by remelting and remobilization of early-formed plagioclase-mafic cumulates remains one of the working hypotheses [28].

Perhaps the fundamental insight to come from research on massif anorthosites in this lab is that their troctolitic/noritic crystallization patterns derive from melting mafic sources at 10 to 13 kbar [26]. The troctolitic/noritic crystallization sequence derives from liquid compositions along the high-pressure $\text{plag}+\text{opx}+\text{cpx}$ cotectics having relatively low Wo content and variable olivine normative character. Not coincidentally, perhaps, most ferroan anorthosites seem to have troctolitic/noritic to troctolitic/gabbro-noritic crystallization patterns [29], and the average LFA-related mafic component of the upper lunar crust [HON - 30] seems to have the same normative character as the parent magmas of the massif anorthosites. Now it is likely that the average ferroan crust contains a cumulus mafic component because HON is distinctly more magnesian than a plausible FAN parent magma [31] with $\text{Mg}' = 0.60$ whose crystallization begins with fo_{82}ol . Yet, despite the lower Mg' , the composition of the LFA parent magma has the same normative character as HON. It would be too remarkable to be a coincidence if the LFA parent magma composition also lies in the plagioclase + pyroxene thermal divide at a pressure where *plag*, *opx*, and *aug* are all on the liquidus. Given the much lower alkali concentrations of LFA parent magmas relative to massif parent magmas, it is likely that the trace of the thermal divide will sweep across the LFA parent composition between 5 and 10 kbar, rather than 10 to 13 kbar. As discussed above, a concurrence of multiple saturation in a parental liquid and crystal + liquid coplanarity is not readily explained except by melting mafic sources. Melting of mafic sources might plausibly be expected from overturn within the cumulate pile created by the solidification

of a disorderly magma ocean. The only other possibility for the troctolitic/noritic/gabbro-noritic character of ferroan anorthosites is derivation of their parent magmas by bottom-up crystallization of an improbably orderly magma ocean [e.g., 32].

Late stage evolution

A combination of field, geochemical, and isotopic evidence point to a series of dikes, sills and small intrusions forming from liquids residual to the massif anorthosites [33,34]. These rocks are commonly referred to as ferrodiorites, monzonorites, or jotunites. And there appears to be a continuum of compositions leading from jotunite to ferro-monzonite to charnockite (orthopyroxene-bearing granite) [35]. The overall jotunite trend has much in common with post-LFA differentiation: evolved ferroan liquids with elevated K, REE, and P and large depletions of Sr, Eu, Ti, and Nb relative to the REE. Our experimental work [20,35] on Norwegian rocks establishes a clear link between primitive jotunites (TJ), fine-grained jotunites represented by the chill margins of dikes, the monzonitic to qtz-monzonitic interiors of some of the dikes, and the most evolved compositions. This work [35] has also demonstrated that plagioclase, a ubiquitous mineral in all these rocks, is absent near the liquidus of the Fe-Ti rich rocks, and that evidence of liquid immiscibility is lacking in the field and in the experiments. The Fe-Ti rich rocks, therefore, are cumulates. On a larger scale, formation of such cumulates could be expected to lead to more efficient density separation of oxides from silicates, and given the observed crystallization order of ilmenite, magnetite, apatite, we could expect to find segregations of ilmenite alone, ilmenite + magnetite, and ilmenite + magnetite + apatite. These assemblages are precisely what are found in oxide deposits of the Rogaland district [36]. These deposits are always found within the anorthosite massifs, most commonly near the contacts, although larger deposits may be found in the interiors of the massifs. The scales of the deposits vary from a few to hundreds of meters and include massive varieties as well as dispersed oxide horizons in silicates. It is likely that all deposits formed by the crystallization of jotunitic liquids squeezed out to the margins of the intruding and deforming anorthosite masses. Some deposits are still associated with their coprecipitating silicates, whereas others formed from post-cumulus gravitational separation and settling. As such, these deposits represent important chemical and physical analogs not only of the ilmenite \pm KREEP layers believed to have formed during the latest stages of the lunar magma ocean, but possibly to a hitherto unrecognized variety of KREEP that may have formed as the end product of crystallization of residual liquids within the anorthosites rather within the magma ocean proper or at least at a lower level within the large magma bodies that gave rise to the ferroan anorthosites. Recognition of this "older" KREEP may be the key to understanding the apparent contradiction between a Mg-suite norite with a 4.46 Ga Nd-Sm isochron age [37] and the 4.36 Ga Nd-Sm age of KREEP [38], which ostensibly marks the end of the magma ocean crystallization. An important feature of most Mg-suite rocks is a sub-chondritic Ti/Sm ratio [39], which indicates assimilation of an evolved component that has a

signature of ilmenite fractionation. This component is KREEP or something very similar [40]. If some of the KREEPy material that was assimilated by Mg-suite magmas formed in long-lived residual pockets of the magma ocean whereas other KREEPy material formed at higher levels in the crust, it would explain rocks that crystallized before the main batch of KREEP but nonetheless carry a KREEP signature. There are no rocks analogous to the Mg-suite cumulates in terrestrial anorthosite complexes, but there clearly are two origins for the evolved rocks: some form by differentiation of liquid squeezed out of the crystallizing anorthosites and others form in the upper portions of layered intrusions, like the Bjerkreim-Sockndal body [41], whose the parental magmas come from lower crustal chambers.

Finally, no granitoids residual to the LFA have been found. Yet our calculations of the crystallization paths of LFA parent magmas shows that such rocks ("Descartesites") are to be expected if crystallization of the anorthosites took place at depths < 20 km [42]. Thus their absence may be the result of crystallization at greater depths. The appearance of a *plag + pyx* thermal divide for LFA magma compositions at $P > 1$ kb (depths > 20 km) prohibits fractionating, olivine-saturated magmas from reaching silica saturation or even silica enrichment. The absence of siliceous lunar anorthosites is readily explicable in terms of a well-behaved magma ocean: no siliceous anorthosites are to be expected as long as the magma ocean developed a floating crust more than 20 km thick before the magma ocean reached the thermal divide. So far pyroxene exsolution barometry has placed 2 similar ferroan anorthosites at cooling depths of 14 and 21 km [43]. More barometry is needed on samples at both the high- and low-Mg' ends of the LFA array to establish any stratigraphic significance. The presence of olivine-bearing "sodic" ferroan anorthosites [3] is consistent with either a different parent magma than that of the 2 calibrated anorthosites or a similar parent magma crystallizing at higher pressure. In either case, a simple MO scenario does not apply, but crystallization at pressures ≥ 1 kb remains essential to avoiding formation of Descartesites.

REFERENCES

- [1] James, O. B. (1987) Magnesian members of the lunar ferroan-anorthosite suite. In *Lunar and Planetary Science XVIII*, The Lunar and Planetary Institute, pp. 456-457.
- [2] Warren, P. A., E. A. Jerde and G. W. Kallemeyn (1991) Pristine moon rocks: Apollo 17 anorthosites. *Proc. Lunar Planet. Sci. Conf. 21st*, 51-61.
- [3] James, O.B., M. M. Lindstrom, and M. K. Flohr (1988) Ferroan anorthosite from lunar breccia 64435: Implications for the origin and history of ferroan anorthosite, *Proc. Lunar Planet. Sci. Conf. 19th*, p. 219-243.
- [4] Wood, J. A., J. S. Dickey Jr., U. B. Marvin, and B. N. Powell (1970) Lunar anorthosites and a geophysical model of the moon, *Proc. Apollo 11 Lunar Sci. Conf.*, pp. 965-988.
- [5] Benz, W., W. L. Slattery and A. G. W. Cameron (1986) Planetary collision calculations: The origin of the Moon, *Icarus*, 66, 515-535.
- [6] Fram, M.S. and J. Longhi (1992) Phase equilibria of dikes associated with Proterozoic anorthosite complexes, *Am. Mineral.*, 77, 605-614.
- [7] Housh, T.B., and Luhr, J.F. (1991) Plagioclase-melt equilibria in hydrous systems. *Amer. Mineral.*, 76, 477-492.
- [8] Emslie, R.F. (1975) Pyroxene megacrysts from anorthositic rocks: a new clue to the sources and evolution of the parent magmas. *Canadian Mineralogist*, 13, 138-145.
- [9] Longhi, J., M.S. Fram, J. Vander Auwera, and J. Montieth (1993) Pressure effects, kinetics, and rheology of anorthositic and related magmas, *Am. Mineral.*, 77, 605-616.
- [10] van der Molen, I., and M.S. Paterson (1979) Experimental deformation of partially molten granite. *Contributions to Mineralogy and Petrology*, 70, 299-318.
- [11] Frost, B.R., Frost, C.D., Lindsley, D.H., Scoates, J.S. & Mitchell, J.N., 1993. The Laramie anorthosite complex and Sherman batholith: geology, evolution and theories of origin In A.W. Snoke, J.R. Steidtmann & S.M. Roberts, eds. *Geology of Wyoming, Geological Survey of Wyoming Memoir no. 5*, 118-161.
- [12] Wiebe, R. A. (1990) Evidence for unusually Feldspathic liquids in the Nain Complex, Labrador, *Am. Mineral.*, 75, 1-12.
- [13] Miller, C.F., E.B. Watson, M.T. and Harrison (1988) Perspectives on the source, segregation and transport of granitoid magmas. *Transactions of the Royal Society of Edinburgh: Earth Sciences*, 79, 135-156.
- [14] German, R.M. (1985) The contiguity of liquid phase sintered microstructures. *Metallurgical Transactions*, 16A, 1247-1252.
- [15] Jurewicz, S.R., and E.B. Watson (1985) The distribution of partial melt in a granitic system: The application of liquid phase sintering theory. *Geochimica Cosmochimica Acta*, 49, 1109-1122.

- [16] Longhi J. and Jurewicz S. R. (1995) Plagioclase-melt wetting angles and textures: implications for anorthosites, *Lunar and Planetary Science XXVI*, The Lunar and Planetary Institute, pp. 859-860.
- [17] LaFrance B., John B.E., and Scoates J.S. (1995) Syn-emplacement recrystallization and deformation microstructures in the Poe Mountain anorthosite, Wyoming. *Contrib. Mineral. Petrol.* 122, 431-440.
- [18] Haskin, L.A., M.M. Lindstrom, P.A. Salpas, and D.J. Lindstrom (1981) On compositional variations among lunar anorthosites. *Proc. Lunar Planet. Sci. Conf. 12th*, 41-66.
- [19] Emslie, R.F. (1985) Proterozoic anorthosite massifs. In A.C. Tobi and J.L.R. Touret, Eds., *The Deep Proterozoic Crust in the North Atlantic Provinces*, p. 39-60. Dordrecht, Netherlands.
- [20] Vander Auwera, J. and J. Longhi (1994) Experimental study of a jotunite: constraints on the parent magma composition and crystallization conditions (P, T, fO₂) of the Bjerkreim-Sokndal layered intrusion (Norway). *Contrib. Mineral. Petrol.*, 118, 60-78.
- [21] Duchesne, J.C., and R. Maquil (1992) The Egersund-Ogna massif. In J.C. Duchesne, Ed., *The Rogaland intrusive massifs: An excursion guide*, p. 7-25, International Geological Correlation Programme Project 290.
- [22] Duchesne, J.C., and J. Hertogen (1988) Le magma parental du lopolithe de Bjerkreim-Sokndal (Norvège méridionale). *Comptes Rendus de l'Académie des Sciences Paris*, 306, 45-48.
- [23] Duchesne, J.C., E. Wilmart, D. Demaiffe, and J. Hertogen (1989) Monzonorites from Rogaland (Southwest Norway): a series of rocks coeval with but not comagmatic with massif-type anorthosites. *Precamb. Res.*, 7, 111-128.
- [24] Duchesne, J.C. (1984) Massif anorthosites: another partisan review. In W.L. Brown, Ed., *Feldspars and feldspathoids*, p. 411-433, Reidel, Boston.
- [25] Wilson, J.R., Robins, B., Nielsen, F.M., Duchesne, J.C. & Vander Auwera, J., 1992. The Bjerkreim-Sokndal layered intrusion, southwest Norway. In R.G. Cawthorn, Ed., *Layered Intrusions*, p.231-255, Elsevier, Amsterdam.
- [26] Longhi, J., J. Vander Auwera, Fram M.S., and Duchesne J.C. (1998) Some phase equilibrium constraints on the origin of Proterozoic (massif) anorthosites and related rocks. *J. Petrol.* 40, 153-166.
- [27] Taylor, S. R., and S. M. McClennnon (1985) *The Continental Crust: its Composition and Evolution*, Blackwell, London.
- [28] Longhi, J. and L. D. Ashwal (1984) A two stage model for lunar anorthosites: An alternative to the magma ocean hypothesis, *Proc. Lunar Planet. Sci. Conf. 15th, J. Geophys. Res.*, 90, C571-C584.
- [29] James, O.B (1980) Rocks of the early lunar crust. *Proc. Lunar Planet. Sci. Conf. 11th*, 365-393.

- [30] Haskin, L.A., M.M. Lindstrom, P.A. Salpas, and D.J. Lindstrom (1981) On compositional variations among lunar anorthosites. *Proc. Lunar Planet. Sci. Conf. 12th*, 41-66.
- [31] Longhi, J. (1989) Fractionation trends of evolved lunar magmas, in *Lunar and Planetary Science XX*, The Lunar and Planetary Institute, Houston, pp. 584-585.
- [32] Warren, P.H. and Wasson, J.T. (1979) Effects of pressure on the crystallization of a moon-sized "chondritic" magma ocean. *Proc. Lunar Planet. Sci. Conf. 10th*, 2051-2083.
- [33] Owens B.E., Rockow M.W., and Dymek R.F. (1993) Jotunites from the Grenville Province, Quebec: Petrological characteristics and implications for massif anorthosite petrogenesis. *Lithos*, 30, 189-206.
- [34] Mitchell J.N. (1993) Petrology and geochemistry of dioritic and gabbroic rocks in the Laramie Anorthosite Complex, Wyoming: implications for the evolution of Proterozoic anorthosite. Ph.D. Thesis, Univ. of Wyoming.
- [35] Vander Auwera J., Longhi J., and Duchesne J.C. (1998) The liquid line of descent of the jotunite (hypersthene monzodiorite) suite. *J. Petrol.*, 39, 439-468
- [36] Duchesne J.-C. (1996) Fe-Ti deposits in Rogaland anorthosites (South Norway): geochemical characteristics and problems of interpretations. in press, *Agricola Volume*, John Wiley.
- [37] Shih C.-Y, L. E. Nyquist, E.J. Dasch, D.D. Bogard, B.M. Bansal, and H. Weismann (1993) Ages of pristine noritic clasts from lunar breccias 15445 nad 15455. *Geochim. Cosmochim. Acta*, 57, 915-931.
- [38] Lugmair G.W. and R.W. Carlson (1978) The Sm-Nd history of KREEP. *Proc. Lunar Planet. Sci. Conf. 9th*, 689-704.
- [39] Longhi J. and A. E. Boudreau (1979) Complex igneous processes and the formation of the primitive lunar crustal rocks. *Proc. Lunar Planet Sci. Conf. 10th*, pp. 2085-2105.
- [40] Warren, P. W. (1986) Anorthosite assimilation and the origin of the Mg/Fe-related bimodality of pristine Moon rocks: Support for the magmasphere hypothesis, *J. Geophys. Res.*, 91, D33-D343.
- [41] Nielsen, F.M. and J.R. Wilson (1991) Crystallization processes in the Bjerkreim-Sokndal layered intrusion, south Norway: evidence from the boundary between two macrocyclic units. *Contrib. Mineral. Petrol.*, 107, 403-414.
- [42] Longhi J. (1997) Descartesites: missing(?) pristine rocks, *Lunar and Planetary Science XXVIII*, pp. 829-830.
- [43] McCallum I.S. and O'Brien H.E. (1996) Stratigraphy of the lunar highland crust: Depths of burial of lunar samples from cooling rate studies. *Am. Mineral.*, 81, 1166-1175.

APPENDIX A. Journal Articles

- *VANDER AUWERA, J. and J. LONGHI (1994) Experimental study of a jotunite: constraints on the parent magma composition and crystallization conditions (P, T, fO₂) of the Bjerkreim-Sokndal layered intrusion (Norway). *Contrib. Mineral. Petrol.*, 118, 60-78.
- *VANDER AUWERA, J., J. LONGHI, and J.C. DUCHESNE (1998) The liquid line of descent of the jotunite (hypersthene monzodiorite) suite. *J. Petrol.*, 39, 439-468.
- *LONGHI J., J. VANDER AUWERA, J.C. DUCHESNE, and M.S. FRAM (1999) Some phase equilibrium constraints on the origin of Proterozoic (massif) anorthosites and related rocks. *J.. Petrol.* 40, 153-166.
- DUCHESNE J.C., J.P. LIÉGEOIS, J. VANDER AUWERA, and J. LONGHI (1999) Tectonic setting and phase diagram constraints on the origin of Proterozoic anorthosites: the Crustal Tongue melting model, submitted to *Tectonophysics*.
- VANDER AUWERA J., J. LONGHI, M.S. FRAM and J.C DUCHESNE (1999) The effect of pressure on DS_r (plag/melt) and DC_r (opx/melt). Implications for anorthosite petrogenesis, submitted to *Contrib. Mineral. Petrol.*

APPENDIX B. Published Abstracts

- *LONGHI J. and J. VANDER AUWERA (1993) The monzonorite-anorthosite connection: the petrogenesis of terrestrial KREEP, *Lunar and Planetary Science XXIV*, The Lunar and Planetary Institute, pp. 897-898.
- *VANDER AUWERA, J., J. LONGHI and J.-C. DUCHESNE (1993) Jotunites from the Rogaland Province (Norway): constraints from experimental data and the partitioning of Sr (plag/melt) and Cr (opx/melt), *EOS*, 74, p. 659.
- *LONGHI J. and VANDER AUWERA, J. (1994) A mantle-derived parent magma for massif anorthosites??? In *Anorthosites, Rapakivi Granites and Related Rocks*, (R. F. Emslie, ed.) International Geological Correlation Programme Joint Meeting IGCP #290 and #315, p. 6.
- *LONGHI J. and S. R. JUREWICZ (1995) Plagioclase-melt wetting angles and textures: implications for anorthosites, *Lunar and Planetary Science XXVI*, The Lunar and Planetary Institute, pp. 859-860.
- *LONGHI J , J. VANDER AUWERA, and M S FRAM (1996) Origin of Proterozoic anorthosites by fusion of the lower crust, *EOS*, 77, p. 760.
- *LONGHI J. (1997) Descartesites: missing(?) pristine rocks, *Lunar and Planetary Science XXVIII*, pp. 829-830.

* - appended

Jacqueline Vander Auwera · John Longhi

Experimental study of a jotunite (hypersthene monzodiorite): constraints on the parent magma composition and crystallization conditions (P , T , f_{O_2}) of the Bjerkreim-Sokndal layered intrusion (Norway)

Received: 2 December 1993 Accepted: 4 May 1994

Abstract The Bjerkreim-Sokndal layered intrusion is part of the Rogaland anorthosite Province of southern Norway and is made of cumulates of the anorthosite-mangerite-charnockite suite. This study presents experimental phase equilibrium data for one of the fine-grained jotunite (Tjörn locality) occurring along its northwestern lobe. These experimental data show that a jotunitic liquid similar in composition to the Tjörn jotunite, but slightly more magnesian and with a higher plagioclase component is the likely parent of macrocyclic units (MCU) III and IV of the intrusion. The limit of the olivine stability field in the experimentally determined phase diagram as well as comparison of the Al_2O_3 content of low-Ca pyroxenes from experiments and cumulates ($\approx 1.5\%$) yields a pressure of emplacement ≤ 5 kbar. Experimentally determined Fe-Ti oxide equilibria compared to the order of cumulus arrival in the intrusion show that the oxygen fugacity was close to FMQ (fayalite-magnetite-quartz) during the early crystallization. It subsequently decreased relative to this buffer when magnetite disappeared from the cumulus assemblage and then increased until the reentry of this mineral. Calculated densities of experimental liquids show a density increase with fractionation at 7, 10 and 13 kbar due to the predominance of plagioclase in the crystallizing assemblage. At 5 kbar and 1 atm (FMQ-1), where plagioclase is the liquidus phase, density first increases and then drops when olivine (5 kbar) or olivine + ilmenite (1 atm: FMQ-1) precipitate. At 1 atm and NNO (nickel-nickel oxide), the presence of both magnetite and ilmenite as near liquidus phases induces a density decrease. In the Bjerkreim magma chamber, oxides are early cumulus phases and liquid

density is then supposed to have decreased during fractionation. This density path implies that new influxes of magma emplaced in the chamber were both hotter and denser than the resident magma. The density contrast inferred between plagioclase and the parent magma shows that this mineral was not able to sink in the magma, suggesting an *in situ* crystallization process.

Introduction

The study of layered intrusions has provided important data for the understanding of the chemical and physical evolution of igneous liquids. Knowledge of the parent magma composition is necessary to allow modeling of this evolution. To assess this initial liquid, one can use the technique of bulk summation of cumulate compositions (Wager 1960; Wager and Brown 1967; Morse 1981) or one can use dikes and chilled margins sometimes occurring around the perimeter of layered intrusions (e.g., Wager 1960; Longhi et al. 1983; Hoover 1989). Assimilation is likely to have occurred in the final stage of the Bjerkreim-Sokndal intrusion evolution (Demaiffe et al. 1979; Barling et al. 1992; Jensen et al. 1993) precluding any use of the first method. This study tests the suitability as a parent magma of a fine-grained jotunite (jotunite = hypersthene monzodiorite = monzonorite) outcropping near the northeastern contact of the intrusion (Maijer et al. 1987; Duchesne and Hertogen 1988) using experimental phase equilibria. Phase relations of this putative parent liquid have been determined as a function of temperature, pressure (1 atm up to 18 kbar) and oxygen fugacity [NNO (nickel-nickel oxide) to MW-2.5]. By comparing these experimentally determined phase relationships with the cumulate stratigraphy of the intrusion, we also constrain estimates of the pressure of emplacement of the intrusion, and the oxygen fugacity during the early stage of crystallization as well as the density changes.

J. Vander Auwera (✉)
L.A. Géologie, Pétrologie, Géochimie, University of Liège,
B-4000 Liège, Belgium

J. Longhi
Lamont-Doherty Earth Observatory, Palisades,
NY 10964, USA
Editorial responsibility: W. Schreyer

Regional geology

The Bjerkreim-Sokndal layered intrusion (BKSJ; Fig. 1) is part of the Rogaland intrusive complex of southern Norway where massif-type anorthosites (Egersund-Ogna; Håland-Helleren; Åna-Sira) and leuconoritic bodies (e.g., Hydra) occupy the largest portion of the surface. The intrusion is deformed and has in its northern part the general form of a syncline plunging SE at about 35° so that a thick sequence of layered rocks is exposed (Michot 1960; Nielsen and Wilson 1991). Abundant inclusions of Egersund-Ogna (Duchesne 1970; Wilson et al. 1992) occur at the base of the intrusion thus indicating a younger age for BKSJ. The intrusion is crosscut by jotunitic dykes among which the most important is the Lomland dyke (Fig. 1) (Duchesne et al. 1985).

Recent geochronological data (Duchesne et al. 1993) suggest that the Rogaland intrusives were emplaced between 920 and 930 Ma. These intrusions have contact metamorphosed the surrounding rocks [M2 stage of Jansen et al. (1985)] which grade from amphibolite to granulite facies conditions ($T = 750\text{--}900^\circ\text{C}$) close to the intrusions (Hermans et al. 1975; Jansen et al. 1985). This metamorphism has intensely overprinted the older metamorphic parageneses (M1 stage) which are only observed as relics in the

Rogaland Province. Several isograds have been mapped (Fig. 1) by Hermans et al. (1975).

The Bjerkreim-Sokndal layered intrusion

The intrusion contains all the major rock types in the anorthositic suite: anorthosite, leuconorite, norite, jotunite, mangerite and quartz mangerite (Fig. 1). Michot (1960, 1965) established the detailed stratigraphy of the massif. He subdivided the Layered Series of the Bjerkreim lobe, which belongs to the lower, northwestern part of the massif, into five major rhythmic units. Following the nomenclature recommended by Irvine (1982), Nielsen and Wilson (1991) refer to these units as macrocyclic units (MCU). Moreover, these authors have argued that MCU V, leuconoritic at its base and noritic in its upper part, does not display any primitive mineral compositions and consider that MCU IV directly grades into the massive mangerites and quartz mangerites belonging to the top of the intrusion through a norite-mangerite Transition Zone defined by Duchesne et al. (1987). More recently, Wilson et al. (1992) have subdivided the Layered Series into 6 megacyclic units

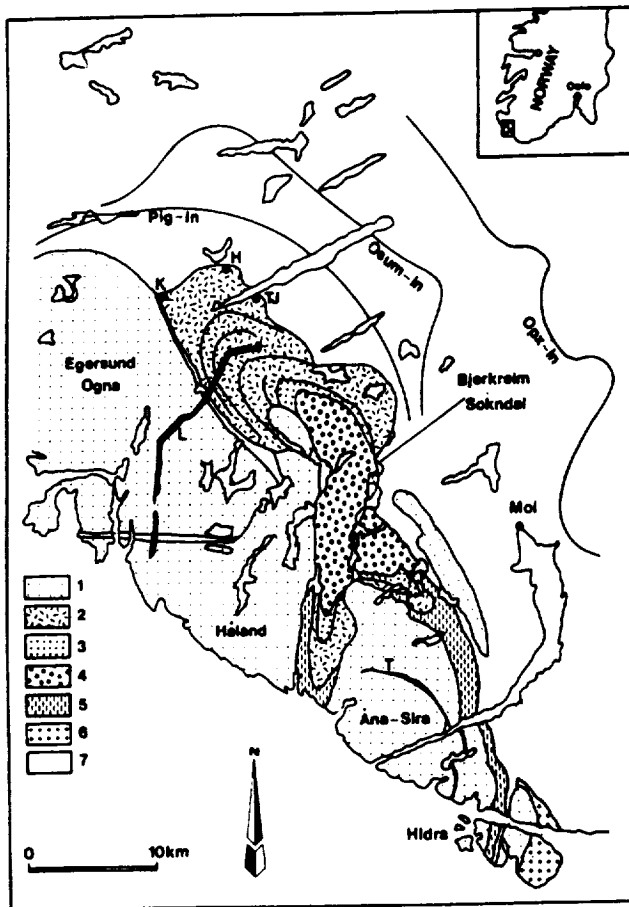


Fig. 1 Schematic geological map of the Rogaland anorthositic complex [after Hermans et al. (1975) and Michot (1960)]. 1 anorthosites. 2 lower part of the Bjerkreim-Sokndal intrusion. 3 mangerites of the Bjerkreim-Sokndal intrusion. 4 quartz-mangerites of the Bjerkreim-Sokndal intrusion. 5 jotunitic complex. 6 Farsund charnockite. 7 metamorphic envelope. jotunitic dykes in black (L Lomland, T Tellnes), K Kløgtveit, H Hellevatnet, TJ Tjörn. Isograd patterns (opx orthopyroxene, osum osumilite, pig pigeonite) after Hermans et al. (1975).

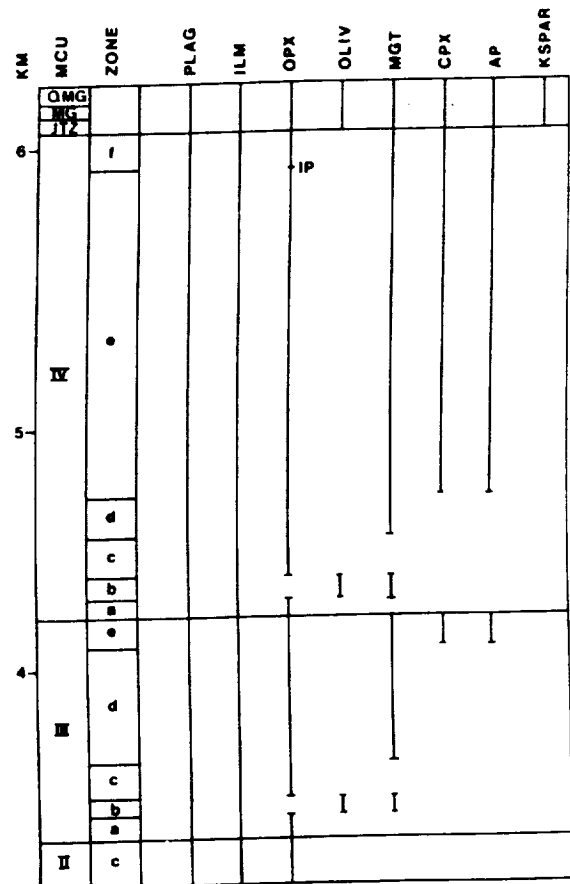


Fig. 2 Internal subdivisions of macrocyclic units (MCU) based on cumulus mineral assemblages [after Jensen et al. (1993) and Nielsen and Wilson (1991)]. (plag plagioclase, ilm ilmenite, opx low-Ca pyroxene, oliv olivine, mgt magnetite, cpx Ca-rich pyroxene, ap apatite, Kspar K-feldspar, IP inverted pigeonite, QMG quartz mangerite, MG mangerite, JTZ jotunite transition zone). Thickness measured from the country-rock contact.

(MCU 0 to IV). In order to maintain the numbering of Michot (1960, 1965: units II, III and IV are equivalent in both nomenclature), they refer to the lowest three units as MCU0, IA and IB. The MCUs 0, I and II are essentially made of anorthositic and leucocratic cumulates and lack norites at the top (Wilson et al. 1992). In MCUs III and IV, the lithological sequence is more complete (Fig. 2) comprising a thin zone of essentially anorthositic composition followed by leucotroctolites which are overlain by plagioclase + hypersthene + ilmenite cumulates and then by norites. The roof of the intrusion was located above the quartz mangerites and has been eroded away. The origin of these quartz mangerites is still in dispute. They were first considered as comagmatic with the rocks of the lower part of the intrusion. Subsequent Sr isotopic data (Demaiffe et al. 1979) have however shown important assimilation of the surrounding gneisses and in 1984, Wiebe proposed that these rocks could correspond to the melted roof of the intrusion. This last hypothesis has been rejected by Wilmart (1988) and Duchesne and Wilmart (1989) who consider that the mangerites, the quartz mangerites and the charnockites are representative of a series of liquids which can be divided into two trends. Based on trace element modeling (Rb, Sr), Wilmart (1988) suggests that in both trends, evolution is not controlled by partial melting but by fractional crystallization processes taking place in more deep-seated magma chambers.

Michot (1960; 1965), Duchesne (1971, 1972a,b), Duchesne et al. (1987), Nielsen and Wilson (1991) and Jensen et al. (1993) emphasized the cryptic layering of the Layered Series with minerals having more evolved compositions towards the top of the sequence. Olivine is absent in the lower part of the massif except at the base of MCU III (Epteland unit: Nielsen and Wilson 1991) and MCU IV (Svalestad horizon: Michot 1960). These two horizons display the least evolved cumulates: Fo_{66-77} and An_{52-43} . Olivine reappears with a more evolved composition (Fo_{50}) in the Transition Zone and in the mangerites. According to the cumulus phase stratigraphy (Nielsen and Wilson 1991; Jensen et al. 1993), the crystallization sequence is $\text{plag} \pm \text{opx} \pm \text{ilm}$ (a) \rightarrow $\text{plag} + \text{oliv} + \text{ilm} + \text{mgt}$ (b) \rightarrow $\text{plag} + \text{opx} + \text{ilm}$ (c) \rightarrow $\text{plag} + \text{opx} + \text{ilm} + \text{mgt}$ (d) \rightarrow $\text{plag} + \text{opx} + \text{ilm} + \text{mgt} + \text{cpx} + \text{ap}$ (e) (Fig. 2, see caption for mineral abbreviations). Duchesne (1972a) suggested that each unit corresponds to the crystallization of a new magma influx which mixes with the resident magma. Recent Sr (Jensen et al. 1993) and Nd (Barling et al. 1992) isotopic data have supported this hypothesis.

Detailed mapping across the MCU III/IV boundary suggests a discordance of 2 to 6° between the base of MCU IV and phase layering in MCU III (Nielsen and Wilson 1991). Moreover, based on the lack of unit IIIe in the central part of the chamber, these authors suggest that crystallization of MCU III occurred in a compositionally zoned magma chamber on an inward-sloping floor by down-dip accretion and that the new dense magma of MCU IV fountained in the chamber and mixed with the residual magma already present in the chamber producing a hybrid unit at the base of MCU IV (MCU IVa).

Parent magma of Bjerkreim-Sokndal and description of the sample used

Michot (1960) suggested that a basaltic composition was precluded for the parental magma of the intrusion since ultramafic cumulates are lacking at the base of the Layered Series. Through modeling of Ca, K and trace elements in plagioclase (Sr, Ba) and apatite (REE), Duchesne (1978) and Roelandts and Duchesne (1979) suggested a jotunitic composition having a REE distribution similar to that of the jotunitic chilled margin of the Hydra body (Demaiffe and Hertogen 1981). Duchesne and Hertogen (1988) argued that a fine-grained jotunitic border facies outcropping at Tjörn was the first direct constraint on the composition of the parent magma of BSKS.

The locality of Tjörn was first described by Majjer et al. (1987) at the north-eastern contact of the intrusion with its envelope.

More recently, detailed mapping has shown that the Tjörn outcrop is actually at 300 m from the contact in the intrusion (J. Sandal, personal communication in Nielsen and Wilson 1991; Fig. 1). Nielsen and Wilson (1991), though also in favor of a jotunitic composition, have questioned the hypothesis that Tjörn unequivocally represents the BSKS parent magma. Other fine-grained jotunitic rocks have now been reported (Wilson et al. 1992) at several places along the northern contact, especially at Klögtveit and Hellevatnet (Fig. 1). These jotunitic rocks are broadly similar in composition to the Tjörn (TJ) samples but display some heterogeneity as usually observed in chilled margins (e.g., Hoover 1989). This heterogeneity is likely to result from accumulation of phenocrysts (plagioclase) or assimilation from wall rock.

The 80.12.3A sample (Table 1) is equigranular and is made of a slightly antiperthitic plagioclase ($\text{An}_{36}\text{Ab}_{64}\text{Or}_2$), inverted pigeonite ($\text{En}_{59}\text{Fs}_{39}\text{Wo}_2$) with augite exsolutions, cpx, oxides, apatite as well as scarce quartz and K-feldspar. The inverted pigeonite is poikilitic interstitial; apatite is small, usually elongated and disseminated in the different minerals of the rock predominantly in the plagioclase and not in oxides. The grain size (0.5–1 mm) is significantly lower than that of the BSKS cumulates (2–3 mm). Moreover, the texture and grain size are similar to those observed in the chilled margins of the jotunitic dykes crosscutting the anorthosites, consistent with the hypothesis that sample 80.12.3A was emplaced as a liquid (Duchesne and Hertogen 1988). Comparison of the CIPW norms of the 80.12.3A sample and the Kiglapait (Ki) Upper Zone liquid at 85PCS (Ki85) (S.A. Morse, personal communication; Morse 1981) shows that both samples are similar in normative apatite (TJ = 1.68%; Ki = 1.34%), magnetite (TJ = 3.02%; Ki = 4.41%), ilmenite (TJ = 6.84%; Ki = 7.14%), anorthite (plag) (TJ = 40.6%; Ki = 44.8%) but TJ is richer in hypersthene (TJ = 19.04%; Ki = 2.68%) as well as orthose (TJ = 6.12%; Ki = 2.22%) and lower in clinopyroxene (TJ = 5.62%; Ki = 22.93%) and olivine (TJ = 1.24%; Ki = 14.45%) than Ki85. Tjörn sample is then jotunitic and Ki85, ferrogabbroic.

Experimental and analytical methods

Starting material and experimental procedure

Powder of sample 80.12.3A was provided by J.C. Duchesne. One atmosphere and high pressure experiments were all performed at Lamont-Doherty. Experimental conditions are reported in Table 2. The 1 atm melting experiments were conducted in a Deltech vertical quenching furnace in a CO/CO_2 atmosphere using the Pt-wire loop technique. To minimize iron loss, Pt-loops (0.1 mm wire diameter) were presaturated in Fe by running them for 48 hours at the experimental conditions with a large amount of sample; then the loops were cleaned in HF and reused for the experiments. Pellets of powder rock were sintered on Pt-wire loops. The $\text{CO}-\text{CO}_2$ gas mixtures were controlled with calibrated flow meters and f_{O_2} was measured using a (Zr, Ca) O_2 electrolyte cell. The 1 atm experiments were carried out at different f_{O_2} : NNO (nickel-nickel oxide) (run nos. TJ-37, 36, 31, 26, 38, 29, 32, 33, 34), MW (magnetite-wüstite) (run no. TJ-27–30), FMQ-1 (fayalite-magnetite-quartz) (run nos. TJ-48, 45, 46, 52, 53, 55) and MW-2.5 (run nos. TJ-49, 50) in order to constrain the f_{O_2} of the Bjerkreim-Sokndal magma chamber and because f_{O_2} is known to play an important role in liquid fractionation (Osborn 1959). This range of oxygen fugacities overlaps the one suggested by ilmenite-magnetite equilibria in the cumulates (Duchesne 1972a). The cell was calibrated against the Ni-NiO solid buffer and f_{O_2} is accurate to within ± 0.10 log units. Temperature was measured and monitored using a Pt-Pt10Rh thermocouple. This thermocouple was calibrated against the melting point of gold and found to agree within $\pm 2^\circ\text{C}$. Temperatures are accurate to within $\pm 2^\circ\text{C}$. In order to reduce Na loss, low gas flow rates (0.1 cm/s) and large amounts of sample were used. After each experiment, the samples were lightly crushed, mounted in epoxy and polished.

Table 1 Composition of the TJ and Hidra jotunites. Values for ferrous iron are by titration (*LOI* loss on ignition)

No.	Locality	SiO ₂	TiO ₂	Al ₂ O ₃	Fe ₂ O ₃	FeO	MnO	MgO	CaO	Na ₂ O	K ₂ O	P ₂ O ₅	LOI	Total
D80.12.1 ^a	Tjörn	49.57	4.95	14.11	6.48	7.72	0.14	5.46	6.21	3.57	1.00	1.07	0.00	100.28
D80.12.3A ^a	Tjörn	49.39	3.67	15.81	5.81	7.88	0.13	4.54	6.87	3.50	0.96	0.71	0.00	99.17
D80.12.4 ^a	Tjörn	49.27	5.22	14.00	5.81	9.08	0.15	5.71	6.18	3.72	1.06	0.79	0.00	100.98
Tjaver ^b	Tjörn	49.70	3.63	15.78	5.00	8.37	0.15	4.44	6.81	3.88	1.05	0.64	nd	99.45
TJ ^c	Tjörn	49.54	3.46	16.04	nd	13.06	0.13	4.54	6.82	3.65	0.94	0.63	nd	98.81
H17234 ^d	Hidra	49.80	4.28	14.10	2.20	11.70	0.17	4.90	6.00	3.50	1.95	0.91	0.32	99.83
H17020 ^d	Hidra	48.00	4.61	14.20	5.00	10.40	0.18	4.60	6.40	3.60	1.08	0.81	0.85	99.81

^a XRF data from Piron (1981)^c Electron microprobe analysis of starting composition^b Average composition of samples 80.12.3A and 83.17.2 from Duchesne and Hertogen (1988)^d From Duchesne et al. (1974)**Table 2** Experimental conditions. See Table 3 for experimental product compositions (*gl* glass, *pl* plagioclase, *opx* low-Ca pyroxene, *pig* pigeonite, *aug* augite, *il* ilmenite, *mt* magnetite, *up* ulvöspinel, *grt* garnet; numbers after phase symbols are phase proportions calculated from mass balance of the experimental products against bulk composition, see text for explanation)

Experiment no.	<i>T</i> (°C)	<i>P</i>	<i>t</i> (h)	<i>f</i> _{O₂}	Products
TJ-37	1190	1 bar	16	NNO	gl ₈₆ , pl ₆ , il ₁ , mt ₇
TJ-36	1175	1 bar	16.5	NNO	gl ₉₇ , pl ₁ , il ₀ , mt ₂
TJ-31	1160	1 bar	18	NNO	gl ₇₅ , pl ₁₅ , il ₁ , mt ₉
TJ-26	1148	1 bar	26.5	NNO	gl ₈₁ , pl ₁₂ , il ₀ , mt ₇
TJ-38	1133	1 bar	22	NNO	gl ₆₄ , pl ₂₄ , opx ₀ , il _{0.5} , mt _{18.5}
TJ-29	1118	1 bar	52	NNO	gl ₆₀ , pl ₂₆ , opx ₃ , il _{0.3} , mt ₁₅
TJ-32	1105	1 bar	46	NNO	gl ₄₅ , pl ₃₆ , opx ₆ , il _{0.3} , mt _{12.7} , up ₀
TJ-34	1085	1 bar	72	NNO	gl ₃₅ , pl ₄₂ , opx ₀ , pig ₇ , aug ₃ , il ₁ , mt ₂₁ , up ₀
TJ-33 1	1071	1 bar	69.5	NNO	gl ₂₀ , pl ₅₁ , opx ₀ , pig ₁₅ , aug ₂ , il ₀ , up ₁₂
TJ-33 2	1071	1 bar	69.5	NNO	gl ₁₆ , pl ₅₃ , opx ₀ , pig ₁₅ , aug ₃ , il ₀ , up ₁₂
TJ-48	1150	1 bar	17.5	FMQ-1	gl ₉₂ , pl ₈
TJ-45	1124	1 bar	92.5	FJQ-1	gl ₆₉ , pl ₂₅ , ol ₅ , il ₁
TJ-46	1090	1 bar	97	FMQ-1	gl ₅₁ , pl ₃₄ , ol ₀ , il ₁ , up ₅
TJ-52	1080	1 bar	192	FMQ-1	gl ₃₉ , pl ₄₃ , ol ₁₄ , pig ₀ , il ₄
TJ-53	1070	1 bar	162	FMQ-1	gl ₃₀ , pl ₄₈ , ol ₁₂ , pig ₅ , il ₄ , mt ₀ , up ₀
TJ-55	1065	1 bar	167	FMQ-1	gl ₂₂ , pl ₅₁ , ol ₁₅ , aug ₆ , il ₀ , pig ₀
TJ-27	1140	1 bar	23	MW	gl ₉₅ , pl ₅
TJ-30	1110	1 bar	52	MW	gl ₇₈ , pl ₁₈ , ol ₃ , il ₁ , up ₀
TJ-49	1125	1 bar	48	MW-2.5	gl ₇₆ , pl ₁₉ , ol ₅ , il ₀
TJ-50	1090	1 bar	92	MW-2.5	gl ₄₈ , pl ₃₈ , ol ₁₁ , il ₃
TJ-17	1170	5 kbar	5		gl
TJ-25	1165	5 kbar	43		gl
TJ-28	1160	5 bar	21		gl
TJ-43	1150	5 kbar	41		gl ₉₂ , pl ₈
TJ-40	1135	5 kbar	48		gl ₈₁ , pl ₁₅ , ol ₄
TJ-23	1130	5 kbar	47		gl ₇₅ , pl ₂₁ , ol ₄
TJ-51	1110	5 kbar	54.5		gl ₇₅ , pl ₂₂ , ol ₃ , il ₀
TJ-47	1100	5 kbar	95		gl ₄₇ , pl ₄₀ , ol ₁₁ , pig ₀ , il ₂
TJ-1	1170	7 kbar	72		gl ₉₇ , pl ₃
TJ-41	1155	7 kbar	48		gl ₈₇ , pl ₁₁ , opx ₂
TJ-9	1145	7 kbar	73		gl ₈₄ , pl ₁₄ , opx ₂ , il ₀
TJ-3	1120	7 kbar	90		gl ₅₁ , pl ₃₃ , opx ₁₄ , ol ₀ , il ₂
TJ-4	1095	7 kbar	144		gl ₂₆ , pl ₄₈ , ol ₀ , pig ₂₂ , il ₄
TJ-5	1190	10 kbar	46		gl
TJ-16	1175	10 kbar	48		gl
TJ-18	1165	10 kbar	44		gl
TJ-20	1160	10 kbar	25		gl ₉₁ , pl ₆ , opx ₃
TJ-7	1130	10 kbar	70		gl ₇₅ , pl ₁₆ , opx ₈ , il ₁
TJ-8	1100	10 kbar	89		gl ₄₈ , pl ₃₂ , opx ₁₂ , pig ₀ , aug ₅ , il ₃
TJ-24	1190	13 kbar	15		gl
TJ-12	1185	13 kbar	50		gl ₉₈ , pl ₀ , opx ₂
TJ-11	1162	13 kbar	94		gl ₇₉ , pl ₁₁ , opx ₆ , pig ₀ , aug ₄ , il ₀
TJ-10	1160	13 kbar	70		gl ₇₃ , pl ₁₃ , opx ₅ , pig ₀ , aug ₈ , il ₁
TJ-13	1130	13 kbar	93		gl ₅₄ , pl ₂₄ , opx ₀ , pig ₁₆ , aug ₃ , il ₃
TJ-35	1215	16 kbar	22		gl ₉₄ , aug ₅
TJ-14	1200	16 kbar	48		gl ₈₆ , aug ₄ , grt ₁₀
TJ-44	1225	18 kbar	50		gl ₈₂ , grt ₁₈

Table 3 Composition of experimental products. Electron microprobe analyses of experimental run products; same symbols as in Table 2; No. is the number of analyses performed on each phase. Units in parentheses represent the standard deviation. For an entry of 48.1(4), the SD is 0.4 for an entry of 1.03(5), the SD is 0.05 and for an entry of 0.30(10), the SD is 0.10. Fo [Mg 100]/(Mg + Fe); En_s [100-Mg]/(Mg + Fe + Ca); An [Ca 100]/(Ca + Na + Na) are given in atomic units for olivine, pyroxene and plagioclase respectively

Experiment	Phase	No.	SiO ₂	TiO ₂	Al ₂ O ₃	Cr ₂ O ₃	FeO	Fe ₂ O ₃	MgO	MnO	CaO	K ₂ O	Na ₂ O	P ₂ O ₅	Total	An, En, Fo
TJ-37	gl	6	54.1(3)	3.34(7)	16.1(2)	0.12(2)	8.54(16)		4.47(5)	0.26(2)	6.96(4)	1.15(6)	3.39(83)	0.96(1)	100.05	
	pl	5	52.7(9)	0.31(24)	28.3(1.1)		1.82(75)		0.29(31)		12.3(7)	0.31(32)	3.91(30)		99.92	62
	il	4	0.10(2)	45.3(7)	2.20(68)	0.01(1)	33.7(4)	9.99	3.93(22)	0.06(3)	0.16(6)				95.41	
	mt	2	0.15	3.55	6.76	0.04	22.08	58.30	8.43	0.26	0.13				99.67	
TJ-36	gl	4	50.3(1)	4.00(1)	15.9(1)	0.11(2)	11.6(11)		4.53(3)	0.24(2)	6.81(6)	0.93(2)	3.35(6)	0.85(1)	98.63	
	pl	4	52.9(3)	0.34(12)	28.8(6)		1.41(16)		0.22(8)		12.4(3)	0.18(2)	4.07(48)		100.30	62
	il	1	1.66	49.90	3.89	0.01	34.90	0.00	4.54	0.05	0.42		0.07		95.39	
	mt	2	0.14(5)	9.7(1)	7.91(24)	0.24(4)	31.2(1)	42.00	5.88(0)	0.20(1)	0.15(5)		0.03		97.37	
TJ-31	gl	6	55.3(2)	3.04(12)	14.9(1)	0.04(6)	8.24(18)		4.80(11)	0.16(7)	6.76(6)	1.03(5)	3.52(7)	0.81(10)	98.56	
	pl	4	53.4(9)	0.31(22)	28.2(1.2)		1.57(53)		0.46(27)		12.2(7)	0.30(17)	4.23(39)		100.71	60
	il	6	0.07(2)	46.2(3)	1.95(84)	0.03(2)	33.3(7)	8.57	4.62(19)	0.06(1)	0.13(4)				95.21	
	mt	5	0.13(2)	4.93(8)	6.14(5)	0.05(2)	24.4(4)	57.30	8.02(20)	0.26(3)	0.15(4)				101.36	
TJ-26	gl	4	53.1(3)	3.52(8)	14.8(1)		10.7(1)		5.04(3)	0.16(2)	6.71(8)	1.10(8)	3.56(9)	0.67(6)	99.35	
	pl	5	52.2(6)	0.18(4)	28.3(2)		1.55(15)		0.19(5)		11.9(3)	0.19(5)	4.44(12)		98.94	59
	mt	1	0.12	9.79	6.07	0.06	30.60	46.20	6.65	0.19	0.08				99.77	
	il	1	0.24	48.40	5.24	0.00	36.20	0.66	4.09	0.06	0.13				94.97	
TJ-38	gl	6	57.6(5)	2.92(4)	14.0(7)	0.11(2)	8.18(21)		4.58(17)	0.31(2)	6.75(15)	1.45(12)	3.10(69)	1.40(14)	100.35	
	pl	6	54.9(1)	0.27(20)	26.6(5)	0.00	1.94(62)		0.43(27)		10.9(7)	0.46(30)	4.96(82)		100.44	53
	opx	3	55.5(9)	0.42(30)	1.58(68)	0.02(1)	10.7(1.2)		30.9(2)	0.39(5)	1.39(51)		0.04(1)		101.02	84
	il	1	0.89	49.80	1.98	0.04	35.80	1.96	5.03	0.08	0.39				95.93	
TJ-29	mt	2	0.12(1)	5.87(9)	4.33(9)	0.06(3)	25.0(1)	55.60	7.46(8)	0.36(2)	0.09(0)				98.83	
	gl	4	56.3(4)	3.09(16)	13.6(1)		9.5(3)		4.34(11)	0.16(1)	6.76(10)	1.61(10)	3.49(13)	0.92(9)	99.80	
	pl	5	53.9(1.4)	0.15(8)	27.6(1.2)		1.31(60)		0.17(11)		10.7(1.0)	0.31(9)	4.94(50)		99.04	53
	opx	7	54.8(4)	0.43(16)	1.55(47)	0.02(2)	12.1(4)		29.0(8)	0.37(7)	1.63(49)		0.11(6)		99.92	79
TJ-32	mt	3	0.31(2)	9.21(34)	3.76(12)	0.02(2)	30.8(4)	50.50	6.07(3)	0.29(2)	0.17(2)				101.13	
	il	3	0.21(5)	51.1(7)	1.69(47)	0.00	37.9(5)	0.74	4.52(13)	0.03(3)	0.18(6)				96.42	
	gl	5	59.1(7)	2.47(7)	13.1(1)	0.12(1)	7.64(23)		3.87(18)	0.29(3)	6.85(16)	1.39(13)	3.02(10)	1.66(10)	99.50	
	pl	5	55.8(2.3)	0.15(8)	27.1(5)	0.00	1.37(62)		0.42(54)		10.7(1.0)	0.33(4)	4.91(71)		100.72	53
TJ-34	il	5	0.48(56)	46.6(2.0)	1.56(11)	0.00	33.1(2.1)	7.89	4.89(43)	0.08(2)	0.28(10)				94.40	
	mt	5	0.15(4)	3.58(10)	3.22(4)	0.04(2)	24.0(3)	62.30	6.92(3)	0.4(4)	0.20(2)				100.79	
	up	5	0.31(46)	20.5(9)	1.04(9)	0.01(1)	43.2(1.2)	27.80	3.85(22)	0.16(1)	0.14(6)				96.91	
	gl	5	60.7(1)	2.34(7)	13.2(2)		7.25(21)		2.98(17)	0.16(4)	5.77(27)	2.20(10)	2.79(23)	1.72(15)	99.11	
TJ-33	pl	4	55.8(9)	0.09(10)	27.5(2)		0.82(50)		0.08(8)		10.3(5)	0.42(10)	5.20(35)		100.21	51
	opx	4	54.9(8)	0.30(5)	1.06(12)	0.02(2)	15.1(9)		27.3(7)	0.51(3)	1.29(21)		0.05(2)		100.47	74
	pig	1	55.00	0.54	0.90	0.03	14.31		26.90	0.42	2.33		0.04		100.43	74
	aug	1	52.50	0.33	1.58	0.05	9.89		13.29	0.24	22.50		0.37		100.68	38
TJ-33	il	1	0.45	47.10	1.45	0.00	34.68	5.97	4.27	0.07	0.25				94.25	
	mt	2	0.11(3)	7.59(6)	3.06(13)	0.11(1)	29.45(5)	51.70	5.15(13)	0.50(1)	0.21(3)				97.87	
	up	3	0.00	28.2(2)	0.81(1)	0.10(2)	50.1(2)	11.50	3.45(10)	0.24(1)	0.16(2)				94.55	
	gl	2	61.5(9)	2.45(2)	13.7(1)		7.70(7)		2.22(1)	0.13(1)	5.32(6)	2.15(33)	2.84(68)	1.64(7)	99.60	
TJ-33	gl2	2	66.1(3)	2.14(13)	13.4(3)		5.81(38)		1.63(12)	0.10(0)	3.73(24)	2.88(4)	2.28(50)	1.05(13)	99.16	
	pl	5	57.5(1.6)	0.31(23)	26.3(1.1)		1.05(56)		0.20(16)		9.65(81)	0.56(12)	5.45(53)		101.07	48
	opx	6	52.3(6)	0.69(70)	0.92(14)	0.01(1)	22.0(6)		21.6(1.0)	0.48(6)	1.17(44)		0.02(2)		99.18	62
	pig	3	53.6(6)	0.52(7)	0.73(35)	0.02(0)	19.0(4)		22.1(4)	0.47(7)	3.51(79)		0.06(3)		100.03	63

Table 3 (continued)

Experiment	Phase	No.	SiO ₂	TiO ₂	Al ₂ O ₃	Cr ₂ O ₃	FeO	Fe ₂ O ₃	MgO	MnO	CaO	K ₂ O	Na ₂ O	P ₂ O ₅	Total	An, En, Fo
TJ-33	aug	2	51.4 (9)	0.80 (76)	1.75 (19)	0.01 (1)	10.9 (3)	15.00	13.9 (7)	0.29 (6)	19.80		0.33 (6)		99.13	41
	il	3	0.20 (16)	44.8 (1)	0.49 (3)	0.01 (1)	32.5 (5)		4.20 (9)	0.31 (5)	0.21 (6)				97.73	
	up	3	0.29 (32)	22.5 (3)	0.98 (7)	0.02 (2)	44.9 (4)	23.30	3.72 (23)	0.14 (2)	0.10 (1)				95.99	
TJ-27	gl	4	49.9 (5)	4.21 (32)	15.6 (3)		13.1 (5)		4.65 (10)	0.14 (2)	6.63 (17)	0.96 (9)	3.69 (19)	0.53 (5)	99.37	
	pl	5	51.6 (7)	0.22 (5)	29.1 (2)		1.15 (8)		0.14 (4)		12.1 (3)	0.20 (2)	4.28 (22)		98.73	60
TJ-30	gl	4	50.2 (6)	4.30 (6)	14.3 (1)		13.7 (2)		4.64 (6)	0.18 (2)	6.20 (4)	1.15 (5)	3.34 (5)	0.57 (4)	98.55	
	pl	5	53.7 (5)	0.22 (3)	27.7 (10)		1.56 (56)		0.25 (15)		11.0 (4)	0.26 (6)	4.82 (14)		99.45	55
	ol	5	37.5 (5)	0.20 (10)	0.31 (26)	0.03 (3)	27.8 (4)		34.4 (5)	0.27 (4)	0.33 (13)		0.04 (2)		100.87	69
	up	4	0.27 (2)	20.5 (1)	5.15 (8)	0.80 (27)	41.7 (1)	26.00	5.75 (5)	0.25 (9)	0.15 (2)		0.02 (2)		100.61	
	il	1	0.06	47.30	0.72	0.21	31.50	13.00	6.09	0.19	0.13				99.13	
TJ-48	gl	4	49.3 (1)	4.12 (4)	15.1 (1)	0.04 (3)	13.0 (3)		4.52 (6)	0.15 (1)	6.44 (4)	1.04 (3)	3.61 (8)	0.61 (2)	97.86	
	pl	7	54.3 (2.2)	0.21 (13)	28.0 (1.2)		0.87 (27)		0.16 (9)		10.8 (1.6)	0.28 (5)	4.58 (59)		99.39	56
TJ-45	gl	4	49.5 (4)	4.57 (1)	13.7 (1)	0.03 (2)	14.2 (1)		4.13 (5)	0.16 (2)	6.18 (6)	1.17 (5)	3.45 (11)	0.85 (4)	97.97	
	pl	6	55.7 (2.2)	0.16 (8)	27.3 (1.1)		0.90 (27)		0.12 (7)		10.0 (1.4)	0.33 (7)	5.24 (57)		99.66	50
	ol	4	36.1 (2)	0.29 (20)	0.04 (0)	0.00	31.8 (4)		30.7 (1)	0.31 (3)	0.25 (2)	0.00	0.01 (1)		99.54	63
	il	5	0.06 (2)	51.7 (3)	0.46 (3)	0.21 (3)	35.6 (1)	4.86	6.02 (5)	0.24 (1)	0.13 (2)				99.26	
	gl	4	52.2 (2)	3.89 (5)	12.5 (2)	0.02 (2)	13.8 (1)		3.35 (7)	0.17 (2)	6.48 (10)	1.56 (4)	3.40 (12)	0.97 (4)	98.35	
TJ-46	pl	6	55.9 (1.8)	0.14 (7)	27.0 (8)		0.78 (19)		0.09 (3)		9.75 (1.08)	0.43 (9)	4.94 (51)		99.01	51
	ol	5	35.3 (4)	0.22 (6)	0.05 (4)	0.03 (2)	35.5 (2)		27.2 (3)	0.41 (2)	0.35 (2)	0.00	0.01		99.13	58
	il	6	0.06 (0)	51.7 (4)	0.34 (2)	0.05 (1)	37.4 (4)	4.26	4.94 (6)	0.28 (3)	0.19 (4)				99.18	
	up	5	0.14 (2)	20.2 (2.4)	5.56 (78)	0.12 (1)	44.3 (3.2)	25.20	3.84 (29)	0.29 (1)	0.07 (3)				99.68	
	gl	4	54.1 (1.2)	3.26 (17)	11.8 (2)	0.03 (2)	13.2 (7)		2.83 (19)	0.20 (1)	6.57 (31)	1.62 (12)	2.83 (15)	1.15 (18)	97.52	
TJ-52	pl	6	56.5 (9)	0.12 (5)	26.9 (7)	0.01 (1)	0.59 (14)		0.08 (6)	0.00	9.27 (73)	0.50 (6)	5.53 (49)	0.01 (2)	99.46	47
	ol	6	34.4 (6)	0.20 (11)	0.15 (14)	0.01 (1)	39.2 (2)		24.1 (14)	0.41 (2)	0.43 (4)	0.05 (4)	0.08 (6)	0.13 (3)	99.17	48
	plg	3	50.8 (6)	0.70 (18)	1.30 (67)	0.00	23.1 (4)		18.6 (1.2)	0.33 (2)	3.20 (27)	0.01 (1)	0.18 (15)	0.03 (3)	99.19	55
	il	5	0.08 (1)	51.8 (2)	0.24 (2)	0.06 (3)	38.6 (3)	3.25	4.28 (7)	0.30 (2)	0.18 (3)				98.82	
	gl	5	53.1 (6)	3.38 (14)	11.4 (1)		15.1 (3)		2.75 (8)	0.16 (1)	7.15 (18)	1.83 (5)	2.61 (5)	1.79 (15)	99.25	
TJ-53	pl	5	57.0 (1.3)	0.07 (5)	26.2 (5)	0.00	0.55 (18)		0.04 (4)	0.01 (1)	8.48 (69)	0.59 (8)	5.73 (30)	0.00	98.61	43
	ol	2	33.6 (1)	0.30 (15)	0.05 (4)	0.02 (1)	41.3 (2)		21.3 (1)	0.41 (3)	0.43 (3)				97.86	48
	plg	5	50.1 (4)	0.60 (8)	0.64 (20)	0.02 (1)	23.9 (5)		17.5 (2)	0.37 (2)	4.54 (40)	0.01 (1)	0.09 (3)	0.03 (3)	97.84	51
	il	5	0.05 (3)	51.5 (7)	0.22 (1)	0.06 (2)	39.6 (2)	3.11	3.60 (3)	0.29 (3)	0.16 (7)				98.59	
	mt	3	0.20 (2)	11.9 (7)	5.39 (26)	0.15 (1)	38.9 (7)	39.60	2.12 (5)	0.20 (3)	0.09 (0)				98.36	
TJ-55	up	1	0.11	28.05	2.74	0.27	51.80	11.20	2.98	0.32	0.11				97.54	
	gl	5	54.9 (1.0)	2.68 (16)	11.8 (2)	0.01 (1)	13.3 (4)		2.26 (16)	0.17 (2)	6.20 (22)	2.30 (11)	2.53 (17)	1.87 (11)	98.01	
	pl	7	57.7 (1.1)	0.09 (8)	25.9 (3)		0.57 (14)		0.04 (4)		8.00 (28)	0.76 (6)	5.42 (29)		98.49	43
	ol	5	33.5 (4)	0.30 (7)	0.20 (11)	0.01 (1)	42.8 (3)		20.6 (2)	0.45 (3)	0.60 (14)				98.50	46
	aug	4	50.7 (5)	0.29 (14)	1.62 (17)	0.05 (3)	11.5 (1.0)		12.6 (2)	0.23 (4)	21.0 (1.2)		0.36 (6)		98.24	37
TJ-49	plg	8	50.2 (4)	0.61 (12)	0.66 (15)	0.03 (1)	24.4 (1.3)	4.08	16.0 (7)	0.41 (5)	5.67 (1.87)		0.04 (4)		98.03	48
	il	5	0.10 (4)	50.4 (3)	0.30 (4)	0.10 (1)	38.9 (3)		3.43 (4)	0.35 (3)	0.24 (5)				97.93	
	gl	5	50.0 (5)	4.66 (17)	14.2 (3)	0.01 (1)	13.9 (2)		4.27 (13)	0.16 (1)	6.20 (9)	1.14 (4)	3.17 (17)	0.79 (6)	98.50	
	pl	6	53.9 (4)	0.22 (10)	28.3 (9)		0.77 (31)		0.15 (12)		11.1 (4)	0.27 (7)	4.58 (59)		99.34	56
	ol	4	35.8 (1)	0.19 (3)	0.03 (0)	0.01 (1)	31.7 (2)		30.3 (2)	0.33 (1)	0.27 (1)		0.01 (1)		98.55	63
TJ-50	il	4	0.06 (1)	52.5 (3)	0.43 (1)	0.19 (2)	35.7 (2)	2.69	6.30 (3)	0.30 (3)	0.24 (1)				98.37	
	gl	4	52.0 (2)	4.04 (11)	12.5 (1)	0.02 (1)	14.3 (2)		3.30 (5)	0.15 (2)	6.71 (9)	1.41 (3)	2.80 (11)	1.17 (5)	98.44	
	pl	6	56.0 (2.5)	0.14 (9)	27.0 (1.4)		0.64 (16)		0.09 (6)		9.68 (1.6)	0.50 (5)	5.26 (73)		99.29	49
	ol	4	34.6 (2)	0.24 (10)	0.03 (2)	0.00	37.1 (2)		25.5 (1)	0.42 (3)	0.35 (2)		0.01 (1)		98.31	55
	il	5	0.10 (5)	52.4 (2)	0.29 (3)	0.06 (4)	38.1 (2)	2.16	4.89 (5)	0.29 (3)	0.24 (4)				98.56	

Table 3 (continued)

Experi- ment	Phase	No.	SiO ₂	TiO ₂	Al ₂ O ₃	Cr ₂ O ₃	FeO	Fe ₂ O ₃	MgO	MnO	CaO	K ₂ O	Na ₂ O	P ₂ O ₅	Total	An, En, Fo
TJ-17	gl	5	49.5 (3)	3.46 (3)	16.0 (1)		13.1 (2)		4.54 (6)	0.13 (1)	6.82 (9)	0.94 (4)	3.65 (11)	0.63 (4)	98.81	
TJ-43	gl	5	49.5 (3)	4.04 (2)	15.3 (1)		13.5 (1)		4.65 (5)	0.13 (1)	6.39 (6)	0.90 (8)	3.62 (10)	0.66 (4)	98.64	
	pl	3	56.4 (1.8)	0.20 (1)	27.3 (1.3)		0.53 (2)		0.08 (2)		9.61 (1.10)	0.36 (6)	5.48 (78)		99.99	48
TJ-40	gl	4	49.5 (3)	4.23 (5)	14.8 (1)		14.0 (2)		4.63 (6)	0.16 (3)	6.36 (9)	1.04 (3)	3.76 (11)	0.69 (5)	99.09	
	pl	5	56.1 (4)	0.21 (1)	27.8 (3)		0.56 (5)		0.09 (1)		9.94 (34)	0.38 (4)	5.53 (27)		100.62	49
	ol	5	36.5 (3)	0.20 (1)	0.08 (1)	0.00	31.2 (3)		31.8 (2)	0.26 (3)	0.29 (2)		0.03 (1)		100.32	64
TJ-23	gl	5	48.2 (3)	4.89 (4)	14.1 (1)		14.2 (1)		4.67 (3)	0.16 (1)	6.37 (6)	1.16 (6)	3.46 (13)	0.79 (5)	98.00	
	pl	8	56.0 (1.6)	0.21 (1.5)	26.6 (8)		0.56 (16)		0.10 (6)		8.99 (1.03)	0.45 (6)	5.70 (28)		98.58	45
	ol	6	37.3 (5)	0.21 (3)	0.09 (8)	0.00	30.9 (3)		32.0 (3)	0.27 (2)	0.27 (3)		0.01 (2)		100.97	65
TJ-51	gl	4	49.4 (8)	5.32 (20)	14.1 (1)	0.01 (1)	13.3 (5)		4.85 (18)	0.17 (1)	6.31 (12)	1.09 (6)	3.59 (15)	0.65 (4)	98.76	
	pl	7	56.7 (1.5)	0.30 (30)	26.7 (1.1)	0.00	0.72 (42)		0.15 (10)	0.00	9.19 (91)	0.43 (7)	5.50 (45)	0.00	99.63	47
	ol	4	36.8 (2)	0.22 (4)	0.06 (1)		28.6 (6)		33.2 (47)	0.28 (2)	0.28 (2)		0.01 (0)		99.37	67
	il	5	0.07 (2)	55.5 (6)	0.58 (1)	0.14 (2)	35.3 (1)	0.00	7.14 (6)	0.26 (1)	0.18 (6)				99.02	
TJ-47	gl	4	50.2 (4)	4.42 (3)	11.5 (7)	0.03 (2)	15.1 (2)		3.39 (3)	0.19 (1)	7.06 (9)	1.69 (4)	3.65 (11)	1.42 (8)	98.72	
	pl	6	56.6 (9)	0.09 (5)	27.3 (7)	0.00	0.49 (11)		0.06 (3)	0.01 (1)	8.89 (94)	0.56 (7)	6.11 (56)	0.01 (0)	100.03	43
	ol	4	34.4 (1)	0.24 (12)	0.03 (1)	0.00	37.2 (3)		25.5 (2)	0.38 (1)	0.39 (3)	0.00	0.01 (1)	0.00	98.17	55
	pig	7	50.4 (4)	0.90 (27)	1.21 (32)	0.05 (2)	22.5 (2.1)		17.9 (9)	0.31 (2)	4.80 (2.11)	0.00	0.11 (4)	0.00	98.15	53
	il	5	0.04 (1)	54.3 (6)	0.26 (1)	0.06 (2)	39.5 (3)	0.00	4.69 (3)	0.31 (3)	0.20 (20)				99.38	
TJ-1	gl	5	50.3 (4)	3.08 (7)	16.0 (1)		12.6 (2)		4.66 (2)	0.14 (1)	6.44 (10)	1.00 (5)	3.53 (14)	1.19 (8)	98.98	
	pl	3	57.7 (6)	0.10 (3)	27.0 (9)		0.48 (9)		0.08 (3)		9.34 (31)	0.41 (2)	5.30 (42)		100.40	48
TJ-41	gl	5	49.7 (2)	3.97 (11)	15.3 (2)		13.6 (2)		4.71 (6)	0.14 (2)	6.58 (7)	0.97 (7)	3.53 (15)	0.62 (5)	99.10	
	pl	4	56.3 (9)	0.19 (2)	27.7 (2)		0.52 (7)		0.08 (2)		9.70 (12)	0.37 (6)	5.69 (16)		100.56	47
	opx	5	51.9 (6)	0.93 (19)	3.15 (19)	0.03 (1)	19.0 (5)		22.8 (6)	0.23 (3)	1.63 (3)		0.08 (1)		99.85	66
TJ-9	gl	6	47.2 (4)	4.76 (9)	14.3 (1)		15.0 (2)		4.80 (7)	0.15 (3)	6.61 (4)	1.05 (4)	3.65 (16)	0.81 (5)	98.22	
	pl	6	56.1 (6)	0.20 (5)	27.0 (5)		0.54 (17)		0.10 (7)		9.16 (40)	0.42 (6)	5.59 (32)		99.10	46
	opx	7	50.2 (9)	1.24 (31)	4.72 (1.34)	0.05 (1)	19.3 (5)		22.1 (1)	0.26 (2)	1.96 (28)		0.11 (2)		99.93	64
	il	5	0.04 (1)	53.6 (9)	0.57 (0)	0.11 (2)	36.6 (4)	1.11	6.36 (7)	0.26 (3)	0.14 (2)				98.7	
TJ-3	gl	3	48.1 (1)	3.88 (8)	13.2 (1)		16.4 (1)		4.02 (2)	0.16 (2)	6.51 (1)	1.36 (2)	3.36 (12)	1.59 (21)	98.54	
	pl	6	56.7 (1.3)	0.14 (16)	27.6 (1.2)		0.69 (41)		0.11 (10)		9.46 (1.05)	0.48 (8)	5.58 (43)		100.82	47
	ol	8	36.0 (2)	0.17 (5)	0.06 (1)	0.01 (1)	35.6 (8)		28.3 (1)	0.32 (4)	0.29 (4)		0.02 (1)		100.69	59
	opx	6	52.5 (8)	0.68 (15)	2.16 (1.00)	0.01 (1)	19.9 (7)		22.8 (4)	0.25 (3)	1.66 (13)		0.05 (1)		99.98	65
	il	5	0.03 (2)	53.5 (4)	0.40 (2)	0.05 (2)	38.7 (1)	0.04	5.10 (4)	0.28 (2)	0.13 (1)				98.17	
TJ-4	gl	6	47.1 (1.1)	4.21 (33)	12.0 (1.2)		17.8 (1.0)		3.40 (25)	0.18 (2)	7.28 (14)	2.02 (17)	2.93 (21)	2.32 (18)	99.20	
	pl	4	57.2 (1.0)	0.16 (4)	27.0 (6)		0.62 (8)		0.06 (1)		9.03 (62)	0.84 (11)	5.58 (34)		100.45	45
	ol	6	34.5 (5)	0.24 (14)	0.10 (7)	0.01 (1)	41.3 (4)		23.1 (4)	0.38 (4)	0.44 (5)		0.04 (2)		100.20	50
	pig	7	50.6 (9)	0.83 (12)	1.81 (38)	0.01 (2)	24.4 (1.1)		16.9 (9)	0.33 (6)	4.15 (67)		0.17 (7)		99.20	50
	il	4	0.04 (3)	53.9 (2)	0.34 (12)	0.06 (2)	40.9 (5)	0.00	4.03 (4)	0.32 (2)	0.18 (3)				99.79	
TJ-5	gl	4	50.6 (1)	3.65 (3)	16.3 (1)		11.9 (1)		4.34 (2)	0.11 (1)	6.56 (3)	0.95 (1)	3.56 (5)	0.59 (5)	98.53	
TJ-18	gl	5	50.1 (1)	3.46 (3)	16.5 (1)		12.4 (1)		4.39 (3)	0.13 (1)	6.73 (6)	1.00 (3)	3.73 (13)	0.63 (3)	99.04	
TJ-20	gl	5	49.6 (1)	3.79 (8)	15.8 (1)		13.0 (2)		4.26 (5)	0.14 (2)	6.59 (6)	1.04 (5)	3.65 (14)	0.63 (4)	98.49	
	pl	5	57.6 (7)	0.11 (6)	26.3 (6)		0.50 (13)		0.07 (3)		8.50 (58)	0.40 (3)	6.27 (38)		99.78	42
	opx	6	51.3 (7)	0.93 (13)	5.28 (87)	0.05 (2)	18.6 (3)		22.0 (1.1)	0.24 (2)	2.21 (48)		0.29 (16)		100.92	65
TJ-7	gl	5	49.2 (2)	3.89 (3)	15.3 (1)		13.7 (1)		3.88 (6)	0.12 (3)	6.76 (4)	1.22 (7)	3.44 (10)	0.83 (6)	98.23	
	pl	5	56.5 (6)	0.12 (2)	26.9 (3)		0.47 (7)		0.05 (1)		8.95 (32)	0.47 (5)	5.66 (18)		99.15	45

Table 3 (continued)

Expe- riment	Phase	No.	SiO ₂	TiO ₂	Al ₂ O ₃	Cr ₂ O ₃	FeO	Fe2O3	MgO	MnO	CaO	K ₂ O	Na ₂ O	P ₂ O ₅	Total	An, En, Fo
TJ-7	opx	6	50.7 (1.1)	0.92 (21)	4.74 (1.1)	0.02 (3)	20.8 (3)		20.5 (1.0)	0.25 (4)	2.26 (30)		0.15 (7)		100.23	61
	il	3	0.14 (4)	52.6 (2)	0.65 (3)	0.10 (2)	37.0 (3)	2.67	5.59 (10)	0.26 (2)	0.23 (1)				99.24	
	gl	4	49.1 (8)	3.22 (7)	14.4 (4)		14.8 (5)		3.20 (32)	0.14 (3)	6.72 (12)	1.70 (11)	3.34 (18)	1.13 (4)	97.72	
	pl	5	57.3 (1.2)	0.09 (5)	26.6 (6)		0.43 (8)		0.03 (2)		8.33 (84)	0.49 (8)	6.11 (59)		99.41	42
	opx	8	49.5 (9)	0.77 (21)	4.6 (1.3)	0.04 (4)	23.2 (7)		19.3 (9)	0.28 (6)	2.24 (41)		0.13 (5)		100.00	57
TJ-8	aug	2	48.8 (5)	1.16 (3)	5.22 (23)	0.04 (0)	16.3 (8)		13.2 (1)	0.25 (4)	13.9 (12)		0.63 (1)		99.48	41
	pig	1	49.90	1.68	6.59	0.04	20.00		15.73	0.26	4.96		0.30		99.53	52
	il	4	0.08 (2)	52.4 (3)	0.46 (2)	0.06 (2)	39.1 (2)	2.66	4.34 (6)	0.24 (3)	0.19 (4)				99.50	
	gl	5	50.6 (1)	4.19 (3)	16.2 (1)	0.14 (2)	12.8 (1)		4.48 (6)	0.25 (3)	6.76 (2)	1.03 (2)	3.52 (2)	0.85 (3)	100.91	
	gl	4	50.1 (3)	3.75 (2)	16.6 (1)		12.3 (2)		4.26 (7)	0.11 (2)	6.67 (9)	0.93 (2)	3.63 (19)	0.58 (4)	98.94	
TJ-12	pl	5	56.4 (4)	0.13 (3)	27.0 (2)		0.47 (4)		0.06 (1)		8.78 (18)	0.38 (4)	6.04 (14)		99.24	44
	opx	7	49.6 (5)	0.81 (9)	7.13 (71)	0.06 (2)	18.0 (1)		22.8 (5)	0.23 (2)	1.78 (6)		0.18 (3)		100.64	67
	gl	4	49.4 (1.1)	4.09 (28)	15.8 (2)		13.2 (5)		3.47 (11)	0.13 (2)	6.40 (21)	1.24 (11)	3.72 (21)	0.85 (15)	98.28	
	pl	6	57.1 (6)	0.12 (5)	26.4 (3)		0.49 (13)		0.05 (2)		8.10 (37)	0.47 (5)	6.35 (26)		99.04	40
	opx	6	48.7 (6)	0.83 (8)	6.62 (75)	0.05 (3)	21.0 (5)		20.3 (5)	0.27 (4)	1.95 (8)		0.19 (2)		99.98	61
TJ-10	pig	5	48.2 (3)	1.16 (4)	7.06 (43)	2.00 (2)	19.4 (1.1)		18.8 (1.3)	0.25 (2)	4.53 (1.78)		0.41 (12)		101.78	57
	aug	4	47.3 (2)	1.78 (3)	8.86 (7)	0.03 (2)	14.1 (1)	1.87	12.9 (2)	0.22 (1)	13.1 (1)		1.14 (4)		99.39	43
	il	5	0.06 (2)	52.2 (5)	0.80 (3)	0.05 (2)	38.5 (3)		4.62 (6)	0.23 (2)	0.17 (6)				98.44	
	gl	4	48.5 (1)	4.42 (8)	15.7 (1)		13.4 (5)		3.71 (11)	0.13 (1)	6.67 (8)	1.11 (5)	3.49 (17)	0.84 (8)	97.94	
	pl	5	57.0 (4)	0.12 (1)	26.6 (2)		0.48 (7)		0.05 (1)		8.37 (13)	0.46 (3)	6.33 (29)		99.40	41
TJ-11	opx	7	49.2 (6)	0.93 (11)	6.34 (83)	0.03 (2)	20.8 (9)		20.7 (1.4)	0.28 (6)	1.91 (13)		0.22 (6)		100.35	61
	aug	6	48.1 (7)	1.65 (16)	8.20 (72)	0.03 (2)	14.7 (9)		14.5 (7)	0.24 (2)	11.7 (1.0)		0.97 (10)		100.11	47
	pig	1	47.90	1.09	8.07	0.05	20.40		19.30	0.28	2.44		0.30		99.83	59
	il	4	0.04 (2)	52.4 (4)	0.79 (2)	0.04 (2)	37.9 (3)	2.49	5.06 (5)	0.21 (2)	0.11 (3)				99.11	
	gl	5	48.6 (7)	3.49 (8)	15.5 (2)		14.0 (2)		2.96 (21)	0.12 (2)	6.44 (7)	1.46 (9)	3.14 (15)	1.38 (19)	97.17	
TJ-13	pl	5	57.3 (4)	0.12 (2)	26.3 (2)		0.54 (6)		0.03 (1)		8.20 (15)	0.52 (4)	6.28 (11)		99.27	41
	opx	4	48.6 (6)	0.72 (16)	5.29 (84)	0.01 (1)	23.2 (5)		19.1 (4)	0.31 (3)	2.04 (25)		0.19 (5)		99.42	59
	aug	7	48.8 (6)	1.40 (15)	7.59 (53)	0.02 (3)	16.4 (8)		12.7 (7)	0.22 (7)	12.3 (9)		0.85 (14)		100.21	41
	pig	1	49.00	0.68	5.46	0.01	21.80		18.70	0.28	3.81		0.42		100.08	56
	il	5	0.05 (0)	51.9 (3)	0.67 (2)	0.05 (2)	39.5 (2)	2.83	3.88 (6)	0.24 (3)	0.15 (3)				99.28	
TJ-35	gl	5	51.0 (2)	4.27 (6)	16.4 (1)	0.14 (2)	12.6 (2)		4.22 (2)	0.26 (2)	6.71 (5)	1.03 (4)	3.57 (11)	0.87 (2)	101.04	
	aug	6	48.26 (24)	1.35 (4)	9.69 (22)	0.06 (1)	14.9 (3)		14.1 (3)	0.25 (2)	9.52 (42)		1.14 (3)		99.33	48
	gl	6	50.6 (7)	4.18 (5)	15.6 (1)	0.01 (1)	11.7 (1)		3.37 (4)	0.10 (1)	6.59 (5)	1.10 (4)	3.93 (18)	134 (12)	98.49	
	aug	6	48.6 (1.0)	1.87 (28)	10.2 (1.1)	0.03 (2)	12.0 (3)		12.6 (4)	0.16 (3)	14.3 (7)		1.77 (25)		101.39	43
	grt	5	39.6 (4)	1.51 (35)	23.0 (1)	0.04 (3)	19.9 (3)		11.8 (4)	0.38 (3)	6.63 (24)		0.07 (2)		103.01	
TJ-44	gl	4	50.7 (2)	4.35 (7)	14.6 (1)	0.00	11.4 (1)		4.00	0.12 (1)	6.51 (3)	1.09 (1)	4.20 (7)	0.70 (0)	96.66	
	grt	5	38.7 (4)	1.06 (10)	21.9 (4)	0.00	19.9 (1)		11.0 (1)	0.37 (4)	6.45 (14)	0.00	0.06 (1)		99.39	

High pressure experiments were all run in a standard Boyd and England (1960) piston cylinder apparatus (1.2") using the cold piston-in method (Johannes et al. 1971). Approximately 0.01 g of rock powder was packed in a graphite cell which was then placed in a dense alumina insulator. This assemblage and crushable alumina insulators were introduced in a pressure cell made of sintered BaCO₃. In order to achieve dry conditions, the entire assembly was dried overnight in a vacuum oven ($T = 110^{\circ}\text{C}$). Using this technique on a powdered anorthositic dike, Fram and Longhi (1992) reported H₂O content less than 0.15% in a superliquidus glass. Temperature was controlled and monitored using a Pt-Pt10Rh thermocouple. The thermocouple was separated from the top of the graphite cell by a crushable alumina wafer (0.5 mm). Thermocouple e.m.f. was not corrected for P . Pressure and temperature have been calibrated for this system by Fram and Longhi (1992). The temperature offset between thermocouple and sample is 20°C and temperatures reported in Table 2 have been corrected for this difference. The difference between the applied and the actual pressure is linear between 5 and 30 kbar (2 kbar at 5 kbar and 4.5 kbar at 30 kbar). A friction correction is not included in the pressures reported in Table 2. After each experiment, the whole cell assembly was mounted in epoxy and polished. The use of unsealed graphite capsules has probably resulted in loss of CO₂ as graphite is porous to fluids at high pressure and temperature (Holloway et al. 1992) and consequently in reduction of ferric iron producing low oxygen fugacity in these experiments. Using the composition of ilmenites present in the high pressure experiments and the geobarometer of Andersen and Lindsley (1988), the oxygen fugacities were estimated to lie between FMQ-4 and FMQ-2, the latter value being close to the CCO buffer.

Analytical method

The experimental charges were analyzed using the CAMEBAX-MICRO wavelength dispersive system at Lamont-Doherty. Accelerating voltage was set at 15 kV and a sample current of 5 nA was used for Na and K and of 25 nA for Si, Ti, Al, Fe, Mg, Mn, Ca, P and Cr. Counting times were 20 s and data were reduced using the PAP corrections program of Cameca. Minerals were analyzed with a point beam and glasses with a defocused beam of 5 μm to minimize alkali loss. Different calibrations were used for glasses (glass standard GLCV = Ca, Mg, Si, Al; fayalite = Fe; rhodonite = Mn; microcline = K; labradorite = Na; rutile = Ti; apatite = P; uvarovite = Cr), plagioclases, oxides (hematite = Fe, ilmenite = Ti; anorthite = Ca, Al; enstatite = Si, Mg; uvarovite = Cr; rhodonite = Mn), as well as pyroxenes and olivines. Major element compositions of the experimental runs are reported in Table 3. The totals for ilmenites and ulvöspinel present in the 1 atm experiments performed at NNO are systematically low with lower totals for ilmenites than ulvöspinel. The origin of this deficiency is still unknown. The possible occurrence of minor components such as Zn, V, Nb and Ta has been checked without success.

Although experimental conditions at 1 atm have been chosen in order to achieve conservation of mass, Fe and Na loss may still have occurred in some experiments. Consequently, mass balance between the bulk composition of the starting material and the compositions of all phases present in one experimental charge (Table 3) (with allowance for Na and Fe loss) has been computed using a least squares multiple regression. With this method, proportions of all coexisting phases (Table 2) are given as well as the extent of Fe and Na loss. Results show that Na loss varies between 0 to 14 relative percent and Fe loss, from 5 up to 9 relative percent. In some cases, mass balance calculations yielded negative proportions for phases that were actually present in the experimental charge. This results from the arrangement of phases in the compositional space. In these cases, mass balances cannot be used to test if mass was conserved during the course of the experiment. Nevertheless, in order to obtain estimates of phase proportions in these experiments, phases with negative proportions have been excluded

(proportion 0 in Table 2) and their components included in the other phases. This results in an increased proportion of the remaining phases. In three experiments (TJ-38, TJ-29, TJ-34) mass balance calculations resulted in proportions of phases that were too high ($\Sigma = 107$ for TJ-38; $\Sigma = 104$ for TJ-29; $\Sigma = 109$ for TJ-34). In these experiments, Na loss ranges from 7 to 14% but important Fe gains are obtained (up to 45%) due to an overestimation of magnetite proportion in mass balance calculation.

Approach towards equilibrium

In the experiments described here, melt proportions are usually high (above 30% except in TJ-33 (20%), TJ-55 (22%) and TJ-4 (26%)). This together with the long experimental durations (from 16 to 144 h) allowed close approach towards equilibrium. Nevertheless, backscattered electron imaging shows a slight zoning in pyroxenes and plagioclase of some runs and the low Wo content of the low-Ca pyroxenes cores is in agreement with an origin as relics of the rock powder (see sample description in section 3). These phases are clearly not in complete equilibrium. Accordingly, only the rims of minerals surrounded by melt have been analyzed and there are several lines of observation which suggest that local equilibrium was approached between rims and liquid. Indeed, the Fe-Mg exchange partition coefficient between low-Ca pyroxene and melt is nearly constant [average $K_D = 0.27 \pm 0.02$ (1 σ)] and in agreement with results from other studies (Kinzler and Grove 1992). Within analytical uncertainty, melt compositions are homogeneous in the experimental charges except in TJ-33 which has been performed at low temperature (melt proportion $\approx 20\%$) and will not be considered in further discussion. Crystals are generally large (50–100 μm) and subehedral to euhedral (oxides usually have a more rounded shape). Finally, two different runs (TJ-10 and TJ-11; $P = 13$ kbar and $T = 1160^{\circ}\text{C}$) were performed at the same P - T conditions and show that the reproducibility of the method is very good. Both experiments display the same phase assemblages (melt + plag + opx + pig + aug + ilm) and phase proportions. Moreover, rims of plagioclase and opx are compositionally identical (An_{40-41} and En_{61} ; see Table 3). Augite and pigeonite have slightly different compositions (pig: $\text{En}_{57}\text{Fs}_{33}\text{Wo}_{10}$ in TJ-10 and $\text{En}_{59}\text{Fs}_{35}\text{Wo}_6$ in TJ-11; aug: $\text{En}_{43}\text{Fs}_{26}\text{Wo}_{31}$ in TJ-10 and $\text{En}_{47}\text{Fs}_{26}\text{Wo}_{27}$ in TJ-11) suggesting that these phases are slower to equilibrate.

Experimental results

The phase equilibria for sample 80.12.3A as a function of pressure and temperature are shown in Fig. 3. For 1 atm experiments, only those performed at MW have been shown on the phase diagram. Plagioclase is the sole liquidus phase from 1 atm up to 7 kbar, followed by olivine at low pressure [1 atm (MW) and 5 kbar] and by low-Ca pyroxene at 7 kbar. At 10 and 13 kbar, the liquid is multiply saturated with plagioclase and low-Ca pyroxene, followed at lower temperature by ilmenite, pigeonite, and augite. At 16 kbar, the liquidus phase is sub-calcic, aluminous augite followed by garnet whereas at 18 kbar, garnet is the liquidus phase.

At 1 atm and NNO, the liquidus temperature is significantly higher ($> 30^{\circ}\text{C}$) than at more reducing conditions. Ilmenite, magnetite and plagioclase are the liquidus phases, joined at lower temperature by low-Ca pyroxene instead of olivine as observed at lower f_{O_2} . This results from the higher a_{SiO_2} in the melt due to early crystallization of oxides. This phenomenon has also de-

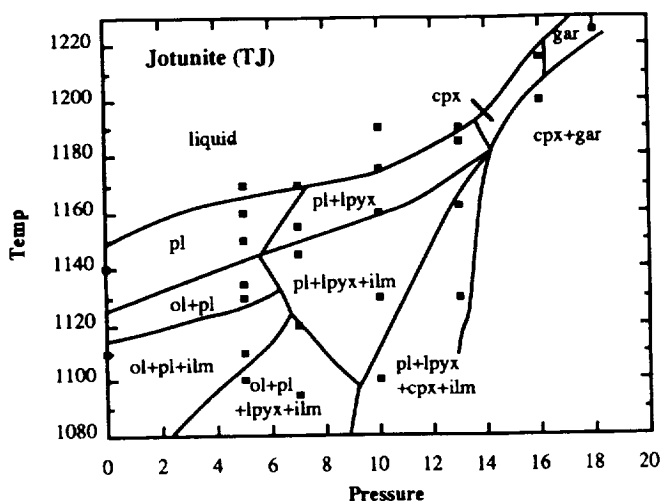


Fig. 3 Pressure (kbar) - Temperature (°C) phase diagram of sample 80.12.3A (TJ). (Symbols: *pl* plagioclase, *ol* olivine, *ilm* ilmenite, *lpyx* low-Ca pyroxene, *cpx* augite or/and pigeonite, *gar* garnet). At 1 atm, only experiments performed at MW are shown

pleted the residual liquids in FeO resulting in a much higher En content of low-Ca pyroxene in TJ-38 (En_{84} ; see Table 3) than at 7 kbar (TJ-41: En_{66}). At lower temperature (TJ-34), pigeonite, augite and ulvöspinel crystallize.

At FMQ-1, MW and MW-2.5, phase equilibria are similar, suggesting that below FMQ, there is little difference in the crystallization sequence. However, ilmenite is more abundant at FMQ-1 than at MW-2.5. At FMQ-1, magnetite (TJ-53) and ulvöspinel (TJ-46, TJ-53) occur in the cores of olivine grains and have not been observed as isolated grains surrounded by melt. Their occurrence as stable phases in these experiments is then questionable. At MW-2.5, ilmenite is the only stable oxide whereas at MW, ilmenite together with ulvöspinel occur in TJ-30.

Ilmenites occurring at NNO have a much higher Al_2O_3 content (0.49–5.24%) than those present at lower f_{O_2} (0.22–0.72%) and in the cumulates of BKSK (0.0–0.6%). The NNO ilmenites crystallized at a higher f_{O_2} than existed in the earlier stages of the intrusion (see below). This high f_{O_2} stabilized the oxides at the expense of the mafic silicates, thus allowing the oxides to precipitate at higher temperatures from liquids with higher Al_2O_3 . This higher Al_2O_3 content of the liquid also results from the smaller proportion of plagioclase in the liquidus assemblage of the NNO experiments. At lower f_{O_2} , the Al_2O_3 content of natural and experimental ilmenites is similar. The MgO content of experimental ilmenites is similar whatever the f_{O_2} (3.43–6.30%) but higher than that of the natural oxides (0.06–2.9%). Duchesne (1972a) has shown that the Fe^{3+} and Ti contents of the natural oxides have been modified during subsolidus cooling. The experimental data presented here suggest that their MgO content might also have been affected by this readjustment. The occurrence of

spinel grains in the reaction rims (spineliferous ilmenite of Duchesne 1972a) at the contact between ilmenite and magnetite grains supports this hypothesis.

The experimental results are consistent with the hypothesis that f_{O_2} , which controls the early appearance of magnetite, can play a key role in determining the course of fractionation, particularly with respect to silica enrichment (Kennedy 1955; Osborn 1959). Nevertheless, it must be emphasized that the liquidus crystallization of both oxides at NNO is also made possible by the high FeO content of the parent composition.

Pressure effects

The anorthite content of the liquidus plagioclase changes from An_{62} at 1 atm to An_{48} at 7 kbar. A large pressure effect on the plagioclase partition coefficients has already been observed by Green (1969) for quartz dioritic, gabbroic anorthositic and high-Al basalt liquids and by Fram and Longhi (1992) for a high-Al basalt composition. It is corroborated by the present experimental data on a more ferrous and potassic composition. This pressure effect is best displayed as the difference between the log of the observed partition coefficient of albite and the log of the Kd_{Ab} calculated at 1 atm as a function of pressure (Fig. 4). The $\log Kd_{Ab}$ at 1 atm has been calculated using the model of Drake (1976) and the model of Weaver and Langmuir (1990; C.H. Langmuir, personal communication). Both models

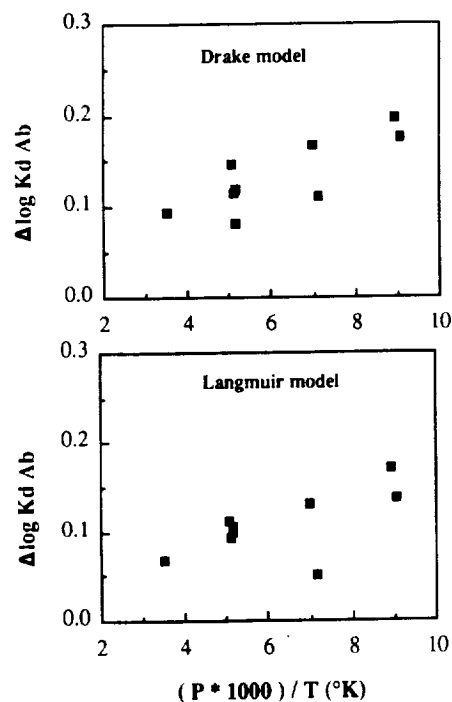


Fig. 4 Compositional change of plagioclase as a function of pressure. $\Delta \log Kd_{Ab}$ is the difference between the observed $\log Kd_{Ab}$ at P and the $\log Kd_{Ab}$ calculated at 1 atm using the models of Drake (1976) or Weaver and Langmuir (1990)

show an increase of the $K_{D_{Ab}}$ with pressure. Nevertheless, there is a spread in data points obtained at a given pressure. This feature results from compositional effects not taken into account in the models as discussed by Longhi et al. (1993).

Figure 5 shows that the Al_2O_3 content of low-Ca pyroxene in equilibrium with plagioclase strongly increases with pressure in agreement with experimental results obtained by Emslie (1975), Maquil (1978), Fram and Longhi (1992) and Longhi et al. (1993). Longhi et al. (1993) have shown that the increasing content of Al_2O_3 with pressure in low-Ca pyroxene results primarily from changes in crystal-liquid partitioning with little contribution from any increase in Al_2O_3 in the liquid. Consequently, comparison of the Al_2O_3 content between natural and experimental orthopyroxenes provides some constraint to the pressure of emplacement of the intrusion. However, the interpretation is clouded somewhat by the fact that our experiments did not produce opx at 5 kbar. The opx-bearing melts at NNO and 1 atm lacked olivine and were probably much different ($> 57\%$ SiO_2) than those in BSKS during the initial stages of opx crystallization ($\approx 50\%$ SiO_2), so direct comparison may not be precise. Furthermore, the low-Ca pyroxenes present in the BSKS cumulates (opx) and in the TJ sample (inverted pigeonite) have exsolved some augite and are lower in CaO than the experimental pyroxenes. Nevertheless, Longhi et al. (1993) have shown that the Al_2O_3 contents of the exsolved crystals are probably not significantly different from the original concentrations. Orthopyroxenes of BSKS display a low Al_2O_3 content close to the 1 atm experimental opx and below those of 7 kbar. Moreover, the mean Al_2O_3 of the TJ inverted pigeonite is 1.05%. This is less than, but close to the 1.21% average Al_2O_3 in the 5 kbar pigeonite (TJ-47; Table 3). Consequently, these data suggest a pressure of emplacement less than or equal to 5 kbar. This will be discussed in more detail in the discussion.

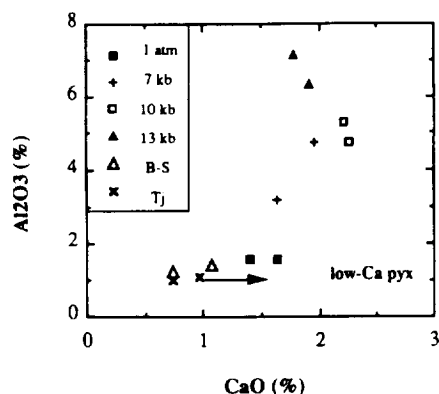


Fig. 5 Al_2O_3 and CaO concentrations (wt%) in experimental low-Ca pyroxenes in equilibrium with plagioclase as a function of pressure. Data on opx from the BSKS cumulates are from Duchesne (1972b). The low-Ca pyroxene of the TJ sample is an inverted pigeonite (see text). Vector indicates mixing path between low-Ca pyroxene host and augite lamellae.

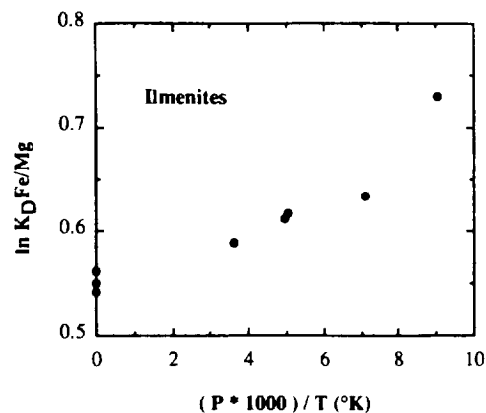


Fig. 6 Exchange partition coefficient (Fe^{2+}/Mg^{2+}) between ilmenite and liquid as a function of pressure. Ilmenites of the NNO experiments (1 atm) have not been considered.

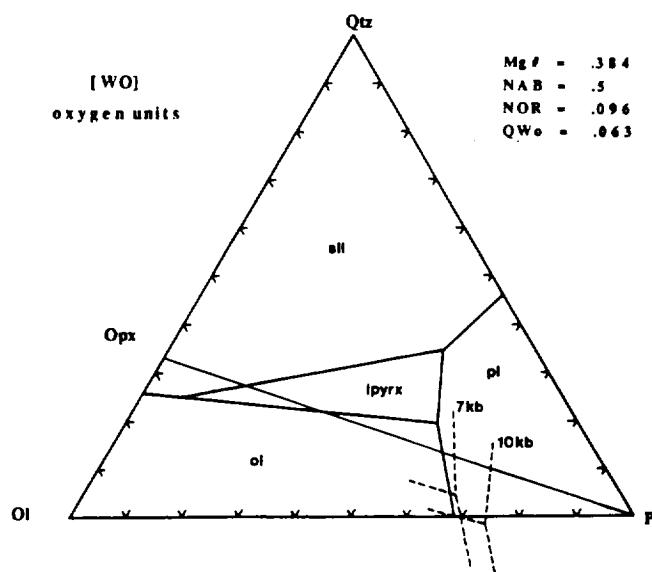


Fig. 7 Projection on the silica-olivine-plagioclase plane from wollastonite. 1 bar phase boundaries were calculated with the method of Longhi (1991). (QWo Quaternary wollastonite component, NAB and NOR albite and orthoclase mole fractions in the normative feldspar, $Mg\#$: $MgO/(MgO + FeO)$ in mole units). The 7 and 10 kbar phase boundaries have been located with TJ-1 and TJ-20, respectively.

The exchange partition coefficient between ilmenite and melt $[(Fe/Mg)_{ilm}/(Fe/Mg)_{melt}]$ is shown as a function of pressure in Fig. 6. Only near-liquidus ilmenites have been considered in order to avoid compositional effect and ilmenites of the NNO experiments are not plotted on the diagram (see above). These experimental data suggest a positive pressure dependence of the exchange partition coefficient as observed for olivine (Ulmer 1989).

Experimental data show that the position of phase boundaries is shifted with pressure (Fig. 7). The 1 atm boundaries shown on Fig. 7 have been calculated with the algorithms of Longhi (1991) which account for the

change of phase boundaries with Mg # and alkali content of the liquid. With increasing pressure, the low-Ca pyroxene field is enlarged at the expense of the plagioclase and olivine fields. The extent of the shift is similar to that found by Fram and Longhi (1992) on a high-Al basalt.

Fractionation paths

The compositions of experimental liquids at 1 atm and high pressure are shown in Figs. 8 and 9, respectively. At 1 atm, SiO_2 is chosen as the differentiation index since in the NNO experiments MgO is nearly constant for most of the crystallization interval due to the late appearance of silicate ferromagnesians. At NNO, the liquidus crystallization of ilmenite and magnetite produces a drastic increase in SiO_2 from 50% to 60% as well as a rapid decrease in FeO and TiO_2 . Oxides Na_2O and Al_2O_3 are progressively depleted due to their incorporation in pla-

gioclase which is always a liquidus mineral whereas K_2O and P_2O_5 are enriched in successive liquids. At FMQ-1, TiO_2 decreases as soon as ilmenite crystallizes, MgO decreases more rapidly than at NNO as olivine is a near liquidus phase and the drop in Na_2O and Al_2O_3 is more important due to the higher proportion of plagioclase.

MgO is used as the differentiation index at high pressure because SiO_2 varies only slightly. In most diagrams (Al_2O_3 - P_2O_5 -FeO- TiO_2 - SiO_2), the 5 kbar and 7 kbar trends strongly differ from those at 10 and 13 kbar because plagioclase is the sole or the most important phase in the high temperature part of the 5 and 7 kbar trends. Plagioclase crystallization induces a slight increase in MgO at 5 and 7 kbar correlated with a rapid increase in FeO, TiO_2 and P_2O_5 , as these components are incompatible in plagioclase, and a decrease in Al_2O_3 and SiO_2 which are incorporated in this mineral. The TiO_2 drops when ilmenite crystallizes. Here too, K_2O and P_2O_5 are progressively enriched in the liquids and

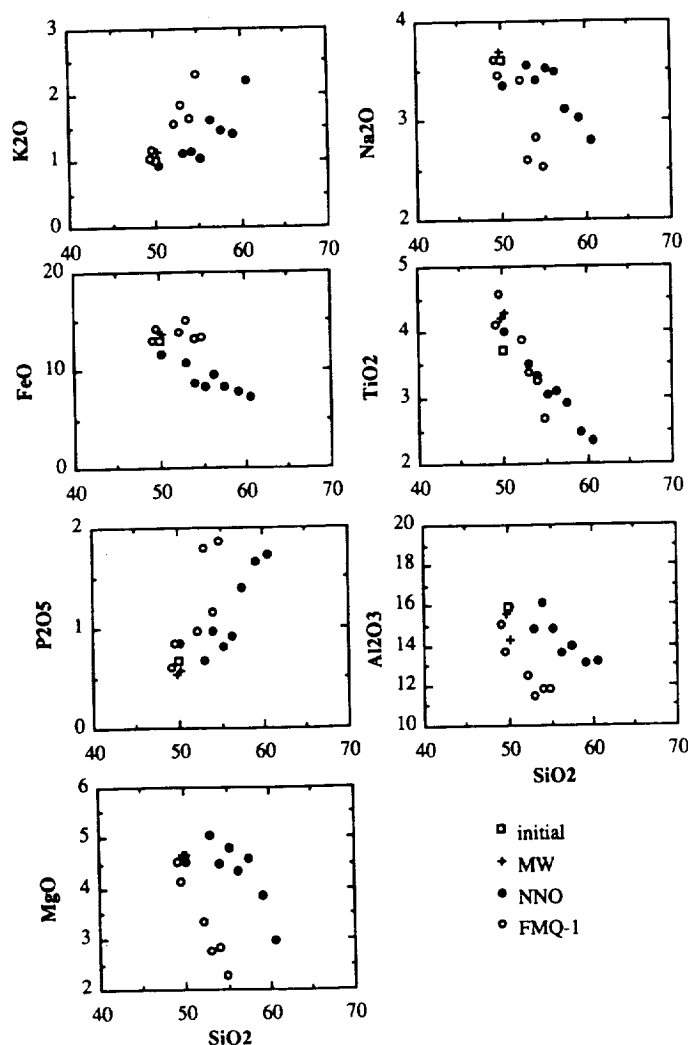


Fig. 8 Fractionation trends in the 1 atm experiments with SiO_2 as a differentiation index

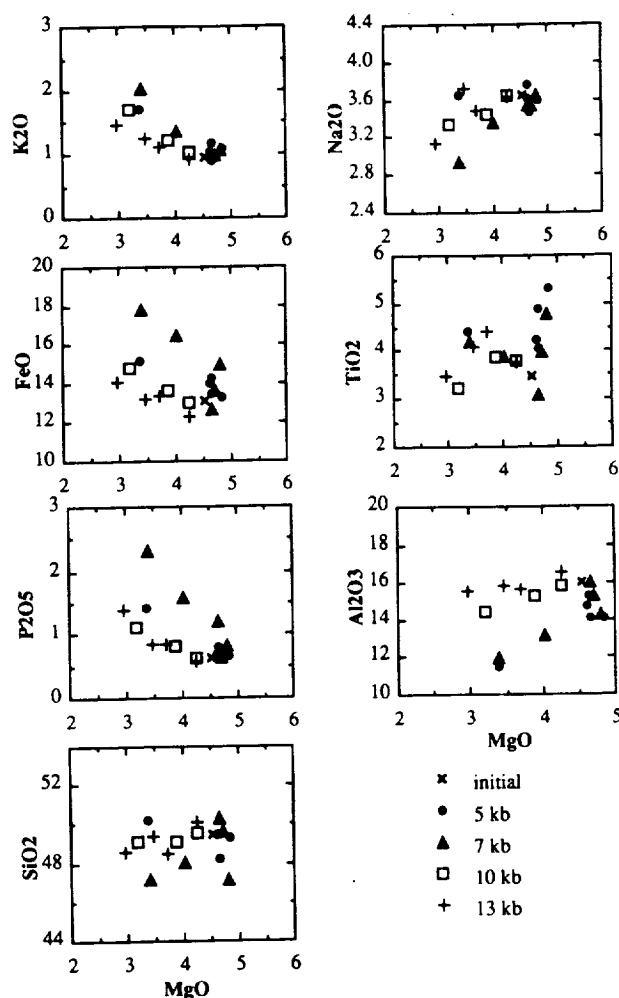


Fig. 9 Fractionation trends in the high pressure experiments with MgO as a differentiation index

the slope of the K_2O trend decreases with pressure as the crystallized pyroxene plagioclase ratio increases. Both FeO and P_2O_5 trends show a reversal with increasing pressure. Their incompatible character increases from 5 to 7 kbar and then decreases from 7 to 10 and 13 kbar. As already pointed out above, the first ferromagnesian mineral to appear is olivine at 5 kbar and low-Ca pyroxene at 7, 10 and 13 kbar. As olivine has a much higher FeO content ($\approx 30\%$, see Table 3) than low-Ca pyroxene ($\approx 19\%$), early crystallization of similar proportions of olivine instead of low-Ca pyroxene will induce a slower increase in FeO . Moreover, FeO is less incompatible at 10 and 13 kbar than at 7 kbar due to the increasing proportion of low-Ca pyroxene with pressure in the crystallizing assemblage. Considering the available data on the partitioning of phosphorous between mineral and liquid (Anderson and Greenland 1969), this element is increasingly incompatible in ilmenite, olivine, pyroxenes and finally plagioclase. This is supported by the measured content of P_2O_5 in minerals occurring in TJ-52 (olivine, 0.13%; pigeonite, 0.03% and plagioclase, 0.01%). Accordingly, the slower increase in P_2O_5 observed at 5 kbar compared to that at 7 kbar is probably due to the early crystallization of olivine at low pressure whereas the increasing proportion of low-Ca pyroxene in the crystallizing assemblage from 7 to 13 kbar decreases the incompatibility of phosphorous.

Discussion

Suitability of TJ as a parental magma of the intrusion

The crystallization sequence observed in the 5 kbar experiments (plag \rightarrow plag + ol \rightarrow plag + ol + ilm) is close to that inferred for the primitive BSKS cumulates of MCUs III and IV (Jensen et al. 1993; Nielsen and Wilson 1991). However, the effect of the relatively lower oxidation state superimposed by the graphite capsules in the high pressure experiments is to reduce the amount of ferric iron and increase the fayalitic component of the starting material. As a result, the Mg # of olivine (Fe_{67} max) and pyroxene (En_{67} max) is somewhat lower than it should be and the stabilities of olivine relative to low-Ca pyroxene and pigeonite relative to orthopyroxene are enhanced. Moreover, this low f_{O_2} prevents early crystallization of ilmenite and magnetite (see below). Consequently, comparison of experimental and natural plagioclase is a more reliable test of Tjörn as a parent magma and the limit of olivine stability at high pressure in the experiments is an upper limit for pressure of crystallization of the intrusion. The least evolved cumulates in the intrusion contain olivine (Fe_{77}) and plagioclase (An_{52}) together with ilmenite and magnetite. The plagioclase composition at the liquidus is An_{48} at 5 and 7 kbar, so TJ is slightly more evolved than the BSKS parent in terms of plagioclase component.

In order to compensate for the difference between the ambient f_{O_2} in the graphite capsules and the probable f_{O_2} of the intrusion (FMQ, see below), the Fe^{3+}/Fe^{2+} ratio of the liquid at the temperature of olivine precipitation at 5 kbar (1130°C) has been calculated following Kress and Carmichael (1991). As Toplis et al. (in press) have shown that P_2O_5 decreases the Fe_2O_3/FeO ratio in a ferrobasic melt, their proposed minimum $d_{P_2O_5}$ factor of -6 has been incorporated in the Kress and Carmichael (1991) model. Then, taking into account the pressure (Ulmer 1989) and compositional dependence (Longhi et al. 1978) of the olivine K_d , the olivine composition in equilibrium with Tjörn has been calculated to be Fe_{71} . Given the large uncertainties associated with the application of the Kress and Carmichael model (estimate of the error propagation suggests that $\ln(X_{Fe_2O_3}/X_{FeO})$ is known within ± 0.35 ln units), this value of Fe_{71} is in agreement with that obtained by Duchesne and Hertogen (1988) (Fe_{73}) who used the Ford et al. (1983) equations (1165°C at 6 kbar) in their calculations and the measured Fe^{3+}/Fe^{2+} ratio of the rock. Thus TJ is somewhat more evolved than the BSKS parent in terms of Mg # [$Mg/(Mg + Fe^{2+})$] as well. The occurrence of pigeonite at 5 kbar (TJ-47, see Table 3) instead of orthopyroxene corroborates this conclusion as the Mg # is the primary factor controlling opx versus pigeonite. Therefore, a jotunitic liquid similar in composition to TJ, but slightly more magnesian and with a more anorthitic plagioclase component, is the likely parent magma of MCUs III and IV of the BSKS intrusion. Perhaps a small amount of wall rock assimilation or transient fractionation en route to the site of emplacement is responsible for the difference.

Based on REE and Sr isotopic compositions, Demaiffe and Hertogen (1981) suggested that the chilled margin observed around the perimeter of the Hydra body is the parent magma of this intrusion. As TJ is compositionally very close to the Hydra margin (Duchesne et al. 1989) (see Table 1), these results show that an important volume of jotunitic magma has been emplaced in Rogaland at the same time or shortly after the emplacement of massif-type anorthosites and yielded the BSKS and Hydra intrusions as well as the jotunitic complex (Fig 1).

Pressure of emplacement of the intrusion and of M2 stage

Given that graphite capsules may have enhanced olivine stability (see above), 5 kbar is a probable maximum for the emplacement of the BSKS intrusion. Comparison of Al_2O_3 contents in experimental and natural opx also suggests a pressure less than or equal to 5 kbar, as discussed above.

The pressure of emplacement of the intrusion has strongly been debated among authors. Jansen et al. (1985) found a pressure of 4 to 5 kbar using the garnet-orthopyroxene-plagioclase-sillimanite geobarometer in

the contact aureole of the intrusion (stage M2). Maijer et al. (1981) suggested that the osumilite occurrence in the northern part of the contact aureole of the intrusion points to a lower pressure of 3 to 4 kbar. Nevertheless, Wilmart and Duchesne (1987) pointed out that according to experimental data (Grew 1982; Hensen 1977; Olesch and Seifert 1981), osumilite is stable up to higher pressures (8–10 kbar) when $P_{\text{H}_2\text{O}}$ is low and suggested a higher pressure of 6 to 7.5 kbar for the emplacement of the Rogaland intrusions (stage M2). Moreover, according to Wilmart et al. (1991) CO_2 -rich fluid inclusions observed in the mangerites of the upper part of the intrusion also point to a pressure of 7.4 ± 1 kbar.

The estimation of Wilmart and Duchesne (1987) is based on the stability of the assemblage olivine ($\text{Fe}_{94}\text{Fo}_6$) + quartz in the upper part of the BSKS intrusion and of Fe-rich opx ($\text{Fs}_{83}\text{En}_{15}\text{Wo}_2$). With these assemblages, they obtained upper (7 kbar) and lower (5.7 kbar) limits for the pressure of emplacement of this intrusion using the Bohlen and Boettcher (1981) geobarometer, which is based on the equilibrium $\text{opx} = \text{olivine} + \text{quartz}$ determined in the FeO-MgO-CaO-SiO_2 system. Increasing Fe content of opx will move this equilibrium towards higher pressure. In their application of this geobarometer, Wilmart and Duchesne (1987) didn't take into account other components such as Na, Al, Mn, Ca and Ti (Duchesne, personal communication) which have a strong influence on the pressure conditions of the $\text{opx} = \text{olivine} + \text{quartz}$ equilibrium (Bohlen et al. 1980). The Ca, Na, Al and Ti are strongly partitioned into opx and extend the stability field of this mineral. According to Bohlen et al. (1980), the magnitude of this extension can unfortunately not be determined with accuracy as pertinent activity data are lacking. Using their proposed two-site ionic model $\{a_{\text{Fe}_2\text{Si}_2\text{O}_6} = [1 - (\text{Na} + \text{K} + \text{Mn} + \text{Ca} + 1/2\text{Mg})] [1 - (\text{Ti} + \text{AlVI} + \text{Cr} + \text{Zn} + 1/2\text{Mg})]\}$ to estimate the effect of these ions when calculating the a_{Fs} in the opx gives an $a_{\text{Fs}} = 0.60$ for $\text{Fs}_{83}\text{En}_{15}\text{Wo}_2$ as opposed to $a_{\text{Fs}} = 0.83$ employed by Wilmart and Duchesne (1987). The lower revised a_{Fs} decreases the lower limit of pressure a few kbar.

The CO_2 -rich inclusions observed in quartz of the upper part of BSKS have been subdivided into three types by Wilmart et al. (1991): scarce Ia inclusions of pure CO_2 ; abundant Ib composed of CO_2 and containing graphite; and late Ic with no graphite. In the P - T plane, the representative isochore of the Ia inclusions lies well above the regional P - T path and may correspond to a density increase as suggested by the authors (volume decrease after their formation). On the other hand, the isochores of the Ib inclusions intersect the P - T path for pressures lower than 6 kbar. At 800°C , the temperature estimated for the upper part of the intrusion by Wilmart et al. (1991) using the Lindsley and Andersen (1983) two-pyroxene model and by Duchesne (1972a) using Fe-Ti oxides, the Ib isochores give a pressure range of 4 to 6 kbar which is in very good agreement with the pressure estimated from phase equilibria of the

TJ composition and by Jansen et al. (1985). We consider then that this pressure is relevant for the emplacement of the Rogaland intrusions and for the contact metamorphism (M2 stage of Maijer et al. 1981) and A stage of Wilmart and Duchesne (1987).

f_{O_2} during differentiation of the intrusion

Due to important subsolidus reequilibration of ilmenite and magnetite compositions (Duchesne 1972a), the T - f_{O_2} path could not be estimated for the early cumulates. Nevertheless, using the compositions of isolated grains, Duchesne (1972a) has estimated the f_{O_2} for two particular levels of the intrusion. With the calibration of Buddington and Lindsley (1964), he suggested an f_{O_2} slightly above NNO for the upper part of MCU IV using magnetite and ilmenite whose compositions were reintegrated optically and an f_{O_2} of FMQ-1 for the quartz mangerites belonging to the upper part of the intrusion based on magnetite compositions. This last estimate has subsequently been confirmed by Wilmart and Duchesne (1987) and is in agreement with the occurrence of fayalitic olivine (Fo_6 ; Duchesne 1972b) in equilibrium with quartz and magnetite in these rocks. Nitsan (1974) has calculated the position of the fayalite-quartz-magnetite assemblage as a function of f_{O_2} , T and the fayalite content of olivine. At $T = 800^\circ\text{C}$ (Duchesne 1972a, Wilmart and Duchesne 1987), Fo_6 gives $\log f_{\text{O}_2} = -16$ which is close to FMQ.

Comparison between experimentally determined phase equilibria at different f_{O_2} with the order of cumulus arrival in the intrusion allows an independent estimate of the f_{O_2} during the early fractionation. Nevertheless, this technique relies on the identification of the cumulus or postcumulus status of oxides and sometimes this distinction cannot be made unequivocally (McBirney 1989). Jensen et al. (1993) have suggested that both ilmenite and magnetite are cumulus phases in MCUs IIIb and IVb (Fig. 2). According to these authors, the two oxides occur as large grains (≈ 1 mm) of similar sizes and are quite abundant in the leucotroctolites (modal proportions from Jensen et al. (1993): ilmenite, 5%; magnetite, 1%). It is worth noting that the abundance of ilmenite in MCU IVb is higher than that observed in the near liquidus experiment at FMQ-1 (TJ-45, see Table 2). Moreover, the high-Al content of magnetite (spinel exsolutions: Duchesne 1972a; Jensen, et al. 1993) as well as the high Cr content of both oxides also gives support to the hypothesis that these oxides are early cumulus phases. A peculiar feature of MCUs III and IV is that magnetite disappears in units c and reappears in units d (Fig. 2) whereas the proportion of ilmenite steadily increases from bottom to top of these MCUs (Duchesne 1972a). Moreover, the proportion of magnetite is always lower than that of ilmenite in the cumulates. At 1 atm and NNO, both oxides are near the liquidus together with plagioclase. Nevertheless, the proportion of magnetite is much higher than that of

Table 4 Calculated densities of liquids in experimental charges

Experiment	T (°C)	d (g/cm ³) ^a	d (g/cm ³) ^b	d (g/cm ³) (3)
1 atm NNO				
TJ-37	1190	—	2.59	—
TJ-36	1175	—	2.66	—
TJ-31	1160	—	2.58	—
TJ-26	1155	—	2.63	—
TJ-38	1133	—	2.57	—
TJ-29	1118	—	2.59	—
TJ-32	1105	—	2.55	—
TJ-34	1085	—	2.52	—
1 atm FMQ-1				
TJ-48	1150	—	2.69	—
TJ-45	1124	—	2.70	—
TJ-46	1090	—	2.67	—
TJ-52	1080	—	2.65	—
TJ-53	1070	—	2.68	—
TJ-55	1065	—	2.63	—
5 kb				
TJ-17	1170	2.78	2.77	2.76
TJ-43	1150	2.79	2.79	2.78
TJ-40	1135	2.80	2.79	2.78
TJ-23	1130	2.81	2.81	2.80
TJ-51	1110	2.80	2.80	2.79
TJ-47	1100	2.80	2.80	2.78
7 kb				
TJ-1	1170	2.80	2.80	2.79
TJ-41	1155	2.83	2.83	2.82
TJ-9	1145	2.87	2.87	2.86
TJ-3	1120	2.87	2.87	2.85
TJ-4	1095	2.90	2.89	2.86
10 kb				
TJ-5	1190	2.84	2.84	2.83
TJ-18	1165	2.85	2.85	2.84
TJ-20	1160	2.87	2.86	2.85
TJ-7	1130	2.88	2.88	2.86
TJ-8	1100	2.89	2.88	2.86
13 kb				
TJ-24	1190	2.91	2.91	2.90
TJ-12	1185	2.91	2.90	2.89
TJ-11	1162	2.94	2.93	2.92
TJ-10	1160	2.92	2.92	2.90
TJ-13	1130	2.93	2.93	2.91
16 kb				
TJ-35	1215	2.96	2.96	2.95
TJ-14	1200	2.94	2.94	2.93
18 kb				
TJ-44	1225	2.97	2.97	2.96

^a Fe₂O₃ and H₂O not taken into account in density calculations^b % Fe₂O₃ in the liquids calculated following Kress and Carmichael (1991) and using the d_{FeO} proposed by Toplis et al. (in press)^c Fe₂O₃ and H₂O taken into account, see text for explanation

nificant except at 13 and 16 kbar when H₂O is taken into account.

At 1 atm and FMQ-1, density first increases as plagioclase is the sole liquidus phase and a subsequent den-

sity drop occurs when ilmenite and olivine join the assemblage. A similar T - ρ path is observed at 5 kbar. At 7 and 10 kbar, there is an overall density increase which is more rapid at high temperature as plagioclase dominates in the liquidus assemblages (see Table 2).

As already discussed above the H₂O content of the superliquidus glasses is less than 0.15%. Nevertheless, due to the low molecular weight of H₂O, small weight percents correspond to significant mole fractions of H₂O (Lange and Carmichael 1990). Consequently, we have calculated the density of the liquids taking into account an initial value of 0.15% and the build up of H₂O as anhydrous phases precipitate (Fig. 10 and Table 4). Density increases are reduced or even absent (at low temperature at 10 kbar) and the density drop observed at 5 kbar is magnified.

At NNO the density curve displays some oscillations with an overall decrease due to the early crystallization of magnetite as well as ilmenite and to the higher proportion of oxides than plagioclase. The small oscillations are correlated with the FeO content and are likely to be due to variable proportions of ilmenite and magnetite. At high temperature magnetite and ilmenite are the sole ferromagnesians at the liquidus and variation in their proportions strongly influence the FeO content and ρ . At lower temperature, opx, augite and pigeonite are also present and lessen the above effect.

Crystallization of both ilmenite and magnetite together with plagioclase in the early cumulates followed by the plag + opx + ilm assemblage is likely to have produced a decrease in liquid density as suggested by Nielsen and Wilson (1991), based on fractionation-density considerations (Sparks and Huppert 1984). Moreover new influxes of jotunitic magma were both hotter and denser than the resident magma.

The calculated density of TJ has to be compared to that of plagioclase in order to estimate the buoyancy of this mineral which is the dominant phase in the primitive cumulates. In 1988, using the expression of Bottinga and Weill (1970), Duchesne and Hertogen obtained a density of 2.65 and 2.62 for an H₂O content of 0 and 0.5% respectively at $T = 1160^\circ\text{C}$. In this estimation, they did not take into account compressibility factors and P₂O₅ as data on its partial molar volume were lacking (Duchesne, personal communication). They also used the measured content of Fe₂O₃ (5.00% Fe₂O₃ and 8.37% FeO) in the rock which was probably increased by subsolidus oxidation. The Fe₂O₃ content has now been recalculated for FMQ at 5 kbar and 1150°C using the regression of Kress and Carmichael (1991). With the expression of Lange and Carmichael (1990) and including the recent data on P₂O₅ (Toplis et al. in press), d equals 2.77 (0% H₂O) and 2.74 (0.5% H₂O). Considering the density of plagioclase crystallizing in the early cumulates [$T = 1150^\circ\text{C}$ -An₅₀, 2.625; $T = 1130^\circ\text{C}$ -An₄₅, 2.615; (Campbell et al. 1978)], it is unlikely that plagioclase could have settled in the BKSK magma chamber. This in turn points to an *in situ* crystallization process. Similar conclusions were already obtained by Bottinga

ilmenite and low-Ca pyroxene is the first ferromagnesian to appear instead of olivine due to the increased a_{SiO_2} induced by the early precipitation of oxides. These two features indicate that f_{O_2} was probably lower than NNO during the early stage of fractionation. At FMQ-1, a few grains of ilmenite occur together with olivine (TJ-45) but magnetite is lacking. Consequently, the early f_{O_2} was probably intermediate between NNO and FMQ-1 and close to FMQ. The disappearance of magnetite in units c of MCUs III and IV which is correlated with the replacement of olivine by low-Ca pyroxene, suggests a subsequent decrease in f_{O_2} (Snyder et al. 1993). The early crystallization of both oxides in units b results in an increase in a_{SiO_2} which drives the liquid into the stability field of low-Ca pyroxene. As for the same $\text{Fe} \# [\text{Fe}^{2+}/(\text{Fe}^{2+} + \text{Mg})]$, olivine contains twice as much Fe^{2+} as low-Ca pyroxene, crystallization of the latter decreases the $\text{Fe}_2\text{O}_3/\text{FeO}$ of the liquid thereby decreasing the f_{O_2} . Subsequently, crystallization of both ilmenite and pyroxene will increase the redox ratio of the liquid until the stability field of magnetite is encountered again (Morse 1980; Snyder et al. 1993). Duchesne (1972a) proposed an f_{O_2} of NNO for the upper part of MCU IV. Nevertheless, according to our experimental data, this f_{O_2} estimate is probably too high as the proportion of magnetite is always much higher than that of ilmenite at NNO (see Table 2) and this is contrary to what is observed in the cumulates. Consequently experimentally determined phase equilibria indicate that f_{O_2} was first close to FMQ (units b), then decreased relative to this buffer (units c) and increased afterwards until magnetite reappearance. This f_{O_2} path cannot be correlated with the value of FMQ found for the quartz mangerites, as the origin of these rocks has not been established clearly (see above). Changes in f_{O_2} during fractionation have been reported in other layered intrusions and are different than those inferred for the BSKS magma chamber. Based on Fe-Ti oxide analyses and the solution model of Lindsley (1977), Morse (1980) suggested that in Kiglapait, f_{O_2} was close to MW in the lower zone, increased to an intermediate value between MW and FMQ at the cumulus arrival of ilmenite and titanomagnetite and subsequently remained at this value in the upper zone. Using experimentally determined oxide phase equilibria, Snyder et al. (1993) have shown that in the Newark Island layered intrusion the f_{O_2} increased relative to FMQ before titanomagnetite precipitation and decreased afterwards. According to these authors, a similar trend is also relevant for the Skaergaard and Somerset Dam intrusions and might be typical of tholeiitic magma differentiation.

Density changes during fractionation

Liquid densities have been calculated following the expression of Bottinga and Weill (1970) and using the partial molar volumes, thermal expansions and compressibilities of oxide components proposed by Lange and

Carmichael (1990). As shown by Toplis et al. (in press), addition of P_2O_5 to a ferrobasaltic melt reduces the density. The P_2O_5 content of the liquids present in the experiments ranges from 0.53% to 2.32% and the partial molar volume of P_2O_5 derived by these last authors on a ferrobasaltic composition at 1200°C has been used in our calculations. Results are shown in Fig. 10 and Table 4.

In the 1 atm experiments, the Fe_2O_3 content is not negligible and has been calculated using the regression of Kress and Carmichael (1991) and the $d_{\text{P}_2\text{O}_5}$ of Toplis et al. (in press). The same technique has been applied to the high pressure experiments in which f_{O_2} was estimated with the composition of ilmenite. As shown on Fig. 10, taking into account this component in the high pressure experiments does not change significantly the density given the large uncertainties associated with the model of Kress and Carmichael.

Density calculations have an accuracy of about 0.5% (Sparks and Huppert 1984). When H_2O is taken into account (see below), accuracy is however less good ($\pm 1.0\%$) due to the considerable uncertainty that still surrounds the value of the partial molar volume of H_2O (Lange and Carmichael 1990). The range of densities observed in our experiments is 4.9% at NNO, 2.6% at FMQ-1, 1.4% at 5 kbar, 3.5% at 7 kbar, 1.4% at 10 kbar, 1.0% at 13 kbar and 16 kbar (Table 4). The observed decrease and increase in density are thus sig-

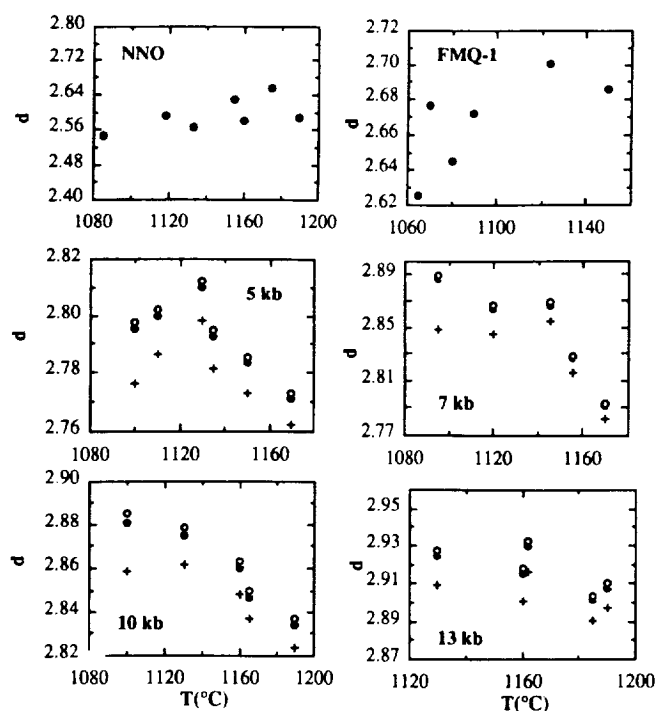


Fig. 10 Density changes (g/cm^3) along fractionation trends in the one atmosphere and high pressure experiments. Liquid densities were calculated following Lange and Carmichael (1990) and with $d_{\text{P}_2\text{O}_5}$ from Toplis et al. (in press): (open circles without Fe_2O_3 and H_2O , filled circles with Fe_2O_3 and without H_2O , crosses with Fe_2O_3 and H_2O ; see text for explanation)

A Liquid Line of Descent of the Jotunite (Hypersthene Monzodiorite) Suite

JACQUELINE VANDER AUWERA^{1*}, JOHN LONGHI² AND JEAN-CLAIR DUCHESNE¹

¹L.A. GÉOLOGIE, PÉTROLOGIE ET GÉOCHIMIE, UNIVERSITÉ DE LIÈGE, B-4000 LIÈGE, BELGIUM

²LAMONT DOHERTY EARTH OBSERVATORY, PALISADES, NY 10961, USA

RECEIVED JANUARY 10, 1997; REVISED TYPESCRIPT ACCEPTED SEPTEMBER 30, 1997

Proterozoic massif anorthosites are usually associated with variable amounts of a characteristic suite of rocks ranging from a melanocratic facies highly enriched in Fe, Ti and P (FTP rocks) to mafic and granitic rocks (the jotunite charnockite suite). Here experimental and geochemical data on fine-grained (chilled) samples from several intrusions of the Rogaland Province are used to decipher their petrogenesis. Modeling of these data supports the hypothesis that extensive fractionation of primitive jotunites can produce quartz mangerites with REE concentrations in the range of jotunites, strong depletions in U, Th, Sr and Ti, and smaller to no relative depletions in Hf and Zr. Experimental and petrographic data indicate that the FTP rocks represent accumulations of a dense oxide apatite pigeonite assemblage from coexisting multisaturated jotunitic to mangeritic liquids. The Rogaland jotunitic charnockitic trend corresponds to a multi-stage process of polybaric fractional crystallization and crystal accumulation. The early stage, in which a primitive jotunitic magma fractionates to produce an evolved jotunite, probably took place several kilometers below the intrusion level of dikes, either in mafic chambers similar to that of the Bjerkreim-Sokndal layered intrusion or in masses of crystallizing andesine anorthosite. The later stage of fractionation, which may have involved flow differentiation, took place within the dikes themselves and produced compositions ranging from evolved jotunite to mangerite to quartz mangerite and charnockite.

INTRODUCTION

Proterozoic massif anorthosites are usually associated with variable amounts of a characteristic suite of mafic to granitic rocks. The least evolved rocks of this suite are enriched in mafic minerals (low- and high-Ca pyroxenes, Fe–Ti oxides, apatite), and in some cases very high concentrations of these phases give rise to melanocratic rocks. Various names including ferrodiorite, monzonorite, jotunite, Fe–Ti–P-rich rocks (FTP) and oxide-apatite gabbonorite have been used; however, in this study, we will refer to them by the collective term of jotunite (hypersthene monzodiorite). Evolved rocks of the suite include mangerites (hypersthene monzonite), quartz mangerites and charnockites (hypersthene granite). We will refer to the suite as a whole as the jotunite suite.

The origin of jotunites remains the subject of considerable debate, despite their similar textural and geochemical characteristics from one anorthosite complex to another. Several hypotheses, not mutually exclusive, have been proposed: (1) jotunites are residual liquids after anorthosite crystallization (Ashwal, 1982; Morse, 1982; Wiebe, 1990; Emslie *et al.*, 1994); (2) they are the parental magmas of the andesine anorthosite suite (Duchesne *et al.*, 1974; Duchesne & Demaiffe, 1978; Demaiffe & Hertogen, 1981); (3) they are products of partial melting of the lower crust (Duchesne *et al.*, 1985, 1989; Duchesne, 1990); (4) they are transitional rocks in a comagmatic sequence from anorthosite to mangerite (Wilmart *et al.*, 1989; Owens *et al.*, 1993; Duchesne & Wilmart, 1997); (5) they are derived by fractionation of mafic magmas unrelated to the anorthositic suite (Emslie, 1985); (6) they are immiscible liquids conjugate to

KEY WORDS: anorthosite; experimental petrology; geochemistry; monzodiorite; Rogaland anorthosite complex

*Corresponding author. Telephone: +32 4 3662253. Fax: +32 4 3662921. e-mail: jvdauwera@ulg.ac.be

mangerites (Philpotts, 1981). In this paper, we present new experimental data on two jotunite samples from the same dike (the Varberg dike) in the Rogaland anorthositic complex as well as new geochemical data (major and trace elements) on fine-grained (chilled) jotunitic rocks from other intrusions in the Rogaland Province. We then use these data as well as published experimental and geochemical data from the literature to: (1) define a liquid line of descent extending from jotunite up to quartz mangerite (or acidic rocks); (2) discuss the possible origins of rocks showing extreme concentrations of FeO, TiO₂ and P₂O₅; and (3) develop models of major and trace element [REE (rare earth elements), Sr, U, Th, Zr, Hf, Ta, Rb, Co, Ni, Cr, Sc] fractionation within the suite.

GEOLOGICAL SETTING AND PETROGRAPHY

The Rogaland intrusive complex of southern Norway (Fig. 1) (Michot, 1960; Michot & Michot, 1969) is one of the group of Proterozoic anorthositic provinces that have been recognized world-wide (Ashwal, 1993). Massif-type anorthosites (Egersund Ognå; Håland Hellen; Åna Sira), leuconoritic bodies (Hidra, Garsaknatt) and a large layered intrusion (Bjerkreim Sokndal: BKSK) occupy most of the surface exposure. Jotunitic rocks mainly occur in a system of dikes and small intrusions (Duchesne *et al.*, 1985, 1989). There are also several Fe–Ti ore bodies within the complex (Krause & Pedall, 1980; Duchesne, 1998). New U–Pb ages obtained from zircon and baddeleyite (Schärer *et al.*, 1996) suggest that emplacement of this complex occurred within <10 my (between 930 and 920 Ma).

The Rogaland jotunitic suite was first described by Michot (1960) and then extensively studied by Duchesne, Demaiffe and coworkers in several papers reviewed by Duchesne (1990). The characteristics of jotunites will only be briefly summarized here. Jotunites are typically medium grained (from 0.1 mm to a few millimeters in size) and contain plagioclase (usually antiperthitic), some perthitic K-feldspar, poikilitic inverted pigeonite, augite, Fe–Ti oxides, and apatite; these minerals plus mesoperthitic K-feldspar and quartz are characteristic of the evolved facies (Duchesne, 1990). Jotunitic rocks occur mostly as dikes crosscutting massif-type anorthosites but those that have been dated have similar absolute ages in the range of 920–930 Ma (Schärer *et al.*, 1996). Among them, the Tellnes dike in the Åna Sira massif as well as the Varberg and Lomland dikes in the Egersund Ognå massif (Fig. 1) have been studied in the most detail (Duchesne *et al.*, 1985; Wilmar *et al.*, 1989). The Tellnes dike, to which we will frequently refer in this study, varies continuously from jotunitic to charnockitic lithologies. It has a well-defined Rb–Sr whole-rock isochron and its

compositional variation can be explained by a process of fractional crystallization without progressive contamination (Wilmar *et al.*, 1989). However, whole-rock Rb–Sr isotopic data from other dikes such as Lomland do not fit tightly to isochrons and there is considerable variation in I_s from dike to dike (0.704–0.710) that does not correlate with other geochemical parameters (Demaiffe *et al.*, 1986; Duchesne *et al.*, 1989), which taken together suggest variable contamination of multiple sources. Jotunites also form small intrusions (e.g. Eia–Rekefjord; Fig. 1) as well as chilled margins to the Hidra and Garsaknatt leuconoritic bodies (Demaiffe & Hertogen, 1981) and, locally, to the Bjerkreim Sokndal layered intrusion (Duchesne & Hertogen, 1988; Wilson *et al.*, 1996). Experiments on a sample from one of these chilled margins, the Tjörn facies [sample 80123a of Duchesne & Hertogen (1988)], have shown the near-liquidus assemblages to be plagioclase (An₁₀) + olivine (Fo₁₀) at 5 kbar and plagioclase (An₁₇) + low-Ca pyroxene (En₆₈) at 7 kbar (Vander Auwera & Longhi, 1994). The compositions of most of the Rogaland jotunitic suite form coherent trends in variation diagrams (Fig. 2), but the least differentiated compositions (high MgO, low K₂O) are chilled margin samples and form a group distinct from the rest of the dike system. In the following, we will refer to the distinctive group of chilled margin samples as primitive jotunites and to the least differentiated samples of the dike trend as evolved jotunites. In this latter group, most samples are chilled margins to the dikes (75202F, 8926, 89115, 7355).

In this study, we took special care to select samples from different occurrences which probably represent liquid compositions [very fine-grained texture (<250 µm), non-porphyrific facies, elongated apatite and oxide grains randomly dispersed in the other minerals, etc.] and their exact locations are given in Table 1. Three of these samples (80123a, 91141 and 7234; Table 1) from the chilled margin of BKSK and Hidra are primitive jotunites. The remainder of the samples are from the dikes and have compositions ranging from evolved jotunite to quartz mangerite. Although the Varberg dike (Fig. 1) displays the typical mineralogy of jotunites (see above), it contains a chilled margin (Table 1; sample 75202F), which has been observed at several places along its contact, as well as a locally developed, Fe–Ti–P-rich melanocratic facies (sample 75372: TiO₂ 6.23%; FeO₂ 27.43%; P₂O₅ 4.20%) in the interior, where mafic minerals (inverted pigeonite, augite, ilmenite, magnetite, apatite) make up ~75% of the rock, and plagioclase and perthitic K-feldspar make up the remaining 25%. Mineral phases from samples taken along strike of the dike have been analyzed with the electron microprobe to test for geographical variations in mineral compositions.

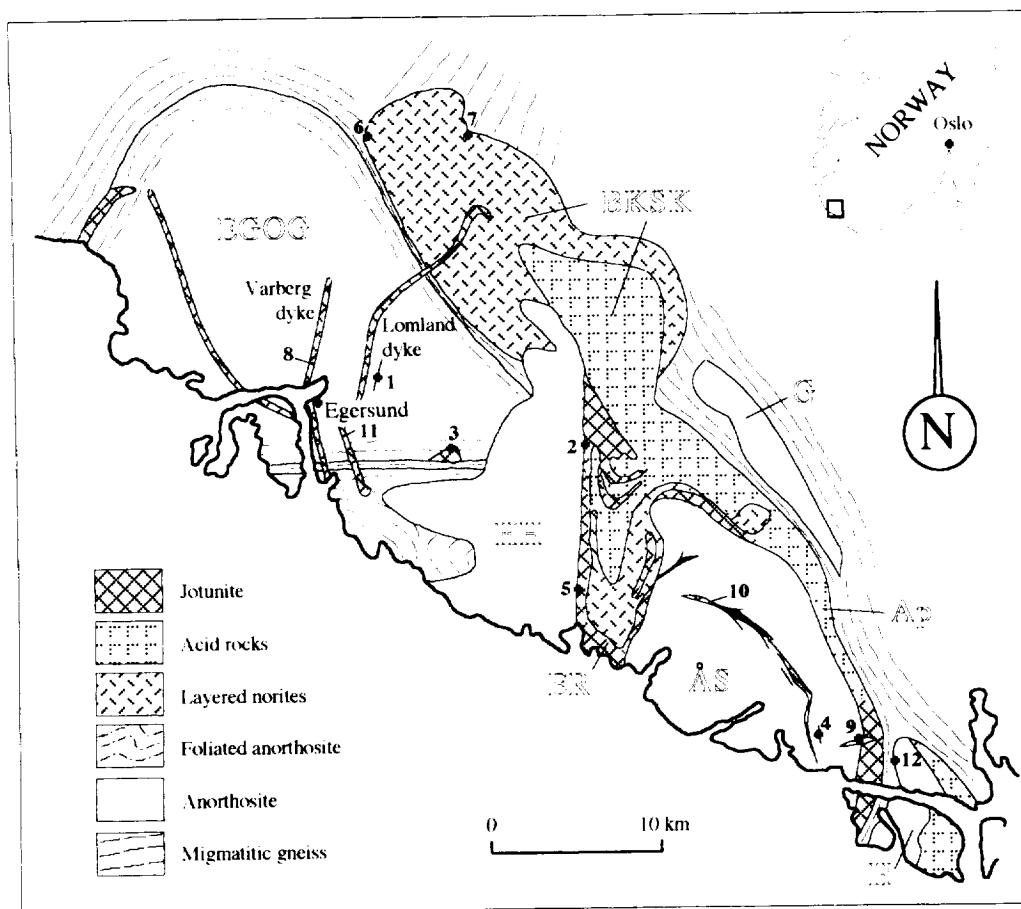


Fig. 1. Schematic geological map of the Rogaland anorthositic complex [after Michot & Michot (1969) and Bolle (1996)]. EGOG, Egersund–Ogna; HH, Haland–Helleren; AS, Ana–Sira; H, Hidra; G, Garsaknatt; ER, Eia–Rekefjord; BKSX, Bjerkreim–Sokndal; Ap, Apophysis. Numbers refer to samples described in Table 1.

SAMPLE PREPARATION, EXPERIMENTAL AND ANALYTICAL METHODS

Experiments were carried out on two powdered rocks of the Varberg dike at Lamont–Doherty either in a standard 1/2 inch piston cylinder apparatus or in a Deltech vertical quenching furnace, following the methods described by Fram & Longhi (1992) and Vander Auwera & Longhi (1994). One sample was from the chill margin (sample 75202F; VB); the other was from the melanocratic facies (sample 75372; MEL). High-pressure experiments were run in graphite capsules at 5 kbar (runs VB-1 to VB-5, VB-13 and VB-14 on sample VB, and runs MEL-1 to MEL-3 on sample MEL), the likely pressure of emplacement of the Rogaland intrusive complex (Jansen *et al.*, 1985; Vander Auwera & Longhi, 1994). Dry run conditions are consistent with the relatively low $f(\text{H}_2\text{O})$

that is a general feature of massif anorthosites and related rocks (see, e.g. Morse, 1982). However, the graphite capsules imposed a relatively low oxygen fugacity in these experiments, probably between FMQ (fayalite–magnetite–quartz) 2 and FMQ 4 (Vander Auwera & Longhi, 1994), which inhibits magnetite stability. To approximate the $f(\text{O}_2)$ of the jotunites and to determine the effects of magnetite, which is a late-stage mineral in the primitive jotunites, on the liquid line of descent, we also performed a few 1 atm melting experiments in a controlled $\text{CO}–\text{CO}_2$ atmosphere. These were carried out at two different $f(\text{O}_2)$ values: NNO (nickel–nickel oxide; runs VB-16 and VB-17) and FMQ (run VB-6); $f(\text{O}_2)$ was measured with a Ca-doped ZrO_2 electrolyte cell. Good agreement was found between $f(\text{O}_2)$ determined directly and $f(\text{O}_2)$ calculated by applying the Andersen & Lindsley (1988) model to the compositions of coexisting ilmenite and spinel produced in the experiments. To minimize

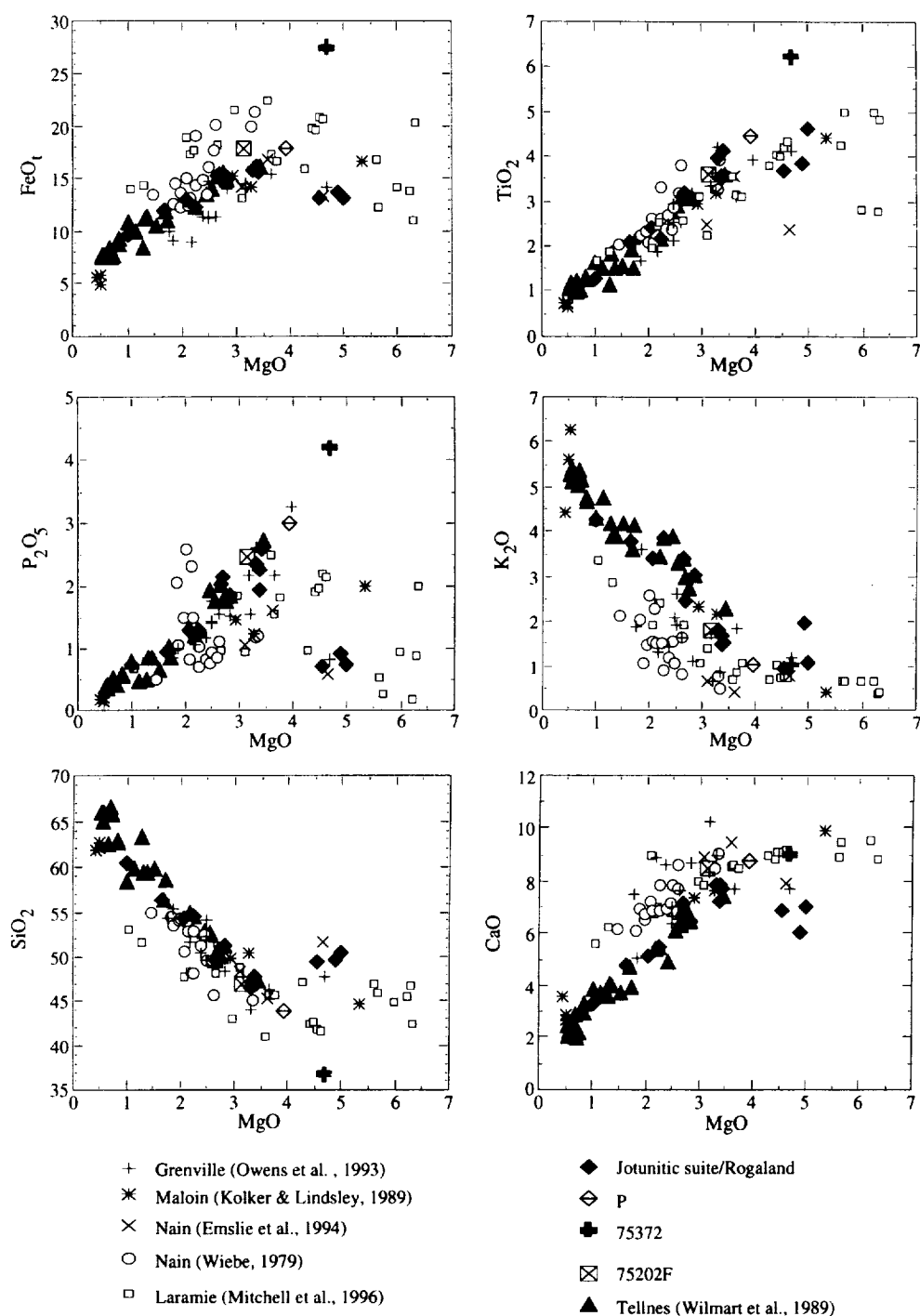


Fig. 2. Major element variation diagrams of the jotunitic suite. Data from fine-grained samples (chills), from the Tellnes dike (Wilmart, 1988; Wilmart *et al.*, 1989) and from other localities [Grenville Province, Quebec: Owens *et al.* (1993); Laramie: Kolker & Lindsley (1989); Mitchell *et al.* (1996); Nain: Wiebe (1979); Emslie *et al.* (1994)] are shown for comparison. P corresponds to the average of four samples from the Puntervoll facies (FTP rocks) of the Lomland dike (Duchesne *et al.*, 1985).

Table 1: Sample description, location and facies of jotunites

Sample	UTM grid: zone 32 VLK	Intrusion
89115/ch (1)*	305–859	Kjervall dike crosscutting the Egersund–Ogna anorthosite
78211/ch (2)	407–825	Eiavatn dike crosscutting the Eia–Rekefjord intrusion
8925, 8926/ch (3)	315–812	dike on top of the Koldal small intrusion: 8925 is from the central part of the dike, and 8926 from the contact
8951/ch (4)	534–615	satellite to the Tellnes dike crosscutting the Åna–Sira anorthosite
7355/ch (5)	399–727	Eia–Rekefjord intrusion
91141/ch (6), 80123a/ch (7)†	273–992; 354–983	fine-grained margin of the Bjerkreim–Sokndal intrusion
75182, 7519, 75202F/ch, 75202G, 75204, 75206, 75372, 78201, 7912(8)	249–883; 249–875; 244–825; 244–825; 244–825; 244–825; 244–838; 251–797; 243–841	Varberg dike crosscutting the Egersund–Ogna anorthosite
7838/ch, 8034/ch (9)	550–624; 554–627	Fidsel dike crosscutting the Apophysis
T2/ch, T221/ch, T82/ch, 7832, 7828, 7252 (10)‡	514–657; 455–701; 517–653; 523–627; 472–698; 477–697	Tellnes dike crosscutting the Åna–Sira anorthosite
66175, 7536, 7533, 7534 (11)	263–803; 267–815; 275–827; 273–829	Punternvold facies (melanorites) of the Lomland dike
7234/ch (12)§	589–602	fine-grained margin of the Hydra leuconoritic body

*Numbers in parentheses correspond to the localities shown in Fig. 1; /ch indicates that the sample corresponds to a chill.
†Duchesne & Hertogen (1988). ‡Wilmart (1988). §Duchesne *et al.* (1974).

iron loss in highly crystalline runs, powdered samples were pressed into disks of 6 mm diameter (bonded with polyvinyl alcohol) and loosely wrapped in Pt wire of 0.254 mm diameter. Run conditions and phase assemblages are given in Table 2.

Analytical method

After each experiment, the charges were mounted in epoxy, polished and analyzed at Lamont Doherty under the Camebax/Micro electron microprobe equipped with a wavelength dispersive system. Accelerating voltage was set at 15 kV and all elements were measured for 20 s at a beam current of 25 nA, except in the case of feldspars, phosphates, and glasses, where Na and K were measured first for 30 s at 5 nA. Rims of minerals were analyzed with a point beam and glasses with a defocused beam of 5 µm to minimize alkali loss. X-ray intensities were reduced using the Cameca PAP correction program. A combination of mineral and glass standards were used for glass analyses whereas only mineral standards were used for plagioclase, oxides, pyroxenes, and olivines.

Major element compositions of the experimental phases are reported in Table 3. Rims and cores of feldspars and pyroxenes occurring in the different facies of the Varberg dike have been analyzed with the Cameca SX50 of the CAMST ('Centre d'Analyse par Microsonde pour les Sciences de la Terre', Louvain-La-Neuve, Belgium; J. Wautier analyst). Standards included natural minerals and synthetic compounds. Accelerating voltage was set at 15 kV and beam current was 20 nA with 10 s counting times. X-ray intensities were reduced using the Cameca PAP correction program. Results are given in Table 4.

Mass balance between the bulk composition of the starting material and the compositions of all phases present in each run has been calculated using a least-squares multiple regression to determine phase proportions and to test if Fe and Na loss occurred in the 1 atm experiments. Results are given in Table 2. Na loss ranges from 4% up to 14% whereas Fe displays a small gain in VB-16 (6%) and a significant one in VB-17 (25%). The latter experiment did not equilibrate pervasively, as the temperature was near the solidus and the charge melted only locally. In run VB-14, the orthopyroxene (opx) coefficient had a negative sign. The opx coefficient

Table 2: Experimental conditions and products

Experiment	T (°C)	P	t (h)	f(O ₂)	Products
VB-1	1150	5 kbar	25		gl
VB-2	1120	5 kbar	26		gl ₉₄ pl ₆
VB-3	1100	5 kbar	36		gl ₉₆ pl ₄
VB-4	1080	5 kbar	47		gl ₈₂ pl ₁₇ ol _{0.2} il _{0.7} ap _{0.1}
VB-14	1078	5 kbar	66		gl ₆₁ pl ₃₀ pig ₆ il ₃ ap _{0.01} opx ₀
VB-13	1074	5 kbar	114		gl pl ol il ap pig
VB-5	1060	5 kbar	71		gl pl pig aug il ksp qtz
VB-6	1050	1 bar	125	FMQ	gl ₅₀ pl ₃₀ ol ₇ il ₃ uvsp ₈ phosph
VB-16	1065	1 bar	46	NNO	gl ₄₇ pl ₂₈ pig ₄ aug ₄ uvsp ₁₃ phosph ₄
VB-17	1060	1 bar	89	NNO	gl ₃₀ pl ₃₃ pig ₄ aug ₅ uvsp ₁₅ phosph ₅
MEL-1	1130	5 kbar	23		gl
MEL-2	1110	5 kbar	18		gl ₉₉ il ₁
MEL-3	1090	5 kbar	25		gl ₉₀ il ₄ ol ₄ ap ₂

The numbers following the phase abbreviations are the weight proportions of the relevant phases present in the experiments, calculated using a weighted least-squares minimization.

was then changed to zero and its components were included in the other phases. This results in an increased proportion of the remaining phases.

The fine-grained samples of jotunites were analyzed for major elements and some trace elements by X-ray fluorescence on a CGR Lambda 2020 Spectrometer at the University of Liège (analyst G. Bologne) (Bologne & Duchesne, 1991). The other trace elements were analyzed either on a VG elemental PQ2 Plus inductively coupled plasma-mass spectrometer at the University of Liège (Vander Auwera *et al.*, 1998) or by neutron activation at the Pierre Sûte Laboratory (CEA, Saclay, France; analyst J. L. Joron). Major and trace element data are presented in Table 5.

(An₃₂Ab₆₆Or₂). There seems to be a correlation between plagioclase composition and bulk composition, as plagioclase displaying the lowest anorthite content (An₃₀ in sample 75206; Table 4) is associated with the bulk composition showing the lowest MgO (2.79%) and highest SiO₂ (49.29%) content observed in the samples from the Varberg dike (Table 5; analysis of sample 75204 is given instead of that of sample 75206). This observation is supported by petrographic data from the Tellnes dike, in which there is a systematic change in the feldspar composition associated with bulk composition: jotunites are characterized by antiperthitic plagioclase and lesser K-feldspar (microperthite), mangerites contain more K-feldspar and mesoperthite-rimmed plagioclase, whereas quartz mangerites display mesoperthite (Wilmart *et al.*, 1989).

EXPERIMENTAL AND ANALYTICAL RESULTS

Mineral compositions

The compositions of plagioclase and pyroxenes from the Varberg dike (Fig. 3) have a limited range and are similar to those observed in jotunites from the Tellnes dike (Wilmart, 1988). In the chill margin plagioclase is not significantly zoned, with cores of An₄₃ and mantles with an average of An₃₄. Augite, whether as lamellae or primary crystals, has an intermediate *mg*-number (0.49). The low-Ca pyroxene (lpyx) is orthopyroxene (Wo_{1.2}En_{83.3}) inverted from pigeonite (Fig. 3, Table 4). In the sample of the melanocratic facies (MEL), the pyroxenes are similar to those elsewhere in the dike, but alkali feldspar is present (An_{0.4}Or_{99.6}) together with plagioclase

Experimental results

At 5 kbar and 1120°C plagioclase (An₁₀) is the sole liquidus phase of VB, the chill margin sample. Olivine (Fo₃₀), ilmenite, and apatite appear approximately together at 1080°C in run VB-4. The SiO₂ and P₂O₅ concentrations in the 1080°C liquid are 46.0% and 2.74%, respectively (Table 3); these values are consistent with the apatite-saturation model of Harrison & Watson (1984). In run VB-14 at 1078°C there is a drastic increase in crystallinity and olivine is replaced by pigeonite and orthopyroxene. At a slightly lower temperature (1074°C, VB-13) olivine reappears as a stable phase. Only the top half of the VB-13 charge shows signs of glass and textural equilibration. Thus the solidus probably lies within the

Table 3: Composition of experimental products

Exp.	No.	Ph	SiO ₂	TiO ₂	Al ₂ O ₃	Cr ₂ O ₃	Fe ₂ O ₃	FeO	MgO	MnO	CaO	K ₂ O	Na ₂ O	P ₂ O ₅	F	Total	'An, Fo, En'
VB-1	4	gl	47.26(34)	3.82(9)	13.97(9)			15.56(19)	3.06(8)	0.25(3)	7.70(3)	1.77(3)	3.28(6)	2.4(4)		99.07	
VB-2	4	gl	47.62(31)	3.85(10)	13.30(14)			16.34(22)	3.16(3)	0.23(2)	7.47(11)	1.92(3)	2.95(11)	2.43(2)		99.27	
5	pl	57.29(60)	0.15(2)	27.52(47)				0.57(7)	0.06(1)	0.00	9.56(34)	0.78(5)	5.61(32)	0.00		101.55	46
VB-3	4	gl	47.51(26)	3.9(2)	13.47(11)			15.74(14)	3.16(3)	0.23(1)	7.57(5)	1.89(3)	3.17(9)	2.53(5)		99.17	
3	pl	56.30(28)	0.14(5)	27.89(47)				0.57(7)	0.07(2)	0.00	9.99(79)	0.62(8)	5.44(18)	0.00		101.01	49
VB-4	4	gl	46.00(52)	4.24(12)	11.57(21)			18.26(46)	3.66(7)	0.27(2)	7.80(11)	1.82(8)	2.80(1)	2.74(8)		99.16	
4	pl	58.5(1.4)	0.05(6)	26.80(99)				0.52(9)	0.03(2)	0.00	8.81(2)	0.82(21)	5.88(55)	0.00		101.36	43
5	ol	34.18(19)	0.22(3)	0.05(1)	0.01(1)			41.44(27)	23.38(21)	0.51(2)	0.40(3)	0.00	0.02(1)	0.00		100.21	50
4	il	0.05(2)	55.93(4)	0.33(3)	0.00			40.42(9)	4.20(6)	0.41(2)	0.19(5)	0.00	0.02(1)	0.00		101.55	
3	ap	0.00	0.00	0.02(3)				0.97(23)	0.18(13)	0.06(0)	53.52(73)	0.08(6)	0.06(1)	41.14(19)	1.85(51)	97.88	
VB-14	7	gl	45.80(36)	4.16(8)	10.87(8)			20.17(22)	3.25(7)	0.32(3)	7.49(7)	2.04(9)	2.69(8)	2.84(7)		99.63	
7	pl	59.60(72)	0.02(3)	25.81(33)				0.39(11)	0.02(1)	0.00	7.24(31)	1.46(51)	5.65(31)	0.00		100.19	38
8	plg	50.93(55)	0.83(14)	1.1525	0.01(1)			26.25(77)	16.41(44)	0.51(4)	4.19(56)		0.08(1)			100.36	48
5	il	0.05(2)	54.35(27)	0.32(2)	0.01(1)			41.76(17)	3.39(8)	0.42(4)	0.11(5)		0.01(1)			100.42	
1	opx	50.50	0.31	0.80				29.46	15.68	0.67	1.85		0.06			99.33	47
4	ap	0.00	0.00	0.00				0.94(48)	0.20(21)	0.08(2)	54.27(51)	0.03(1)	0.07(2)	40.92(28)	1.93(55)	98.44	
VB-13	2	gl1	50.24(1.1)	2.92(8)	10.48(3)			19.58(48)	1.85(4)	0.33(6)	6.52(5)	2.72(4)	2.84(32)	2.47(3)		99.95	
1	gl2	51.01	2.61	10.92				17.15	1.59	0.32	7.32	3.20	3.07	3.28		100.47	
1	gl3	55.18	2.33	11.79				15.58	1.39	0.22	5.12	4.04	4.68	1.73		102.06	
3	gl4	50.50(87)	2.82(19)	10.63(25)				18.77(1.4)	1.76(15)	0.33(4)	6.79(46)	2.88(28)	2.91(26)	2.74(47)		100.13	
9	pl	59.80(57)	0.06(7)	25.59(33)				0.41(14)	0.02(2)	0.00	7.14(40)	1.52(46)	5.70(24)	0.00		100.24	37
7	plg	49.84(69)	0.79(7)	0.95(19)	0.01(1)			30.89(91)	12.70(60)	0.59(4)	4.42(62)		0.08(2)			100.27	38
1	ol	31.96	0.46	0.04	0.06			54.39	12.07	0.75	0.61		0.02			100.36	28
5	il	0.08(2)	53.17(38)	0.21(1)	0.02(2)			43.63(27)	1.98(3)	0.43(5)	0.17(9)		0.02			99.71	
5	ap	0.00	0.00	0.05(3)				1.24(12)	0.23(1)	0.08(4)	52.64(38)	0.06(1)	0.07(2)	40.84(48)	2.15(20)	97.36	
VB-5	3	gl	67.64(1.4)	0.77(11)	14.85(2.0)	0.01(1)		4.49(1.3)	0.32(9)	0.04(2)	1.47(17)	6.17(77)	3.70(42)	0.31(5)		99.77	

Table 3: continued

Exp.	No.	Ph	SiO ₂	TiO ₂	Al ₂ O ₃	Cr ₂ O ₃	Fe ₂ O ₃	FeO	MgO	MnO	CaO	K ₂ O	Na ₂ O	P ₂ O ₅	F	Total	'An, Fo, En'
VB-6	6	gl	54.41(64)	2.54(6)	12.18(11)	0.00		14.16(31)	2.22(4)	0.25(3)	6.11(11)	2.92(15)	3.00(24)	1.86(6)		99.65	
	11	pl	59.04(13)	0.07(5)	26.22(77)	0.00		0.65(20)	0.04(3)	0.00	8.27(92)	1.05(19)	5.46(55)	0.00		100.80	43
	5	ol	34.49(51)	0.19(4)	0.13(10)	0.00		42.81(26)	21.64(32)	0.67(4)	0.52(10)		0.03(1)			100.48	47
	4	il	0.03(1)	46.9(3.7)	0.45(21)	0.02(2)	12.65	35.92(2.3)	3.26(10)	0.44(1)	0.14(6)					99.81	
VB-16	6	uvsp	0.13(1)	23.88(25)	2.23(3)	0.03(2)	21.05	48.81(61)	2.64(7)	0.47(4)	0.22(6)					99.46	
	7	gl	56.69(2.0)	2.18(21)	12.53(40)	0.03(2)		11.02(1.2)	2.34(34)	0.22(4)	5.59(66)	2.83(30)	3.06(8)	1.65(32)		98.14	
	12	pl	57.12(1.7)	0.07(5)	26.51(1.1)	0.00		0.56(22)	0.03(3)	0.00	8.9(1.2)	0.80(17)	5.00(58)	0.00		98.97	47
	8	plg	50.76(43)	0.77(8)	1.25(22)	0.02(1)		19.9(1.3)	17.9(1.1)	0.58(3)	7.5(2.1)		0.11(4)			98.85	52
VB-17	1	aug	49.57	0.96	1.70	0.05		17.45	15.50	0.48	11.98		0.17			97.86	46
	5	uvsp	0.16(3)	19.76(54)	2.46(6)	0.02(1)	28.10	44.08(53)	2.99(7)	0.50(2)	0.12(7)		0.01(1)			98.20	
	6	phosp	0.00	0.00	0.11(9)			3.45(11)	3.75(4)	0.18(2)	44.90(25)	0.23(23)	0.49(17)	43.87(22)	0.00	96.98	
	5	gl	66.94(73)	1.24(12)	13.97(7)			5.71(21)	1.03(7)	0.10(2)	2.65(8)	4.13(20)	3.48(15)	0.57(4)		99.82	
MEL-1	9	pl	58.3(1.5)	0.11(6)	26.52(97)			0.67(27)	0.04(4)	0.00	8.62(91)	0.92(22)	5.00(62)	0.00		100.15	44
	3	plg	51.06(94)	0.61(21)	0.97(40)	0.02(2)		22.6(1.5)	17.3(1.6)	0.73(5)	6.2(2.5)		0.09(4)			99.59	50
	9	aug	50.19(43)	0.88(15)	1.43(20)	0.02(1)		17.8(1.3)	14.1(1.0)	0.58(12)	14.1(2.1)		0.20(3)			99.32	41
	5	uvsp	0.37(25)	16.41(31)	2.32(8)	0.02(1)	35.07	41.73(40)	2.57(12)	0.61(4)	0.29(11)		0.02(1)			99.41	
MEL-2	4	phosp	0.00	0.00	0.34(16)			3.59(10)	3.72(4)	0.22(2)	45.49(30)	0.24(19)	0.46(13)	43.56(61)	0.00	97.62	
	4	gl	36.59(16)	7.08(2)	7.34(4)			27.05(8)	4.51(4)	0.34(3)	9.13(8)	0.62(6)	1.87(8)	4.40(7)		98.93	
	5	gl	36.95(37)	6.56(18)	7.13(15)			27.19(39)	4.61(2)	0.37(2)	9.29(7)	0.57(4)	1.66(5)	4.51(8)		98.85	
	4	il	0.04(1)	54.53(25)	0.31(2)	0.01(1)	0.00	41.35(31)	3.66(5)	0.36(1)	0.20(6)		0.01(1)	0.00		100.47	
MEL-3	6	gl	39.56(21)	5.78(5)	8.14(8)			25.66(28)	3.99(7)	0.35(2)	9.01(7)	0.61(7)	1.98(11)	3.91(8)		98.98	
	5	ol	33.19(16)	0.24(3)	0.03(1)	0.05(1)		46.13(23)	19.36(8)	0.53(3)	0.42(2)	0.00	0.02	0.00		99.98	43
	4	il	0.03(1)	55.38(37)	0.29(2)	0.01(1)	0.00	41.68(26)	3.34(4)	0.43(3)	0.15(2)	0.00	0.00	0.00		101.31	
	3	ap	0.00	0.00	0.01(1)			1.46(40)	0.24(19)	0.05(2)	53.78(41)	0.04(2)	0.04(1)	41.21(51)	1.69(39)	98.52	

gl, glass; ol, olivine; pig, pigeonite; opx, orthopyroxene; pl, plagioclase; il, ilmenite; uvsp, ulvöspinel; aug, augite; ap, apatite; phosp, whitlockite. For each phase, the average of several analyses (No. is the number of analyses) is given and the standard deviation is in parentheses. Fo [Mg × 100/(Mg + Fe)], En [Mg × 100/(Mg + Fe + Ca)], An [Ca × 100/(Ca + Na + K)] are given in atomic units.

Table 4: Microprobe analyses of the Värberg dike feldspars and pyroxenes

Sample:	75202F	7912	7912	75202G	75182	75182	75372	75372	75206	78201
Phase:	Plag	Plag	FK	Plag	Plag	FK	plag	FK	Plag	Plag
No.:	6	6	2	4	8	2	8	4	7	8
<i>Feldspars</i>										
SiO ₂	61.06	60.89	64.88	61.38	61.34	64.33	61.16	64.90	61.81	60.90
Al ₂ O ₃	24.62	24.78	18.29	24.48	24.43	18.40	24.63	18.43	24.16	24.66
FeO	0.21	0.18	0.06	0.15	0.11	0.08	0.12	0.05	0.22	0.10
CaO	6.96	7.15	0.04	6.65	6.65	0.06	6.67	0.11	6.15	7.01
K ₂ O	0.35	0.36	16.06	0.35	0.36	15.22	0.40	14.77	0.32	0.37
Na ₂ O	7.38	7.28	0.82	7.43	7.47	0.93	7.49	1.14	7.79	7.30
Total	100.58	100.64	100.15	100.45	100.36	99.01	100.48	99.39	100.45	100.34
Si	2.7032	2.6950	2.9957	2.7160	2.7165	2.9915	2.7075	2.9983	2.7321	2.7008
Al	1.2842	1.2923	0.9952	1.2763	1.2751	1.0082	1.2851	1.0031	1.2586	1.2890
Fe	0.0076	0.0065	0.0025	0.0056	0.0039	0.0030	0.0045	0.0021	0.0080	0.0038
Ca	0.3300	0.3393	0.0019	0.3153	0.3153	0.0030	0.3166	0.0056	0.2914	0.3329
Na	0.6333	0.6246	0.0738	0.6372	0.6416	0.0836	0.6431	0.1023	0.6673	0.6273
K	0.0201	0.0204	0.9457	0.0200	0.0205	0.9027	0.0224	0.8701	0.0181	0.0211
Catsum	4.9783	4.9781	5.0146	4.9704	4.9730	4.9919	4.9791	4.9813	4.9755	4.9748
% An	33.56	34.46	0.19	32.42	32.27	0.30	32.23	0.57	29.83	33.93
% Ab	64.40	63.46	7.22	65.53	65.64	8.45	65.49	10.46	68.32	63.93
% Or	2.04	2.08	92.60	2.06	2.10	91.25	2.28	88.97	1.85	2.15

Table 4: continued

Sample:	75202F	75202F	7912	7912	7912	75202G	75202G	75202G	75182	75182	75372	75372	75206	75206	78201	78201	78201	78201
Phase:	opx	cpx	opx	opx	cpx	opx	opx	cpx	cpx	opx	opx	opx	opx	opx	opx	opx	opx	cpx exs.†
No.:	4	4	4	3	3	7	3	3	1	4	4	6	4	4	4	2	2	2
<i>Pyroxenes</i>																		
SiO ₂	49.84	51.25	49.69	51.45	51.23	49.61	51.23	50.98	49.73	51.34	49.74	51.13	50.39	51.92	50.02	51.14	51.50	
TiO ₂	0.10	0.14	0.06	0.16	0.21	0.10	0.21	0.24	0.10	0.17	0.12	0.24	0.07	0.17	0.11	0.25	0.23	
Al ₂ O ₃	0.59	1.24	0.58	1.29	1.26	0.71	1.26	1.33	0.60	1.16	0.67	1.31	0.61	1.19	0.65	1.33	1.34	
Cr ₂ O ₃	0.04	0.02	0.05	0.05	0.03	0.03	0.03	0.00	0.03	0.01	0.04	0.06	0.00	0.01	0.04	0.00	0.01	
FeO	37.93	17.52	37.74	17.61	16.65	37.14	16.65	16.75	39.11	18.28	37.79	17.92	35.06	15.36	37.36	18.97	16.61	
MgO	11.69	9.35	11.30	9.02	9.46	11.98	9.46	9.35	10.28	8.20	11.03	8.79	13.14	9.96	11.65	9.17	9.59	
MnO	0.81	0.39	0.95	0.40	0.41	0.76	0.41	0.31	0.84	0.36	0.82	0.37	0.92	0.44	0.82	0.46	0.34	
CaO	0.56	20.63	0.77	21.24	21.34	0.80	21.34	21.78	0.87	21.27	0.83	19.81	0.64	20.71	0.79	18.84	21.38	
K ₂ O	0.03	0.01	0.00	0.01	0.01	0.01	0.01	0.00	0.02	0.01	0.01	0.01	0.00	0.01	0.00	0.00	0.01	
Na ₂ O	0.01	0.33	0.00	0.34	0.34	0.00	0.34	0.34	0.00	0.33	0.00	0.34	0.00	0.37	0.00	0.37	0.31	
Total	101.61	100.90	101.14	101.58	101.14	101.14	100.93	101.07	101.57	101.13	101.05	100.22	100.83	100.25	101.44	100.54	101.32	
Si	1.9754	1.9676	1.9800	1.9653	1.9627	1.9702	1.9627	1.9540	1.9840	1.9756	1.9826	1.9798	1.9849	1.9863	1.9805	1.9735	1.9631	
Ti	0.0030	0.0040	0.0019	0.0046	0.0029	0.0029	0.0062	0.0069	0.0031	0.0048	0.0037	0.0070	0.0020	0.0049	0.0031	0.0074	0.0067	
Al	0.0275	0.0561	0.0270	0.0581	0.0334	0.0334	0.0568	0.0602	0.0283	0.0526	0.0316	0.0597	0.0283	0.0536	0.0302	0.0607	0.0600	
Cr	0.0012	0.0007	0.0016	0.0016	0.0010	0.0010	0.0008	0.0000	0.0009	0.0004	0.0013	0.0018	0.0001	0.0006	0.0012	0.0001	0.0004	
Fe	1.2571	0.5625	1.2575	0.5626	1.2334	1.2334	0.5335	0.5368	1.3047	0.5882	1.2598	0.5803	1.1547	0.4914	1.2369	0.6126	0.5293	
Mg	0.6908	0.5352	0.6712	0.5133	0.7091	0.7091	0.5404	0.5341	0.6114	0.4703	0.6553	0.5072	0.7714	0.5679	0.6877	0.5275	0.5450	
Mn	0.0272	0.0126	0.0321	0.0129	0.0256	0.0256	0.0133	0.0100	0.0282	0.0118	0.0276	0.0120	0.0306	0.0144	0.0276	0.0150	0.0110	
Ca	0.0237	0.8486	0.0327	0.8692	0.0341	0.0341	0.8759	0.8943	0.0372	0.8770	0.0353	0.8220	0.0269	0.8489	0.0333	0.7785	0.8731	
K	0.0015	0.0006	0.0001	0.0003	0.0006	0.0006	0.0004	0.0000	0.0012	0.0005	0.0004	0.0004	0.0000	0.0005	0.0002	0.0000	0.0004	
Na	0.0005	0.0248	0.0000	0.0255	0.0000	0.0000	0.0249	0.0253	0.0000	0.0244	0.0002	0.0254	0.0004	0.0274	0.0002	0.0275	0.0230	
Catsum	4.0081	4.0127	4.0040	4.0132	4.0101	4.0101	4.0150	4.0216	3.9989	4.0055	3.9977	3.9954	3.9991	3.9957	4.0009	4.0027	4.0118	
% En	35.03	27.50	34.22	26.39	27.71	35.87	27.71	27.18	31.30	24.30	33.60	26.56	39.50	29.76	35.12	27.49	27.99	
% Fs	63.76	28.89	64.12	28.93	27.36	62.40	27.36	27.32	66.80	30.39	64.59	30.39	59.13	25.75	63.18	31.91	27.18	
% Wo	1.20	43.61	1.67	44.69	44.93	1.73	44.93	45.51	1.90	45.31	1.81	43.05	1.37	44.49	1.70	40.60	44.84	
mg-no.	0.36	0.49	0.35	0.48	0.50	0.37	0.50	0.50	0.32	0.44	0.34	0.47	0.40	0.54	0.36	0.47	0.51	

*No., number of analyses per sample.
 tets., cpx exsolution in opx.

Table 5: Major and trace analyses of whole rocks

Sample	75372	66175	75336	P	75202G	7534	7533	7519	78201	7912	89115	8925	75202F	8926	75182	72521	7355	75204	80123	721	72345	78211	91141	72211	8951	7821	8034	78381	7832		
Location	8	11	11	11	8	11	11	8	8	8	1	3	8	3	8	10	5	8	7	10	12	2	6	10	4	10	10	9	9	10	
Major elements as wt % oxide																															
SiO ₂	36.79	42.75	43.50	43.88	44.61	44.62	44.66	45.06	45.40	45.63	46.45	46.90	46.93	47.17	47.31	47.32	47.85	49.29	49.39	49.52	49.53	49.82	50.38	51.16	54.33	54.51	56.38	56.40	60.41	65.7	
TiO ₂	6.23	4.36	4.80	4.45	4.10	4.20	4.42	4.22	4.70	3.57	3.98	4.14	3.59	3.56	3.59	3.60	3.50	3.43	3.67	3.11	3.82	3.18	4.62	3.08	2.41	2.18	1.90	2.09	1.27	0.99	
Al ₂ O ₃	7.16	12.18	13.31	12.89	11.80	12.95	13.13	11.79	12.92	12.75	13.22	13.16	13.45	13.76	12.92	12.80	13.40	15.81	15.81	15.81	14.50	13.13	14.50	13.13	14.50	12.30	11.86	11.87	9.65	7.54	
FeO	27.43	18.58	17.73	17.81	18.21	17.40	17.52	19.38	17.74	17.24	15.72	15.55	15.35	15.68	17.55	16.04	16.03	15.01	13.11	15.25	13.68	14.98	13.20	14.82	12.96	12.30	11.85	11.87	9.65	7.54	
MnO	0.41	0.26	0.27	0.26	0.18	0.24	0.27	0.27	0.25	0.20	0.24	0.27	0.21	0.21	0.27	0.21	0.22	0.22	0.22	0.13	0.17	0.21	0.21	0.22	0.19	0.21	0.16	0.15	0.16	0.11	
MgO	4.68	4.26	3.93	3.94	3.62	3.85	3.73	3.70	3.67	3.68	3.30	3.42	3.38	3.44	3.38	3.44	3.38	2.79	4.54	2.66	4.90	2.70	4.98	2.84	2.08	2.26	1.69	1.65	1.01	0.65	
CaO	9.02	9.13	8.82	8.76	8.69	8.57	8.50	7.20	7.92	8.68	7.81	7.69	8.44	7.33	7.43	7.43	7.43	7.13	6.87	6.33	6.00	7.17	7.01	5.09	5.43	4.66	4.74	3.31	2.56	3.07	
Na ₂ O	1.67	3.01	3.10	3.26	2.99	3.46	3.47	3.11	3.48	3.62	3.54	3.32	3.40	3.63	3.63	3.53	3.72	3.41	3.50	3.14	3.50	3.02	3.53	3.05	2.80	3.58	3.31	3.78	3.41	3.07	
K ₂ O	1.02	0.90	0.90	1.02	1.72	1.21	1.05	1.80	1.37	1.72	1.32	1.52	1.80	1.70	1.81	2.28	1.49	2.20	0.96	3.41	1.95	2.46	1.07	3.03	3.38	3.60	3.77	4.24	5.04	5.04	
P ₂ O ₅	4.20	3.40	2.98	2.99	3.10	2.89	2.70	2.40	2.42	2.98	2.35	2.59	2.50	2.26	2.47	2.74	1.95	2.06	0.71	2.03	0.91	2.15	0.73	1.84	1.31	1.29	1.04	0.95	0.75	0.51	
Total	98.61	98.83	99.34	99.25	99.02	98.39	99.45	98.83	98.87	100.28	98.40	98.51	98.84	98.58	100.27	99.39	99.42	99.05	98.69	99.23	99.56	98.62	100.34	99.78	98.19	98.84	98.59	99.27	97.97	99.5	
Trace elements as ppm																															
Ni	<10	<10	<10	40.7	<10	21	—	—	—	17	—	—	16	—	—	—	6.60	—	25	60	23	55	—	—	—	—	11	1.4	—	—	—
Cr	3.15	2.71	—	76.2	1.88	—	—	—	—	—	—	—	66.0	—	—	—	22.0	—	65.7	28.0	48.8	31.8	—	—	—	60	34	4	1	21	
V	219	171	152	160	176	151	164	—	—	178	109	187	159	164	—	—	128	231	116	216	87	300	142	284	66	78	60	35	—	72	
Co	56.0	51.0	45.0	45.8	41.1	40.0	47.0	—	—	24.0	48.9	56.9	34.7	51.1	—	—	36.0	49.6	30.9	49.0	27.1	46.5	47.1	72.9	30.8	35.1	23	17	20.2	11.5	7.2
Zn	306	200	213	202	234	176	218	—	—	216	214	226	190	233	—	—	197	—	212	144	258	—	—	133	223	204	243	186	—	—	151
Ga	—	—	—	—	—	—	—	—	—	—	31.6	30.7	—	36.1	—	—	—	30.4	—	—	—	—	—	32.1	21.7	—	33.9	—	—	—	—
Rb	6.4	5.1	3.7	5.3	8.5	6.9	5.6	10.6	7.0	9.0	10.6	12.7	10.6	12.6	13.0	—	17.0	16.6	20.4	18.0	25.4	43.0	28.5	5.8	19.2	37.0	39	34	34.0	48.0	71.0
Sr	268	438	465	458	380	473	436	399	431	438	465	463	415	465	375	354	412	375	530	342	382	341	461	349	311	316	272	310	211	128	
Y	110	53	52	51	98	45	52	75	63	70	64	69	72	57	69	79.0	107	87	72	95	—	—	70	33	78	65	95	78	68	52	
Zr	402	56	21	55	205	85	56	663	221	148	253	203	191	402	598	442	509	250	262	687	300	473	241	598	620	626	717	952	1251	1387	
Nb	—	—	—	—	—	—	—	—	—	—	39.9	43.6	26.0	22.6	—	—	27.0	32.5	27.0	—	—	—	27.2	21.9	28.0	31.6	29.0	26.0	—	—	18
Ba	708	576	745	721	1334	775	788	1262	980	1085	1602	1435	1362	1400	1175	1212	1130	1009	470	1541	580	1346	801	1542	1557	1348	1533	1801	1979	1842	
La	86.1	42.4	39.0	40.0	59.9	39.7	39.0	—	—	—	65.3	60.7	48.8	50.8	—	54.7	79.9	63.7	58.0	131	82	132	31	52.1	58.5	62.1	47.5	57.7	54.5	33.7	
Ce	224	109	121	112	145	99.3	119	152	128	132	130	142	112	119	152	138	180	151	236	131	82	132	31	52.1	58.5	62.1	47.5	57.7	54.5	33.7	
Pr	—	—	—	—	—	—	—	—	—	—	19.6	21.4	—	17.7	—	—	26.5	—	—	—	—	—	19.4	4.91	—	18.8	—	—	—	—	—
Sm	140	727	79.0	73.50	—	—	—	—	—	—	92.1	99.0	—	78.6	—	—	106	119	—	39.0	96.0	52.9	89.5	24.1	—	83.4	108	83.0	87.0	85.0	57
Nd	36.1	20.1	—	19.0	18.9	17.8	—	—	—	—	21.7	22.4	14.1	18.9	—	—	20.4	27.7	16.9	8.50	17.8	11.5	21.4	6.24	18.8	19.8	16.6	16.2	18.0	17.8	11.7
Eu	8.08	6.52	—	6.80	8.40	6.77	—	—	—	—	7.93	7.55	7.50	7.07	—	—	7.40	7.31	7.40	2.86	7.70	3.31	7.39	2.83	7.54	6.84	6.50	6.40	6.62	6.77	5.7
Gd	—	—	—	—	—	—	—	—	—	—	18.6	19.6	—	16.0	—	—	26.0	—	—	—	—	—	25.6	4.53	—	16.0	—	—	—	—	—
Tb	4.21	2.39	—	2.27	2.89	2.15	—	—	—	—	2.69	2.86	2.15	2.26	—	—	2.40	3.72	2.58	1.13	2.43	1.59	2.73	0.99	2.37	2.50	2.41	2.11	2.46	2.50	1.68
Dy	—	—	—	—	—	—	—	—	—	—	12.5	13.3	—	10.9	—	—	18.8	—	—	—	—	—	13.2	0.95	12.1	—	—	—	—	—	—
Ho	—	—	—	—	—	—	—	—	—	—	2.34	2.50	—	2.12	—	—	4.04	—	—	—	—	—	2.49	1.15	—	2.35	—	—	—	—	—
Er	—	—	—	—	—	—	—	—	—	—	5.19	5.53	—	4.63	—	—	9.84	—	—	—	—	—	5.80	2.85	—	5.79	—	—	—	—	—
Tm	—	—	—	—	—	—	—	—	—	—	0.65	0.69	—	0.59	—	—	1.28	—	—	—	—	—	0.78	0.46	—	0.74	—	—	—	—	—
Yb	7.43	2.78	—	2.63	4.20	—	—	—	—	—	3.49	4.04	3.60	3.33	—	—	3.80	8.05	4.80	2.00	4.30	3.55	4.38	2.89	4.81	4.21	4.50	3.90	4.70	5.50	4
Lu	1.11	0.43	—	0.39	—	—	—	—	—	—	0.48	0.51	—	0.43	—	—	1.16	—	0.33	0.77	0.52	0.56	0.43	—	0.59	0.92	—	0.69	0.85	—	
Hf	8.94	2.57	—	2.78	—	—	—	—	—	—	5.20	4.40	—	6.91	—	—	11.0	9.68	5.40	6.50	16.2	7.30	8.80	5.50	12.2	12.1	15.5	17.3	22.10	28.5	32.5
Ta	2.86	1.05	—	1.16	—	—	—	—	—	—	1.71	2.23	—	1.04	—	—	1.68	1.32	1.82	1.31	1.67	1.22	2.05	0.77	1.75	1.50	1.90	1.27	1.89	1.62	0.94
Pb	—	—	—	—	—	—	—	—	—	—	8.55	7.97	—	7.05	—	—	8.72	—	—	—	—	—	11.0	8.08	10.0	12.1	—	—	—	—	—
Th	0.59	0.71	—	0.60	—	—	—	—	—	—	—	—	—	—	—	—	0.79	1.19	1.15	0.50	0.66	3.60	0.23	—	0.67	0.29	0.75	0.59	0.67	0.87	0.66
U	0.17	0.31	—	0.30	—	—	—	—	—	—	—</																				

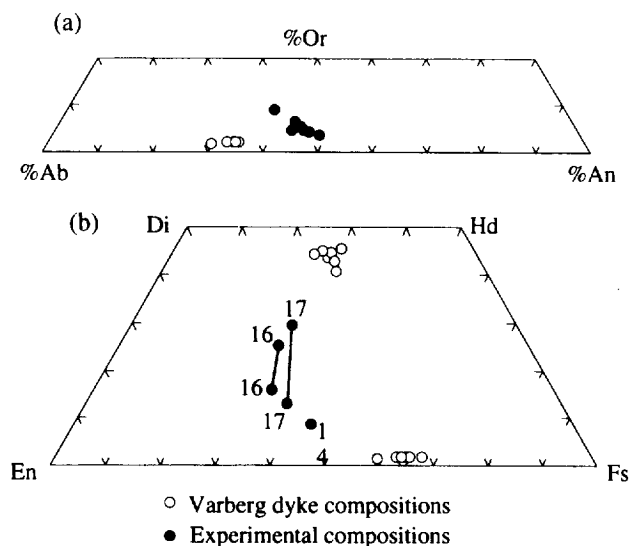


Fig. 3. Anorthite content of plagioclase (a) and pyroxene compositions (b) [En (MgSiO₃) Fs (FeSiO₃) Di (CaMgSi₂O₆) Hd (CaFeSi₂O₆) quadrilateral] in the Varberg dike (Table 4) as well as in liquidus and near-liquidus experiments (VB runs) (Table 3). Numbers in the pyroxene quadrilateral are run numbers.

charge. The few areas of glass are chemically heterogeneous (Table 3), and thus represent local surface equilibrium. Mass balance calculations show that there is a precipitous drop in percent liquid between 1080°C (82%) and 1078°C (61%), so encountering the solidus a few degrees lower is not surprising; however, in VB-5 at 1060°C, which should have been below the solidus, a small amount of glass with 67.6% SiO₂ was observed adjacent to K-feldspar. An explanation of these phenomena can be deduced from Fig. 4, in which liquidus phase diagrams are drawn from experimental phase compositions. In a plagioclase-ilmenite-apatite projection (Fig. 4a), the compositions of liquid, pigeonite, and olivine (plus plagioclase, ilmenite, and apatite) in VB-14 are nearly coplanar, implying a thermal divide on the olivine-pigeonite (+ plagioclase, ilmenite, and apatite) liquidus boundary, which in turn promotes extensive crystallization in a narrow temperature interval. Moreover, both the plagioclase-ilmenite-apatite projection (Fig. 4a) and the wollastonite-ilmenite-apatite projection (Fig. 4b) indicate that the VB-14 liquid composition is also close to a second thermal divide plagioclase-pigeonite (+ augite, apatite, and ilmenite) and a eutectic olivine + plagioclase + pigeonite (+ augite + apatite + ilmenite). This latter thermal divide restricts SiO₂ enrichment at 5 kbar and low $f(\text{O}_2)$ and prevents olivine-saturated liquids from ever reaching quartz saturation. Had magnetite been stable or the pressure lower, it is likely that the eutectic would become a peritectic (olivine in reaction) and that liquids would be able to breach the augite-pigeonite thermal divide. Given the absence of magnetite in the various runs and

the array of phase relations in Fig. 4, we believe that the high-SiO₂ glass in VB-5 is primarily the result of local equilibrium in the experimental charge where more mafic domains having a higher solidus temperature remained entirely crystalline, whereas more felsic domains having a lower solidus temperature yielded a small amount of high-SiO₂ melt. Therefore, as with VB-13, even though run VB-5 did not achieve bulk equilibrium, the liquid is probably multiply saturated nonetheless, so we have used the VB-5 glass composition to approximate the multiple saturation surface of charnockitic (high-SiO₂) liquids. A second curious point is the apparent absence of olivine in VB-14, despite the fact that olivine is present in runs immediately above (VB-4) and below (VB-13) this temperature. Given that the composition of the olivine + plagioclase + pigeonite (+ augite, apatite, and ilmenite) pseudo-invariant point lies close to a line from the Pl component through the VB composition, it is likely that a small difference in pressure between the two runs produced a different crystallization sequence: lower pressure in VB-4 (ol, no pyx) shifted the pseudo-invariant point away from the Ol component and stabilized olivine; whereas higher pressure in VB-14 shifted the pseudo-invariant point toward the Ol component and stabilized low-Ca pyroxene. Accordingly, olivine should be stable at the same pressure as, but at a lower temperature than VB-14, which is what is observed in VB-13.

At 1 atm and the NNO buffer, pigeonite, augite, plagioclase, and phosphate are stable together near the solidus with the only Fe-Ti oxide being titanomagnetite (actually ferri-ulvöspinel: $\text{uvsp}_{38}\text{mgt}_{12}$ in VB-16), whereas

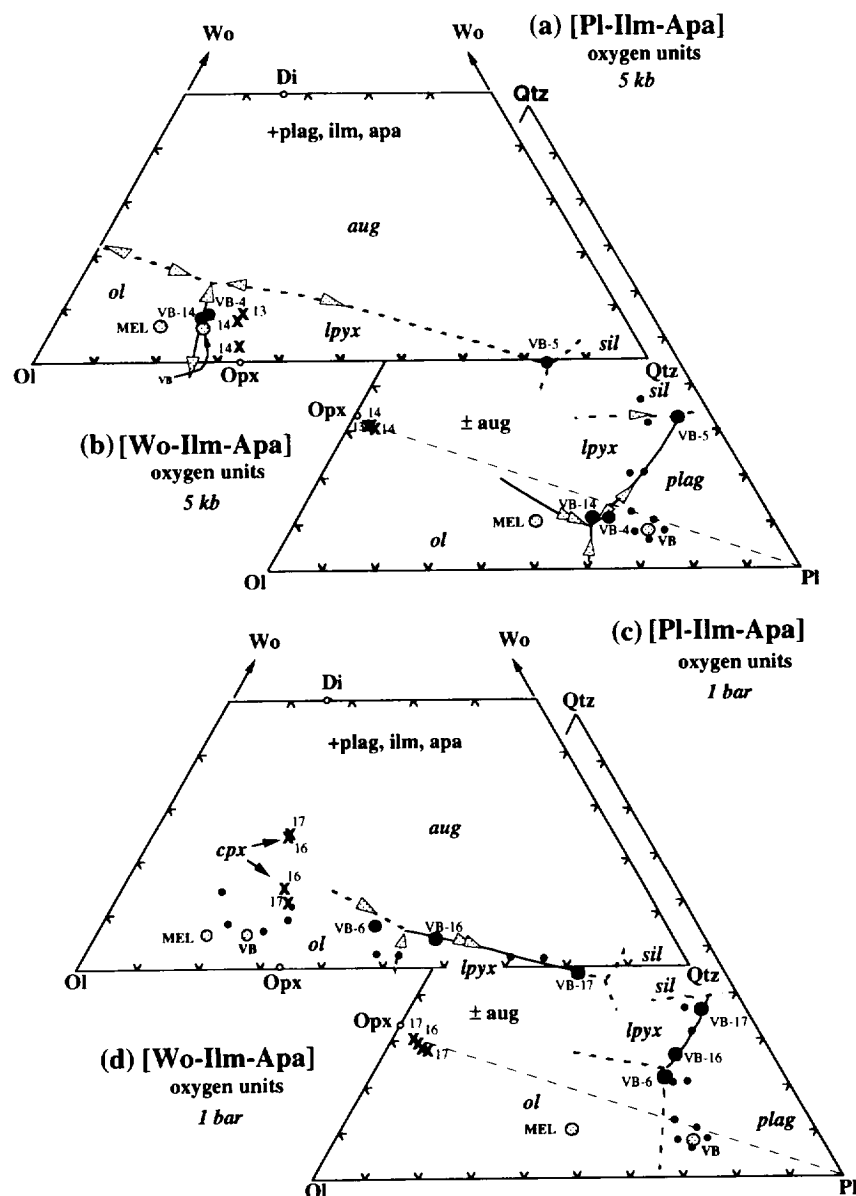


Fig. 4. Projections according to Longhi (1991) on the silica-olivine wollastonite plane from plagioclase, ilmenite and apatite and on the silica-olivine plagioclase plane from wollastonite, ilmenite and apatite. In (a) and (b), 5 kbar experiments are shown; in (c) and (d), 1 bar experiments. In all diagrams except (a), the small black dots correspond to the fine-grained samples and the large stippled points to starting compositions (VB and MEL). Low-Ca pyroxene (lpyx) composition (x) are from VB-13 and VB-14 in (a) and (b) and from VB-16 and VB-17 in (c) and (d). In (a) and (b), VB-4 and VB-14 glasses (●) were used to position the ol + plag + lpyx boundary and the VB-5 glass provides some constraint on the sil + lpyx + plag (+ aug) point. In (c) and (d), the ol + plag + lpyx boundary has been constrained with the VB-6 (●) and VB-16 (●) glasses whereas the VB-17 glass fixes the plag + lpyx + aug boundary.

at the FMQ buffer, both ilmenite and ferri-ulvöspinel ($uvsp_{69}mgt_{31}$ in VB-6) precipitate (Table 2). We presume that olivine would be stable at higher temperatures at NNO, as it is at FMQ. Phosphate analyses (Table 3) indicate that fluorine is present in the 5 kbar experiments

but not in the 1 atm experiments, suggesting that the phosphate is probably fluoroapatite in the former and whitlockite in the latter. The liquidus boundaries drawn on the basis of the 1 atm experiments are shown in Fig. 4c and d. They indicate that under moderately oxidizing

low-pressure conditions the thermal divide involving augite + low-Ca pyroxene + plagioclase is not stable and that olivine is in reaction with liquid when low-Ca pyroxene is stable. Thus olivine, which is the first mafic phase to crystallize in the jotunite compositions at low pressure, will be replaced by low-Ca pyroxene and plagioclase (Fig. 4d) at a peritectic reaction, and further fractional crystallization will drive the liquid toward silica saturation, and produce SiO_2 enrichment. The liquidus topology is consistent with petrological variations observed in the Tellnes orebody and its associated dike (Wilmart *et al.*, 1989) where olivine-bearing ilmenite norite contains the minerals with the most primitive compositions, and other lithologies are olivine free and grade continuously from jotunite to mangerite to quartz mangerite.

Titanomagnetite is present together with ilmenite in the matrix of the Varberg dike; however, both oxides have been exsolved and subjected to strong subsolidus re-equilibration (Duchesne, 1972a), so their compositions provide no constraint on redox conditions in the dike. Accordingly, we have estimated redox conditions in the dike on the basis of experimental Fe-Ti oxide assemblages. At 1 atm and the FMQ buffer, two Fe-Ti oxides are stable, $\text{ilm}_{10}\text{hem}_{11}$ and $\text{uvsp}_{10}\text{mgt}_{11}$, whereas at 1 atm and the NNO buffer, only spinel precipitates ($\text{uvsp}_{10}\text{mgt}_{12}$ in VB-16; $\text{uvsp}_{10}\text{mgt}_{12}$ in VB-17). Also, previous work on a primitive jotunite has shown that FMQ

1 marks the low- $f(\text{O}_2)$ stability limit for spinel in these compositions (Vander Auwera & Longhi, 1994). Thus, inasmuch as both spinel (magnetite) and ilmenite are present in the dike, the $f(\text{O}_2)$ was probably close to the FMQ buffer during crystallization.

Natural and experimental pyroxene compositions have been plotted in a Al_2O_3 vs CaO diagram (Fig. 5) in an attempt to glean some information about the pressure of crystallization of the dike. The situation is complicated by inversion and exsolution in the pyroxene; however, the primary pyroxene compositions are constrained to lie on mixing lines between host and lamellae. Both the 1 atm and 5 kbar data fall above (higher Al_2O_3) the mixing lines of the natural pyroxenes in Fig. 5, indicating no simple relationship. Comparison of pyroxene compositions in the two 5 kbar runs suggests that the lower Al_2O_3 content observed in the natural pyroxenes may result from continued equilibration to the solidus and into the subsolidus. Even so, there is no way to discriminate between 1 atm and 5 kbar on the basis of Al_2O_3 concentrations. However, the experimental data suggest that CaO decreases systematically with increasing pressure. Consequently, we have calculated the CaO concentration of the primary pigeonite from the compositions of orthopyroxenes and exsolved augites in samples 78201 and 75202G (Table 4) and the modal proportions of

orthopyroxene hosts and augite exsolutions (optical determination). The range of calculated compositions of natural pyroxenes (4.8–5.9 wt % CaO) is slightly higher than the value calculated by Duchesne (1972b) for inverted pigeonites from BKS (3.7–4.7% CaO). The values indicate a pressure of emplacement between 1 atm and 5 kbar (Fig. 5), the latter pressure being consistent with estimates for the crystallization of the Bjerkreim-Sokndal intrusion (Vander Auwera & Longhi, 1994).

Because the chill margin composition (VB) projects well into the plagioclase field in Fig. 4b and d, it is clear that the chill margin is not itself a quenched liquid at pressures of 5 kbar or less. In the 5 kbar near-liquidus run, VB-2, plagioclase has the composition An_{46} , whereas the most anorthitic plagioclase in the chill margin sample is only An_{30} . So the chill margin is not even a simple quenched liquid. In Fig. 4b (5 kbar) the chill margin lies nearly on a line between the plagioclase component and the pseudo-invariant point. These relations, together with the abrupt simultaneous appearance of olivine, ilmenite, and apatite in the crystallization sequence, are consistent with the chilled margin being a multi-saturated liquid, like VB-4 or -14, enriched with 15–30% plagioclase by weight. It should be noted that plagioclase in run VB-14 has an average composition of An_{30} , which is close to that observed in the dike, and which supports a multi-saturated liquid composition similar to that of VB-14. Alternatively, if the jotunite magma was derived by fractionation at a higher pressure where multi-saturated liquids sustain higher plagioclase components (Vander Auwera & Longhi, 1994), some portion of the apparent excess plagioclase component would be due to decompression, and the actual liquid composition would be displaced toward the Pl component, but not as far as the chill margin composition (Vander Auwera & Longhi, 1994). So, despite the fine grain size of the chill margin and the absence of phenocrysts, the material flowing along the margins of the dikes contained some plagioclase crystals in suspension. The more evolved compositions of the fine-grained samples with higher Qtz components do fall close to the plagioclase + pyroxene cotectics in Fig. 4b and d, so it is likely that the more evolved fine-grained samples within the dikes closely approximate liquid compositions.

Whole-rock analyses

The fine-grained samples from the Varberg dike and various other dikes display high total Fe as FeO_t (9.65–16.03%), TiO_2 (1.27% up to 4.62%), K_2O (0.96% up to 4.24%), and P_2O_5 (0.71% up to 2.59%) concentrations together with a modest range in SiO_2 (46.45% up to 60.41%) (Table 5, Fig. 2). In variation diagrams (Fig. 2), the primitive jotunites form a group distinct from the

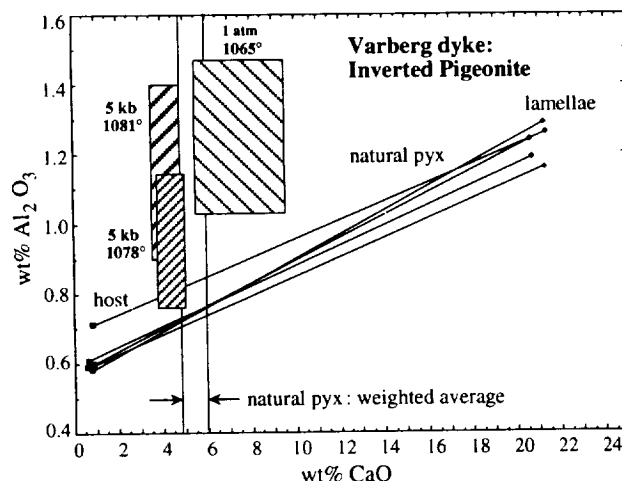


Fig. 5. Al_2O_3 and CaO contents of natural and experimentally obtained pyroxenes. For the experimental compositions, boxes correspond to 1 SD. The calculated compositions of natural pyroxenes correspond to their compositions before exsolution (see text for explanation).

jotunites of the dike system, which define trends of decreasing FeO , TiO_2 , P_2O_5 and CaO, and increasing SiO_2 and K_2O , with decreasing MgO. Samples of jotunites from other localities have been included in Fig. 2 for comparison. Among them, two [sample 738: Owens *et al.* (1993); sample EC90-216: Emslie *et al.* (1994)] are very similar to the primitive jotunites of Rogaland whereas the others fall near or on the trend of the dike system. Nevertheless, a group of samples from Nain (Wiebe, 1979) and Grenville (Owens *et al.*, 1993) define a trend higher in CaO/MgO and lower in $\text{K}_2\text{O}/\text{MgO}$ than samples from the other localities. This probably results mainly from different fractionation paths from locality to locality (see discussion) and from accumulation of plagioclase + mafics. This latter process can also explain the dispersion observed in samples from the Laramie complex (Mitchell *et al.*, 1996) especially in the FeO/MgO , TiO_2/MgO and $\text{P}_2\text{O}_5/\text{MgO}$ diagrams.

La concentrations in the fine-grained samples and other representative samples range from 15 ppm to 80 ppm (Table 5). The evolved jotunites, mangerites and quartz mangerites (Fig. 6) are higher in total REE content than the primitive jotunites, except the quartz mangerite 7832 which is in the range of primitive jotunites. The fine-grained samples display similar light REE (LREE) enrichment [average $(\text{La}/\text{Yb})_N = 9$] except for one sample [91141: $(\text{La}/\text{Yb})_N = 4$]. Eu anomalies are either weak slightly negative or slightly positive (e.g. 91141) or absent.

In a multielement diagram (Fig. 7), the primitive jotunites display variable concentrations of several trace elements, especially for Th, Rb, and REE (see also U in Table 5), whereas their major element concentrations

are rather constant except for K. Duchesne *et al.* (1989) previously pointed out this feature and attributed it to the variability of the source of jotunites. Apart from the enormous variation in Th, the primitive jotunites have relatively featureless patterns in contrast to the highly fractionated patterns of the evolved jotunites, mangerites and quartz mangerites. Primitive jotunites show small depletions of Ta (not Nb) and Hf (but not Zr in all cases) relative to the adjacent REE, whereas Ti shows a small excess as does P. Also, Sr may show a small depletion (80123a, 7234 in Fig. 7), where Eu shows no depletion (Fig. 6), or Sr may show no depletion (91141) where Eu shows a small excess. However, all the evolved jotunites, mangerites and quartz mangerites show prominent depletions in Sr relative to Ce and Nd, yet Eu anomalies remain small and may even be positive in the quartz mangerites. The Sr depletions indicate extensive crystallization of plagioclase despite the evidence for plagioclase accumulation in some samples. The unexpected behavior of Eu is discussed below. Interestingly, P, which shows small relative excesses in the primitive jotunites, shows larger excesses in the evolved jotunites and then little or no excess or depletion in the mangerites, and finally prominent depletions in the quartz mangerites. This pattern signals the onset of apatite crystallization as the magma changes from jotunitic to mangeritic. Relative depletions of Nb-Ta become more pronounced, and pronounced relative depletions of Ti develop with differentiation, whereas relative depletions of Hf and Zr diminish in the mangerites and even become slight enrichments in the quartz mangerites, which are consistent with Ti-oxide crystallization, but not zircon. Th shows huge depletions relative to the LREE in all of the evolved

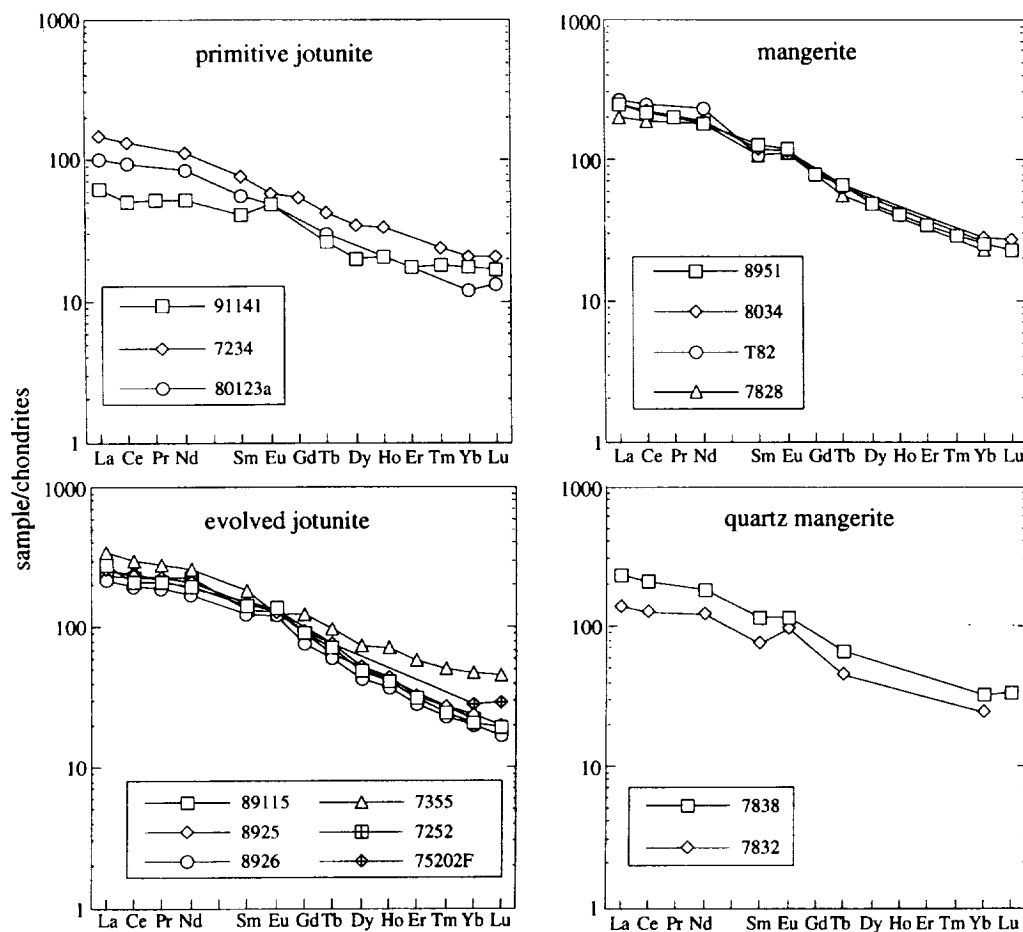


Fig. 6. REE patterns of the jotunitic suite [7234 (Duchesne *et al.*, 1974); 80123a (Duchesne & Hertogen, 1988); 7252, 7828, T82, 7832 (Wilmart *et al.*, 1989)]. REE abundances normalized to C1 chondrite of Sun & McDonough (1989).

jotunites despite its variability in the primitive jotunitites, suggesting that the Th-REE relation is a characteristic of the parental magma, and of the three primitive jotunitites only 80123a could be parental to the evolved jotunitites. Primitive jotunitites also show considerable range in K_2O with limited variation in MgO (Figs 2 and 8). These features suggest variable contamination of the large intrusions by country rock gneisses during emplacement (Hoover, 1989; Wilson *et al.*, 1996). For all the samples the K/Rb ratio varies from 376 to 1535 and Zr/Hf from 40 to 58. These trace elements compositions are in the range of those previously reported by Duchesne (1990) for the jotunitic suite of the Rogaland Province and are similar to those reported in other anorthositic complexes [e.g. Grenville Province: Emslie *et al.* (1994); Laramie Complex: Kolker *et al.* (1990); Mitchell *et al.* (1996)].

A LIQUID LINE OF DESCENT OF THE JOTUNITE SUITE AND ORIGIN OF ROCKS WITH EXTREME Fe-Ti-P CONTENT

Liquid line of descent (LLD)

A series of samples presented in this study display petrographic features typical of chilled rocks that suggest they are close to liquid compositions and thus constrain a liquid line of descent of the jotunitic suite under dry conditions. Nevertheless, projection of the fine-grained samples in the Ol Pl-Qtz diagram (Fig. 4) seems to indicate that some of them are enriched in plagioclase. We have already mentioned that the fine-grained samples define in variation diagrams (Fig. 2) two clusters of

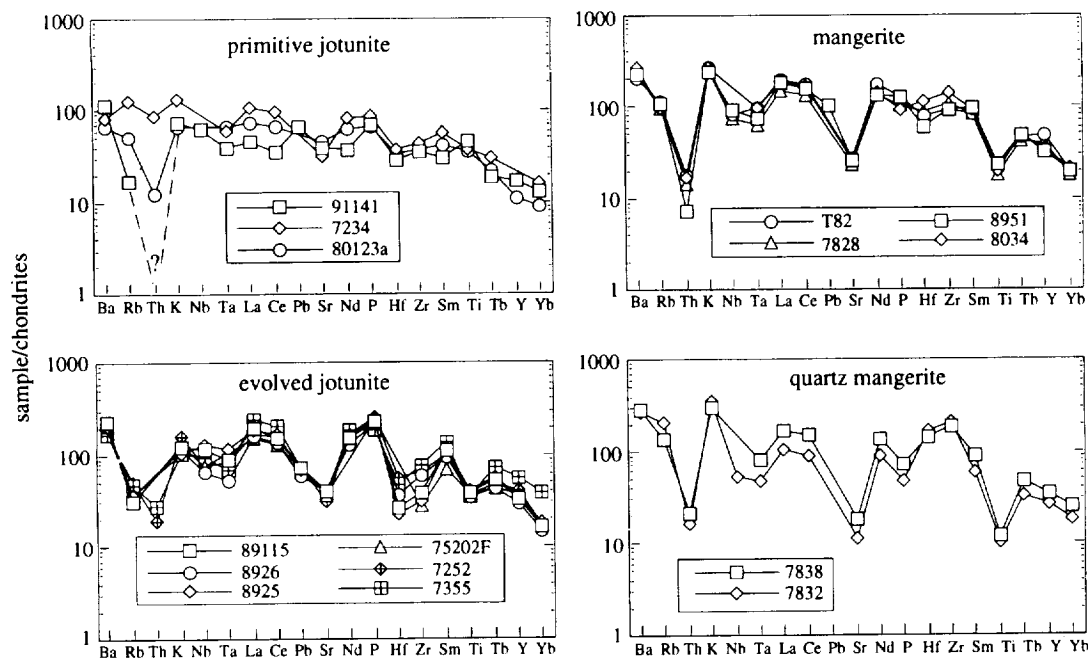


Fig. 7. Multielement diagrams of the jotunitic suite [7234 (Duchesne *et al.*, 1974); 80123a (Duchesne & Hertogen, 1988); 7252, 7828, T82, 7832 (Wilmar *et al.*, 1989)]. Abundances normalized to chondrites (Thompson, 1982).

points, one with a narrow range of intermediate MgO , corresponding to the primitive jotunites (chilled margins of large intrusions), and the other, offset from the first, forming linear trends ranging from evolved jotunites to quartz mangerites, in which FeO_t , TiO_2 , and CaO decrease, whereas K_2O and SiO_2 increase, versus decreasing MgO . These trends are repeated by samples from other dikes in the Rogaland system. The compositions of samples from the Tellnes dike, for example, overlap those from the Varberg dike and extend the trend to higher SiO_2 (charnockite). Thus in Rogaland there is an apparent discontinuity between primitive jotunite and evolved jotunite, but continuous chemical variation from evolved jotunite, through quartz mangerite, to charnockite.

The experimental data obtained on the two Varberg dike samples plus previous data on the Tjorn jotunite (Vander Auwera & Longhi, 1994), which belongs to the group of primitive jotunites, bring additional constraints on the LLD. However, some care must be taken because the compositions of the experimental liquids vary by equilibrium crystallization, whereas the jotunite LLD more probably results from a partially fractional crystallization process, and also because the pressure–redox conditions of the experiments do not match those of the dikes. Delayed crystallization of ilmenite, the absence of magnetite near the solidus, and decreased $m\text{-number}$ of ferromagnesian phases all are effects of the low $\text{Fe}^{1+}/$

Fe^{2+} ratio imposed by the graphite capsules; and even though the 1 atm experiments have been run at the appropriate $f(\text{O}_2)$, the lower pressure increases the proportion of plagioclase and olivine crystallization relative to pyroxene. These difficulties turn out to be relatively minor if one compares a combination of the 1 atm and high-pressure (5 and 7 kbar) data with the variation pattern of the dikes, as illustrated in Fig. 8, where the shaded areas correspond to the compositional ranges of the Rogaland jotunites shown in Fig. 2.

The most important feature is that the FMQ VB point (run VB-6) lies on or very near the dike trend in all of the panels (Fig. 8). The track of NNO VB is parallel to the dike trend, but is offset from the dikes in the direction of higher SiO_2 and lower FeO_t and TiO_2 , because of the crystallization of too high a proportion of Fe–Ti-oxides. The track of 5 kbar VB follows a path of much higher FeO_t and lower SiO_2 than the dikes, as the reducing conditions imposed by the graphite capsules delay the crystallization of Fe–Ti oxides, which in turn induces an excessive ferrous iron content in the liquid. It thus seems likely that crystallization of a liquid with VB-like composition at modest pressures and with $f(\text{O}_2)$ close to FMQ would produce a track very close to the dike trend, and that following eventual crystallization of titanomagnetite the track would extend to high SiO_2 (charnockitic) concentrations.

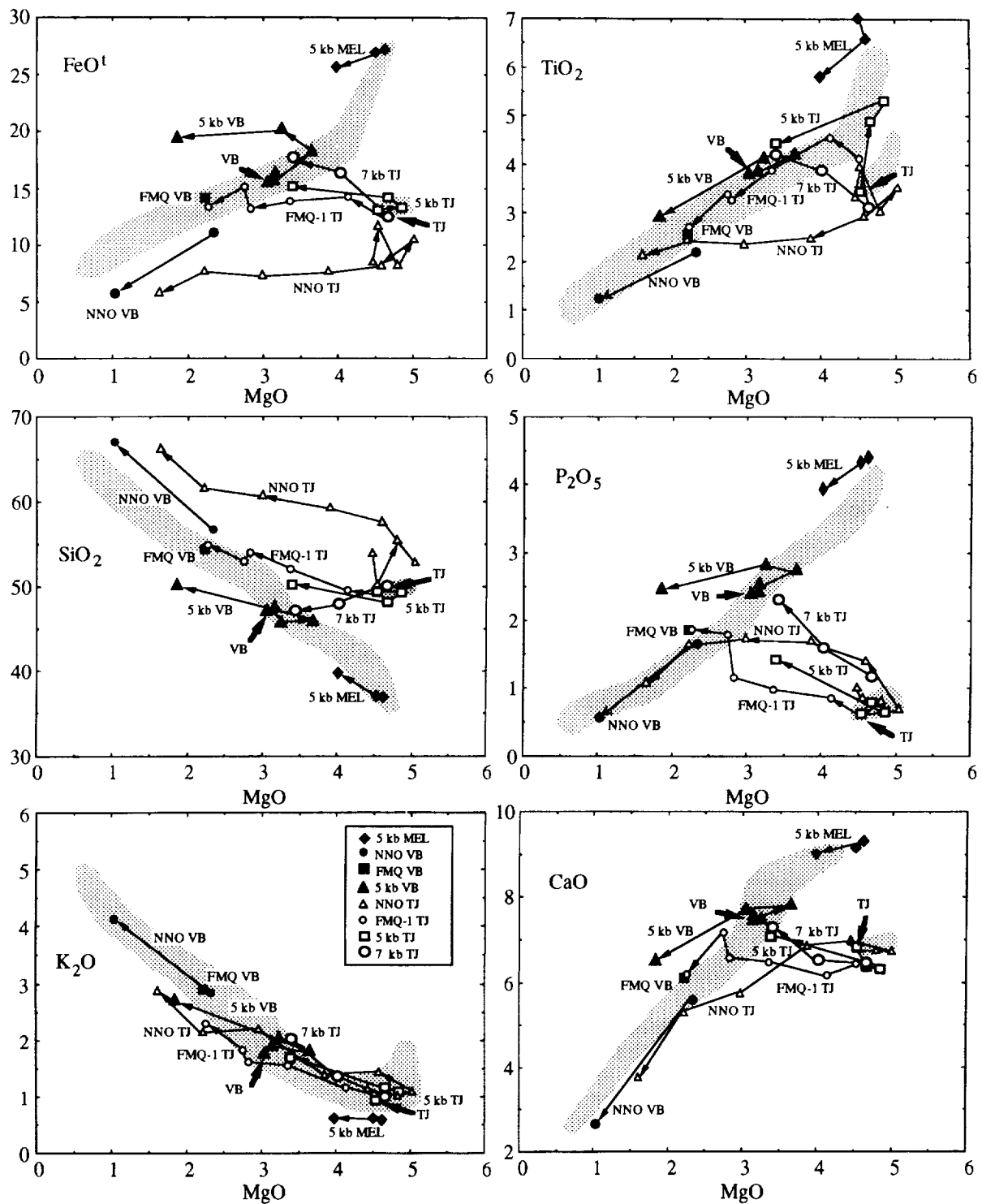


Fig. 8. Comparison of experimental data (wt % oxides) on VB (75202F), MEL (75372), and TJ (Vander Auwera & Longhi, 1994) with the Rogaland jotunite trend from Fig. 2 (shaded areas).

Comparison of the data on a primitive jotunite (TJ) from a previous study (Vander Auwera & Longhi, 1994) with data on the evolved jotunite (VB) from the present study provides further constraints on their possible relationship. In all sets of experiments on TJ, TiO_2 and FeO increase with decreasing temperature until ilmenite becomes a liquidus phase. While plagioclase is the sole crystallizing phase, the initial TiO_2 and FeO tracks show an increase with decreasing temperature. The effect of ilmenite saturation is probably best illustrated by the TJ experiments run at 1 atm (FMQ - 1 TJ). In this case, the maximum TiO_2 concentration (~4.5 wt %) is reached at ~4 wt % MgO. As temperature decreases further, TiO_2 and FeO decrease with MgO, whereas SiO_2 increases. The tracks of TiO_2 , FeO , and SiO_2 for FMQ - 1 TJ eventually all join the trend of the dike compositions: FeO and SiO_2 at MgO lower than that of sample VB; TiO_2 at MgO higher than VB. Crystallization of TJ at higher pressure will move the tracks of the FeO and SiO_2 closer to VB. If titanomagnetite were to crystallize after ilmenite at 5 kbar, the 5 kbar tracks of both VB and TJ would move closer to and follow the dike trend. P_2O_5 concentration in the liquid increases with decreasing temperature until phosphate crystallizes in experiments on both TJ and VB. In the VB experiments, apatite begins to crystallize simultaneously with ilmenite and olivine (VB-4); this liquid is probably very close to the Varberg liquid composition (see above). The TJ data also show that the early increase in P_2O_5 appears more pronounced at high pressure. This pressure effect derives from a greater proportion of pyroxene crystallizing relative to olivine at higher pressure: olivine can incorporate a small amount of P_2O_5 [more than low-Ca pyroxene; see Vander Auwera & Longhi (1994)] and Mg decreases more rapidly because of the higher Mg content of olivine. SiO_2 decreases with temperature in TJ liquids at 7 kbar because of co-crystallization of high-Si plagioclase and orthopyroxene and a low proportion of ilmenite; whereas at 5 kbar SiO_2 increases weakly because olivine is the sole mafic silicate phase near the liquidus. K_2O always increases and the residual experimental TJ liquids reach the K_2O content observed in dikes.

An important feature of Fig. 8 is thus the bridge made between the field of primitive jotunites and the trend of evolved jotunites by liquids residual to TJ. At 5–7 kbar the paths of the TJ liquids join the evolved jotunite trend close to the multi-saturated VB experimental liquids that most closely approximate the parental liquid of the Varberg dike. Consequently, the apparent discontinuity between primitive and evolved jotunites shown in Fig. 2 could result from a lack of exposures of this early fractionation stage. This process probably took place below the intrusion level of the dikes.

Origin of the extreme concentrations of Fe, Ti and P in some jotunites

Jotunites characterized by very high concentrations of FeO , TiO_2 and P_2O_5 (FTP) have been recognized in all anorthosite complexes (Ashwal, 1982; Owens & Dymek, 1992; Owens *et al.*, 1993; McLelland *et al.*, 1994). Emslie *et al.* (1994) and McLelland *et al.* (1994) have proposed that the unusually high Fe–Ti–P content is characteristic of a liquid derived from the processes of anorthosite crystallization under reducing conditions. FTP-rich jotunites from Rogaland have been recognized in the Varberg and Lomland dikes. In the latter, they constitute the Puntervoll facies, which passes progressively along strike into jotunites, mangerites and quartz mangerites. An average of four analyses of the Puntervoll facies (Duchesne *et al.*, 1985) plots on an extension of the trend of evolved jotunites at 3.9 wt % MgO (P' in Fig. 2). In the Varberg dike, the transition between the FTP rocks and the common jotunites is not observed in the field but these FTP rocks (e.g. MEL with 4.20% P_2O_5 , 6.23% TiO_2 and 27.43% FeO) plot with higher FeO and TiO_2 than simple extensions of the dike trend (Figs 2 and 8). The chemical variation toward low- SiO_2 compositions is more nearly continuous in anorthosite complexes from the Grenville Province (Owens & Dymek, 1992; McLelland *et al.*, 1994).

Variation diagrams combining experimental and geochemical data (Fig. 8) indicate that the composition of sample MEL cannot be simply explained by fractionation from a primitive jotunite even under very reducing conditions [f(O_2) in the 5 and 7 kbar TJ experiments lies between FMQ - 2 and FMQ - 4]. Consequently, given that field evidence indicates that sample MEL is comagmatic with VB, three alternatives are left: the FTP-rich jotunites may correspond to immiscible liquids conjugate to the mangerites found in the same dikes (e.g. Lomland) or they can represent liquids more or less heavily laden with Fe–Ti oxides and apatite or possibly cumulates injected as a crystal mush (Ashwal, 1982).

The position of sample VB in the jotunitic differentiation trend corresponds to the culmination of FeO and TiO_2 concentrations in the jotunite trend and thus it is the most likely candidate to plot within the immiscibility field (Roedder, 1979). However, the experimental MEL liquid compositions (Fig. 8) trend toward the array of evolved jotunite compositions with decreasing temperature, i.e. SiO_2 and K_2O increase as MgO, FeO , P_2O_5 , and TiO_2 decrease. Therefore the VB and MEL compositions are not situated on opposite sides of some immiscibility field. There is also no evidence (globules, menisci) of two liquids of any kind (silicate/silicate or silicate/oxide) in any of the experiments. Plagioclase is not a near-liquidus phase of the MEL composition, nor is there any textural or petrographic evidence for

immiscibility in the dike itself. Moreover, if we assume that, in the Varberg dike, the melanorite represented by sample MEL and the mangeritic composition represented by the Kungland facies (Duchesne *et al.*, 1985) correspond to conjugate immiscible liquids, the partition coefficients of P, Zr, REE, Ba and Sr are much lower than those measured by Watson (1976). We therefore conclude that immiscibility is not a relevant process for the formation of the FTP rocks, which leaves crystal accumulation (perhaps achieved through flow differentiation) as the only viable mechanism to produce FTP rocks.

Given that plagioclase is texturally primitive (hypidiomorphic) in the Varberg dike and is ubiquitous in the cumulates (BKSK intrusion), the absence of plagioclase near the liquidus of the melanorite MEL is a clear indication that the rock has accumulated non-felsic minerals. However, experiments performed on the MEL sample show that its liquidus temperature (1110°C) is similar to that of the chilled margin (1120°C) of the Varberg dike, and is only marginally higher than the temperature of the likely parental liquid (~1080°C; VB-14), despite its having higher FeO₁ and lower SiO₂. If a rock is a chilled suspension of a single phase in a liquid, the liquidus temperature of the rock will be higher than the temperature at the time of accumulation and the liquidus phase is likely to crystallize over a large temperature interval. However, if several phases have accumulated then there is the possibility of little or no increase in liquidus temperature as in the case of eutectic accumulation. Multi-phase accumulation appears to be the case for the relatively low liquidus temperature of MEL, and the similarity of the liquidus temperatures of VB and MEL is thus partly coincidental. Nevertheless, the situation is more complex here, as only the non-felsic part of the saturating assemblage – ilmenite, magnetite, apatite, and possibly orthopyroxene – appears to have accumulated to form the melanocratic facies. In the projections (Fig. 4), though, there appears to be a displacement of the MEL composition away from liquids saturated with the dike's assemblage not toward orthopyroxene, but toward the olivine component. This disparity may be attributed to Fe³⁺ incorporated in the accumulated Fe–Ti oxides, but treated as Fe²⁺ in the projections. Subtraction of this Fe will drive the projected MEL composition toward Qtz on a line parallel to the Ol–Qtz join, thus increasing the proportion of orthopyroxene relative to olivine in the apparent accumulated component.

Major element modeling

To model the trace element variations in the jotunitic trend, we must first constrain the phase proportions and, hence, the major element variation. In the following,

we will present a three-stage model based on previous petrogenetic studies of other Rogaland dikes (Duchesne *et al.*, 1985; Wilmart *et al.*, 1989) as well as of the BKSK layered intrusion (Duchesne, 1978). Stage 1 of the model involves fractionating a primitive jotunite, similar to the parental magma of BKSK (TJ: sample 80123a) to produce an evolved jotunite; the second stage involves fractionating an evolved jotunite, similar to VB to produce a mangeritic composition; and the third stage involves fractionating a mangeritic composition to produce quartz mangerite.

Variation diagrams in Fig. 8 show that subtraction of a leuconoritic assemblage from TJ drives the residual liquid toward the field of evolved jotunite compositions, close to the chilled margin composition of the Varberg dike (VB). In the different sets of experiments on TJ (Vander Auwera & Longhi, 1994), cumulus assemblages in equilibrium with the liquid closest to VB are: 64% plag + 30% low-Ca pyroxene + 6% ilm at 7 kbar, 74% plag + 20% ol + 2% pig + 4% ilm at 5 kbar, and 70% plag + 18% ol + 12% oxides at 1 atm and FMQ – 1. These phase proportions closely match the leuconoritic cumulate deduced by Duchesne (1978) (74% plag + 16% low-Ca pyroxene + 10% ilm) from the Sr–Ca modeling of the leuconoritic stage of BKSK, except that olivine is the major ferromagnesian phase at 5 kbar and 1 atm instead of low-Ca pyroxene. Moreover, the fraction of liquid is 0.47 at 5 kbar and 0.51 at 1 atm, which is close to the value ($f = 0.47$) calculated by Duchesne (1978). The phase proportions observed in the experimental cumulates correspond to an equilibrium crystallization process whereas those derived for BKSK are based on a fractional crystallization process. Nevertheless, as a fractional crystallization process is more relevant for the jotunitic trend discussed here, we have chosen a cotectic leuconoritic cumulate made of 74% plag + 16% low-Ca pyroxene + 10% ilm with $f = 0.5$ for the first stage.

To further model the fractional crystallization process along the jotunitic trend, there is the possibility to use simulations based either on partition coefficients (Nielsen, 1990) or on minimization of the Gibbs free energy (Ghiorso & Sack, 1995). Nevertheless, it has been shown that these simulations do not predict well the saturation of Fe–Ti oxides (Toplis & Carroll, 1996). We have therefore used mass balance calculations to further model the major element variations in the jotunitic trend. In the case of fractional crystallization, the mineral phase compositions must be in equilibrium with the starting liquid and this will be true for a certain amount of crystallization after which a new set of mineral compositions must be selected. We assume that the parent magma of the Lomland dike was close to the Varberg chilled margin (VB) and to the Eia–Rekefjord chill (7355) but we must point out that these compositions are probably slightly enriched in plagioclase, so that we use parent

Table 6: Three-stage major element model

Calculated cumulates

Primitive jotunite

C1 = 74% plag (An₄₃) + 16% low-Ca pyrx + 10% ilm (f1 = 0.5, F = 0.5)

Evolved jotunite

C2 = 43.3% plag + 19.6% low-Ca pyrx + 8.5% high-Ca pyrx + 9.3% ilm + 11.3% mgt + 8% ap (f2 = 0.6, F = 0.3)

Mangerite

C3 = 46.9% plag + 11.3% low-Ca pyrx + 12.7% high-Ca pyrx + 2.8% ilm + 21.1% mgt + 5.2% ap (f3 = 0.67, F = 0.2)

Least-squares fractionation model for cumulate 2 (C2)

	Evolved jotunite*	Mangerite	Cumulate	Mineral compositions used in fit					
				Plag (An ₄₀)	Opx (mg-no. 0.56)	Cpx (mg-no. 0.66)	Ilm (Hem ₂)	Mgt (Uvsp ₁₅)	Apa
SiO ₂	47.30	51.60	40.55	58.52	50.38	51.22	0.49	1.74	0.00
TiO ₂	3.55	2.41	5.25	0.00	0.14	0.42	48.81	4.84	0.00
Al ₂ O ₃	13.70	14.65	12.42	26.31	1.22	2.12	0.39	3.10	0.00
FeO _t	15.83	13.28	19.48	0.00	25.90	11.53	44.71	78.98	0.00
MgO	3.20	2.26	4.90	0.00	18.62	12.44	0.55	0.46	0.00
MnO	0.25	0.19	0.29	0.00	0.00	0.00	0.00	0.00	0.00
CaO	7.65	6.21	9.86	7.86	0.74	20.34	0.10	0.11	54.80
Na ₂ O	3.56	3.96	2.95	6.50	0.13	0.65	0.00	0.00	0.00
K ₂ O	1.70	3.00	0.35	0.80	0.00	0.00	0.00	0.00	0.00
P ₂ O ₅	2.27	1.44	3.40	0.00	0.00	0.00	0.00	0.00	41.70
$\Sigma r^2 = 0.086$									

Least-squares fractionation model for cumulate 3 (C3)

	Mangerite†	Quartz mangerite	Cumulate	Mineral compositions used in fit					
				Plag (An ₃₀)	Pig VB-16 (mg-no. 0.62)	Cpx (mg-no. 0.67)	Ilm (Hem ₀)	Mgt (Uvsp ₃₁)	Apa
SiO ₂	57.02	65.71	39.93	61.00	51.66	51.06	0.40	1.22	0.00
TiO ₂	1.92	0.99	4.32	0.00	0.78	0.51	52.79	11.05	0.00
Al ₂ O ₃	14.16	13.31	12.33	24.70	1.27	2.36	0.10	2.13	0.00
FeO _t	11.98	7.54	21.91	0.00	20.30	11.51	45.05	79.50	0.00
MgO	1.71	0.65	4.75	0.00	18.20	13.04	1.31	0.91	0.00
CaO	4.71	2.56	9.29	6.10	7.67	21.00	0.08	0.16	56.79
Na ₂ O	3.35	3.07	3.47	7.20	0.11	0.53	0.00	0.00	0.00
K ₂ O	3.64	5.04	0.47	1.00	0.00	0.00	0.00	0.00	0.00
P ₂ O ₅	1.05	0.51	2.59	0.00	0.00	0.00	0.00	0.00	43.21
$\Sigma r^2 = 0.057$									

*For stage 2, the starting composition corresponds to the average of several evolved jotunites including 75202F and 7355 whereas the mangerite is the average of the Kungland facies of the Lomland dike (Duchesne *et al.*, 1985).

†For stage 3, the starting and final compositions are samples 7828 and 7832 of the Tellnes dike, respectively (Wilmart, 1988; Wilmart *et al.*, 1989).

'magma' instead of 'liquid'. The composition of this parent magma is given in Table 6 (evolved jotunite). Calculation of the virtual olivine composition, using the Ford *et al.* (1983) relationship, in equilibrium with that

liquid gives Fo₃₆ at 5 kbar (1094°C). This olivine constrains the *mg*-number of the pyroxenes in equilibrium with that liquid and permits selection of the other minerals (plag, ilm and magnetite) in the series of BKSK cumulate

assemblages. Given these compositions, it is possible to calculate by least-squares fitting the proportions of the minerals in the cumulate which subtracted from an evolved jotunitic liquid close to VB give a mangeritic composition close to that of the Lomland dike (Klungland facies) which is also close to that of sample 78211 (2.7% MgO). The fitting is excellent (sum of the squared residues <0.1). The composition of the assemblage is given in Table 6, as well as the whole-rock composition of the calculated cumulate and the mangeritic composition. It is worth noting that this latter composition is close to the melt phase obtained in the VB-16 run in which the cumulate is also very rich in oxide [53% plag + 7.5% pig + 7.5% aug + 25% uvsp + 7.5% phosph: uvsp is the sole oxide as the experiment was conducted at NNO and the proportion of pyroxenes is less than in the calculated cumulate because the VB-16 liquid is higher in SiO₂ (56.69%) than the calculated mangerite (51.60%)]. On the other hand, the noritic cumulate deduced from trace element modeling of the second stage (noritic) of BKSK (Duchesne, 1978) as well as the noritic cumulate calculated for the Tellnes dike (Wilmart *et al.*, 1989) bracket the assemblage calculated here.

In a study of the Tellnes dike, Wilmart *et al.* (1989) have modeled the formation of a charnockite from an evolved jotunitic (similar to VB). The presence of a quartz mangerite (7838) among the series of fine-grained samples confirms the general nature of this differentiation process. Stage 3 of our modeling, which employs samples 7828 (mangerite) and 7832 (quartz mangerite) from the Tellnes dike (Wilmart *et al.*, 1989) as the starting and final compositions, respectively, is now a refinement of their calculations. The results show that an oxide gabbro cumulate (C3; Table 6) can account for fractionation from a mangerite to a quartz mangerite. The C3 plagioclase contains 1% K₂O, in agreement with the VB-16 plagioclase (0.80% K₂O). Petrographic and experimental data indicate that olivine is not stable in the evolved liquids of the differentiation trend, which justifies the presence of pigeonite instead of olivine (Wilmart *et al.*, 1989) in our cumulate. Mass balance calculations thus indicate that differentiation and silica enrichment along the jotunitic trend can be explained by extraction of magnetite-ilmenite-rich cumulates (C2 and C3) whose bulk SiO₂ values are lower than that of the evolved jotunitic and mangerite, as already pointed out by Hunter & Sparks (1987) for the Skaergaard intrusion. This conclusion is further supported by several other lines of evidence. As already mentioned, the mangeritic liquid of run VB-16 is in equilibrium with an assemblage containing 25% uvsp. Moreover, the BKSK evolved cumulates are characterized by thick layers of ultramafic rock containing up to 50% of Fe-Ti oxides, interleaved with norites or mangerites (Duchesne *et al.*, 1987). Finally, the calculated cumulates are close to sample MEL, and the occurrence

of FTP rocks such as MEL indicates that it is possible to accumulate large amounts of Fe-Ti oxides from these magmas.

Constraints from trace elements

We have also modeled the abundances of various trace elements (REE, Sr, U, Th, Zr, Hf, Ta, Rb, Ba, Co, Ni, Cr, Sc) in three stages using the same proportions of minerals that proved successful for the major elements. Partition coefficients are listed in Tables 7 and 8, and are taken from the literature, except where noted. Apatite and plagioclase are likely to be the most important phases because apatite has the highest D_{REE} values of the calculated minerals (Watson & Green, 1981), whereas plagioclase is the most abundant phase in the model cumulates, and apatite and plagioclase fractionate Eu and Sr relative to the REE in opposite directions. We have attempted to account for compositional variations in partition coefficients and to fill in gaps in the experimental data base with various approximations. For example, D_{Eu} (plag) has been calculated using Drake's equation (Drake, 1975) taking $D_{\text{Eu}2+} = D_{\text{Sr}} = 1.4$ (Watson & Green, 1981) and determining $D_{\text{Eu}3+}$ by extrapolating the other trivalent REE. The set of D_{REE} (plag) (Table 7) has been estimated by normalizing trace element concentrations measured in plagioclase separates (An_{50}) from the anorthositic cumulates of the Hydra leuconoritic body (Demaiffe & Hertogen, 1981) to concentrations of the same elements in Hydra chilled margin samples (Duchesne *et al.*, 1974; Demaiffe & Hertogen, 1981). In the case of apatite in stage 2, for example, the D_{REE} values have been calculated by normalizing the REE concentrations of apatite separated from sample MEL to the REE concentrations of bulk sample 8951, which is close to a liquid composition. For stage 3, the data of Fujimaki (1986) have been adopted.

Results of the model calculations using sample 80123a [IJ; Duchesne & Hertogen (1988); Vander Auwera & Longhi (1994)] as the starting composition are shown in Figs 9 and 10. The REE (Fig. 9a) show a strong increase during stage 1, then decrease from stage 2 to stage 3 as apatite crystallizes. A slight negative Eu anomaly appears in stage 1 and then disappears in stage 2 as a result of the appearance of apatite in the cumulate. Finally, fractionation of apatite with high D values in stage 3 induces the appearance of a positive Eu anomaly. The calculated REE contents closely, but not exactly, match the patterns observed in the jotunitic suite (Fig. 6). Small positive Eu anomalies in some evolved jotunitics and lack of any Eu anomaly in others probably reflect minor accumulations of plagioclase in the evolved jotunitics inferred from phase equilibria considerations. For the other trace elements, results are shown in Fig. 9b and

Table 7: REE partition coefficients selected for the modeling

	plag (1)	apa,2 (2)	apa,3 (3)	opx (4)	cpx (5)	ilm (6)	mgt (1)
La	0.13	12.0	14.5	0.0019	0.04	0.0023	0.006
Ce	0.11	15.0	21.1	0.0035	0.075	0.0019	0.006
Pr	0.1	17.0	26.9	0.0059	0.113	0.0016	0.006
Nd	0.09	19.0	32.8	0.013	0.15	0.0012	0.006
Sm	0.06	20.0	46.0	0.063	0.22	0.0023	0.006
Eu	0.46	13.0	25.5	0.059	0.2	0.0009	0.006
Gd	0.052	20.0	43.9	0.069	0.25	0.006	0.006
Tb	0.05	19.0	39.4	0.11	0.258	0.0095	0.006
Dy	0.048	18.0	34.8	0.15	0.267	0.013	0.006
Ho	0.046	16.8	28.8	0.2	0.275	0.022	0.006
Er	0.044	15.5	22.7	0.24	0.283	0.031	0.006
Tm	0.042	14.2	19.1	0.315	0.292	0.044	0.006
Yb	0.04	13.0	15.4	0.39	0.3	0.057	0.008
Lu	0.038	10.0	13.8	0.47	0.3	0.07	0.008

1, Demaiffe & Hertogen (1981); 2, see text for explanation; 3, Fujimaki (1986); 4, Dunn & Sen (1994); 5, McKay (1989) for 40% Wo; 6, Nakamura *et al.* (1986); 2 and 3 correspond to the cumulates c2 and c3 of Table 6. Values of *D* not given in the literature were extrapolated.

Table 8: Trace elements partition coefficients selected for the modeling

	plag1	plag2	plag3	opx	ilm	apa2	apa3	cpx	mgt
Sr	1.9 (1)	2.3 (1)	3.9 (1)	0.0034 (2)		1.4 (3)	2.2 (3)	0.09 (5)	
U	0.34 (2)	0.34 (2)	0.34 (2)	0.0002 (8)		25 (12)	25 (12)	0.0009 (13)	
Th	0.04 (6)	0.04 (6)	0.04 (6)	0.0001 (8)	0.09	23	19	0.0015 (13)	0.025 (19)
Zr				0.021 (2)	0.33 (10)			0.25 (14)	0.12 (19)
Hf	0.01 (7)	0.01 (7)	0.01 (7)	0.004 (8)	0.419 (10)			0.29 (15)	0.97 (19)
Ta	0.018 (6)	0.018 (6)	0.018 (6)	0.004 (21)	3.7			0.03	0.04
Rb	0.1 (6)	0.1 (6)	0.1 (6)	0.025 (4)					
Ba	0.38 (2 & 22)	0.38 (2 & 22)	0.38 (2 & 22)	0.00015 (8)				0.0023 (16)	
Co	0.05 (6)	0.05 (6)	0.05 (6)	0.7 (8)	9			1.2 (4)	5 (20)
Ni				9.5 (8)	17			2 (17)	44 (19)
Cr	0.03 (7)	0.03 (7)	0.03 (7)	1 (8)	16 (11)			2.7 (18)	350 (11)
Sc	0.015 (7)	0.015 (7)	0.015 (7)	2 (9)	2 (9)			4 (9)	2 (9)

(1) Duchesne (1978) and Vander Auwera *et al.* (1993); (2) Dunn & Sen (1994); (3) Watson & Green (1981); (4) Henderson (1982); (5) Ray *et al.* (1983); (6) calculated from Demaiffe & Hertogen (1981) and Duchesne *et al.* (1974); (7) Phinney & Morrison (1990); (8) Kennedy *et al.* (1993); (9) Duchesne *et al.* (1985); (10) McKay *et al.* (1986); (11) Jensen *et al.* (1993); (12) J. C. Duchesne, personal communication (1996); (13) Beattie (1993); (14) Johnson & Kinzler (1989); (15) Hart & Dunn (1993); (16) average of values given by Hart & Dunn (1993), Beattie (1993) and Hauri *et al.* (1994); (17) Steele & Lindstrom (1981); (18) average of values given by Hart & Dunn (1993) and Hauri *et al.* (1994); (19) Nielsen *et al.* (1994); (20) Horn *et al.* (1994); (21) Forsythe *et al.* (1994); (22) Duchesne & Demaiffe (1978). 1, 2 and 3 are for the three cumulates c1–c3 of Table 6. When the *D* value is not specified in a mineral, it is assumed equal to zero. Partition coefficients in italics have been calculated.

compared with the observed compositions of the different types of rocks in Table 9. Sr, U, Th, Co, Ni and Cr decrease with fractionation; Zr, Hf, Rb and Ba increase; Ta slightly increases; and, finally, Sc displays a slight

increase in the first stage and then decreases in the subsequent stages as magnetite crystallizes. The uniformly incompatible nature of Zr and Hf suggests that zircon is not a liquidus phase in the jotunitic suite. These results

Table 9: Comparison between observed and calculated trace element content

	Primitive jotunites		Evolved jotunites		Mangerites		Quartz mangerites	
	80123a	Observed range	Calculated	Observed range	Calculated	Observed range	Calculated	Observed range
Sr	530	382–784	400	412–465	377	272–310	257	128–211
U	0.10	0.1–1.3	0.17	0.32	0.09	0.1–18	0.08	0.1–0.2
Th	0.50	0.5–3.8	0.97	0.51–1.19	0.63	0.59–0.67	0.63	0.66–0.87
Zr	262.00	155–292	510.96	89–558	821.85	717–952	1193.36	1251–1387
Hf	6.50	4.5–8.2	12.56	5.4–11	19.10	17.3–22.1	25.71	28.5–32.5
Ta	1.31	0.8–1.31	2.01	1–2.2	2.78	1.3–1.9	3.95	0.94–1.62
Rb	17.00	5.8–44	32.21	9.7–13.4	52.38	34	76.63	48–71
Ba	469.00	469–801	771.87	1065–1602	1182.61	1533–1801	1643.05	1842–1979
Co	49.00	30–72.9	47.36	34.7–56.9	33.76	17–20.2	26.96	7.2–11.5
Ni	60.00	53–60	12.88	6.6–16.1	0.27	0–1.4	0.00	
Cr	28.00	28–50	16.28	22–66	0.00	4–34	0.00	1–21
Sc	13.80	13.8–25.9	19.10	8.15–28.1	17.69	19–21.1	16.20	16–17.7

For each type of rock, the composition calculated using the three-stage major element model (see text for explanation) is compared with the range observed in the fine-grained samples. In the case of the primitive jotunites, these samples are 80123a, 7234, 91141; 7020 (Duchesne *et al.*, 1974); 200/22, 259/11 (DemaiFFE & Hertogen, 1981); B90, B93, B95 (Wilson *et al.*, 1996). For the evolved jotunites, the samples are 75202F, 7355, 89115, 8925, 8926 as well as 7252 (Wilmart *et al.*, 1989). For the mangerites, the samples are 7838 and 7832 (Wilmart *et al.*, 1989).

are similar to those obtained for the Tellnes dike (Wilmart, 1988; Wilmart *et al.*, 1989). For most elements the agreement between observed and calculated values is very good, which supports the major element modelling proposed above. It should be noted especially that the Sr concentration decreases with crystallization, whereas the LREE show a small overall increase; hence the development of a pronounced Sr depletion relative to the LREE in the most evolved rocks – a clear sign of plagioclase fractionation. Continuous enrichment of Hf and Zr smooths out the depletions of Hf and Zr relative to the middle REE (MREE) in the transition from evolved jotunite to quartz mangerite as observed in the rocks (Fig. 7). For U and Th, our calculated values increase in stage 1 and then slowly decrease in stages 2 and 3, as observed in the rocks, reflecting the crystallization of apatite in stages 2 and 3, with high partition coefficients for these elements (Duchesne & Wilmart, 1997). Also, the calculated Rb concentration increases as expected with differentiation, but, starting with 17 ppm in 80123a, the concentrations after stages 1 and 2 are higher than those measured in the evolved jotunites and the mangerites. When a starting composition lower in Rb is chosen, as, for example, 5–80 ppm in primitive jotunite 91141, the calculated values in stages 2 (17.87 ppm) and 3 (26.17 ppm) are lower than the observed ranges. The highly variable Rb contents of the primitive jotunites (Duchesne *et al.*, 1989) probably reflect different degrees

of contamination in the various batches of the parental jotunite magma. Although some additional contamination during fractionation of the Varberg and Lomland dikes cannot be excluded, Rb–Sr isotopic data prohibit any significant contamination of the Tellnes dike during fractionation (Wilmart *et al.*, 1989). The same conclusion can also be drawn regarding the K₂O evolution. Small variations in the K₂O content of the parental magma batches, noted by Duchesne *et al.* (1989), are amplified by fractionation of a low-K cumulate. Contamination of the dikes is curious because most of the outcrop of the jotunite dikes lies within anorthositic rocks which are very low in K and Rb. The unsuitability of the anorthosite as a source of contamination for the dikes suggests that the dikes intruded the anorthosites already contaminated.

DISCUSSION

Results presented here indicate that quartz mangerites occurring in the vicinity of anorthositic complexes can be produced by extensive fractionation of primitive jotunites. Their compositions will be dependent upon the composition of the parental jotunite, but some generalizations are possible: such quartz mangerites will be characterized by REE concentrations in the range of jotunites with a weak Eu anomaly that is more positive (or less negative)

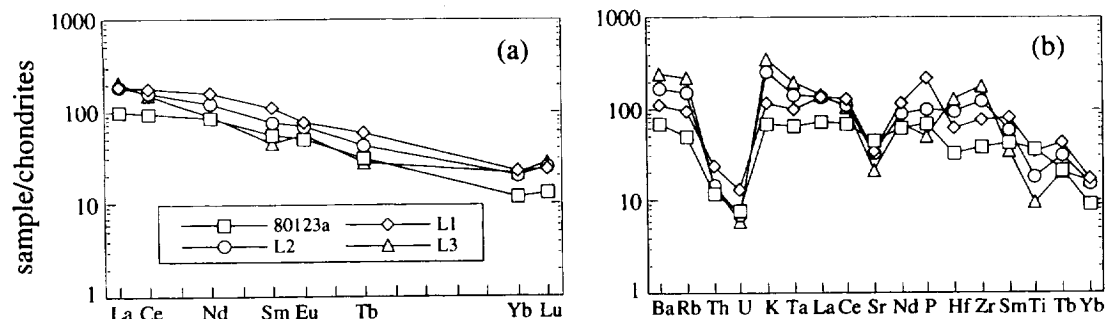


Fig. 9. Calculated REE (a) and trace elements (b) content of the evolved jotunite (L1), the mangerite (L2) and the quartz mangerite (L3) using sample 80123a as a starting composition and the three cumulates deduced from the major element modeling (in Table 6). Partition coefficients used in the model are given in Tables 7 and 8.

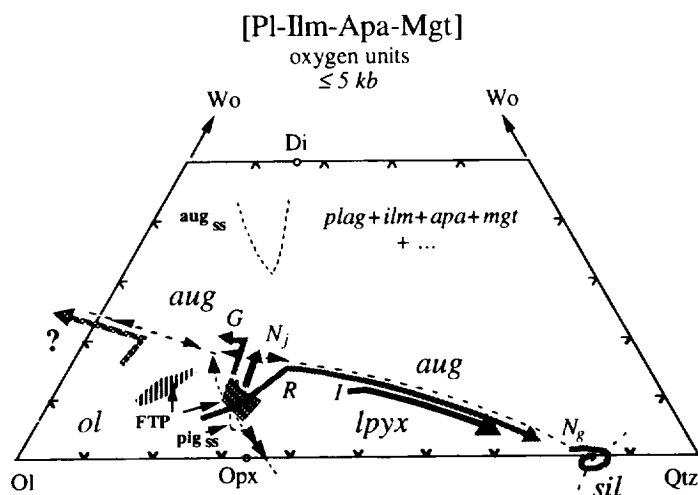


Fig. 10. Schematic representation of liquidus equilibria of ilmenite-apatite-magnetite-plagioclase saturated liquids projected onto the olivine-wollastonite-quartz plane. Arrows show direction of decreasing temperature; single arrows indicate cotectics; double arrows indicate reaction curves. Shaded paths indicate lines of descent consistent with mineral assemblages as explained in text. *G*, Laramie and Marcy trends; *Nj*, Nain jotunite (ferrodiorite) trend; *Ng*, Nain granitoids; *R*, Rogaland trend (see text); *I*, hypothetical trend of crustal melt with intermediate composition.

than its parent; and on multi-element plots there will be locally strong depletions of U, Th, Sr, and Ti with smaller to no relative depletions of Hf and Zr. Complementary to the quartz mangerite will be a series of cumulates rich in oxides and apatite which will form melanocratic rocks. Recently, Owens *et al.* (1993) described a broadly similar scenario for derivation of quartz mangerite from jotunite in the Grenville Province of Quebec. These observations differ in detail from those of Mitchell *et al.* (1996) and Emslie *et al.* (1994). Mitchell *et al.* (1996) described monzodiorite (~jotunite) evolving to monzonite (mangerite) and then monzosyenite instead of quartz monzonite (~quartz mangerite) along with the formation of complementary oxide-apatite-rich rocks in the Laramie Complex of Wyoming. Emslie *et al.* (1994) observed an absence

of evolved compositions in the range of 52–62 wt % SiO_2 , but a continuum in SiO_2 from 62 (quartz mangerite) to 74% (charnockite) in the Nain Complex of Labrador. Not surprisingly, Emslie *et al.* (1994) ascribed their high-Si compositions to partial melting of the lower crust, not fractionation. The Nain high-Si compositions have much in common with the Rogaland quartz mangerites in terms of mineralogy and trace element abundance patterns; however, the Nain granitoids show small negative Eu anomalies and more pronounced relative depletions of Sr and P, which might reflect more extensive fractionation of plagioclase and apatite, but might also reflect partial melting of a mafic crustal source. Also, the Rogaland quartz mangerites are found only within fractionated dikes or as the upper portion of a much larger jotunitic

intrusion such as BSKK (Duchesne & Wilmart, 1997), whereas some of the Nain granitoids comprise entire discrete intrusions or substantial fractions of others. Although the difference in field relations between Rogaland and Nain may be due in part to the level of exposure, we cannot exclude the possibility of deriving some quartz mangerites by partial melting of the lower crust. Indeed, as discussed below, there is a wide range of pressure and composition for which fractionation of a jotunitic magma cannot yield quartz mangerite.

Our conclusions on the liquid line of descent of jotunitites, as well as those of Owens *et al.* (1993) and Mitchell *et al.* (1996), contradict those presented by McLelland *et al.* (1994), who modeled the compositions of P-Ti-Fe-rich mafic dikes and sheets from the contact zone of the Marcy massif in the Adirondack mountains. In variation diagrams, the trends defined by these rocks show extreme enrichments in FeO_1 (up to 25%), TiO_2 (up to 7.6%), P_2O_5 (3.6%) correlated with extreme depletion in silica (down to 36% SiO_2). McLelland *et al.* (1994) admitted that these rocks are likely to represent crystal-laden liquids but nevertheless contended that the liquid line of descent followed at least in part a trend of decreasing Si and increasing P, Ti, and Fe. However, comparison with the data from this study indicates that the highest Fe, Ti, P and lowest Si concentrations are similar to those of Rogaland sample MEL, which is demonstrably a partial cumulate of a multiphase liquidus assemblage (pyroxene, apatite, ilmenite, magnetite); furthermore, experiments show that FeO_1 , TiO_2 , and P_2O_5 decrease as oxides and apatite crystallize from this composition. In projections such as Fig. 4a and b, the FTP-rich model magmas M6-M9 from McLelland *et al.* (1994) (Table 1) define a trend (not shown) pointing away from the 5 kbar pseudo-eutectic toward the Ol component; whereas model magmas M4-M6 plot close to the pseudo-eutectic. As explained above, the highest apparent contents of the Ol component may be in part a mixture of pyroxene and magnetite. The presence of pyroxene + oxide + apatite + plagioclase in M8 followed by the initial appearance of olivine in M9 is also consistent with a eutectic-like pseudo-invariant point. Thus the Marcy FTP enrichment is due primarily to accumulation from a multisaturated jotunitic liquid.

Interestingly, McLelland *et al.* (1994) pointed out the existence of a 'coeval, but not comagmatic' suite of rocks including mangerites and charnockites, which suggests a second jotunitic magma series characterized by silica enrichment similar to Rogaland (e.g. De Waard & Romey, 1968). The various differentiation paths of these and other jotunitic suites are illustrated in Fig. 10 by schematic versions of Fig. 4a in which magnetite is included as a projection component. The overall topology of Fig. 10 is the same as in Fig. 4a, but points project differently (higher Qtz component) because some of the

Fe has been removed from the Ol component to form an Fe_3O_4 (Mgt) component. Liquid lines of descent are represented by shaded lines and FTP trends by patterned areas. Because different suites probably crystallized at different pressures the topology of the entire diagram may not be appropriate to a single pressure or composition (with decreasing pressure or increasing *mg*-number the olivine pseudo-eutectic becomes peritectic and the pyroxene plagioclase thermal divide disappears). However, the diagram was constructed such that the local liquidus topologies would be appropriate. The diagram shows that the plagioclase + low-Ca pyroxene + augite thermal maximum is stable on the aug + lpx liquidus boundary and that the Wo-rich portion of the ol + lpx curve is even, whereas the low-Wo portion is odd and truncates the thermal ridge that crosses the lpx liquidus field. This configuration allows olivine to react out of magmas along the *R* curve and be replaced by pigeonite (lpx); and it also allows the fractionating magma to eventually reach silica saturation. Rogaland, some of the Grenville intrusions (Owens *et al.*, 1993) and parts of the Adirondacks (De Waard & Romey, 1968) are examples. The *G* curve represents magmas in which olivine crystallizes after pigeonite at the pseudo-eutectic, such as in the Greaser Intrusion in the Laramie Complex (Mitchell *et al.*, 1996) and the Marcy trend of McLelland *et al.* (1994). The *N* curve [Nain: Emslie *et al.* (1994); Maloin Ranch pluton: Kolker & Lindsley (1989)] is an example of a trend in which the liquid lies in the pyroxene + plagioclase thermal divide, so neither olivine nor quartz crystallizes, even after extensive fractionation. As a result, jotunitic (ferrodioritic, monzonoritic) rocks grade into two-pyroxene mangerites, and subsequently into syenites. Such rocks will show a modest increase in SiO_2 concentration because the high-Si felsic components increase at the expense of the low-Si mafic components in the residual liquids (e.g. Longhi, 1991). Because the decrease in the Qtz component is so small along the *G* trend, SiO_2 will also increase weakly in the residual liquid as it progressively forms olivine-free jotunitites (ferrodiorites), olivine-bearing mangerites, and ol syenites. Thus FTP cumulates apparently have developed from liquids that underwent pronounced SiO_2 enrichment (*R*) as well as from residual liquids in which SiO_2 increased only modestly (*N*, *G*). Finally, the curve labeled with the question mark is an example of a line of descent along which SiO_2 concentration and Qtz content decrease, and FeO_1 , TiO_2 and P_2O_5 increase, even though ilmenite and apatite are crystallizing. Such behavior is possible because the solubilities of TiO_2 and P_2O_5 increase with decreasing SiO_2 (e.g. Harrison & Watson, 1984). Rocks formed from such magmas would contain olivine, plagioclase, and highly aluminous augite, in addition to apatite and oxides, but no low-Ca pyroxene. We are not aware of any

examples of such a rock series in Proterozoic anorthositic complexes.

It follows that lpx-bearing granitoids cannot be consanguineous with coeval jotunitic rocks, if the parent magma of the jotunites evolved either on the low-Qtz side of the pyroxene-plagioclase thermal divide (e.g. *G*) or in the divide itself (e.g. *A*₁). Charnockitic granitoids could only have been derived from parent magmas that project to the high-Qtz side of the thermal divide; there are three possible options: (1) the granitoid magmas may have fractionated from a jotunitic liquid with low-Wo content like *TJ* that was able to breach the trace of the thermal divide before low-Ca pyroxene precipitated (*R*); (2) they may have fractionated from crustal melts with intermediate composition (*I*); (3) the granitoids may have crystallized directly from high-SiO₂ crustal melts (*V*₁), as suggested by Emslie *et al.* (1994). In the first case, continuous variation in SiO₂ concentration is expected. In the second case, a gap in SiO₂ is problematical; however, a bimodal volume distribution vs SiO₂ is likely even if SiO₂ variation is apparently continuous. In the third case, a gap in SiO₂ concentration is inevitable.

CONCLUSIONS

The Rogaland jotunitic trend presented above (Fig. 2) is the latter part of a multi-stage process of polybaric fractional crystallization, crystal accumulation, and probably flow differentiation within dikes. The high MgO-FeO, TiO₂, P₂O₅ rocks are accumulations of a dense oxide-apatite-pigeonite assemblage into coexisting jotunitic to mangeritic liquids. The accumulation is probably the result of flow differentiation within the dike system causing separation of a crystal-rich suspension into high- and low-density components, liquid \pm plagioclase being the low-density component. Indeed, the dike chill margins appear to be mixtures of multi-saturated liquid and 15–30% plagioclase. Evidence of K and Rb increasing faster than can be accounted for by fractional crystallization suggests contamination of the suspension before its intrusion into the anorthositic terrane. Estimated CaO concentrations of the bulk compositions of inverted pigeonites are intermediate to those produced at 1 bar and those at 5 kbar, suggesting crystallization of the Varberg dike, at least, in this pressure range. The earlier part of the process was fractional crystallization of a primitive jotunitic magma that is similar to the parental liquid of the Bjerkreim-Sokndal layered intrusion. Major and trace element modeling are consistent with extraction of an ilmenite-norite component from the primitive jotunitic to form an evolved jotunitic similar to the Varberg chill margin. Liquids generated in melting experiments (Vander Auwera & Longhi, 1994) on a primitive jotunitic (*TJ*) at 5–7 kbar are saturated not only with the requisite

ilmenite-norite assemblage, but also intersect the jotunitic major element trend closest to the Varberg chill margin composition. Trace element modeling also is consistent with such a scheme. This early stage of fractionation probably took place several kilometers below the intrusion level of dikes in a chamber evolving similarly to BKSK and provides the link between primitive and evolved jotunites.

Other researchers have argued that the jotunitic (ferrodioritic) suite was derived by fractionating liquids residual to the anorthosites themselves (e.g. Owens *et al.*, 1993; Mitchell *et al.*, 1996). Although we have presented evidence from Rogaland that seemingly contradicts these arguments in detail, we agree in the larger sense because we believe that primitive jotunites may be parental not only to mafic bodies such as BKSK, but also to a substantial portion of the Rogaland anorthosites (Duchesne, 1978; Longhi & Vander Auwera, 1992) – the amount of suspended plagioclase determines whether the intrusion is anorthositic or mafic, but the liquid is similar and so is its line of descent. Thus the jotunitic dikes may just as well have been spawned by fractionation within a deep-seated anorthositic intrusion as in a layered, mafic body similar to BKSK. Furthermore, although there is widespread belief that a mantle-derived high-Al basalt is parental to the massif anorthosites (Morse, 1982; Emslie *et al.*, 1994; Mitchell *et al.*, 1996), there is evidence of a continuum in composition between such high-Al basalts and primitive jotunites, which have higher concentrations of Ti, P, and K but are otherwise similar (Longhi & Vander Auwera, 1992). And, most importantly, both high-Al basaltic and primitive jotunitic compositions, which are suitable as parental magmas of anorthosites, lie in thermal divides (maxima) at lower crustal pressures, which effectively precludes their having been derived by fractional crystallization, with or without crustal assimilation, of more primitive mantle-derived melts (Longhi & Vander Auwera, 1992).

Further crystallization and flow of the evolved jotunitic magma within the dikes produced a series of mangeritic, quartz-mangeritic, and charnockitic rocks displaying a continuous increase in SiO₂ concentration. There are also low-SiO₂ facies of the dikes enriched in FeO, TiO₂, and P₂O₅ (FTP rocks), which are partial cumulates of pigeonite, oxides, and apatite complementary to the SiO₂ enrichment trend. Trace element modeling of this fractionation scheme closely reproduces the observed rock compositions, in particular the lack of a significant Eu anomaly despite extensive plagioclase fractionation. Whether jotunitic magmas fractionate continuously to quartz-mangerite and charnockite or to mangerite and syenite is determined by their disposition relative to the pyroxene-plagioclase thermal divide, which becomes stable at ~3–4 kbar in these compositions. Jotunitic magmas that crystallize either in the thermal divide or

on the low-Qtz side of the divide will not yield high-SiO₂, quartz-bearing derivatives; consequently, coeval granitoids are either direct crustal melts or derived from crustal melts with intermediate composition. If low-pressure and/or low Wo content permit a jotunitic magma to breach the pyroxene-plagioclase thermal divide, then continued fractionation will yield consanguinous granitoids as in Rogaland.

ACKNOWLEDGEMENTS

We would like to thank J. L. Joron for analysing some samples, as well as G. Bologne and G. Delhaze for help with the chemical analyses and sample preparation. The microprobe analyses were performed under the supervision of G. Wauthier. Financial support to J.V.A. and J.C.D. was provided by the Belgian Fund for Joint Basic Research, and to J.L. by NASA Grants NAG-9-329 and NAGW 3407. This work was also part of the International Geological Correlation Program, Project 290. This paper is Lamont-Doherty Earth Observatory Contribution 5741.

REFERENCES

- Andersen, D. J. & Lindsley, D. H. (1988). Internally consistent models for Fe-Mg-Mn-Ti oxides: Fe-Ti oxides. *American Mineralogist* **73**, 714-726.
- Ashwal, L. D. (1982). Mineralogy of mafic and Fe-Ti oxide-rich differentiates of the Marcy anorthosite massif, Adirondacks, NY. *American Mineralogist* **67**, 14-27.
- Ashwal, L. D. (1993). *Anorthosites*. Berlin: Springer-Verlag.
- Beattie, P. (1993). The generation of uranium series disequilibria by partial melting of spinel peridotite: constraints from partitioning studies. *Earth and Planetary Science Letters* **117**, 379-391.
- Bolle, O. (1996). The Apophysis of the Bjerkreim Sokndal layered intrusion (southwestern Norway). In: Demaiffe, D. (ed.) *Petrology and Geochemistry of Magmatic Suites of Rocks in the Continental and Oceanic Crusts (J. Michot volume)*. Bruxelles: MRAC & ULB, pp. 129-144.
- Bologne, G. & Duchesne, J. C. (1991). Analyse des roches silicatées par spectrométrie de fluorescence X: précision et exactitude. *Belgian Geological Survey Professional Paper* **249**, 11 pp.
- Demaiffe, D. & Hertogen, J. (1981). Rare earth geochemistry and strontium isotopic composition of a massif-type anorthositic charnockitic body: the Hidra massif (Rogaland, SW Norway). *Geochimica et Cosmochimica Acta* **45**, 1545-1561.
- Demaiffe, D., Weis, D., Michot, J. & Duchesne, J. C. (1986). Isotopic constraints on the genesis of the Rogaland anorthositic suite (southwest Norway). *Chemical Geology* **57**, 167-179.
- De Waard, D. & Romey, W. D. (1968). Petrogenetic relationships in the anorthositic charnockite series of Snowy Mountain Dome, south central Adirondacks. In: Isachsen, Y. W. (ed.) *Origin of Anorthosite and Related Rocks*. New York State Museum and Science Service, Memoir **18**, 307-315.
- Drake, M. J. (1975). The oxidation state of europium as an indicator of oxygen fugacity. *Geochimica et Cosmochimica Acta* **39**, 55-64.
- Duchesne, J. C. (1972a). Iron-titanium oxide minerals in the Bjerkreim-Sogndal Massif, south-western Norway. *Journal of Petrology* **13**, 57-81.
- Duchesne, J. C. (1972b). Pyroxènes et olivines dans le massif de Bjerkreim-Sogndal (Norvège méridionale). Contribution à l'étude de la série anorthosite-mangérite. *24th International Geological Congress, Montreal Section 2*, **2**, pp. 320-328.
- Duchesne, J. C. (1978). Quantitative modeling of Sr, Ca, Rb and K in the Bjerkreim-Sogndal lopolith (SW Norway). *Contributions to Mineralogy and Petrology* **66**, 175-184.
- Duchesne, J. C. (1990). Origin and evolution of monzonorites related to anorthosites. *Schweizerische Mineralogische und Petrographische Mitteilungen* **70**, 189-198.
- Duchesne, J. C. (1998). Fe-Ti deposits in Rogaland anorthosites (south Norway): geochemical characteristics and problems of interpretation. In: Rickard, D. (ed.) *Agricola Volume*. New York: John Wiley.
- Duchesne, J. C. & Demaiffe, D. (1978). Trace elements and anorthosite genesis. *Earth and Planetary Science Letters* **38**, 249-272.
- Duchesne, J. C. & Hertogen, J. (1988). Le magma parental du lopolithe de Bjerkreim-Sokndal (Norvège méridionale). *Comptes Rendus Hebdomadaires des Séances de l'Académie des Sciences* **306**(2), 45-48.
- Duchesne, J. C. & Wilmart, E. (1997). Igneous charnockites and related rocks from the Bjerkreim-Sokndal layered intrusion (Southwest Norway): a jotunitic (hypersthene monzodiorite)-derived A-type granitoid suite. *Journal of Petrology* **38**, 337-369.
- Duchesne, J. C., Roelandts, L., Demaiffe, D., Hertogen, J., Gijbels, R. & de Winter, J. (1974). Rare-earth data on monzonoritic rocks related to anorthosites and their bearing on the nature of the parental magma of the anorthositic series. *Earth and Planetary Science Letters* **24**, 325-335.
- Duchesne, J. C., Roelandts, L., Demaiffe, D. & Weis, D. (1985). Petrogenesis of monzonoritic dykes in the Egersund-Ogna anorthosite (Rogaland, SW Norway): trace elements and isotopic (Sr, Pb) constraints. *Contributions to Mineralogy and Petrology* **90**, 214-225.
- Duchesne, J. C., Denoix, B. & Hertogen, J. (1987). The noritic-mangérite relationships in the Bjerkreim-Sokndal layered lopolith (southwest Norway). *Lithos* **20**, 1-17.
- Duchesne, J. C., Wilmart, E., Demaiffe, D. & Hertogen, J. (1989). Monzonorites from Rogaland (Southwest Norway): a series of rocks coeval but not comagmatic with massif-type anorthosites. *Precambrian Research* **45**, 111-128.
- Dunn, T. & Sen, C. (1994). Mineral/matrix partition coefficients for orthopyroxene, plagioclase, and olivine in basaltic to andesitic systems: a combined analytical and experimental study. *Geochimica et Cosmochimica Acta* **58**, 717-733.
- Emslie, R. F. (1985). Proterozoic anorthosite massifs. In: Tobin, A. C. & Touret, J. L. R. (eds) *The Deep Proterozoic Crust in the North Atlantic Provinces*. NATO Advanced Study Institute C158. Dordrecht: D. Reidel, pp. 39-60.
- Emslie, R. F., Hamilton, M. A. & Thériault, R. J. (1994). Petrogenesis of a Mid-Proterozoic Anorthosite-Mangérite-Charnockite-Granite (AMCG) complex: isotopic and chemical evidence from the Nain Plutonic Suite. *Journal of Geology* **102**, 539-558.
- Ford, C. E., Russell, D. G., Craven, J. A. & Fisk, M. R. (1983). Olivine-liquid equilibria: *T*, *P* and composition dependence of the crystal/liquid cation partition coefficients for Mg, Fe, Ca and Mn. *Journal of Petrology* **24**(3), 256-265.
- Forsythe, L. M., Nielsen, R. L. & Fisk, M. R. (1994). High-field-strength element partitioning between pyroxene and basaltic to dacitic magmas. *Chemical Geology* **117**, 107-125.
- Fram, M. & Longhi, J. (1992). Phase equilibria of dikes associated with Proterozoic anorthosite complexes. *American Mineralogist* **77**, 605-616.
- Fujimaki, H. (1986). Partition coefficients of Hf, Zr and REE between zircon, apatite and liquid. *Contributions to Mineralogy and Petrology* **94**, 42-45.

- Ghiorsio, M. S. & Sack, R. O. (1995). Chemical mass transfer in magmatic processes. IV. A revised and internally consistent thermodynamic model for the interpolation and extrapolation of liquid–solid equilibria in magmatic systems at elevated temperatures and pressures. *Contributions to Mineralogy and Petrology* **119**, 197–212.
- Harrison, T. M. & Watson, E. B. (1984). The behavior of apatite during crustal anatexis: equilibrium and kinetic considerations. *Geochimica et Cosmochimica Acta* **48**, 1467–1477.
- Hart, S. R. & Dunn, T. (1993). Experimental cpx/melt partitioning of 24 trace elements. *Contributions to Mineralogy and Petrology* **113**, 1–8.
- Hauri, E. H., Wagner, T. P. & Grove, T. L. (1994). Experimental and natural partitioning of Th, U, Pb and other trace elements between garnet, clinopyroxene and basaltic melts. *Chemical Geology* **117**, 149–166.
- Henderson, P. (1982). *Inorganic Geochemistry*. Oxford: Pergamon Press.
- Hoover, J. (1989). The chilled marginal gabbro and other contact rocks of the Skaergaard intrusion. *Journal of Petrology* **30**(2), 441–476.
- Horn, I., Foley, S. F., Jackson, S. E. & Jenner, G. A. (1994). Experimentally determined partitioning of high field strength- and selected transition elements between spinel and basaltic melt. *Chemical Geology* **117**, 193–218.
- Hunter, R. H. & Sparks, R. S. J. (1987). The differentiation of the Skaergaard intrusion. *Contributions to Mineralogy and Petrology* **95**, 451–461.
- Jansen, B., Blok, A. & Scheelings, M. (1985). Geothermometry and geobarometry in Rogaland and preliminary results from the Bamble area, south Norway. In: Tobin, A. & Touret, J. L. R. (eds) *The Deep Proterozoic Crust in the North Atlantic Provinces*. NATO Advanced Study Institute C158. Dordrecht: D. Reidel, pp. 499–518.
- Jensen, J., Nielsen, F., Duchesne, J., Demaille, D. & Wilson, J. (1993). Magma influx and mixing in the Bjerkreim-Sokndal layered intrusion, south Norway: evidence from the boundary between two macrocyclic units at Storeknuten. *Lithos* **29**, 311–325.
- Johnson, K. T. M. & Kinzler, R. J. (1989). Partitioning of REE, Ti, Zr, Hf, and Nb between clinopyroxene and basaltic liquid: an ion microprobe study. *EOS Transactions, American Geophysical Union* **70**, 1388.
- Kennedy, A. K., Lofgren, G. E. & Wasserburg, G. J. (1993). An experimental study of trace element partitioning between olivine, orthopyroxene and melt in chondrules: equilibrium values and kinetic effects. *Earth and Planetary Science Letters* **115**, 177–195.
- Kolker, A. & Lindsley, D. H. (1989). Geochemical evolution of the Maloin Ranch pluton, Laramie Anorthosite Complex, Wyoming: petrology and mixing relations. *American Mineralogist* **74**, 307–324.
- Kolker, A., Lindsley, D. H. & Hanson, G. N. (1990). Geochemical evolution of the Maloin Ranch pluton, Laramie Anorthosite Complex, Wyoming: trace elements and petrogenetic models. *American Mineralogist* **75**, 572–588.
- Krause, H. & Pedall, G. (1980). Fe–Ti mineralizations in the Åna–Sira anorthosite, southern Norway. Metallogeny of the Baltic shield. In: Joakim-Siivola (ed.) *Geological Survey of Finland Bulletin* **307**, 56–83.
- Longhi, J. (1991). Comparative liquidus equilibria of hypersthene normative basalts at low pressure. *American Mineralogist* **76**, 785–800.
- Longhi, J. & Vander Auwera, J. (1992). Polybaric fractionation and the connection between high-Al gabbro and monzonite (abstract). *IGCP 290: Origin of Anorthosites and Related Rocks*, Liège: University of Liège.
- McKay, G., Wagstaff, J. & Yang, S. R. (1986). Zirconium, Hafnium, and Rare Earth partition coefficients for ilmenite and other minerals in high-Ti lunar mare basalts: an experimental study. *Proceedings of the 16th Lunar and Planetary Science Conference, Journal of Geophysical Research* **91**, Supplement, D229–D237.
- McKay, G. A. (1989). Partitioning of rare earth elements between major silicate minerals and basaltic melts. In: Lipin, B. R. & McKay, G. A. (eds) *Geochemistry and Mineralogy of Rare-earth Elements*. Mineralogical Society of America, *Reviews in Mineralogy* **21**, 45–78.
- McLelland, J., Ashwal, L. & Moore, L. (1994). Composition and petrogenesis of oxide-, apatite-rich gabbroanorthosites associated with Proterozoic anorthosite massifs: example from the Adirondack Mountains, New York. *Contributions to Mineralogy and Petrology* **116**, 225–238.
- Michot, J. & Michot, P. (1969). The problem of anorthosites. In: Isachsen, Y. (ed.) *Origin of Anorthosites and Related Rocks*. New York State Museum Science Service, *Memoir* **18**, 399–410.
- Michot, P. (1960). La géologie de la catazone: le problème des anorthosites, la paléogénèse basique et la tectonique catazonale dans le Rogaland méridional (Norvège méridionale). *Norges Geologisk Undersøkelse* **212**, 1–54.
- Mitchell, J. N., Scoates, J. S., Frost, C. D. & Kolker, A. (1996). The geochemical evolution of anorthosite residual magmas in the Laramie Anorthosite Complex, Wyoming. *Journal of Petrology* **37**, 637–660.
- Morse, S. A. (1982). A partisan review of Proterozoic Anorthosites. *American Mineralogist* **65**, 1087–1100.
- Nakamura, Y., Fujimaki, H., Nakamura, N., Tatsumoto, M., McKay, G. & Wagstaff, J. (1986). Hf, Zr, and REE partition coefficients between ilmenite and liquid: implications for lunar petrogenesis. *Proceedings of the 16th Lunar and Planetary Science Conference, Journal of Geophysical Research* **91**, Supplement D239–D250.
- Nielsen, R. L. (1990). Simulation of igneous differentiation processes. In: Nicholls, J. & Russell, J. K. (eds) *Modern Methods of Igneous Petrology: Understanding Magmatic Processes*. Mineralogical Society of America, *Reviews in Mineralogy* **24**, 65–105.
- Nielsen, R. L., Forsythe, L. M., Gallahan, W. E. & Fisk, M. R. (1994). Major- and trace-element magnetite–melt equilibria. *Chemical Geology* **117**, 167–191.
- Owens, B. E. & Dymek, R. F. (1992). Fe–Ti–P-rich rocks and massif anorthosite: problems and interpretation illustrated from the Labrieville and St-Urbain pluton. *Canadian Mineralogist* **30**, 163–190.
- Owens, B. E., Rockow, M. W. & Dymek, R. F. (1993). Jotunites from the Grenville Province, Quebec: petrological characteristics and implications for massif anorthosite petrogenesis. *Lithos* **30**, 57–80.
- Philpotts, A. R. (1981). A model for the generation of massif-type anorthosites. *Canadian Mineralogist* **19**, 233–253.
- Phinney, W. C. & Morrison, D. A. (1990). Partition coefficients for calcic plagioclase: implications for Archean anorthosites. *Geochimica et Cosmochimica Acta* **54**, 1639–1654.
- Ray, G. L., Shimizu, N. & Hart, S. R. (1983). An ion microprobe study of the partitioning of trace elements between clinopyroxene and liquid in the system diopside albite anorthite. *Geochimica et Cosmochimica Acta* **47**, 2131–2140.
- Roedder, E. (1979). Silicate liquid immiscibility in magmas. In: Yoder, H. S. (ed.) *The Evolution of the Igneous Rocks*. Princeton, NJ: Princeton University Press, pp. 15–57.
- Schärer, U., Wilmar, E. & Duchesne, J. C. (1996). The short duration and anorogenic character of anorthosite magmatism: U–Pb dating of the Rogaland complex, Norway. *Earth and Planetary Science Letters* **139**, 335–350.
- Steele, I. M. & Lindstrom, D. J. (1981). Ni partitioning between diopside and silicate melt: a redetermination by ion microprobe and recognition of an experimental complication. *Geochimica et Cosmochimica Acta* **45**, 2177–2183.
- Sun, S. S. & McDonough, W. F. (1989). Chemical and isotopic systematics of oceanic basalts: implications for mantle composition and processes. In: Saunders, A. D. & Norry, M. J. (eds) *Magma-tism*

- in the Ocean Basins. *Geological Society, London, Special Publication* **42**, 313–345.
- Thompson, R. N. (1982). British Tertiary volcanic province. *Scottish Journal of Geology* **18**, 49–107.
- Toplis, M. J. & Carroll, M. R. (1996). Differentiation of ferro-basaltic magmas under conditions open and closed to oxygen: implications for the Skaergaard intrusion and other natural systems. *Journal of Petrology* **37**, 837–858.
- Vander Auwera, J. & Longhi, J. (1994). Experimental study of a jotunite (hypersthene monzodiorite): constraints on the parent magma composition and crystallization conditions (P , T , fO_2) of the Bjerkreim-Sokndal layered intrusion (Norway). *Contributions to Mineralogy and Petrology* **118**, 60–78.
- Vander Auwera, J., Longhi, J. & Duchesne, J. C. (1993). Jotunites from the Rogaland Province (Norway): constraints from experimental data and the partitioning of Sr (plag/melt) and Cr (opx/melt). *EOS Transactions, American Geophysical Union* **74**, 659.
- Vander Auwera, J., Bologne, G., Roclandts, I. & Duchesne, J. C. (1998). Inductively coupled plasma-mass spectrometry (ICP-MS): analysis of silicate rocks and minerals. *Annales de la Société Géologique de Belgique* (in press).
- Watson, E. B. (1976). Two-liquid partition coefficients: experimental data and geochemical implications. *Contributions to Mineralogy and Petrology* **56**, 119–134.
- Watson, E. B. & Green, T. H. (1981). Apatite/liquid partition coefficients for REE and Sr. *Earth and Planetary Science Letters* **56**, 405–421.
- Wiebe, R. A. (1979). Fractionation and liquid immiscibility in an anorthositic pluton of the Nain Complex, Labrador. *Journal of Petrology* **20**, 239–269.
- Wiebe, R. A. (1990). Dioritic rocks in the Nain complex, Labrador. *Schweizerische Mineralogische und Petrographische Mitteilungen* **70**, 199–208.
- Wilmart, E. (1988). Étude géochimique des charnockites du Rogaland (Norvège méridionale). *Mémoire en Sciences de la Terre, Université Pierre et Marie Curie, Paris* **88-20**, 341 pp.
- Wilmart, E., Demaiffe, D. & Duchesne, J. C. (1989). Geochemical constraints on the genesis of the Tellnes ilmenite deposit, southwest Norway. *Economic Geology* **84**, 1047–1056.
- Wilson, J. R., Robins, B., Nielsen, F. M., Duchesne, J. C. & Vander Auwera, J. (1996). The Bjerkreim-Sokndal layered intrusion, Southwest Norway. In: Cawthorn, R. G. (ed.) *Layered Intrusions*. Amsterdam: Elsevier, pp. 231–255.

Some Phase Equilibrium Constraints on the Origin of Proterozoic (Massif) Anorthosites and Related Rocks

JOHN LONGHI¹*, JACQUELINE VANDER AUWERA²,
MIRANDA S. FRAM³ AND JEAN-CLAIR DUCHESNE²

¹LAMONT DOHERTY EARTH OBSERVATORY, RT. 9W, PALISADES, NY 10964, USA

²L.A. GÉOLOGIE, PÉTROLOGIE, GÉOCHIMIE, UNIVERSITÉ DE LIÈGE, 4000 LIÈGE, BELGIUM

³DEPARTMENT OF GEOLOGY, UNIVERSITY OF CALIFORNIA, DAVIS, CA 95616, USA

RECEIVED MAY 20, 1997; REVISED TYPESCRIPT ACCEPTED JUNE 26, 1998

Experimental data in the range of 1 bar to 13 kbar enable us to map the liquidus equilibria relevant to Proterozoic (massif) anorthosites and related mafic rocks. Massif anorthosites are widely believed to have formed by accumulation of plagioclase into high-Al basaltic liquids. Mantle-derived basaltic liquids, fractionating at pressures sufficiently high (10–13 kbar) to crystallize the highly aluminous orthopyroxene megacrysts typically observed in anorthosite massifs, reach plagioclase saturation at low normative silica contents. Peritectic-like equilibria (e.g. $liq + opx \rightarrow plag + cpx + sp$) and a thermal divide on the plagioclase + pyroxene liquidus surface ensure that mantle-derived liquids become nepheline normative with further crystallization and crustal assimilation at depth. Such liquids cannot produce the full range of troctolitic noritic to troctolitic gabbroic mineral assemblages observed in anorthosite massifs without extensive low-pressure granite assimilation. Conversely, the array of plausible anorthosite parental liquids not only lies along the trace of the plagioclase + two-pyroxene cotectic from 10 to 13 kbar, but also straddles the thermal divide on the plagioclase + pyroxene liquidus surface. This condition requires mafic source regions, such as lower continental crust or foundered mafic plutons, for liquids parental to massif anorthosites and associated mafic intrusions.

INTRODUCTION

There is hardly a consensus on the petrogenesis of Proterozoic (massif) anorthosites, but many investigators believe in a petrogenetic scheme that involves at least two major stages: (1) extensive crystallization (\pm assimilation) of a mantle-derived magma ponded at or near the base of the crust that produces suspensions of plagioclase in Fe-rich, high-Al gabbroic liquids; followed by (2) intrusion of these suspensions into the mid upper crust where they form complex magma chambers (e.g. Duchesne, 1984; Emslie, 1985; Ashwal, 1993; Wiebe, 1994). A key component of the scheme is the presence in most massifs of high-Al orthopyroxene megacrysts (HAOM, Emslie, 1975) that appear to preserve a record of the high-pressure stage (Maquil & Duchesne, 1984; Longhi *et al.*, 1993). The structures of massifs vary from those that are composites of multiple diapiric intrusions (Harp Lake, Emslie, 1980; Rogaland, Duchesne, 1984) to intrusive bodies with well-developed layering of leucocratic troctolites and leuconorites or leucogabbros overlain by masses of anorthosite (Michikamau, Emslie, 1970; Laramie, Frost *et al.*, 1993), so there may be different modes of transport of the suspensions through the crust. Associated mafic rocks are found on all scales from large layered intrusions, such as Kiglapait (Morse, 1979) and Bjerkreim-Sokndal (Duchesne, 1987; Wilson *et al.*, 1996), with dimensions on the same scale as the anorthositic bodies, to lenses, dikes, and small ferrodioritic

KEY WORDS: anorthosite; lower crust; megacryst; thermal divide; troctolite

*Corresponding author.

(jotunitic) to monzonitic (mangeritic) intrusions that appear to have formed from liquids residual to either the crystallization of the anorthositic masses (e.g. Mitchell *et al.*, 1996) or the more primitive mafic intrusion (e.g. Vander Auwera *et al.*, 1998). Many workers believe the parental magmas of the large layered intrusions to have been relatively plagioclase-free residual liquid from the deep-seated chambers (e.g. Wiebe, 1994). Finally, most workers ascribe formation of associated granitoids (quartz monzonite, charnockite) to melting of the lower crust (e.g. Emslie *et al.*, 1994), although some examples of continuous differentiation from jotunitic to charnockite exist (Vander Auwera *et al.*, 1998).

The major alternative to derivation of the anorthosites' parental magma from the mantle is melting of the lower crust. Trace element modelling provides the basis for this hypothesis (Simmons & Hanson, 1978; Taylor *et al.*, 1984), although there is some experimental work to support melting of the lower crust as well (Green, 1969).

Most anorthositic and related rocks have isotopic compositions that depart to some degree from depleted mantle evolution curves in the direction of crustal contamination—usually the mafic rocks are more contaminated—leading to the concept that most mafic rocks are 'coeval, but not consanguineous' with the anorthosites (e.g. Duchesne *et al.*, 1989). Where massifs lie on either side of a major tectonic boundary, there are systematic differences in the isotopic compositions that correlate with tectonic province (Ashwal & Wooden, 1983; Emslie *et al.*, 1994). Assimilation of different crustal types in the ponded, deep-seated chamber and possibly additional assimilation during transit of the magmas to the upper crust are believed to account for departures of the isotopic systems from mantle evolution curves (e.g. Emslie *et al.*, 1994).

The purpose of this paper is to examine the viability of evolved mantle-derived magmas as parental magmas not only to the anorthositic rocks, but to the mafic rocks and high-Al orthopyroxene megacrysts. To this end we have employed new and published experimental phase equilibrium data in the range of 1 bar to 13 kbar to map out permissible liquid lines of descent of mantle-derived magmas, to constrain the compositions of liquids parental to massif anorthosites based on crystallization sequences, and to predict the compositions of possible lower-crustal melts under anhydrous conditions. We have distinguished two groups of compositions for consideration on the basis of *mg*-number [molar $\text{MgO}/(\text{MgO} + \text{FeO})$] and the composition of the normative feldspar: a high-Al basaltic group (*mg*-number = 0.5–0.4; $\text{Ab}_{12-30}\text{Or}_{1-8}$) represented by HLCA, the proposed parent magma of the Harp Lake complex (Emslie, 1980), and a jotunitic group (*mg*-number = 0.4–0.25; $\text{Ab}_{51-60}\text{Or}_{9-20}$) represented by TJ, a chill margin sample from the Bjerkreim Sokndal intrusion of southern Norway (Duchesne & Hertogen,

1988). Although the liquidus temperatures of the jotunitic rocks are much lower than those of the HLCA group, their phase relations are broadly similar, and it is likely that the groupings represent distinct portions of a larger continuum of compositions.

EXPERIMENTAL METHODS

New experiments were carried out on a powdered rock from the Hettasch Intrusion in Nain, Labrador (Berg, 1980) and on a series of synthetic crystal–glass mixtures. The Hettasch sample (HT76E) is one of a series of samples from quenched pillow-like masses within the layered cumulates. Interpretations of these rocks range from chilled pulses of new liquid (Berg, 1980) to negatively buoyant mixtures of crystals and liquid detached from the top of the magma chamber. The synthetic materials include HLCA, the average high-Al gabbro and proposed parental magma composition of the Harp Lake anorthosite in Nain, Labrador (Emslie, 1980), and HLOL, a composition designed to yield olivine-bearing multi-saturated liquids at moderate pressures. A mechanical mixture of HLCA and HT76E was also used as starting material. The synthetic materials were fused mixtures of oxides and carbonates that were partially crystallized at the fayalite–magnetite–quartz (FMQ) buffer. All experiments were performed at Lamont Doherty Earth Observatory in a standard 1/2 inch piston cylinder apparatus, utilizing a BaCO_3 pressure medium, and calibrating pressure against the melting curve of gold, as described by Fram & Longhi (1992). Temperature was measured with Pt_{100} $\text{Pt}_{90}\text{Rh}_{10}$ thermocouples and power consumption was monitored to guard against thermocouple drift. Charges were run in unsealed graphite capsules. Comparison of oxide assemblages produced in graphite capsules at 5 kbar with 1 atm controlled $f\text{O}_2$ experiments indicates that $f\text{O}_2$ is approximately at MW (magnetite wüstite) 2 in the graphite capsule experiments (Vander Auwera & Longhi, 1994). Also, IR spectra of glass produced with the same assembly indicated $\leq 0.1\%$ each of H_2O and CO_2 (Fram & Longhi, 1992). Bulk compositions of the starting materials are listed in Table 1. Run conditions and phase assemblages are given in Table 2.

After each experiment, the charges were mounted in epoxy, polished and analyzed with the CAMEBAX electron microprobe utilizing the wavelength dispersive system. Accelerating voltage was set at 15 kV and all elements were measured for 20 s at a beam current of 25 nA except in the case of feldspars, phosphates, and glasses, when Na and K were measured first for 30 s at 5–10 nA. For glasses the beam was rastered over square areas 10–20 μm on a side to minimize alkali loss. X-ray intensities were reduced using the Cameca PAP

Table 1: Analyzed and nominal compositions of starting materials and parent magmas (wt % oxides)

	HL0L*†	HT80E*‡	HLCA*†	HT/HL§	TJ*‡	KIMOD¶
SiO ₂	46.9	46.9	50.0	48.9	49.5	49.1
TiO ₂	1.78	1.10	1.85	1.49	3.46	0.79
Al ₂ O ₃	16.7	19.6	17.5	18.7	16.0	18.7
Cr ₂ O ₃	0.03	0.02	0.03	0.02	0.00	
FeO	12.2	10.8	10.8	10.9	13.1	10.3
MgO	10.5	7.75	6.67	7.29	4.54	7.78
MnO	0.13	0.15	0.15	0.15	0.13	0.15
CaO	8.49	8.78	8.78	8.86	6.82	9.52
K ₂ O	0.47	0.40	0.44	0.42	0.94	0.27
Na ₂ O	2.85	2.82	2.93	2.90	3.65	3.08
P ₂ O ₅	0.18	0.15	0.16	0.16	0.63	0.11
Sum	100.2	98.5	99.5	99.8	98.8	99.8
mg-no.	0.607	0.539	0.520	0.544	0.383	0.574
NAb	0.428	0.391	0.423	0.399	0.506	0.409
NOr	0.046	0.034	0.042	0.038	0.089	0.065

mg-number = molar MgO/(MgO + FeO).

NAb = 2Na₂O/(Al₂O₃ + Na₂O + K₂O);

NOr = 2K₂O/(Al₂O₃ + Na₂O + K₂O).

* Analyzed compositions.

† Devitrified synthetic glass.

‡ Rock powder.

§ A 50:50 mixture of normalized HT80E and HLCA.

¶ Model Kiglapait parent magma from Nolan & Morse (1986).

correction program. A combination of mineral and glass standards were used for glass analyses, whereas only mineral standards were used for plagioclase, Fe-Ti oxides, pyroxenes, and olivines. Major element compositions of the experimental phases are reported in Table 3.

Mass balance between the bulk composition of the starting material and the compositions of all phases present in each run has been calculated using a least-squares multiple regression to determine phase proportions and to evaluate the approach to bulk equilibrium. Results are given in Table 2. In each case residual sums of the squares are acceptably low, but in some runs the regression yields negative amounts of low-Ca pyroxene. In the case of the runs with powdered rock starting materials (HT80E-1 and -5) the negative values for orthopyroxene are the result of the regression compensating for non-negligible proportions of relict olivine (armored by clinopyroxene) that is not included in the regression. In the case of run HLCA-53 the negative value for pigeonite (0.016) is probably the result of incomplete re-equilibration of the high-pressure phases grown in the first stage of this experiment (note the relatively high RSSQ in Table 2). In the case of run HL0L-3 the slightly negative proportion of orthopyroxene (0.0079) is probably a combination of a small analytical error and a reaction between orthopyroxene and liquid to form low-Ca clinopyroxene gone nearly to completion. Although the presence of relict olivine and calculated negative proportions of low-Ca pyroxene reflect incomplete bulk equilibration, it is very likely that these runs closely approached equilibrium

Table 2: Experiments and run conditions

Run	T (°C)	P (kbar)	Time (h)	Run products	Phase proportions*	RSSQ	$K_D^{opx-liq}$
HT80E-1	1265	11.5	51.5	gl, cpx, plag, sp, opx, [ol]	0.697, 0.225, 0.053, 0.042, -0.018†	0.03	0.281
HT80E-4	1300	13	53.5	gl, gar, cpx, plag, [ol]	0.744, 0.193, 0.046, 0.013	0.10	
HT80E-5	1265	10	49.0	gl, pig, plag, aug, sp, opx, [ol]	0.676, 0.240, 0.122, 0.055, 0.039, -0.135†	0.02	0.264
HT80E-6	1350/1265	13	2/92.5	gl, gar, cpx, plag	0.344, 0.342, 0.205, 0.110	0.20	
HT80E-7	1275	10	24.0	gl, opx, plag, sp	0.883, 0.047, 0.044, 0.025	0.05	0.279
HT/HL-1	1270	11.5	44.7	gl, plag, opx, cpx	0.628, 0.187, 0.094, 0.089	0.08	0.280
HLCA-25	1250	13	34.0	gl, plag, cpx, opx	0.674, 0.154, 0.136, 0.029	0.11	0.297
HLCA-44	1175	6	48.0	gl, plag, pig	0.326, 0.433, 0.232	0.14	
HLCA-53	1270/1200	11.5/6	72/116	gl, plag, opx, ol, pig	0.725, 0.194, 0.097, 0.007, -0.016	0.37	0.259
HLCA-55	1200/1260	6/11.5	67/119	gl, plag, cpx, opx	0.756, 0.118, 0.082, 0.046	0.11	0.279
HL0L-3	1265	11.5	49.0	gl, cpx, sp, opx	0.573, 0.402, 0.039, -0.007	0.55	0.249
HL0L-4	1300	11.5	29.5	gl, cpx, opx, sp	0.807, 0.146, 0.035, 0.014	0.14	0.289

gl, glass; ol, olivine; opx, orthopyroxene; cpx, clinopyroxene; aug, augite; gar, garnet; sp, spinel; [], relict mineral; plag, plagioclase; pig, pigeonite. RSSQ, residual sum of squares in regression of phase proportions. $K_D^{opx-liq} = [(FeO)^{opx}/(FeO)^{liq}] \times [(MgO)^{liq}/(MgO)^{opx}]$.

*Weight fraction of phases in order listed under 'run products'; where available, analyzed bulk compositions (Table 1) are used in the regressions.

†Negative opx compensates for relict olivine that is not included in the regressions.

Table 3: Composition of phases in weight percent oxides

Run	Phase	Pts*	SiO ₂	TiO ₂	Al ₂ O ₃	Cr ₂ O ₃	FeO	MgO	MnO	CaO	K ₂ O	Na ₂ O	P ₂ O ₅	Sum
HLOL-3	liq	5	47.6(3)†	2.43(5)	17.8(2)	0.01(1)	13.0(1)	5.57(9)	0.12(2)	7.45(5)	0.78(2)	3.88(15)	0.25(2)	98.8
	opx	6	50.1(1.1)	0.49(9)	8.78(1.57)	0.06(2)	14.2(5)	24.4(7)	0.14(1)	1.94(11)		0.18(1)		100.3
	cpx	7	49.2(4)	0.85(7)	9.74(25)	0.07(3)	11.7(3)	16.8(5)	0.16(4)	10.8(4)		0.87(4)		100.1
	sp	4	46(16)	0.46(4)	62.4(7)	0.83(41)	18.8(2)	17.2(3)	0.06(1)	0.14(3)		0.02(1)		100.3
HLOL-4	liq	8	46.1(2)	1.97(3)	17.4(1)	0.03(3)	12.5(1)	7.80(5)	0.15(2)	8.67(7)	0.58(2)	3.08(5)	0.19(1)	98.5
	cpx	18	49.1(7)	0.66(6)	8.56(41)	0.08(4)	10.5(4)	19.6(8)	0.16(2)	9.08(87)		0.55(5)		98.3
	opx	3	51.6(1.2)	0.37(8)	6.46(2.15)	0.10(2)	12.1(3)	26.1(7)	0.13(2)	2.27(7)		0.15(1)		99.3
	sp	6	0.27(9)	0.40(13)	63.0(1.4)	1.51(1.05)	15.3(4)	19.0(5)	0.10(2)	0.10(3)		0.01(1)		99.6
HT80E-1	liq	6	48.0(0)	1.29(3)	18.3(1)	0.01(1)	12.7(2)	5.58(4)	0.15(1)	7.89(6)	0.60(4)	3.55(8)	0.22(6)	98.3
	cpx	9	47.3(8)	0.58(7)	12.3(1.2)	0.02(1)	11.4(5)	15.2(5)	0.20(2)	11.3(1.1)		0.85(5)		99.3
	opx	7	49.3(8)	0.35(8)	11.0(1.0)		15.0(3)	23.4(5)	0.22(1)	2.05(26)		0.18(2)		101.5
	opx†	1	52.9(0)	0.20(0)	8.42(0)		10.3(0)	28.3(0)	0.19(0)	2.21(0)		0.13(0)		102.7
	olt	1	38.0(0)	0.00(0)	0.00(0)	0.04(0)	27.6(0)	36.2(0)	0.24(0)	0.26(0)		0.03(0)		102.4
	sp	6	0.18(10)	0.21(1)	65.8(1.5)	0.39(36)	18.2(1)	17.1(2)	0.10(2)	0.07(3)		0.01(1)		102.0
	plag	10	54.8(8)		29.0(5)		0.43(4)	0.16(17)		11.4(6)	0.24(6)	4.98(26)		101.0
HT80E-4	liq	5	48.2(1)	1.19(3)	18.5(1)	0.01(1)	11.6(1)	5.77(6)	0.12(1)	8.56(7)	0.51(0)	3.62(6)	0.23(1)	98.3
	gar	6	40.2(5)	0.63(11)	23.9(1)	0.03(2)	14.2(2)	15.0(3)	0.33(1)	6.48(18)		0.02(1)		100.8
	cpx	7	47.4(6)	0.54(8)	13.1(5)	0.02(2)	8.18(59)	13.7(2)	0.14(1)	15.1(6)		1.08(5)		99.2
	plag	12	52.8(1.4)	0.03(2)	29.5(9)		0.49(8)	0.09(3)		12.3(1.0)	0.21(5)	4.24(57)		99.6
HT80E-5	liq	6	47.2(3)	1.37(7)	17.8(1)	0.02(1)	13.3(1)	6.09(5)	0.18(2)	8.44(7)	0.51(2)	3.40(8)	0.23(2)	98.5
	aug	10	48.6(8)	0.68(20)	10.1(1.0)	0.03(2)	10.7(6)	16.0(7)	0.20(3)	12.6(9)		0.73(14)		99.6
	opx	4	49.7(8)	0.45(22)	9.31(1.24)	0.00(0)	13.9(5)	24.1(8)	0.19(1)	2.04(10)		0.11(2)		99.9
	pig	1	49.7(0)	0.41(0)	7.96(0)	0.00(0)	14.0(0)	21.8(0)	0.23(0)	4.50(0)		0.21(0)		98.9
	plag	11	53.1(1.3)	0.04(2)	29.3(8)		0.48(6)	0.09(2)		12.1(9)	0.24(5)	4.31(44)		99.6
HT80E-6	liq	8	49.4(5)	1.53(4)	18.4(1)	0.00(0)	11.1(1)	3.81(5)	0.07(1)	6.45(5)	1.17(4)	5.21(12)	0.53(4)	97.6
	cpx	8	48.2(4)	0.94(8)	12.0(7)	0.02(1)	9.98(74)	11.9(5)	0.14(3)	14.5(8)		1.47(6)		99.2
	gar	5	40.0(3)	0.71(14)	22.5(2)	0.03(1)	17.4(3)	12.4(2)	0.29(2)	6.65(11)		0.02(1)		100.0
	plag	6	57.0(4)	0.08(1)	27.3(2)		0.46(8)	0.07(2)		9.06(20)	0.36(2)	5.75(14)		100.1
HT80E-7	liq	7	46.8(2)	1.09(4)	18.0(0)	0.01(1)	12.2(1)	6.88(4)	0.14(2)	9.11(7)	0.40(3)	3.10(8)	0.19(1)	98.0
	opx	6	50.0(6)	0.27(3)	9.06(52)	0.02(1)	12.4(3)	25.0(3)	0.18(1)	2.14(15)		0.10(1)		99.1
	sp	5	0.06(8)	0.19(2)	65.9(1.2)	0.18(5)	15.2(2)	17.2(3)	0.10(1)	0.07(2)		0.00(0)		98.0
	plag	6	52.1(4)	0.06(1)	29.7(2)		0.43(10)	0.16(3)		12.5(2)	0.15(2)	3.99(14)		99.1
HT/HL-1	liq	6	48.0(1)	1.29(3)	18.3(1)	0.01(1)	12.7(2)	5.58(4)	0.15(1)	7.89(6)	0.60(4)	3.55(8)	0.22(6)	98.3
	opx	9	49.2(51)	0.38(5)	9.47(92)	0.12(6)	14.9(3)	23.4(3)	0.20(3)	2.05(23)		0.12(1)		99.8
	cpx	5	48.8(8)	0.65(12)	9.94(97)	0.13(2)	11.6(9)	16.4(1.4)	0.22(2)	10.9(1.8)		0.69(11)		99.5
	plag	10	54.1(1.1)	0.00(0)	29.3(7)		0.55(6)	0.13(2)		11.8(8)	0.20(3)	4.77(52)		100.8
HLCA-25	liq	6	49.0(2)	2.33(7)	18.6(1)	0.01(1)	12.4(1)	5.27(6)	0.17(1)	8.23(5)	0.62(4)	2.98(11)	0.19(2)	97.9
	cpx‡	8	48.6(7)	0.76(9)	9.75(82)	0.21(6)	13.1(8)	16.7(9)	0.23(2)	9.65(1.42)		0.61(10)		99.6
	opx	5	49.7(5)	0.50(5)	9.06(58)	0.25(9)	15.5(7)	22.2(5)	0.19(3)	2.29(45)		0.15(2)		99.9
	plag	10	54.5(1.0)	0.11(1)	27.8(4)		0.71(5)	0.11(2)		10.8(5)	0.27(2)	4.92(26)		99.3

with respect to the crystalline phases in contact with liquid. For example, sample HT80E is a troctolite, but olivine is clearly not stable in any of the runs at 10–13 kbar, thus demonstrating the instability of olivine in plagioclase-saturated liquids of this general type at pressures ≥ 10 kbar. On the other hand, neither aluminous spinel nor garnet is present in the starting rock material, yet they grow readily and mutually exclusively at 10–11.5 and 13 kbar, respectively. Furthermore, the Fe–Mg exchange coefficient (K_D) for orthopyroxene–liquid pairs

(Table 2) has a limited range of values that is approximately the same for isothermal experiments with devitrified glass starting material (0.297–0.249) as it is for polythermal experiments or those with powdered rock starting material (0.281–0.259). These observations are consistent with our previous work based on reversals of plagioclase and orthopyroxene compositions, demonstrating that isothermal experiments on devitrified glass starting materials produced equilibrium phase assemblages and compositions (mantles, rims) in runs with

Run	Phase	Pts*	SiO ₂	TiO ₂	Al ₂ O ₃	Cr ₂ O ₃	FeO	MgO	MnO	CaO	K ₂ O	Na ₂ O	P ₂ O ₅	Sum
HLCA-44	liq	4	45.8(1.1)	4.00(42)	12.2(1.5)	0.00(0)	20.9(1.3)	4.30(75)	0.23(2)	7.47(60)	1.12(31)	3.42(82)	0.35(5)	99.8
	plg	8	52.0(4)	0.71(7)	3.23(47)	0.14(4)	16.9(2)	21.8(4)	0.30(2)	3.95(47)		0.16(4)		99.2
	plag	4	53.8(6)	0.28(9)	28.7(4)		1.20(33)	0.43(11)		11.6(34)	0.36(12)	4.48(8)		100.9
HLCA-53	liq	4	48.1(3)	2.74(5)	15.4(1)	0.15(2)	12.7(1)	5.94(5)	0.34(1)	8.41(7)	0.69(9)	3.56(7)	0.40(1)	98.4
	opx	16	52.9(5)	0.83(4)	4.70(69)	0.35(5)	14.2(4)	25.6(4)	0.38(3)	2.26(28)		0.15(2)		101.4
	plg	1	53.3(0)	0.40(0)	2.99(0)	0.28(0)	14.1(0)	26.2(0)	0.28(0)	3.72(0)		0.15(0)		101.4
	ol	3	38.3(0)	0.07(3)	0.10(4)	0.03(1)	25.7(4)	37.4(6)	0.28(1)	0.36(4)				102.2
	plag	7	53.5(5)	0.09(2)	30.0(3)		0.46(4)	0.12(1)		12.4(2)	0.19(3)	4.38(15)		101.1
HLCA-55	liq	5	48.8(2)	2.59(1)	17.2(1)	0.14(2)	12.1(2)	5.56(5)	0.29(3)	8.43(3)	0.67(4)	3.06(16)	0.39(2)	99.2
	cpx	3	49.1(1.1)	0.71(4)	8.93(31)	0.24(6)	12.1(5)	17.0(3)	0.23(4)	11.6(7)		0.68(2)		100.6
	opx	11	51.0(5)	0.31(13)	8.06(42)	0.26(8)	14.8(7)	24.4(2)	0.22(3)	2.20(13)		0.16(2)		101.5
	plag	12	54.7(4)	0.03(1)	28.8(3)		0.50(9)	0.13(3)		11.4(1)	0.20(4)	4.60(20)		100.4

Abbreviations as in Table 2. Blanks indicate element not analyzed.

* Number of spots or areas analyzed.

† Units in parentheses are 1 SD of replicate analyses in terms of least unit(s) cited.

‡ Relict mineral grain.

§ Possibly two near-critical clinopyroxenes present.

≥60% liquid on a time scale of 1–2 days (Longhi *et al.*, 1993). Therefore, we are confident of the reported phase assemblages and liquid compositions in all of the runs, but would caution against the use of crystal/liquid partitioning data derived from runs with ≤60% liquid or from polythermal runs.

RESULTS

Although we have new data at several pressures, the most complete set is for the HLCA series at 11.5 kbar. Accordingly, we will illustrate these data first, and then go on to examine the effects of pressure and composition. The compositions of coexisting crystals and liquids from the HLCA series at 11.5 kbar are shown in two projections of the quartz/olivine/plagioclase/wollastonite (Qtz–Ol–Pl–Wo) system (Longhi, 1991) in Fig. 1. The HLCA series liquids have the characteristics expected of moderately evolved basalts: intermediate *mg*-number (0.5–0.4) and intermediate normative feldspar ($Ab_{10-30}Or_{70}$). Although the liquids in this figure are not saturated with ilmenite, the compositions are projected from an ilmenite component ($[Fe,Mg]TiO_3$) for the sake of consistency with subsequent figures, which illustrate jotunitic compositions that are saturated with ilmenite. In this figure and in those that follow, we will try to limit the range of *mg*-number and normative feldspar composition as much as possible. This means that the diagrams are a useful means of predicting phase saturation and the nature of invariant points for a family of compositions, but because the liquidus boundaries shift with composition, the fractionation paths of individual compositions will in general

diverge from the depicted liquidus boundaries [see fig. 5 of Longhi (1991)]. Also, because it is not feasible to make *mg*-number and normative feldspar composition precisely constant everywhere even with multiple bulk compositions, it is inevitable that low-temperature portions of some liquidus boundaries may have been defined with experimental liquids having higher *mg*-number or more anorthitic normative feldspar than liquids used to define the ostensibly higher temperature portions of the same or a related boundary. Thus it is possible that the reported temperatures of some of the experimental liquids may apparently violate the direction of falling temperature inferred from the topology of the coexisting phases. In such cases, the reader should keep in mind that the boundary curves are not strictly isobaric-univariant, and topology takes precedence.

Figure 1a illustrates the array of liquidus boundaries saturated with augitic clinopyroxene. Projecting from the Wollastonite ($Wo = CaSiO_3$) component rather than Diopside is useful when clinopyroxene (*cpx*) is a late-crystallizing phase in the experiments, because the Wo projection causes less parallax dispersion of the subjacent, clinopyroxene-absent liquidus surfaces, e.g. the olivine (*ol*) + plagioclase (*plag*) liquidus surface projects as a narrow band under the *ol* + *plag* + *cpx* liquidus boundary curve rather than as a broad band off to the side [see fig. 10 of Longhi (1987)]. This feature makes the Wo projection useful in representing the limits of the primary liquidus volumes of compositions with relatively low Wo contents. Pyroxene compositions in Fig. 1a plot approximately on the trace of the Orthopyroxene ($Opx = [Mg,Fe]_2Si_2O_6$)–Mg-Tschermak ($[Mg,Fe]Al_2SiO_6$) join.

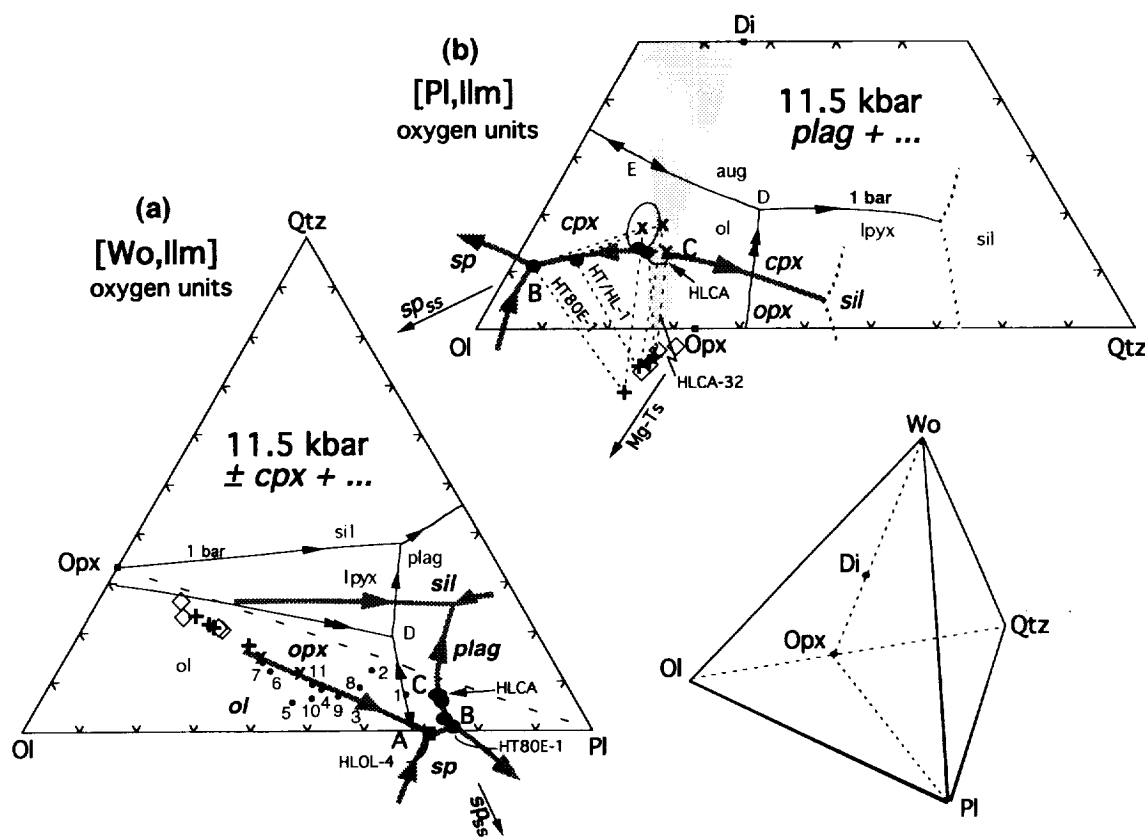


Fig. 1. Liquidus equilibria at 11.5 kbar projected into the model system olivine plagioclase wollastonite ilmenite orthoclase quartz (Ol-Pl-Wo-Ilm-Or-Qtz) in terms of oxygen units, modified after Longhi (1991). (a) Subprojection of clinopyroxene-saturated and -undersaturated liquidus boundaries from the Wo, Or and Qtz components onto the plane Ol-Pl-Qtz. (b) Subprojection of plagioclase-saturated liquids and crystals from the Pl, Or and Ilm components onto the Ol-Qtz-Wo plane. Light continuous lines show augite-saturated and plagioclase-saturated liquidus boundaries at 1 bar calculated for HLCA-like compositions (mg -number = 0.52, NAb = 0.42, NOr = 0.04) from the algorithms of Longhi (1991). Bold lines show 11.5 kbar liquidus boundaries based on data from Fram & Longhi (1992) and this study. Arrows show direction of decreasing temperature; double arrows indicate a reaction boundary. 'sil' refers to silica phase – cristobalite, tridymite, or quartz. Experimental data: ●, liq (+ aug + lpx + $plag$); ■, liq (+ aug + lpx + sp); ○, liq (+ lpx + $plag$); ×, cpx ; +, opx ; ◇, opx megacryst compositions with mg -number ≥ 0.70 from Emslie (1980) and Maquil & Duchesne (1984). Numbered dots are primitive magma compositions from Basaltic Volcanism Study Project (BVSP) (1981): 1 and 2, mid-ocean ridge basalt (MORB) (cols 1 and 4, table 1.2.5.3); 3–7, continental flood basalts (Svartenhuk and Baffin Island *ol*-tholeiites, table 1.2.3.7; cols 15 and 16, table 1.4.2.1; col. 2, table 1.2.2.10); 8 and 9, Hawaiian tholeiites (cols 1 and 2, table 1.2.6.14); 10, Gorgona basaltic komatiite (col. 9, table 1.4.2.1); 11, high-Mg ophiolite dike (col. 11, table 1.2.5.3). Shaded area is the range of clinopyroxene solid solution. Ellipse shows the range of cpx analyses in run HT80E-1. Dashed lines connect coexisting phases. A, B, C, D, E are pseudo-invariant points described in the text. Projection equations, oxygen units:

$$Ol[Wo,Ilm] = 2(FeO + MgO + MnO - TiO_2) / \Sigma[Wo,Ilm]$$

$$Pl[Wo,Ilm] = 8(Al_2O_3 + Na_2O - K_2O) / \Sigma[Wo,Ilm]$$

$$Qtz[Wo,Ilm] = [2SiO_2 - (FeO + MgO + MnO - TiO_2) - 2Al_2O_3 - 2CaO - 10(Na_2O + K_2O)] / \Sigma[Wo,Ilm]$$

$$Ol[Pl,Ilm] = 2(FeO + MgO + MnO - TiO_2) / \Sigma[Pl,Ilm]$$

$$Wo[Pl,Ilm] = 3(CaO - Al_2O_3 + Na_2O + K_2O) / \Sigma[Pl,Ilm]$$

$$Qtz[Pl,Ilm] = [2SiO_2 - (FeO + MgO + MnO - TiO_2) - 2Al_2O_3 - 2CaO - 10(Na_2O + K_2O)] / \Sigma[Pl,Ilm]$$

where $[Wo,Ilm]$ and $[Pl,Ilm]$ identify the main projection components, $\Sigma[Wo,Ilm]$ and $\Sigma[Pl,Ilm]$ refer to the sums of the right-hand sides of the equations, and the oxides are mole fractions.

which crosses the base of the triangle at $Ol_{0.333}Pl_{0.667}$. Figure 1b illustrates a more conventional projection from the Plagioclase and Ilmenite components $[Pl,Ilm]$ of

phase relations on the plagioclase liquidus surface. The compositions of clinopyroxene coexisting with orthopyroxene (opx) and/or spinel (sp) define the limits of the

shaded *cpx* solid solution field. Pyroxene phase relations are rather complex for the compositions considered here: at pressures ≥ 10 kbar clinopyroxenes in HLCA-like composition appear to have a continuous (or nearly so) range of composition between Di and Opx; whereas at lower pressures (see below) distinct high- and low-Ca clinopyroxenes are stable. Following the convention of Longhi & Bertka (1996), we will refer to apparently hypersolvus clinopyroxene as *cpx*, and reserve the terms augite (*aug*) and pigeonite (*pig*) for subsolvus clinopyroxene. Where the *cpx* solid solution is not continuous, there may be two closely spaced liquidus curves involving two pyroxenes for liquids with intermediate *mg*-number, *opx* + *pig* + *plag* and *pig* + *aug* + *plag*; whereas for more magnesian or more ferroan compositions there may be only one two-pyroxene curve, *opx* + *aug* + *plag* (*pig* stable only in *plag*-undersaturated liquids) or *pig* + *aug* + *plag* (*opx* unstable), respectively [see Longhi (1991)]. To avoid unnecessary complexity, we will depict only one two-pyroxene liquidus curve at a time, and we will refer to low-Ca pyroxene (*lpx*) to signify either *opx* or *pig*. In Fig. 1 and subsequent figures the compositions of all clinopyroxenes are represented with a 'x', whereas orthopyroxene is marked by a '+'.

The new data plus data from Bartels *et al.* (1991) and Kinzler & Grove (1992) constrain the nature of three pseudo-invariant points involving olivine, orthopyroxene, clinopyroxene, plagioclase, and aluminous spinel. One is a *plag*-absent *ol* peritectic (A): *liq* + *ol* = *opx* + *cpx* + *sp*. The second is an *ol*-absent *opx* peritectic (B): *liq* + *opx* = *cpx* + *plag* + *sp*. The third is a thermal maximum (C) on the *plag* + *opx* + *cpx* liquidus boundary where the compositions of crystals and liquid are coplanar (note the coplanar arrangement can be adequately depicted only in the [Pl,Ilm] projection). Even though the *cpx* compositions in runs HT80E-1 and the HT/HL-1 do not define tight limits on *cpx* solid solution (because of incomplete equilibration of the clinopyroxene in the charges containing natural rock powders), the data for these runs plus HLCA-32 (Fram & Longhi, 1992) describe three three-phase triangles with the *liq* corners pointing away from Qtz. However, the HLCA-32 three-phase triangle is nearly collapsed to the *opx* + *cpx* tie-line. It should be obvious, therefore, that an apparent collinearity of coexisting pyroxenes and liquid occurs on the *plag* + *opx* + *cpx* liquidus boundary slightly to the right of the HLCA-32 liquid point and that a set of three-phase triangles pointing toward Qtz must exist for liquids on this curve to the right of the Opx-Di join. The locus of the apparent collinearity on the boundary curve is a thermal maximum and has a temperature $\geq 1275^\circ\text{C}$ (run HLCA-32) for liquids with similar *mg*-number and alkalis. Baker & Eggler (1987; fig. 5) have demonstrated

the existence of this thermal maximum in melts of calc-alkaline basalts at 8 kbar and their data are illustrated below.

The nature of point A is well known from other studies (e.g. Kinzler & Grove, 1992), but may be partially inferred by noting that in Fig. 1a the compositions of liquid, orthopyroxene, olivine, and spinel describe the corners of an irregular quadrilateral with liquid and olivine at opposite corners. Analogously, the *opx* + *liq* reaction at point B may be inferred in Fig. 1b by observing that the coexisting *opx* and *liq* compositions lie at opposite corners of a quadrilateral with the *aug* and *sp* compositions at the other two corners.

The array of liquidus curves constrains the crystallization paths of basaltic magmas and the permissible range of crustal melts. Initially *ol*-saturated liquids, crystallizing either *ol* + *opx* + *cpx* or *ol* + *cpx* + *sp*, will reach point A (Fig. 1a), react out olivine, and crystallize an interval of *opx* + *cpx* + *sp* before reaching point B. It is possible that for some compositions *opx* will be in reaction with liquid between A and B (*opx* + *liq* \rightarrow *cpx* + *sp*) — it should be noted in Table 2 that the proportion of *opx* decreases between 1300°C (HL01-4) and 1265°C (HL01-3) — so some fractionating liquids may reach *plag* saturation with only *cpx* stable. At B any orthopyroxene reacts out and further crystallization proceeds along the *cpx* + *plag* + *sp* cotectic, away from the Qtz and Opx components. In this way it is possible to produce high- Al_2O_3 liquids (≥ 18 wt % Al_2O_3) that are also nepheline-normative (liquids that lie to the low-silica side of the Ol-Di join in Fig. 1b) and a series of cumulates that begin with either spinel wehrlite or olivine pyroxenite, followed by spinel pyroxenite (A \rightarrow B), and then spinel gabbro. The data of Kinzler & Grove (1992) and Walter & Presnall (1994) show that for liquids with similar normative feldspar, but higher *mg*-number, all five crystalline phases may coexist with liquid. In these cases, three dimensions are not adequate to represent the liquidus boundaries as curves; and, instead of the *liq* + *opx* + *cpx* + *sp* curve joining the *ol* and *plag* surfaces, portions of the *ol* and *plag* surfaces will overlap with a smeared-out combination of points A and B (*liq* + *ol* + *opx* + *cpx* + *sp*) joining *plag*-free portions of the *ol* saturation surface to *ol*-free portions of the *plag* saturation surface. The net result of these two topologies is similar: initially *ol*-saturated, fractionating liquids will eventually wind up on the *ol*-absent portion of the *plag* saturation surface. Because of the plagioclase + pyroxene thermal divide (C), however, there is no way for a fractionating basaltic liquid to move toward the Qtz component. Conversely, low-degree melts of crustal rocks containing plagioclase and orthopyroxene may access a wide range of Qtz contents. Such melts are restricted to only the vicinity of the *plag* + *opx* + *cpx* liquidus boundary, which extends from high- SiO_2 granitic compositions

at silica saturation to high- Al_2O_3 , nepheline-normative compositions at spinel saturation.

To discuss crystallization and melting paths throughout the crust, we must first understand how the topologies shown in Fig. 1 change with pressure. The topologies of the *aug* and *plag* saturation surfaces are well known at 1 bar over a range of composition (e.g. Grove & Juster, 1989; Longhi, 1991), so intermediate topologies between 1 bar and 11.5 kbar may be interpolated and successive topologies extrapolated to higher pressures. Once a given topology is recognized, its compositional and pressure range may even be constrained by a single key experimental datum. In this way a progression of phase diagrams has been constructed from 1 bar to 13 kbar and illustrated in Fig. 2 for liquids with the same general character (intermediate *mg*-number and normative feldspar) as those in Fig. 1. Figure 3 illustrates a similar set of constructions for jotunitic liquids, which have lower *mg*-number (0.4–0.25) and more alkaline normative feldspar ($\text{Ab}_{30}\text{Or}_{70}$). The bulk compositions of H1CA and TJ are plotted for reference in all panels of Figs 2 and 3, respectively.

The progressions of topologies in Figs 2 and 3 are relatively similar: in the [Wo, Ilm] projections (Figs 2a and 3a) the major features are the shift of the *ol* + *lpx* + *aug* + *liq* boundary away from the Qtz component with increasing pressure (where *lpx* signifies orthopyroxene and/or pigeonite); whereas in the [Pl, Ilm] projections (Figs 2b and 3b) the major feature is the shift of the *ol* + *lpx* + *plag* + *liq* boundary away from Qtz. In both projections the *lpx* and *sp* saturation surfaces eventually intersect and with still higher pressure garnet (*gar*) replaces spinel. At 1 bar the *ol* + *plag* + *lpx* + *aug* + *liq* pseudo-invariant point (D) is an *ol* peritectic and there is a thermal maximum on the *ol* + *plag* + *aug* + *liq* boundary (E) that separates liquids that may fractionate to *lpx* saturation from those that fractionate toward nepheline saturation. By 5 kbar, point D has migrated across the pyroxene-plagioclase plane (the trace of Opx Pl in Figs 2a and 3a or the Opx Di join in Figs 2b and 3b). This movement precipitates two changes: first, a thermal maximum (C) is exposed on the *lpx* + *aug* + *plag* + *liq* boundary curve where the liquid composition appears to be collinear with those of the coexisting *lpx* and *aug*; and second, because the *ol* + *plag* + *lpx* + *aug* + *liq* pseudo-invariant point (D) now lies between two thermal maxima, D must be a eutectic. If the *ol* + *plag* + *lpx* + *liq* boundary is curved as shown in Figs 2b and 3b, then the boundary curve crosses the line of pyroxene solid solutions at an angle, which enables olivine to be in reaction with liquid along the low Wo portion of the curve and to crystallize from liquids along the high Wo portion of the boundary. Thus at the same pressure there can be similar liquids, differing

only slightly in Wo content, with very different crystallization paths: one that produces marked silica enrichment and *qtz*-bearing assemblages, whereas the other produces little or no silica enrichment and *ol*-bearing assemblages. These paths will be illustrated below.

By 6 kbar (Figs 2b and 3b) point D has overtaken the *ol* + *plag* + *aug* + *liq* thermal maximum (E). Once it does, the *ol* + *plag* + *aug* + *liq* thermal maximum (E) disappears and the equilibrium relations at point D must necessarily change to an *opx*(*lpx*) peritectic (Fig. 2b, 8 kbar). With further increases in pressure, the *lpx* and *sp* fields intersect (~10 kbar) and separate the *ol* and *plag* liquidus fields as described above, generating pseudo-invariant points A and B (see Fig. 1a). The disposition of coexisting *opx*, *opx*, *sp*, and *liq* (B) compositions at 10 and 11.5 kbar in Fig. 2b is also quadrilateral and, thus, B remains an *opx*(*lpx*) peritectic. By 13 kbar garnet has replaced spinel in pyroxene-saturated liquids on the plagioclase surface; but none the less, the new pseudo-invariant point involving garnet (B') remains an *opx* peritectic. Other important shifts in liquidus boundaries with increasing pressure include movement of the *plag* + *lpx* + *aug*/*opx* liquidus boundary away from Wo in the [Pl, Ilm] projections and away from Opx in the [Wo, Ilm] projections. The movement of the *plag* + *lpx* + *aug* liquidus boundary away from Opx in the [Wo, Ilm] projections is apparently much greater in high- than in low-silica compositions such that an inflection of the curve occurs in the vicinity of the plagioclase + pyroxene thermal divide.

Although these shifts in liquidus boundaries are general features of basalts, the shifts are compositionally dependent. Specifically, for liquids with higher *mg*-number the boundary curves involving olivine and low-Ca pyroxene project at higher Qtz contents and the *lpx* + *augite* boundary lies at higher Wo, as illustrated in Fig. 2 with 10 kbar data (dashed lines) from Bartels *et al.* (1991; run H142). Consequently, the transitions in topology described above take place at higher pressures in more magnesian liquids and, in extreme cases, may not occur at all. For example, the data from run H130 [*mg*-number(*liq*) = 0.64] of Kinzler & Grove (1992) show the transition of point D from a eutectic to an *opx* peritectic occurring at 9 kbar (their fig. 1) vs at ~6 kbar for the less magnesian compositions of the present study, whereas, in the CMAS system, the data of Presnall *et al.* (1979) and Walter & Presnall (1994) show that point D crosses neither the Ol Pl Di join nor the line of coexisting *opx* and *aug* (diopside); consequently, D remains an *ol* peritectic until spinel separates the liquidus volumes of olivine and anorthite at 9.3 kbar. The *mg*-number value of 0.64 from run H130 is a likely upper limit to the *mg*-number of *plag*-saturated liquids at lower-crustal pressures because ascending mantle-derived melts are likely to be saturated only in olivine and will thus require moderate

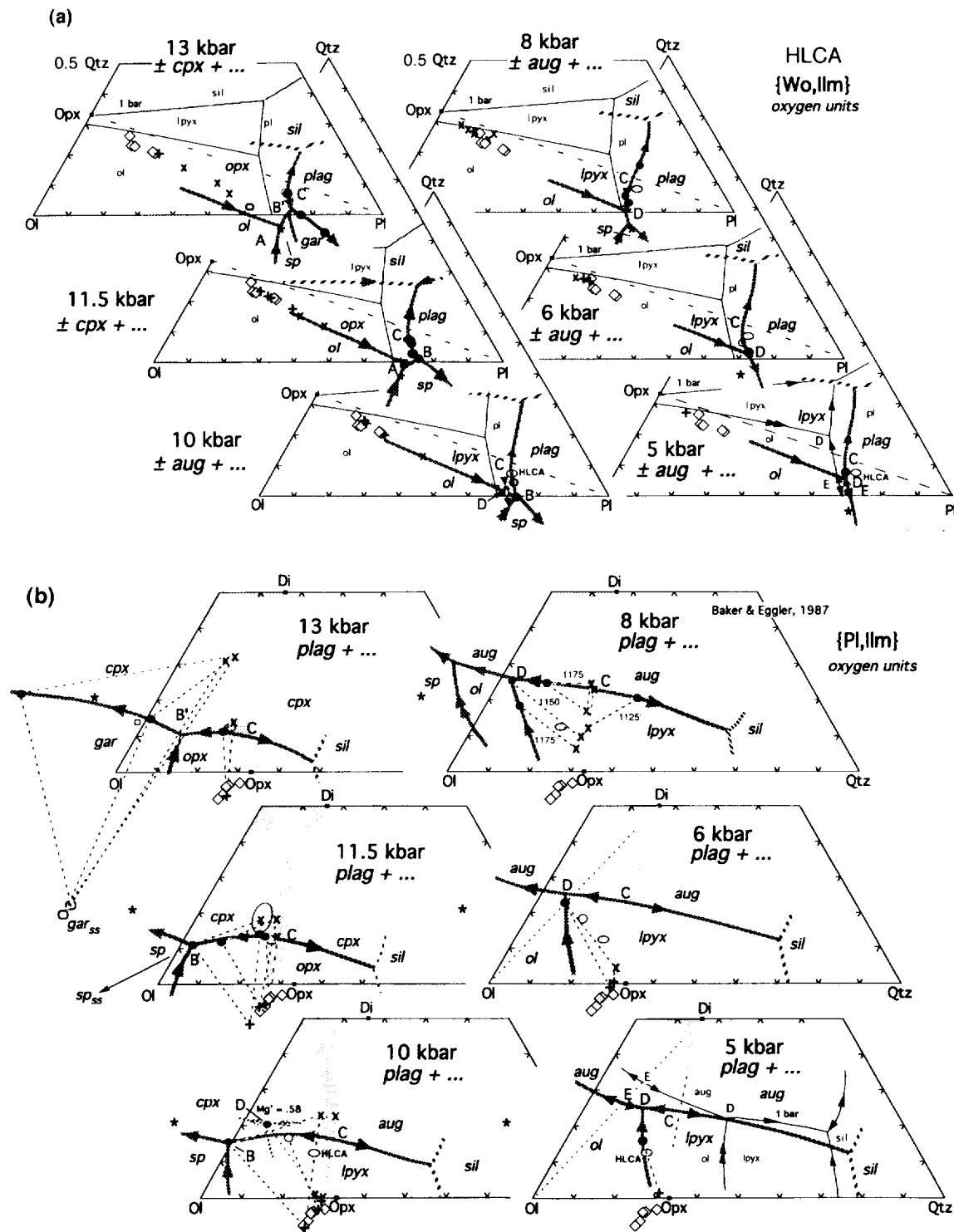


Fig. 2. Progression of liquidus equilibria and solid solutions for HLCA-like compositions from 1 bar to 13 kbar. Projection schemes as in Fig. 1. Light solid lines in 5 kbar panel are 1 bar liquidus boundary curves. \bullet , liq (+ aug/cpx + lpyx + plag) or liq (+ ol + lpyx + plag); blunted ellipses are garnet compositions; \circ , liq (+ lpyx + plag); shaded areas indicate estimated limits of clinopyroxene solid solution; dashed curves indicate estimated positions of liquidus boundaries; shaded diamond, HXOM 860C from Wiebe (1986); *, host dike 860C from Wiebe (1985) with $\text{Fe}^{2+}/\text{Fe}^{3+} = 0.1$; otherwise symbols as in Fig. 1. The 8 kbar data are from Baker & Eggler (1987); 10 kbar high mg -number data are run H142 from Bartels *et al.* (1991); rest of experimental data from Fram & Longhi (1992) and this study.

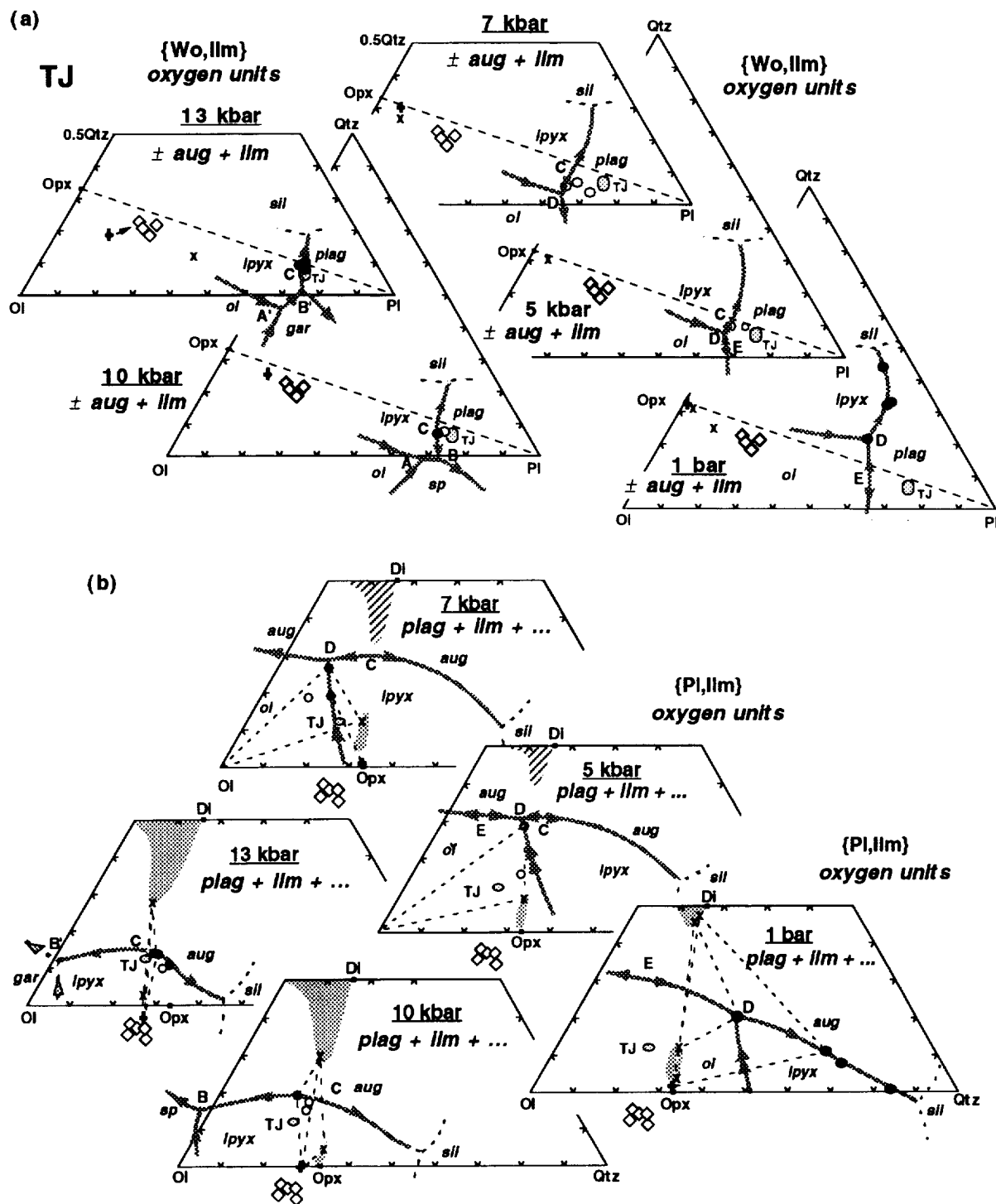


Fig. 3. Progression of liquidus equilibria and solid solutions for TJ-like compositions from 1 bar to 13 kbar. Projection schemes as in Fig. 1. Data from Vander Auwera & Longhi (1994). All liquids are near or at ilmenite saturation. The 1 bar liquids include runs at FMQ - 1, low Qtz, $mg\text{-number}(liq) = 0.25$, and at NNO (nickel nickel oxide), high Qtz, $mg\text{-number}(liq) = 0.42\text{--}0.33$. The higher $mg\text{-number}$ in the NNO liquids produces a relative expansion of the $lpx + liq$ field that is responsible for the strong curvature of the $lpx + aug + plag$ liquidus boundary. Diamonds are Rogaland megacryst compositions from Duchesne & Maquil (1987).

crystallization of olivine and probably pyroxene before reaching plagioclase saturation. For example, the compositions of several proposed parental (if not primary) liquids with *mg*-number ranging from 0.63 to 0.76 (BSVP, 1981) are shown as numbered dots in Fig. 1a. These compositions include primitive MORB (1 and 2), picritic flood basalts (3–7), parental Hawaiian tholeiites (8 and 9), Gorgona basaltic komatiite (10), and a high-Mg ophiolite dike (11). Because the *ol* + *opx* ± *cpx* liquidus boundary shifts away from the *Ol* component as *mg*-number increases, all of these magnesian compositions except the two MORBs will be saturated with *ol* ± *opx* ± *cpx* at 11.5 kbar and will evolve toward the vicinity of point A along their respective *ol* + *opx* + *cpx* boundary curves. Crystallization calculations based upon the pressure-dependent algorithms of Longhi (1992) indicate that the liquids derivative to compositions 3–11 at 11.5 kbar will all have *mg*-number ≤ 0.60 upon reaching point A. Thus, the *mg*-number values of compositions like HLCa (0.51), TJ (0.45), and those of the experimental liquids along the *plag* saturation surface are consistent with values expected of even more evolved liquids.

The two MORB compositions, which project well into the *opx* liquidus field at 11.5 kbar, represent equilibration along the *ol* + *opx* + *cpx* liquidus boundary at 8–9 kbar. Thus the crystallization paths of these primitive MORBs cannot be considered to be representative of mantle-derived liquids at 11.5 kbar. However, at 8 kbar, where these compositions do represent plausible mantle-derived liquids, their derivatives would probably reach *plag* saturation with sufficiently high *mg*-number that D would be eutectic-like. But with continued crystallization *mg*-number would fall into the range appropriate for Fig. 2 (≤ 0.5); and as *mg*-number decreased, the composition of D would migrate away from Qtz and Wo until it crossed the plane of coexisting *ol*, *aug*, and *plag* compositions, at which point D would become a nepheline-normative *opx* peritectic – consistent with Fig. 2. Thus the differentiates of primitive MORBs at 8 kbar would ultimately become nepheline-normative and react out *opx*, even though they may have initially encountered eutectic-like equilibria at D.

As liquidus boundaries are shifting in response to increasing pressure, the solid solution limits of the pyroxenes are expanding too as the result of enhanced solubility of Al components in all pyroxenes and of enhanced solubility of En Fs components in cpx. An important consequence of the increased solubility of the aluminous components is that the location of the plagioclase + pyroxene thermal divide moves away from the Qtz component with increasing pressure. Thus in Fig. 3b this thermal divide sweeps across the TJ composition between 10 kbar (three-phase triangles point to the left) and 13 kbar (three-phase triangles point to the right); whereas in Fig. 2b the thermal divide has not

quite reached the HLCa point at 13 kbar. Also important are the changes in orthopyroxene composition. In Fig. 2a and b the experimental orthopyroxenes at 11.5 kbar overtake the composition of an aluminous *opx* megacryst with 8.4 wt % Al₂O₃ from Harp Lake (Emslie, 1980); similarly, orthopyroxenes produced in the TJ experiments nearly overtake the compositions of the Rogaland megacrysts (Duchesne & Maquil, 1987) by 13 kbar. Finally, the liquidus boundaries involving *plag*, *hpx*, and high-Ca pyroxene move across the HLCa and TJ bulk compositions in both projections at pressures of 11–13 kbar.

The only significant difference in the phase equilibria between the HLCa and TJ series is in terms of clinopyroxene composition: at 10–13 kbar a low-Ca pigeonite coexists with subcalcic augite and orthopyroxene along the TJ *plag* + *hpx* + *aug* liquidus boundary (Fig. 3b); whereas a single clinopyroxene with intermediate Wo content coexists with orthopyroxene along the HLCa *plag* + *opx* + *cpx* liquidus boundary (Fig. 2b). This intermediate *cpx* is probably a supercritical clinopyroxene, resulting from the intersection of the crest of the clinopyroxene solvus with the solidus that rapidly terminates all *aug* + *plg* boundary curves at critical end points with increasing pressure (Longhi & Bertka, 1996). Despite the lower *mg*-number the TJ clinopyroxenes are subsolvus because of their lower temperatures (~100°C lower than HLCa), caused in part by lower *mg*-number and in part by the fluxing action of TJ's higher TiO₂, K₂O, and P₂O₅ concentrations.

Finally, despite significant differences in their chemical compositions, HLCa and TJ display remarkably similar liquidus equilibria. It should be noted that at low pressure the bulk compositions project within the *plag* (± *aug*) liquidus field in the [Wo] projections (Figs 2a and 3a) and within the *plag* + *ol* liquidus field in the [Pl,Ilm] projections (Figs 2b and 3b). As pressure increases, not only do the liquidus boundaries shift such that the *plag* + *opx* + *cpx* boundary curve sweeps across each composition in both projections at approximately the same pressure (11–13 kbar), but the *opx* + *cpx* tie-lines sweep across HLCa and TJ as well. This means that not only are the two bulk compositions multi-saturated in the same pressure range, albeit at different temperatures, but that they also lie in the plagioclase + pyroxene thermal divide. Therefore, neither composition can be derived by fractional crystallization of mantle-derived basaltic magmas; but each can be produced by melting of a (distinct) mafic source.

DISCUSSION

Effects of H₂O on liquidus equilibria

Anorthosites and associated rocks are widely believed to have crystallized from relatively anhydrous magmas (e.g.

Morse, 1982). Evidence is both direct and indirect: amphibole usually appears only as a late-stage replacement mineral; thermometry on ternary feldspars in associated mafic intrusions indicates only modest depression of the dry liquidus (Fuhrman *et al.*, 1988); typically there are no hydrothermal deposits or vein systems; and contact metamorphic aureoles characteristically reach the granulite facies with anhydrous assemblages (e.g. Berg, 1977). Nevertheless, water can have dramatic effects on liquidus equilibria, so it is wise to look for evidence of its effects. A number of recent experimental studies involving melting of mafic materials in the range of 3–7 kbar and $P_{\text{H}_2\text{O}} < P_{\text{total}}$ show that even modest amounts of water (as little as 2 wt % at 5 kbar) produce high-SiO₂ liquids (Baker & Eggler, 1987; Beard & Lofgren, 1991; Springer & Seck, 1997). Conversely, Figs 3b and 4b predict a eutectic-like nature for D and stability of the plagioclase + pyroxene thermal divide at 5 kbar, both of which should inhibit silica enrichment. The Qtz content of point D will increase with decreasing anhydrous pressure, causing D to become an *ol* peritectic and eliminating the plagioclase + pyroxene thermal divide. Thus lower pressures of crystallization should enhance the potential for silica enrichment in evolved liquids. Increasing H₂O content in *liq* at constant pressure has a similar effect, so lack of silica enrichment at 3 or 4 kbar places even stronger restrictions on the permissible amount of dissolved water. As will be discussed shortly, limited silica enrichment is observed in several massifs that crystallized at $P \leq 5$ kbar; and in those cases where extensive fractional crystallization does lead to silica saturation, the paucity of amphibole in evolved rocks attests to relatively low H₂O in the parental liquids. Thus there is little evidence of water exerting an important control on crystallization processes.

Megacrysts and their parent magmas

The close correspondence of 10–13 kbar experimental orthopyroxene compositions and those of highly aluminous (7–9 wt % Al₂O₃) *opx* megacrysts (HAOM) in Figs 2 and 3 is good evidence for a high-pressure (10–13 kbar) origin for these large crystals. At the same time, various geobarometric techniques have yielded much lower pressures, i.e. 3–5 kbar (Ashwal, 1993), for the crystallization of the anorthositic massifs, thus forming the basis for polybaric models in which the megacrysts are rafted by plagioclase-rich suspensions from the depths where they formed to magma chambers in the upper crust (e.g. Duchesne, 1984; Emslie, 1985). Yet, many megacrysts have Al₂O₃ concentrations in the range of +6 wt % and it is not clear whether these compositions represent primary crystallization or re-equilibration. In

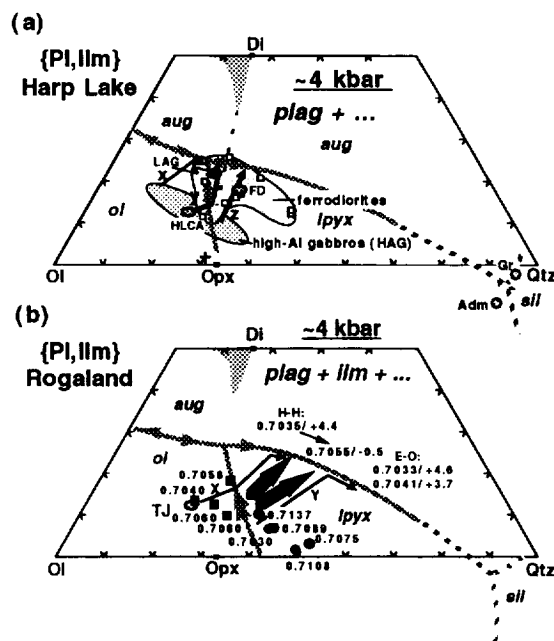


Fig. 4. Crystallization paths of anorthositic and mafic magmas at (a) Harp Lake and (b) Rogaland. Projection schemes as in Fig. 1b. (a) LAG, average low-Al gabbro; FD, average ferrodiorite; Gr, average granite; Adm, average adamellite; □, ferrodiorite compositions projected from Pl, Ilm, Apa and Mgt components. All rock data from Emslie (1980). Heavy cross is 5 kbar experimental *opx* as in Fig. 2. Paths x, y and z show range of mafic crystallization sequences; y and z also show two major low-pressure anorthosite crystallization paths. (b) ■, Bjerkreim Sokndal (Bk Sk) and Hydra chill margins from Duchesne *et al.* (1989); ●, Bk Sk chill margins from Wilson *et al.* (1992); adjacent numbers are initial ⁸⁷Sr/⁸⁶Sr ratios (Demaijff *et al.*, 1986; Robins *et al.*, 1997). Large arrows are anorthositic crystallization paths at low pressure; adjacent numbers are initial ⁸⁷Sr/⁸⁶Sr ratios and ϵ_{Nd} (Demaijff *et al.*, 1986; Menuge, 1988); small arrows are mafic fractional crystallization paths. E-O: Egersund Ognå body; H-H: Haland Hellenen body.

Fig. 3, which is based on experiments from one composition (TJ), *opx* compositions show a progressive increase in Mg-Ts component (hence Al₂O₃) with increasing pressure, and *opx* from the TJ experiments just reaches the range of Rogaland HAOM compositions at 13 kbar. In Figs 1b and 2b, however, it is clear that *opx* coexisting with *plag*, *cpx*, and *liq* has a range of Mg-Ts contents at constant pressure depending on liquid composition. Thus *opx* coexisting with *liq* at the low-Qtz end of the *opx* + *aug*/*cpx* + *plag* boundary curve (D → B → B') reaches the field of HAOM compositions by 6 kbar (Fig. 2) and moves past the HAOM field by 13 kbar; whereas *opx* coexisting with liquids close to the plagioclase + pyroxene thermal divide (C) has lower Mg-Ts contents and reaches only the center of the HAOM field by 13 kbar. Predictably, *opx* coexisting with *liq* on the *opx* + *aug*/*cpx* + *plag* boundary curve at silica saturation will have still lower Mg-Ts contents. Thus there is an intrinsic

uncertainty in estimating pressure from HAOM compositions alone, whether the means be graphical or by algorithm (e.g. Emslie *et al.*, 1994), and the best one can do is to estimate a minimum pressure, i.e. the pressure at which the composition of the most aluminous *opx* sweeps across the HAOM composition of interest. The range of minimum pressures for the HAOM compositions plotted in Fig. 2b is thus ~6 kbar for the least aluminous HOAM to ~10 kbar for the most aluminous (8.3 wt % Al_2O_3) HAOM.

The one exception to this large uncertainty is a case where the liquid composition is known. Wiebe (1985, 1986) described nepheline-normative Proterozoic dikes from Nain containing HAOM as separate, anhedral crystals and as parts of nodules intergrown with *plag*. One of these HAOM compositions with $\text{Al}_2\text{O}_3 = 6.2$ wt % and *mg*-number = 0.74 (shaded diamond) and its host dike composition (asterisk) are illustrated in Fig. 2. Wiebe (1986) argued that comparison of Cr and incompatible element abundances in the HAOM and the dike matrices indicates that the HAOM crystallized from more primitive liquids. This argument is consistent with the projections which indicate that at no pressure is the liquid composition close to *opx* saturation. However, at pressures ≥ 6 kbar this liquid could easily have fractionated from liquids that had reacted *opx* out at D or B or B' depending on the pressure. If the parental liquids of the HAOM were less differentiated relatives of the host dikes, then it is reasonable to assume that HAOM crystallized from a liquid close to the low-Qtz end of the *opx* + *aug*/*cpx* + *plag* liquidus boundary. In this case the true pressure estimate would be equivalent to the maximum pressure estimate. At 6 kbar the most aluminous experimental *opx* has not yet reached the HAOM composition, whereas at 10 kbar the most aluminous *opx* is well past the HAOM composition. This progression yields an estimate of 8 ± 1 kbar for the minimum crystallization pressure, which in this case is possibly the actual pressure.

Crystallization of anorthositic and related magmas at Harp Lake and Rogaland

There is little direct evidence of crystallization pressure in anorthositic rocks themselves; however, application of various geobarometers to mineral assemblages in contact metamorphosed country rocks (e.g. Berg, 1977; Jansen *et al.*, 1985) and in associated mafic intrusions (e.g. Kolker & Lindsley, 1989; Vander Auwera & Longhi, 1994) in most cases yields pressures in the range of 3–5 kbar. There is now emerging a combination of field and geochemical evidence that various Fe-rich dioritic to monzonitic bodies ranging in size from small lenses to small layered intrusions formed by segregation of liquids residual to the crystallization of the anorthosites (e.g.

Owens *et al.*, 1993; Mitchell *et al.*, 1996). The crystallization paths of these intrusions combined with the pressure constraints provide important limits on the compositions of the liquids in the later stages of anorthosite crystallization. Other, evolved intrusive bodies, e.g. the Rogaland dikes (Duchesne *et al.*, 1989), have been shown to be plausible differentiates of more primitive mafic bodies intruded at the same level as the anorthosites (Vander Auwera *et al.*, 1998). These primitive mafic bodies not only have the same minerals as the anorthosites, but overlapping mineral compositions and in some cases similar crystallization patterns. Examples of such bodies include the Maloin Ranch and Greaser plutons in the Laramie Complex of Wyoming (Kolker & Lindsley, 1989; Mitchell *et al.*, 1996) and the Hydra and Bjerkreim Sokndal bodies in Rogaland, Norway (Demaille & Hertogen, 1981; Duchesne, 1987; Wilson *et al.*, 1996). It must be emphasized, however, that massif anorthosites are complex, composite intrusions typically involving several parental liquids, so individual mafic bodies may not display the crystallization patterns seen in the associated anorthosites.

Figure 4 is an attempt to portray the crystallization patterns of both the mafic rocks and anorthosites from the Harp Lake and Rogaland massifs at the final level of emplacement. In each case a set of 4 kbar liquidus boundaries has been interpolated from the diagrams in Figs 2b and 3b. For the HLCA series (Fig. 4a) the liquidus boundaries are drawn such that the *ol* + *lpx* + *aug* + *plag* + *liq* pseudo-invariant point (D) is a eutectic, whereas the *ol* + *lpx* + *plag* + *liq* boundary is a reaction curve with *ol* reacting with *liq*. The *ol* + *lpx* + *plag* + *liq* boundary curve crosses the plagioclase + pyroxene thermal divide (dotted line in Fig. 4a). Thus there are some high-Al gabbroic liquids with relatively low Wo components that may cross the trace of the divide in the *ol* + *plag* field and subsequently crystallize *lpx* + *plag* \pm *aug* en route to eventual saturation with a silica phase, even in the absence of water. Liquids with higher Wo, which reach the *ol* + *lpx* + *plag* + *liq* boundary curve on the low-silica side of the thermal divide may still react *ol* out in favor of *lpx*. However, progress toward silica saturation is thwarted by the plagioclase + pyroxene thermal divide, which forces such liquids to crystallize *aug* after *opx* and then reprecipitate *ol* at the eutectic D. In Fig. 4b the effects of higher concentrations of alkalis in the TJ series overwhelm the effects of lower *mg*-number and shift the *ol* + *lpx* + *plag* + *liq* boundary curve entirely to the high-Qtz side of the pyroxene join rendering the thermal divide metastable and constraining pseudo-invariant point D to be an *ol* peritectic.

Harp Lake

Figure 4a shows some of the compositional relations at Harp Lake. Emslie (1980) reported that the bulk of

the plagioclase-rich rocks are either plagioclase + olivine cumulates, in which orthopyroxene commonly rims olivine, or plagioclase cumulates with interstitial orthopyroxene; orthopyroxene + plagioclase cumulates are present, but rare; and plagioclase + augite cumulates have not been observed. These features indicate magmas that project either in the *ol* + *plag* or the *lpx* + *plag* liquidus fields. These features also require that *ol* reacts along the *ol* + *lpx* + *plag* + *liq* boundary curve. However, the textures of the noritic anorthosites suggest that plagioclase was the sole liquidus phase, so that the parental liquid did not acquire its high Qtz component by differentiation of a troctolitic liquid near the level of emplacement. The presence of the plagioclase + pyroxene thermal divide is problematical because Emslie (1980) did not describe the reappearance of *ol* as a residual phase in leuconoritic rocks, whereas he did note minor quartz in the matrices of some gabbroic rocks. Emslie (1980) suggested that high-Al gabbroic (more properly 'gabbronoritic' or 'noritic') magmas (HAG) similar in composition to HLCA (Fig. 4a), were parental to the anorthositic rocks and the low-Al gabbros (LAG). As described above, with the *ol* + *lpx* + *plag* boundary curve crossing the trace of the pyroxene join as is in Fig. 4, HLCA can satisfy the crystallization paths of the troctolitic anorthositic magmas (y) and fractionate to low-Al gabbro as well because of the influence of the plagioclase + pyroxene thermal divide; whereas a slightly more Qtz-rich composition can yield the noritic anorthosites (z). No equivalent to path x (troctolite → olivine gabbro) has been reported among the anorthosites.

Even more evolved than the low-Al gabbros are the ferrodiorites, which contain abundant oxides and apatite. Although Emslie (1980) did not identify the various opaque minerals, similar rocks in other localities typically contain a titanomagnetite as well as ilmenite (Vander Auwera *et al.*, 1998). Therefore, we have projected these compositions from apatite and magnetite components, as well as plagioclase and ilmenite, to minimize the effects of accumulation of these phases. As a result of a different projection scheme plus lower *mg*-number, the liquidus boundaries drawn in Fig. 4a are not appropriate to the ferrodiorites; however, the position of the thermal divide remains relevant. The compositions of the ferrodiorites occupy an irregular-shaped area with two lobes: one sits astride the plagioclase + pyroxene thermal divide; the other prominent lobe extends toward granitoid compositions. This second lobe is presumably the locus of the *lpx* + *aug* + *plag* liquidus boundary for these compositions. It is thus possible that there are at least two types of ferrodiorite: one derived from liquids close to the LAG composition that were prevented from evolving toward Qtz by the thermal divide; the other from liquids on the high-Qtz side of the thermal divide. In the latter case, the parental liquids may have derived from a

troctolitic parent with low-Wo (dashed portions of the z trend), or from a parent similar to HLCA but with higher H₂O content, or from a primary liquid with intermediate composition (solid portion of the z trend).

Finally, the field of the ferrodiorites stops far short of the compositions of the average adamellite (Adm) and granite (Gr) in Fig. 4a, which have far more extensive outcrops than any of the mafic rocks (Emslie, 1980). The gap in composition between the ferrodiorites and granitic rocks [discussed in some detail for the Nain Province by Emslie *et al.* (1994)] is readily explicable if the plagioclase + pyroxene thermal divide is stable: most liquids derivative to the high-Al gabbros will either be trapped on the low-Qtz side of the divide or 'perched' in the divide itself; even liquids with sufficiently low Wo or high H₂O to breach the divide in the *ol* + *plag* field will none the less require relatively large amounts of crystallization to reach silica saturation because of the orientation of the *opx* *liq* tieline and the small compositional contrast between crystals and liquid when orthopyroxene begins to crystallize. In addition to the difficulty in producing granitic liquids by fractional crystallization of anhydrous mafic magmas, there is also the fact that the volume of granitoids at Harp Lake is much greater than that of the mafic rocks. Both observations are consistent with the arguments made by Emslie *et al.* (1994) that the Nain granitoids were produced by distinct episodes of crustal melting.

Our analysis lends further support to the proposals by Emslie (1980) and Fram & Longhi (1992) that a high-Al gabbro composition was parental to Harp Lake, but we do not imply that any single pulse of magma or even single composition generated all of the anorthositic rocks, gabbros, and ferrodiorites. High-Al gabbros formed from magmas that reached the intrusion level as mostly liquid, whereas the leucocratic rocks formed from magmas that intruded with as much as 70% plagioclase suspended in at least two different high-Al gabbroic liquids (Longhi *et al.*, 1993); and ferrodiorites may have formed as derivatives of either the anorthositic or gabbroic magmas.

Rogaland

The situation in Rogaland is somewhat different from that at Harp Lake. There are three distinct, apparently diapiric anorthositic massifs [Egersund-Ogna (E-O), Haland-Heleren (H-H), Åna Sira (A-S)] plus a large layered mafic intrusion [Bjerkreim-Sokndal (Bk-Sk)] (Duchesne & Michot, 1987). The anorthositic rocks appear more uniform mineralogically than at Harp Lake—plagioclase and orthopyroxene in varying sizes, shapes, and proportions being dominant with minor oxides only in H-H and A-S—but in the Egersund-Ogna massif there is a cryptic geographical variation in plagioclase composition. Plagioclase crystals from the center of this massif have

compositions that cluster independent of size or texture in the range of An_{45-55} with Sr concentrations in the range of 800–1100 ppm. There are two typical crystallization sequences at the level of emplacement of the three massifs, represented in part by the large arrows in Fig. 4b: one is *plag*, *plag* + *opx*, *plag* + *opx* + *ilm* with augite apparently absent (E–O); the other is *plag*, *plag* + *ilm*, *plag* + *plg* + *ilm* (H–H, A–S). A sequence similar to (H–H, A–S) with augite appearing late (path y) is observed in the lower macrocyclical units of the adjacent Bk–Sk layered intrusion (Wilson *et al.*, 1996). The upper Bk–Sk macrocyclical units (III, IV) display a crystallization sequence similar to that illustrated for the TJ composition in Fig. 4b (path x), in which olivine reacts to form orthopyroxene and ilmenite with augite appearing late. Previously, Vander Auwera & Longhi (1994) showed that TJ was similar to, but slightly less primitive than the magma parental to the upper Bk–Sk macrocycles. A comparison between phases from the high-pressure experiments on TJ and the E–O megacrysts suggests that a liquid generally similar to TJ was parental to the E–O anorthosites. At 13 kbar, where TJ is cosaturated with *opx* and *plag*, the liquidus *opx* contains 7.1% Al_2O_3 and 410 ppm Cr with *mg*-number = 0.69, and the coexisting *plag* is An_{44} and contains 1140 ppm Sr (Vander Auwera *et al.*, 1993). Both *opx* and *plag* compositions are similar to, but less primitive than typical megacrysts (*opx*: 7.9% Al_2O_3 , 600–900 ppm Cr, *mg*-number = 0.77–0.59; *plag*: An_{45-55} , 800–1100 ppm Sr) from the center of the E–O massif (Duchesne & Maquil, 1987). Although Cr in the high-pressure *opx* falls well below the range of Cr in the megacrysts, it should be noted that the TJ Cr concentration lies in the center of a range in Cr concentrations from the various Bk–Sk chill margin samples that varies by a factor of four (Duchesne *et al.*, 1989; Robins *et al.*, 1997), so postulating a jotunitic magma with Cr content greater than TJ is certainly plausible. Furthermore, the compositions of plagioclase from the central portion of the E–O massif overlap those from Bk–Sk in terms of Na, K, Ba, and Sr, yet are distinct from those of modern basalts as well as those from Precambrian layered intrusions such as the Bushveld and Stillwater (Duchesne & Demaiffe, 1978; Emslie, 1985). So it is reasonable to conclude that jotunitic magmas, similar to TJ, but with higher *mg*-number and Cr, were parental not only to the Bk–Sk intrusion (path x in Fig. 4b) but also to the *opx* megacrysts and much of the plagioclase in the central portion of the E–O massif. As more data come available, it may turn out that TJ and the parental liquid of the upper Bk–Sk macrocyclical units were more similar to the H–H and A–S parental liquids, whereas the parental liquids of the lower Bk–Sk macrocyclical units were more similar to the central E–O parent liquid. The absence of

primary olivine in the anorthosite massifs and the initiation of the noritic (lower) Bk–Sk macrocycles by plagioclase accumulation (pC) argue for parental liquids, saturated only in plagioclase, that acquired their relatively high Qtz components below the level of emplacement (y in Fig. 4b). Thus in Rogaland there were both troctolitic and noritic parental liquids, and all of these liquids were jotunitic, but only the noritic liquids produced anorthositic intrusions.

Initial $^{87}Sr/^{86}Sr$ -isotope ratios (I_{Sr}) and ϵ_{Nd} are shown for the E–O *opx* and *plag* megacrysts (0.7033/ + 4.6, 0.7041/ + 3.7; Demaiffe *et al.*, 1986) and H–H anorthosites (0.7035/ + 4.4, 0.7055/ + 0.5; Menuge, 1988) are shown in Fig. 4b, as are I_{Sr} ratios for various chill margins of associated mafic intrusions (squares and circles). As in other complexes, the megacrysts have the most isotopically primitive compositions (e.g. Ashwal, 1993) and there is an obvious correlation of weakly increasing I_{Sr} with more strongly decreasing ϵ_{Nd} among the anorthosites, which is generally agreed to be the result of crustal contamination following accumulation of *plag* with high Sr and low Nd concentrations. Given the size of the massifs and their intrusion as heavily crystalline masses (Duchesne, 1984), most of the contamination must have occurred before emplacement. Among the Bk–Sk chill margin samples (filled circles; Robins *et al.*, 1997) I_{Sr} generally increases as Qtz content increases and Wo decreases, which is consistent with progressive high-level granitic gneissic contamination of the Bk–Sk parent magmas. Wilson *et al.* (1996) have also documented progressive Sr-isotopic contamination within the Bk–Sk intrusion (0.7049–0.7085). There are no Nd-isotopic data available for Bk–Sk, but ϵ_{Nd} varies from 0.3 to 2.7 in the chill margin samples (the five circles with the highest Qtz component in Fig. 4b) reported by Robins *et al.* (1997) with no apparent covariation with I_{Sr} . The most significant features of these data are that (a) the most isotopically primitive anorthosites have compositions overlapping those of both the plagioclase and orthopyroxene megacrysts, and (b) the most isotopically primitive Bk–Sk chill margin composition ($^{87}Sr/^{86}Sr$ = 0.7040) is in the range of the megacrysts and most primitive anorthosites. Given the likelihood that the megacrysts reflect high-pressure processes, the anorthosite and Bk–Sk parental liquids thus reached relatively high Qtz and low Wo contents at high pressures, enabling them to crystallize *opx* at lower pressures without extensive assimilation of a granitic component.

Survey of anorthositic and related magmas

From the previous discussions it should be clear that despite large differences in isotopic composition and even some significant differences in minor element concentrations (Ti, K, P) the overall petrological characters

of the magmas parental to the Harp Lake and Rogaland massif anorthosites are similar: the troctolitic noritic and noritic mineralogies require liquid compositions with relatively low W_o and moderate Qtz contents. In Fig. 5 we explore the relation between composition and phase equilibria for a wider range of complexes. Figure 5a, which emphasizes crystallization at the level of emplacement, depicts crystallization paths from various anorthositic massifs as large arrows. Pointed tips show the direction of further crystallization; blunt tips indicate magmas in thermal divides. Also shown are the compositions of some potentially parental mafic rocks. Two features are important. First, the crystallization paths of many of the anorthosites are consistent either with parental liquids (i.e. the beginnings of the arrows) that project near HLCA and TJ in the high-pressure locus of the plagioclase + pyroxene thermal divide or with more noritic compositions that project to the high-Qtz side of the divide. This feature, along with the presence of the highly aluminous *opx*-megacrysts, which ties the anorthosite parent magma to an episode of high-pressure crystallization, prohibits derivation of the parental magma at depth from an even more primitive liquid with significantly lower Qtz content. The second feature is the wide array of mafic compositions (tick marks show the displacement of the projection points caused by removal of 10% of the Fe as ferric), some of which are obviously not parental to the bulk of the associated anorthosites. Perhaps the best example is the Kiglapait intrusion (*Kg*) in the Nain province of Labrador, which has extensive accumulations of troctolite overlain by olivine gabbro that contains no primary low-Ca pyroxene (Morse, 1979). The parental liquids to such sequences of cumulates should logically project well within the *ol* + *plag* liquidus field on a line between the *Ol* component and the thermal maximum on the *ol* + *plag* + *aug* liquidus boundary (compare the blunt-ended arrow in Fig. 5a); and, indeed the chill margin composition of Nolan & Morse (1986) does plot close to this thermal divide. However, no anorthosites with comparable mineral parageneses have been reported in the Nain region (e.g. Ranson, 1981; Xue & Morse, 1993). Interestingly, though, the Kiglapait crystallization sequence is similar to that described in the central dome of the Laramie Complex (LaC) by Frost *et al.* (1993).

Some of the fine-grained high-Al gabbroic dike compositions from the Greaser (and Strong Creek) intrusions at Laramie (Mitchell *et al.*, 1995) also project close to the olivine + augite + plagioclase thermal divide, as do dikes from the Newark Island intrusion (Wiebe & Snyder, 1993), and the Hettasch chill margin (Berg, 1980), although crystal accumulation may have compromised these compositions somewhat.

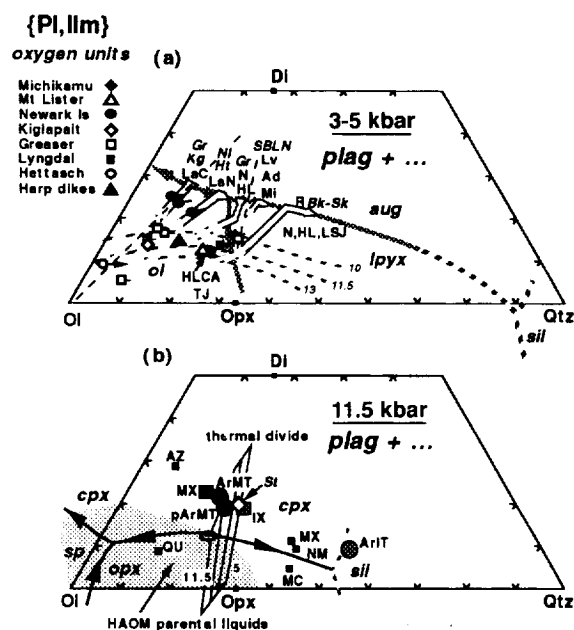


Fig. 5. Comparison of rock, parental magma and potential source compositions. (a) Schematic plagioclase liquidus surface at 3-5 kbar. Open arrows indicate inferred crystallization paths; blunt ends indicate magma perched in or trapped by a thermal divide; dotted portions of the arrows indicate greater ranges of composition for some of the listed localities. Abbreviations (italics, mafic intrusion; plain text, anorthosite): *Kg*, Kiglapait; *Gr*, Greaser; *Ni*, Newark Island; *HL*, Hettasch; *SBLN*, Slam Bang Leuconorite; *Bk-Sk*, Bjerkreim Sokndal; *LaC*, Laramie central dome; *LaN*, Laramie northern dome; *N*, Nain; *HL*, Harp Lake; *Lx*, Labrieville; *Ad*, Adirondacks; *Mi*, Michikamau; *R*, Rogaland; *LSJ*, Lac St Jean. Short lines attached to symbols show the effect of removing 10% of the total Fe as ferric. Dashed curves are the traces of the *lpx* + *aug* + *plag* cotectics at 10, 11.5 and 13 kbar from Fig. 2b. Sources of data: Michikamau, Emslie (1970); Mt Lister dikes, Emslie *et al.* (1994); Newark Island intrusion, Wiebe & Snyder (1993); Kiglapait, Nolan & Morse (1986); Greaser dikes, Mitchell *et al.* (1995); Lyngdal hyperites, gabbro-norites, Demaille *et al.* (1990); Hettasch, Berg (1980); Harp dikes, Meyers & Emslie (1977). (b) Plagioclase liquidus surface at 11.5 kbar from Fig. 2b; thermal divide is constructed from *opx* + *aug* liquidus from 5 to 11.5 kbar. Large filled symbols from Rudnick & Fountain (1995) table 6: MX, mafic xenoliths; ArMT, Archean mafic terranes; pArMT, post Archean mafic terranes; IX, intermediate xenoliths; ArIT, Archean intermediate terranes. Small filled squares, average feldspathic granulitic xenoliths from Emslie *et al.* (1994) table 6: AZ, Arizona; QU, Queensland; MX, Mexico; NM, New Mexico; MC, Massif Central; \diamond , *St.* is bulk composition of the Stillwater Banded Zone, Hess (1960). Shaded area, constructed from Fig. 2b, shows plagioclase-saturated liquids that may coexist with *opx* containing ≥ 8 wt % Al_2O_3 .

Greaser (Laramie)

There are several compositions involved in the Greaser intrusion. Frost *et al.* (1993) described layers of olivine gabbro-norite, gabbro-norite, and ferrogabbro, but no troctolite in the Greaser intrusion. This description is generally consistent only with the Greaser dike composition (open box) that projects close to the *ol* + *lpx* + *plag* liquidus boundary (the reappearance of

Fe-rich olivine without quartz in the residua of some ferrogabbros is an indication that after reacting out olivine the liquid was blocked from silica enrichment by the plagioclase + pyroxene thermal divide). The Greaser composition with very high Ol content probably reflects olivine accumulation, but the cluster of three dike compositions close to Kiglapait chill margin are probably very similar to the liquids parental to the anorthosites of the central dome described above.

Newark Island (Nain)

The three Newark Island dike compositions are from rocks that contain hornblende and biotite, but no olivine, despite their being obviously olivine-normative (Wiebe & Snyder, 1993). None the less, the compositions are generally consistent with the cumulate sequence of troctolite followed by olivine gabbro with minor late-stage gabbro-norite, as suggested by the open arrow. However, the stratigraphic sections presented by Wiebe (1983, 1988) suggest 30–40% troctolite crystallization rather than the ~20% predicted from the projection points in Fig. 5a, thus supporting the existence of a parent magma with even lower Wo than the dikes.

Hettasch (Nain)

The Hettasch chill margin composition (Berg, 1980) apparently reflects olivine (+ plagioclase) accumulation (supported by comparison of most magnesian olivine in the intrusion Fo₇₃ with a calculated Fo₆₂ liquidus olivine for the composition). The proximity of the Hettasch point (O) to the Ol component makes its predicted crystallization sequence especially sensitive to small analytical errors or non-isochemical alteration. Berg (1980) described a thick cumulus sequence of troctolite overlain by gabbro-norite, which suggests a parental liquid projecting approximately on a line between Ol and the pseudo-invariant point this requires a small displacement of the composition toward the Qtz component. As removal of about 50% troctolite component is needed to make the liquidus olivine of the chill margin composition equivalent to those observed in the intrusion, the Hettasch parent liquid (tip of the small arrow) should project approximately in the center of the *ol* + *plag* liquidus field, close to and to the right of the Kiglapait chill composition.

Although neither the Newark Island nor the Hettasch crystallization sequence is prominent among the anorthositic rocks of Nain (Morse, 1982), the major sequence in anorthositic rocks of the northern dome (LaN) at Laramie (Frost *et al.*, 1993), where *ol* + *plag* accumulation gives way to *ol* + *plag* + *aug* + *lpx*, is similar to that of the Hettasch, whereas the Newark Island sequence is apparently transitional between those of the northern

and central domes at Laramie. Thus, although the predominant parental magma of massif anorthosites appears to be troctolitic noritic, it is evident that troctolitic gabbroic magmas with lower Qtz contents also formed anorthosite massifs. What all these magmas seem to have in common is low Wo content, which leads to extensive intervals of *ol* + *plag* crystallization in liquids with low to intermediate Qtz and extensive *lpx* + *plag* crystallization in liquids with higher Qtz, but only in the Laramie Complex have the magmas with lower Qtz contents formed major anorthositic units. Thus the liquids that formed the more primitive mafic intrusions have much the same range in composition and crystallization order as the liquids entrained in suspensions that formed the anorthositic rocks. Not surprisingly, both groups of liquids have similar lines of descent (Vander Auwera *et al.*, 1998) and determining the parentage of highly evolved rocks within the complexes may accordingly be difficult.

Isotopes

Although the Harp Lake and Rogaland massifs do not encompass the full range of petrological and structural variation in Proterozoic anorthosites, they none the less span a sufficiently wide range of variation that both common ground and differences are likely to be characteristic of the group. For example, most massif anorthosites are either noritic or troctolitic noritic (Ashwal, 1993). Laramie, where augite is the dominant mafic mineral (Frost *et al.*, 1993), is a notable exception. Also, differences in the range of ϵ_{Nd} correlate with basement. For example, $\epsilon_{Nd} = -3$ to -6 in anorthosites at Harp Lake, which is situated in Archean terrane, whereas $\epsilon_{Nd} = 0$ to $+5$ in Rogaland, which is situated in Proterozoic terrane (Demaiffe *et al.*, 1986). This correlation of ϵ_{Nd} with basement is characteristic not only of the massifs as a group (Ashwal & Wooden, 1983), but also of individual provinces where anorthositic intrusions span major tectonic boundaries (e.g. Nain, Emslie *et al.*, 1994; Laramie, Mitchell *et al.*, 1995). Within complexes megacrysts of pyroxene and plagioclase tend to have among the lowest I_{Sr} ratios and highest ϵ_{Nd} values (Demaiffe *et al.*, 1986; Ashwal, 1993; Scoates & Frost, 1996). There also appears to be a widespread pattern of ϵ_{Nd} being typically higher and I_{Sr} being lower in troctolitic anorthosites than in associated noritic anorthosites (Ashwal, 1993; Wiebe, 1994). Where there are extensive data available (e.g. Nain, Emslie *et al.*, 1994; Laramie, Scoates & Frost, 1996) there is an overall negative correlation of I_{Sr} and ϵ_{Nd} , indicating a mixing process between a local basement component (high I_{Sr} and low ϵ_{Nd}) and another more primitive component. Scoates & Frost (1996) showed that the entire range in Nd and Sr isotopic composition at Laramie can be accounted for by mixing only 10% Archean basement with the most isotopically

primitive high-Al gabbro. Similarly, it can also be shown that the entire Nd isotopic range in Nain can be accounted for by mixing $\leq 20\%$ Archean basement with the most primitive mafic composition listed by Emslie *et al.* (1994). Even the most extreme examples of a primitive component, however, fall short of unambiguous depleted mantle values ($I_{\text{Sr}} < 0.7030$, $\epsilon_{\text{Nd}} > +5.5$ at ~ 1 Ga). Emslie *et al.* (1994) suggested that the primitive component is enriched mantle; but crustal components can satisfy the constraints equally well (Demaiffe *et al.*, 1986; Owens *et al.*, 1994).

There are numerous examples of conflicting major element and isotopic trends that collectively suggest that most of the isotopic mixing occurs at depth. For example, at Laramie there are examples of apparently local progressive contamination of individual anorthosite intrusions (e.g. Poe Mountain, Scoates & Frost, 1996), which suggest assimilation following emplacement, but the observed variations form only a small part of the isotopic array for the complex. On the other hand, high-Al gabbros span the entire range of ϵ_{Nd} at Laramie with little change in major element composition (Mitchell *et al.*, 1995); whereas among the anorthosites the highest normative An contents (50–55) are observed with both the lowest (0.7042 Poe Mountain) and the highest (0.7055–Snow Creek) I_{Sr} ratios (Scoates & Frost, 1996). Similarly, Owens *et al.* (1994) showed a clear positive correlation between I_{Sr} and normative An in anorthosites from Labrieville, St Urbain, and Morin. These observations suggest that most of the isotopic mixing occurred before emplacement of the anorthositic magmas with only subtle effects on the major element composition of the parent magmas. There are, however, no firm isotopic constraints that distinguish between assimilation at depth by a mantle-derived magma and melting of mixed sources. So other lines of evidence are needed.

High-pressure phase relations

The fact that parental compositions such as HLCA and TJ lie in or near a thermal divide at the pressures where they coexist with two pyroxenes and plagioclase implies not only that their source regions consist of these minerals, but also that the source compositions project in or near this thermal divide. The same constraints do not apply to the low-Qtz mafic liquids that formed the Kiglapait, Hettasch, and Newark Island mafic intrusions, the Greaser dikes, or the Laramie anorthosites. Indeed, considered in isolation such liquids might reasonably be interpreted to be unusual varieties of mantle-derived liquids. None the less, their parental liquid compositions project on or close to the traces of the 10–13 kbar *plag* + *lpx* + *aug/cpx* liquidus boundaries (Fig. 5a), so these compositions are also consistent with melting of mafic sources – but sources with lower Qtz contents than

that of the thermal divide. Probably these lower Qtz contents are produced by some aluminous spinel that formed during subsolidus reaction of olivine and plagioclase and is exhausted during melting. Similarly, noritic parental magmas project on the traces of the 10–13 kbar *plag* + *lpx* + *aug/cpx* liquidus boundaries on the high-Qtz side of the thermal divide. Such magmas are consistent with melting a *plag* + *lpx* + *aug/cpx* source that contains a few percent quartz.

Olson & Morse (1990) and Wiebe (1994) have called attention to 'regional Fe–Al magmas' parental to mafic rocks that are probably, but not so obviously, related to associated anorthositic rocks. Our analysis indicates that these magmas form the low-silica end of a spectrum of anhydrous melts of mafic sources at lower-crustal pressures. It is perhaps a matter of chance and geography that in some complexes (e.g. Harp Lake, Rogaland) mafic rocks that crystallized from liquids similar to those parental to the anorthosites are readily apparent; whereas in other complexes (e.g. Nain) they are not. However, even if magmas similar to the parental magmas of the mafic bodies did not form anorthosites in one complex (e.g. Kiglapait, Hettasch, and Newark Island intrusions in Nain), similar Fe–Al magmas did produce anorthosites elsewhere (e.g. Laramie).

Compositions attributable to the lower crust from compilations of xenolith suites (Emslie *et al.*, 1994; Rudnick & Fountain, 1995) and from averages of granulitic terranes of various ages (Rudnick & Fountain, 1995) are shown in Fig. 5b. These compositions reflect mineralogies dominated by pyroxene and plagioclase, so if anhydrous melting of the lower crust at 10–13 kbar (pressures necessary to produce the HAOM) were to take place, we could reasonably expect liquid compositions with relatively low Wo contents but a petrologically significant range of Qtz contents. Because many of the compositions, including estimates of the average composition of the lower crust (ArMT or pArMT in Fig. 5b), actually project in the polybaric trace of the plagioclase + pyroxene thermal divide, there reasonably might be a clustering of liquid compositions near the pyroxene–plagioclase thermal divide. Additionally, various estimates of the trace element composition of the lower crust are consistent with generation of the parent magmas of the massif anorthosites, such as high Sr concentrations and a lack of Eu anomalies (Taylor *et al.*, 1984; Taylor & McLennan, 1985; Owens *et al.*, 1994) in what would otherwise be evolved compositions. Owens *et al.* (1994) also argued that the observed Sr concentrations in Labrieville plagioclase (~ 2000 ppm) cannot be produced by contaminating a mantle-derived magma with any likely crustal component.

Melting of the lower crust does pose numerous problems, however. In some cases, isotopic compositions of the anorthositic rocks lie close to mantle evolution curves

and thus appear to support a mantle-derived parent magma. However, the constraints may generally be satisfied if the crustal source separated from the mantle no more than a few hundred million years before the melting event (e.g. Demaiffe *et al.*, 1986; Owens *et al.*, 1994). Another problem is *mg*-number: the Archean and post-Archean mafic terrane averages compiled by Rudnick & Fountain (1995) have *mg*-number = 0.54–0.58, whereas HLCA has a bulk *mg*-number = 0.52. Even if the requisite extensive melting were possible, orthopyroxene would not be a residual phase at $P \geq 11.5$ kbar under anhydrous conditions because of the high *Wo* content in these compositions. Sources similar to the average Queensland mafic xenoliths (QU, Emslie *et al.*, 1994) with higher *mg*-number (0.68) and lower *Wo* are more suitable for HLCA, but obviously are not as widespread. Possibly a small amount of H_2O could lower the solidus sufficiently to increase the width of the *opx* + *cpx* two-phase field so as to allow residual orthopyroxene in more typical lower-crustal compositions. Melting of the lower crust, either by magmatic heating from below or by crustal thickening or by thrusting tongues of lower crust into the mantle (Andersson *et al.*, 1996), is not the only possible scenario, however. Arndt & Goldstein (1989) and Glazner (1994) have pointed out that mafic to ultramafic intrusions in the mid- to upper crust will be gravitationally unstable and will tend to sink into the lower crust or upper mantle, especially if heating lowers the effective viscosity of the crust. In such cases upwelling asthenosphere or large magma bodies ponded in the upper mantle might supply both the conductive heat that causes the mafic ultramafic masses to sink out of the crust and the local heat of contact melting. Interestingly, the bulk composition of the Stillwater Banded Zone (Hess, 1960) also projects close to the plagioclase + pyroxene thermal divide and has a relatively high *mg*-number (0.73), although a lower *Wo* content would be preferable. Furthermore, the upper portions of mafic layered intrusions, which contain more sodic plagioclase, more ferroan pyroxene, plus cumulus Fe–Ti oxides and phosphate, are especially attractive sources for jotunitic magmas: the lower *mg*-number plus higher concentrations of K, Ti, and P can lower the solidus sufficiently such that the *opx* + *aug/cpx* tielines extend far enough even at 13 kbar (see Fig. 3b) to encompass compositions with *Wo* contents as high as that of the Stillwater. A third possibility is that of two-stage partial melting in which the first stage of melting removes a silica-saturated melt from an intermediate source leaving a granulitic (*px* + *plag*) restite, whose bulk composition necessarily projects in the thermal divide; a second stage of melting at a higher temperature produces a liquid whose composition also plots in or near the thermal divide. Emslie *et al.* (1994) suggested that such restites would be ideal assimilants to impart many of the trace element features of

anorthosites onto mantle-derived melts. However, nearly 100% assimilation would be needed to make a composition like HLCA or TJ.

Fractionation paths

Finally, questions about the mechanism of crustal melting and what conditions led similar liquids to accumulate plagioclase in one case but not in another are beyond the scope of this paper. But lest this deferment raises inappropriate doubts, we wish to emphasize that the phase equilibria presented herein are not only consistent with generating the parental magmas of HAOM, anorthosites, and related mafic rocks by melting of a lower-crustal mafic source, but also generally preclude derivation from melts of peridotitic mantle and not merely at 11.5 kbar as argued above. The polybaric phase equilibria illustrated in Figs 2 and 3 allow us to consider fractionation paths taken by mantle-derived magmas that pond in upper-mantle or lower-crustal chambers, differentiate, and reach plagioclase saturation with intermediate *mg*-number. Figure 6 shows the trace of the pseudo-invariant points involving *plag*, *lpx*, *ol*, and *aug/cpx* (heavy patterned curves) taken from Fig. 2 and illustrates the permissible anhydrous fractionation paths (open arrows) in three different pressure regimes. At $P \leq 4$ kbar (region I) where the pseudo-invariant point (D) is an olivine peritectic, the high-silica portion of the *aug* + *lpx* + *plag* liquidus boundary is accessible. Between ~4–6 kbar point D is a eutectic (region II), so high-silica liquids are no longer accessible (opposing arrows), at least not to typical basaltic liquids. Above ~6 kbar point D is an *lpx* peritectic (region III), so typical evolved basalts will react out *lpx* and move away from the Qtz component. Only at $P \leq 4$ kbar can assimilation of granitic crust coupled with fractionation (AFC; shaded arrow) cause a multiply saturated liquid to depart significantly from its simple fractionation path because at higher pressures the hybrid liquid either cannot escape the eutectic or it follows the cotectics down temperature away from Qtz.

Also illustrated in Fig. 6 are the compositions of average MORB glasses from the Atlantic and the Pacific, a highly differentiated MORB suite from the East Pacific Rise (filled squares), and some continental tholeiites (filled circles and stars) with relatively low volatile contents that are widely believed to have evolved in lower-crustal chambers before high-level intrusion or eruption. As expected, the locus of these compositions tracks the regions where *lpx*, *aug*, and *plag* ± *ol* co-crystallize and misses the compositional range necessary to form HAOM together with the troctolitic noritic crystallization sequences.

It is possible for primitive mantle melts to access compositions similar to HLCA under special conditions.

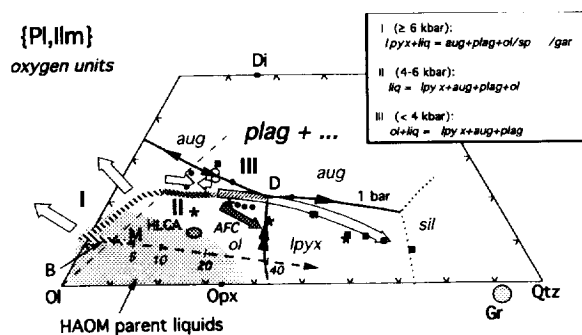


Fig. 6. Fractionation paths of mantle-derived liquids. Heavy dashed curves show the locus of pseudo-invariant points involving *lpx* from Fig. 2b; pressure increases from right to left. Inset box gives the pressure range for each melting equilibrium. Large arrows show direction of the liquid evolution once a fractionating basaltic liquid has reached the pseudo-invariant point appropriate for a given pressure; opposing arrows indicate eutectic relations. Shaded arrow shows assimilation-fractionation (AFC) path for pressure regime III; AFC paths in pressure regimes I and II are similar to simple fractionation paths. Graded line shows wt % mixing of average Harp Lake granite (Gr, Fig. 5a) with liquid at B (Fig. 1). M is representative melt of low-silica mafic source at 10–13 kbar. ■, rocks and glasses from East Pacific Rise (Bender *et al.*, 1986); ○, average Atlantic and Pacific MORB glasses (BSVP, 1981); ●, continental flood basalts; average Askja Myvatn Qtz tholeiite, Iceland, average Siberian traps, average upper and lower Deccan flows (BVSP, 1981), average Picture Gorge basalt, average Yakima basalt, average Karoo diabase, average Palisades diabase (Carmichael, 1974). *Individual representative analyses of Keweenaw flows (BVSP, 1981).

For example, a melt with composition equal to HLCA + Ol could reach *plag* saturation near the HLCA projection point at $P \leq 4$ kbar (Fig. 2a), but at such pressures this residual composition would contain less Pl component than HLCA and such a scenario would preclude HAOM. Assimilation of a granitic component into a primitive melt with lower Qtz and Wo than HLCA could change the crystallization trajectory such that the AFC path trends across the projected HLCA composition (Fig. 6). If the evolving liquid composition remains on the *ol* + *plag* liquidus surface and decreases in temperature, then the process is limited to pressures where the plagioclase + pyroxene thermal divide is not stable, i.e. $P \leq 4$ kbar, once again precluding the existence of HAOM. At higher pressures where HAOM are stable and mantle-derived liquids are nepheline-normative, the plagioclase + pyroxene thermal divide creates a barrier even to the most favorable conditions of AFC (e.g. Kelemen, 1990), such that assimilation of granitic material will induce crystallization that drives the hybrid liquid away from the divide, increasing its nepheline content.

Perhaps, the most hopeful scenario for assimilation arises when the magma is saturated only with plagioclase. If a fractionating mantle-derived liquid arrived at the *plag* liquidus surface at 11.5 kbar, the closest its composition could be to HLCA or TJ would be B in Figs 2a

and 6. If this liquid rose quickly enough to a depth corresponding to 4 kbar, it would be situated entirely within the plagioclase liquidus volume, and, in a [Pl,Ilm] projection, its initial AFC path would appear to be on a direct line toward the assimilate composition (Gr from Fig. 4a in this case). We recall, on the other hand, that noritic anorthosite magmas from Harp Lake and Rogaland intruded saturated only with *plag*. This constraint limits the amount of *plag* crystallization before emplacement, i.e. pressure release from 13 kbar to 4 kbar. The amount of *plag* that will crystallize alone can be estimated to be ≤ 15 vol. % by applying the lever law to the 11.5 and (interpolated) 4 kbar liquidus boundaries in Fig. 2a. If the ascending magma was a suspension and retained all of its superheat, it could dissolve as much as 4% suspended *plag* (Table 4). Gradations on the mixing path in Fig. 6 show that if all of the heat released from crystallizing this potential plagioclase (15% from expansion of the plagioclase liquidus field, 4% from superheat) went into assimilating a comparable amount of granitic component, it would indeed be possible to move the B composition to the high-Qtz side of HLCA. Because the amount of *plag* crystallized from the superheated liquid is approximately the amount that was melted, ~19% assimilation would produce a net crystallization of ~15% *plag* from composition B, thus allowing the hybrid liquid to remain at least marginally in the *plag* liquidus field.

Although the major elements permit this idealized AFC scenario, other considerations mediate against it. First, mantle-derived magmas could make norites only if they assimilated at least 20% granitic component (Gr). Yet many leuconorites have relatively primitive isotopic ratios that preclude 20% assimilation of granitic material. Second, energy sinks (heating of country rock to its solidus, heating the granitic melt to the temperature of the mafic liquid) are likely to make this process less efficient. Also, survival of HAOM, even in suspensions, is a testament to their host liquids having never become significantly superheated. Finally, because the olivine + augite + plagioclase thermal divide (dashed line in Fig. 6) is stable below ~6 kbar for compositions with intermediate *mg*-number, the liquidus surface must be saddle shaped with respect to temperature in the vicinity of the thermal divide. This saddle shape produces an exception to the observation of Ghiorso & Kelemen (1987) that mixtures of primitive liquids and eutectic liquids inevitably have temperatures above the liquidus of the mixture. The mixing trend beginning at B in Fig. 6 cuts across the trace of the thermal ridge (dashed line in Fig. 6) and, therefore, could proceed only in the unlikely event that the granitic melt was generated and its temperature was raised to nearly that of liquid B without withdrawing any heat from B on a regional scale. This condition applies to almost all possibly mantle-derived liquids derived

Table 4: Thermal constraints on superheat and melting (liq = HT80E-1)

Terms

ρ (density; g/cm³), T (temperature; K), P (pressure; bars), V (volume; cm³)

α_p (isobaric thermal expansion; K⁻¹) $\left(\frac{1}{V} \right) \left(\frac{dV}{dT} \right)_p$

\hat{C}_p^{liq} (isobaric heat capacity of liquid)

x_i (mole fraction of oxide i)

$(dT/dP)_s$ (adiabatic temperature gradient) $= \left(\frac{\alpha_p T}{\rho \hat{C}_p} \right)$ (Ref. 1)

$(dT/dP)^L$ (liquidus slope)

$(dT/dF)_p$ (temperature drop per wt unit of crystallinity)

$(d\rho/dP)^L$ (liquidus density gradient)

Calculations

gram-atomic weight of HT80E-1 = 64.6 g/mol

$(d\rho/dP)^L = 0.007$ g/cm³ per kbar (Ref. 2)

$\hat{C}_p^{liq} = \sum_i (x_i \hat{C}_p^{liq}) = 940$ cm³ bar/K per mol = 14.6 cm³ bar/K per g (Ref. 3)

$(dT/dP)^L$ (HLCA, 0–10 kbar) = 4.2 K/kbar (Ref. 4)

$(dT/dF)_p$ (from 500B-30 and -32) = 1.67 K/wt % (Ref. 4)

ΔT^L (11.5–4 kbar) $= (dT/dP)^L (\Delta P) = -31.5$ K

$\alpha_p = 0.000088$ /K (from liquid density model) (Ref. 5)

ρ^{liq} (HT80E-1, 1 bar) = 2.70 g/cm³ @ 1265 °C (Ref. 5)

ρ^{liq} (HT80E-1, 11.5 kbar) = 2.70 + $(d\rho/dP)^L (\Delta P) = 2.78$ g/cm³

$(dT/dP)_s = (0.000088 \times 1538)/(2.78 \times 4.6) = 0.0033$ K/bar = 3.3 K/kbar

potential superheat: $\Delta T^S = \Delta T^L - \Delta T^{adiabatic} = -31.5 - (dT/dP)_s (\Delta P) = -31.5 - (3.3 \times -7.5) = -6.8$ K

plagioclase remelting potential: $F = \Delta T^S / (dT/dF)_p = -4.0$ wt %

References: 1, Stacey (1969); 2, Agee & Walker (1989); 3, Stebbins *et al.* (1984); 4, Fram & Longhi (1992); 5, Bottinga & Weill (1970).

throughout region I. The only exceptions are those that lie along the short portion of region I that extends to the high-Qtz side of the thermal divide. Region I terminates because the increasing pressure stabilizes a garnet-bearing assemblage ($P \geq 13$ kbar) – a condition that appears to be excluded by REE modeling (Simmons & Hanson, 1978). Thus there is a narrow range of possibly mantle-derived liquids projecting near the terminus of Region I (and thus representing fractionation only in the range of 13 kbar $> P > 11.5$ kbar) that could assimilate granite during ascent through the crust and transform into noritic liquids saturated only with *plag*. As illustrated in Fig. 6, a minimum of ~20% granite assimilation would be required to produce noritic liquids by this mechanism. However, the primitive isotope compositions of some noritic anorthosites do not permit such extensive assimilation. Furthermore, Duchesne & Michot (1987) described the Rogaland massifs as being composed nearly entirely of noritic anorthosites and leuconorites with no mention of troctolitic rocks. It is difficult to envision how 20% granite component could become so uniformly mixed throughout such large volumes of suspension so as to not leave patches of troctolitic anorthosite where only 5 or 10% granite was mixed in.

More silicic troctolitic melts (e.g. M) produced on the *opx* + *cpx* + *plag* liquidus boundary on the low-Qtz side of the plagioclase + pyroxene thermal divide at pressures of 10–13 kbar would be able to intrude upward, assimilate granitic material, remain saturated in only plagioclase, and appear to evolve along a mixing line toward granite, as described above. The same cautions against copious assimilation apply here, too, but as M begins with a higher Qtz component than B, less assimilation is required to move the hybrid composition to noritic compositions. Of course, even less assimilation is needed if the starting point is HLCA. In this way it may be possible to transform crustally derived troctolitic magmas into noritic magmas saturated only in *plag* with a relatively small amount of assimilation of granitic material. Indeed, only a few percent granite assimilation is needed to account for the observation that ϵ_{Nd} is typically lower and $T^{87}Sr/T^{86}Sr$ is higher in noritic anorthosites than in associated troctolitic anorthosites (Ashwal, 1993; Wiebe, 1994).

CONCLUSIONS

Massif anorthosites and their associated mafic rocks crystallized from liquids with low Wo contents and

intermediate *mg*-number. These liquids span a considerable range in Qtz content from nearly nepheline-normative compositions that crystallize troctolitic (ol + plag) and gabbroic (ol + aug + plag) assemblages with no low-Ca pyroxene (e.g. the central dome at Laramie and the Kiglapait intrusion in Nain) to quartz-normative compositions that crystallize noritic assemblages (opx + plag \pm ilm) followed by augite-bearing assemblages (e.g. portions of Harp Lake and Nain in Labrador plus Egersund-Ogna, and Bjerkreim-Sokndal in Norway). We have shown here that two compositions that had previously been shown to be suitable parental liquids—HLCA for the Harp Lake anorthosites (Fram & Longhi, 1992) and TJ for the Bk-Sk intrusion (Vander Auwera & Longhi, 1994)—are simultaneously saturated with HAOM-like orthopyroxene, clinopyroxene, and intermediate plagioclase on their respective liquidus at 10–13 kbar and also lie in the plagioclase + pyroxene thermal divide. Despite multisaturation, these compositions cannot be residual liquids to any more primitive liquid derived by melting peridotitic mantle. Such compositions must be melts of pyroxene + plagioclase sources whose compositions already lie in the thermal divide. Although these constraints do not apply to the entire range of liquids parental to the anorthosites, the compositions of these liquids are none the less consistent with partial melting of heterogeneous mafic source regions in the range of 10–13 kbar. The ideal source for HLCA-like liquid is apparently more magnesian than averages of mafic terranes, which are thought to be representative of the lower continental crust (e.g. Rudnick & Fountain, 1995). Other potential sources include restite left after an initial stage of melting and foundered layered intrusions that have sunk out of heated (weakened) crust into the upper mantle (e.g. Glazner, 1994). The more evolved portions of layered intrusions, which contain cumulus ilmenite and apatite, appear to be especially attractive sources for melts similar to TJ, i.e. jotunites or monzonorites.

Isotopic analyses of anorthositic rocks from a given massif typically define mixing arrays between a more evolved crustal component and a more primitive component, whose provenance (enriched mantle, mafic crust) remains unclear. The overall isotopic variations show no consistent correlation with major elements except for a general tendency for troctolitic anorthosites to be more primitive isotopically than noritic anorthosites from the same massif (Ashwal, 1993; Wiebe, 1994). The overall lack of correlation of isotopic and major element variations suggests that the variations were imparted at depth where mantle-derived liquids fractionate away from the compositions characteristic of liquids parental to massif anorthosites, even while assimilating granite. The more isotopically evolved compositions of many noritic anorthosites are consistent with a few percent high-level

assimilation of granitic component into a more troctolitic plagioclase suspension. Mantle-derived magmas not only require more granitic component for this transformation than the isotopes allow in many cases, but they are probably blocked by the olivine + augite + plagioclase thermal divide as well.

ACKNOWLEDGEMENTS

We thank D. J. Ellis and R. A. Wiebe for critical reviews that helped us to improve our presentation. We also thank J. H. Berg for providing us with samples from the Hettasch intrusion. Financial support to J. Vander Auwera and J. C. Duchesne was provided by the Belgian Fund for Joint Basic Research and to J. Longhi by NASA Grants NAG-9-329 and NAGW 3407. This work was also part of the International Geological Correlation Programme, Project 290. This paper is Lamont-Doherty Earth Observatory Contribution 5856.

REFERENCES

- Agee, C. A. & Walker, D. (1989). Static compression and flotation in ultrabasic silicate liquid. *Journal of Geophysical Research* **93**, 3437–3449.
- Andersson, M., Lie, J. E. & Husebye, E. S. (1996). Tectonic setting of post-orogenic granites within SW Fennoscandia based on deep seismic and gravity data. *Terra Nova* **8**, 558–566.
- Arndt, N. T. & Goldstein, S. L. (1989). An open boundary layer between lower continental crust and mantle: its role in crust formation and crustal recycling. *Tectonophysics* **161**, 201–212.
- Ashwal, L. D. (1993). *Anorthosites*. Berlin: Springer-Verlag, 422 pp.
- Ashwal, L. D. & Wooden, J. L. (1983). Isotopic evidence from the eastern Canadian shield for geochemical discontinuity in the Proterozoic mantle. *Nature* **306**, 679–680.
- Baker, D. R. & Eggler, D. H. (1987). Compositions of anhydrous melts coexisting with plagioclase, augite and olivine or low-Ca pyroxene from 1 atm to 8 kbar: application to the Aleutian volcanic center of Atka. *American Mineralogist* **72**, 12–28.
- Bartels, K. S., Kinzler, R. J. & Grove, T. L. (1991). High pressure phase relations of a near-primary high alumina basalt from Medicine Lake Highland, N. California. *Contributions to Mineralogy and Petrology* **108**, 253–270.
- Basaltic Volcanism Study Project (BSVP) (1981). *Basaltic Volcanism on the Terrestrial Planets*. New York: Pergamon, 1286 pp.
- Beard, J. S. & Lofgren, G. E. (1991). Dehydration melting and water-saturated melting of basaltic and andesitic greenstones and amphibolites at 1, 3, and 6.9 kbar. *Journal of Petrology* **29**, 365–401.
- Bender, J., Langmuir, C., Natland, J. & Batiza, R. (1986). Petrogenesis of East Pacific Rise high-silica glasses. *Eos Transactions, American Geophysical Union* **67**, 1254.
- Berg, J. H. (1977). Dry granulite mineral assemblages in the contact aureoles of the Nain Complex, Labrador. *Contributions to Mineralogy and Petrology* **64**, 32–52.
- Berg, J. H. (1980). Snowflake troctolite in the Hettasch Intrusion, Labrador: evidence for magma-mixing and supercooling in a plutonic environment. *Contributions to Mineralogy and Petrology* **72**, 339–351.

- Bottinga, Y. & Weill, D. F. (1970). Densities of liquid silicate systems calculated from partial molar volumes of oxide components. *American Journal of Science* **267**, 169–182.
- Carmichael, I. S. E. (1974). *Igneous Petrology*. New York: McGraw-Hill, 739 pp.
- Demaiffe, D. & Hertogen, J. (1981). Rare earth element geochemistry and strontium isotopic composition of a massif-type anorthositic charnockitic body: the Hydra massif (Rogaland, SW Norway). *Geochimica et Cosmochimica Acta* **45**, 1545–1561.
- Demaiffe, D., Weis, D., Michot, J. & Duchesne, J. C. (1986). Isotopic constraints on the genesis of the Rogaland anorthositic suite, southwest Norway. *Chemical Geology* **57**, 167–179.
- Demaiffe, D., Bingen, B., Wertz, P. & Hertogen, J. (1990). Geochemistry of the Lyngdal hyperites, S.W. Norway: comparisons with the monzonorites associated with the Rogaland anorthosite complex. *Lithos* **24**, 237–250.
- Duchesne, J. C. (1984). Massif anorthosites: another partisan review. In: Brown, W. L. (ed.) *Feldspars and Feldspathoids*. Boston, MA: Reidel, pp. 411–433.
- Duchesne, J. C. (1987). The Bjerkreim-Sokndal massif. In: Majner, C. & Padget, P. (eds) *The Geology of Southernmost Norway: an Excursion Guide. Norges Geologiske Undersøkelse, Special Publication 1*, 56–59.
- Duchesne, J. C. & Demaiffe, D. (1978). Trace elements and anorthosite genesis. *Earth and Planetary Science Letters* **38**, 249–272.
- Duchesne, J. C. & Hertogen, J. (1988). Le magma parental du lopolithe de Bjerkreim-Sokndal, Norvège méridionale. *Comptes Rendus de l'Académie des Sciences* **306**, 45–48.
- Duchesne, J. C. & Maquil, R. (1987). The Egersund-Ogna massif. In: Majner, C. & Padget, P. (eds) *The Geology of Southernmost Norway: an Excursion Guide. Norges Geologiske Undersøkelse, Special Publication 1*, 50–56.
- Duchesne, J. C. & Michot, J. (1987). The Rogaland intrusive masses. In: Majner, C. & Padget, P. (eds) *The Geology of Southernmost Norway: an Excursion Guide. Norges Geologiske Undersøkelse, Special Publication 1*, 48–50.
- Duchesne, J. C., Wilmart, E., Demaiffe, D. & Hertogen, J. (1989). Monzonorites from Rogaland, Southwest Norway: a series of rocks coeval with but not comagmatic with massif-type anorthosites. *Pre-cambrian Research* **7**, 111–128.
- Emslie, R. F. (1970). The geology of the Michikamau intrusion, Labrador. *Geological Survey of Canada Paper* **68-57**, 85 pp.
- Emslie, R. F. (1975). Pyroxene megacrysts from anorthositic rocks: a new clue to the sources and evolution of the parent magmas. *Canadian Mineralogist* **13**, 138–145.
- Emslie, R. F. (1980). Geology and petrology of the Harp Lake Complex, central Labrador: an example of Elsonian magmatism. *Geological Survey of Canada Bulletin* **293**, 1–136.
- Emslie, R. F. (1985). Proterozoic anorthosite massifs. In: Tobin, A. C. & Touret, J. L. R. (eds) *The Deep Proterozoic Crust in the North Atlantic Provinces*. Dordrecht: Reidel, pp. 39–60.
- Emslie, R. F., Hamilton, M. A. & Theriault, R. J. (1994). Petrogenesis of mid-Proterozoic anorthosite-mangerite-charnockite granite, AMCG complex: isotopic and chemical evidence from the Nain Plutonic Suite. *Journal of Geology* **102**, 539–558.
- Fram, M. S. & Longhi, J. (1992). Phase equilibria of dikes associated with Proterozoic anorthosite complexes. *American Mineralogist* **77**, 605–614.
- Frost, B. R., Frost, C. D., Lindsley, D. H., Scoates, J. S. & Mitchell, J. N. (1993). The Laramie anorthosite complex and Sherman batholith: geology, evolution and theories of origin. In: Snodgrass, A. W., Steidtmann, J. R. & Roberts, S. M. (eds) *Geology of Wyoming. Geological Survey of Wyoming Memoir* **5**, 118–161.
- Fuhrman, M. L., Frost, B. R. & Lindsley, D. H. (1988). Crystallization conditions of the Sybille monzonite, Laramie Anorthosite Complex, Wyoming. *Journal of Petrology* **29**, 699–729.
- Ghiorsso, M. S. & Kelemen, P. B. (1987). Evaluating reaction stoichiometry in magmatic systems evolving under generalized thermodynamic constraints: examples comparing isothermal and isenthalpic assimilation. In: Mysen, B. O. (ed.) *Magmatic Processes: Physicochemical Principles. Geological Society Special Publication 1*, 319–336.
- Glazner, A. F. (1994). Foundering of mafic plutons and density stratification of continental crust. *Geology* **22**, 435–438.
- Green, T. H. (1969). High pressure experimental studies on the origin of anorthosites. *Canadian Journal of Earth Science* **6**, 427–440.
- Grove, T. L. & Juster, T. C. (1989). Experimental investigation of low-Ca pyroxene stability and olivine-pyroxene-plagioclase liquid equilibria at 1-atm in natural basaltic and andesitic liquids. *Contributions to Mineralogy and Petrology* **103**, 287–305.
- Hess, H. H. (1960). Stillwater igneous complex, Montana—a quantitative mineralogical study. *Geological Society of America Memoir* **80**, 230 pp.
- Jansen, J. B. H., Blok, R. J. P., Bos, A. & Scheelings, M. (1985). Geothermometry and geobarometry in Rogaland and preliminary results from the Bamble area. In: Tobin, A. C. & Touret, J. L. R. (eds) *The Deep Proterozoic Crust in the North Atlantic Provinces*. Dordrecht: Reidel, pp. 499–516.
- Kelemen, P. B. (1990). Reaction between ultramafic rock and fractionating basaltic magma I. Phase relations, the origin of calc-alkaline magma series and the formation of discordant dunite. *Journal of Petrology* **31**, 51–98.
- Kinzler, R. J. & Grove, T. L. (1992). Primary magmas of mid-ocean ridge basalts. I: Experiments and methods. *Journal of Geophysical Research* **97**, 6885–6906.
- Kolker, A. & Lindsley, D. H. (1989). Geochemical evolution of the Maloin Ranch pluton, Laramie Anorthosite Complex, Wyoming. *American Mineralogist* **74**, 415–446.
- Longhi, J. (1987). Liquidus equilibria and solid solution in the system Anorthite-Forsterite-Wollastonite-Silica at low pressure. *American Journal of Science* **287**, 265–331.
- Longhi, J. (1991). Comparative liquidus equilibria of hypersthene-normative basalts at low pressure. *American Mineralogist* **76**, 785–800.
- Longhi, J. (1992). Origin of green glass magmas by polybaric fractional fusion. *Proceedings of Lunar and Planetary Science* **22**. Houston, TX: The Lunar and Planetary Institute, pp. 343–353.
- Longhi, J. & Bertka, C. M. (1996). Graphical analysis of pigeonite-augite-liquidus equilibria. *American Mineralogist* **81**, 685–695.
- Longhi, J., Fram, M. S., Vander Auwera, J. & Monteith, J. (1993). Pressure effects, kinetics and rheology of anorthositic and related magmas. *American Mineralogist* **77**, 605–616.
- Maquil, R. & Duchesne, J. C. (1984). Géothermométrie par les pyroxènes et mise en place du massif anorthositique d'Egersund-Ogna (Rogaland, Norvège méridionale). *Annales de la Société Géologique de Belgique* **107**, 27–49.
- Menage, J. F. (1988). The petrogenesis of massif anorthosites: a Nd and Sr isotopic investigation of the Proterozoic of Rogaland/Vest-Agder, SW Norway. *Contributions to Mineralogy and Petrology* **98**, 363–373.
- Meyers, R. E. & Emslie, R. F. (1977). The Harp dikes and their relationship to the Helikian record in central Labrador. *Canadian Journal of Earth Science* **14**, 2683–2696.
- Mitchell, J. N., Scoates, J. S. & Frost, C. D. (1995). High-Al gabbros in the Laramie anorthosite complex, Wyoming: implications for the composition of melts parental to Proterozoic anorthosites. *Contributions to Mineralogy and Petrology* **119**, 166–180.
- Mitchell, J. N., Scoates, J. S., Frost, C. D. & Kolker, A. (1996). The geochemical evolution of anorthosite residual magmas in the Laramie anorthosite complex, Wyoming. *Journal of Petrology* **37**, 637–660.

- Morse, S. A. (1979). Kiglapait geochemistry I: systematics, sampling and density. *Journal of Petrology* **20**, 555–590.
- Morse, S. A. (1982). A partisan review of Proterozoic anorthosites. *American Mineralogist* **77**, 1087–1100.
- Nolan, K. M. & Morse, S. A. (1986). Marginal rocks resembling the estimated bulk composition of the Kiglapait Intrusion. *Geochimica et Cosmochimica Acta* **50**, 2381–2386.
- Olson, K. E. & Morse, S. A. (1990). Regional Al–Fe mafic magmas associated with anorthosite-bearing terranes. *Nature* **344**, 760–762.
- Owens, B. E., Rockow, M. W. & Dymek, R. F. (1993). Jotunites from the Grenville Province, Quebec: petrological characteristics and implications for massif anorthosite petrogenesis. *Lithos*, **30**, 57–80.
- Owens, B. E., Dymek, R. F., Tucker, R. D., Brannon, J. C. & Podosek, F. A. (1994). Age and radiogenic isotopic composition of a late- to post-tectonic anorthosite in the Grenville Province: Labrieville massif, Quebec. *Lithos* **31**, 189–206.
- Presnall, D. C., Dixon, J. R., O'Donnell, T. H. & Dixon, S. A. (1979). Generation of mid-ocean ridge tholeiites. *Journal of Petrology* **20**, 3–35.
- Ranson, W. A. (1981). Anorthosites of diverse types in the Puttāluk Lake area, Nain complex, Labrador. *Canadian Journal of Earth Science* **18**, 26–41.
- Robins, B., Tumyr, O., Tysseland, M. & Garman, L. D. (1997). The Bjerkreim–Sokndal layered intrusion, Rogaland, SW Norway: evidence from marginal rocks for a jotunite parent magma. *Lithos* **39**, 121–133.
- Rudnick, R. L. & Fountain, D. M. (1995). Nature and composition of the continental crust: a lower crustal perspective. *Reviews of Geophysics* **33**, 267–309.
- Scotese, J. & Frost, C. D. (1996). A strontium and neodymium isotopic investigation of the Laramie anorthosites, Wyoming, USA: implications for magma chamber processes and the evolution of magma conduits in Proterozoic anorthosites. *Geochimica et Cosmochimica Acta* **60**, 95–107.
- Simmons, C. & Hanson, G. N. (1978). Geochemistry and origin of massif-type anorthosites. *Contributions to Mineralogy and Petrology* **66**, 119–135.
- Springer, W. & Seck, H. A. (1997). Partial fusion of basic granulites at 5 to 15 kbar: implications for the origin of TTG magmas. *Contributions to Mineralogy and Petrology* **127**, 30–45.
- Stacey, F. D. (1969). *Physics of the Earth*. New York: John Wiley, 324 pp.
- Stebbins, J. F., Carmichael, I. S. E. & Moret, L. K. (1984). Heat capacities and entropies of silicate liquids and glasses. *Contributions to Mineralogy and Petrology* **81**, 1–17.
- Taylor, S. R. & McLennan, S. M. (1985). *The Continental Crust: its Composition and Evolution*. London: Blackwell, 312 pp.
- Taylor, S. R., Campbell, I. H., McCulloch, M. T. & McLennan, S. M. (1984). A lower crustal origin for massif-type anorthosites. *Nature* **311**, 372–374.
- Vander Auwera, J. & Longhi, J. (1994). Experimental study of a jotunite: constraints on the parent magma composition and crystallization conditions. *P. T. fO₂* of the Bjerkreim–Sokndal layered intrusion, Norway. *Contributions to Mineralogy and Petrology* **118**, 60–78.
- Vander Auwera, J., Longhi, J. & Duchesne, J.-C. (1993). Jotunites from the Rogaland Province, Norway: constraints from experimental data and the partitioning of Sr (plag/melt) and Cr (opx/melt). *Eos Transactions, American Geophysical Union* **74**, 659.
- Vander Auwera, J., Longhi, J. & Duchesne, J. C. (1998). A liquid line of descent of the jotunite (hypersthene monzodiorite) suite. *Journal of Petrology* **39**, 439–468.
- Walter, M. J. & Presnall, D. C. (1994). Melting behavior of simplified lherzolite in the system CaO–MgO–Al₂O₃–SiO₂–Na₂O from 7 to 35 kbar. *Journal of Petrology* **35**, 329–360.
- Wiebe, R. A. (1983). The geologic setting of the Tegalak layered intrusion. In: Morse, S. A. (ed.) *The Nain Anorthosite Project, Labrador: Field Report 1981*. Amherst: University of Massachusetts, pp. 75–78.
- Wiebe, R. A. (1985). Proterozoic basalt dikes in the Nain anorthosite complex, Labrador. *Canadian Journal of Earth Sciences* **22**, 1149–1157.
- Wiebe, R. A. (1986). Lower crustal cumulate nodules in Proterozoic dikes of the Nain complex: evidence for the origin of Proterozoic anorthosites. *Journal of Petrology* **27**, 1253–1275.
- Wiebe, R. A. (1988). Structural and magmatic evolution of a magma chamber: the Newark Island layered intrusion, Nain, Labrador. *Journal of Petrology* **29**, 383–411.
- Wiebe, R. A. (1994). Proterozoic anorthosite complexes. In: Condie, K. C. (ed.) *Proterozoic Crustal Evolution*. Amsterdam: Elsevier, pp. 215–261.
- Wiebe, R. A. & Snyder, D. (1993). Slow, dense replenishments of a basic magma chamber: the layered series of the Newark Island layered intrusion, Nain, Labrador. *Contributions to Mineralogy and Petrology* **113**, 59–72.
- Wilson, J. R., Robins, B. & Duchesne, J. C. (1992). The Bjerkreim–Sokndal intrusion. In: Duchesne, J. C. (ed.) *The Rogaland Intrusive Massifs: an Excursion Guide, International Geological Correlation Programme Project 290*, 26–39.
- Wilson, J. R., Robins, B., Nielsen, F. M., Duchesne, J. C. & Vander Auwera, J. (1996). The Bjerkreim–Sokndal layered intrusion, south-west Norway. In: Cawthorn, R. G. (ed.) *Layered Intrusions*. Amsterdam: Elsevier, pp. 231–255.
- Xue, S. & Morse, S. A. (1993). Geochemistry of the Nain massif anorthosite: magma diversity in five intrusions. *Geochimica et Cosmochimica Acta* **57**, 3925–3948.

THE MONZONORITE-ANORTHOSITE CONNECTION: THE PETROGENESIS OF TERRESTRIAL KREEP. J. Longhi, Lamont-Doherty Earth Observatory, Palisades, NY 10964 and J. Vander Auwera, LA Géologie, Pétrologie, Géochimie, Université de Liege, B-4000 Sart Tilman, Belgium.

There is a suite of rocks typically associated with Proterozoic massif anorthosites that bear some interesting similarities to lunar KREEP. In many cases (e.g., Laramie [1]) these rocks are plutonic and have traditionally been referred to as the jotunite-mangerite- \pm charnockite- \pm syenite suite. However, in the Rogaland district of southwestern Norway, where they are referred to as "monzonorites", these rocks are also present as fine-grained dikes and as the chill margin of a layered intrusion [2,3], and thus approximate magmatic liquid compositions are readily obtained by chemical analysis. Monzonorites are typically enriched in incompatible lithophile elements such as K (alkali feldspar is present), the rare earths (REE), and P. They have intermediate to low Mg, low-Ca pyroxene, and more evolved types have low Ti/Sm ratios. Much debate has developed over attempts to explain the link between monzonorites and massif anorthosites. One feature seems clear: monzonorites and associated anorthosites have different initial isotopic ratios [3,4], so a simple relation is not possible. However, there is apparently a continuum in major elements between the monzonorites and gabbros believed to represent magmas parental to the anorthosites. This continuum suggests a link via high pressure fractionation coupled with assimilation. Although more complicated, this scenario is similar that evoked for the early Moon: following the formation of ferroan anorthosites, continued fractional crystallization of the residual liquids at the base of the crust led to the formation of KREEP [5]. An attempt is made here to establish a link between monzonorites and high-Al gabbros which are nearly always found as ancillary intrusions associated with anorthosites, and which may record processes in lower crustal magma chambers.

Fig. 1 illustrates some of the evidence for a link by fractionation between monzonorites and gabbros. The upper panels show a continuous variation in TiO_2 , P_2O_5 , and MgO between gabbros and ferrodiorites of the Harp Lake Complex of Labrador [6] and the monzonoritic dikes of the Rogaland district of Norway [3]. Patterns for other elements (SiO_2 , Al_2O_3 , FeO, etc.) versus MgO are also continuous. Interpretation of the elemental variations are not straightforward, however. The peaked TiO_2 -MgO pattern is as expected for fractional crystallization of a magma that eventually becomes saturated in ilmenite. Except for the subset of analyses with P_2O_5 above 2 wt %, the P_2O_5 -MgO pattern is generally similar and indicates crystallization of a phosphate (apatite) between 2 and 3 wt % MgO. The samples with the highest P_2O_5 also have lower SiO_2 (43-45 wt%) and higher FeO (15-20 wt%) than those on the main trend. These samples are from dikes that show large regional variation in composition, and it seems possible that these dikes underwent an internal differentiation caused by differential flow of a crystalline matrix and interstitial liquid. The high-P-Fe, low-Si samples thus may be partial cumulates. If so, then the highest TiO_2 concentrations may be enhanced by accumulation as well. Experimental liquids obtained from gabbroic (HLCA) and monzonoritic (TJ) starting materials tend to mimic the high-MgO portion of the natural trend although it is clear that the specific compositions employed cannot be directly related. The steep trend of increasing TiO_2 with decreasing MgO for the natural samples in Fig. 1 indicates that fractionation must have involved extensive Fe-Mg equilibration.

Trace elements provide evidence of further complications. Several of the monzonoritic dikes lack negative Eu anomalies in their REE patterns and have only weak depletions of chondrite-normalized Sr relative to the light REE [3] — hardly what is expected from liquids residual to the formation of anorthosite. Phase equilibria complicates matters still more. Experiments on one of the most primitive monzonorites (sample TJ, the chill margin of the Bjerkeim-Sokndal intrusion [7]) show that plagioclase(pl) and orthopyroxene(opx) are together on the liquidus from 10 to 13 kbar. This pressure is consistent with experiments that showed aluminous opx megacrysts found in anorthosite plutons to have formed in this pressure range [8]. However, as Fig. 2 illustrates, the TJ composition is close to a thermal divide on the pl-opx(\pm pigeonite)-augite(aug) liquidus boundary in this pressure range, yet it would be extremely fortuitous for a residual liquid to remain on a thermal divide. One way to generate a liquid on a thermal divide would be in a second stage fusion of the lower crust: the first stage removes a granitic component leaving a pyroxene-plagioclase residuum, which would necessarily produce melts on the thermal divide at these pressures. This residuum would likely be depleted in incompatible elements and have positive Eu and Sr anomalies with respect to the other REE, so it would be necessary to invoke small degrees of melting to produce incompatible element enrichments and flatten out the Eu and Sr anomalies. Such a scenario would not, however, readily explain the continuous variation in major elements evident in Fig. 1 nor the continuous variation in mineral compositions between anorthositic and monzonoritic rocks [1].

A final option is assimilation-fractionation. In this scenario the compositions of the monzonoritic parent magmas (derived by high pressure crystallization of gabbroic liquids) are altered by assimilation of

granitic crust at lower pressures (i.e. ≤ 7 kbar) where the pyroxene-plagioclase thermal divide is no longer present. Thus the present location of the TJ composition near the thermal divide is accidental and the incompatible element patterns are hybrids. Further work is needed to verify this hypothesis.

REFERENCES

- [1] Kolker A. and Lindsley D. H. (1989) *Amer. Mineral.*, 74, 307-324. [2] Duschene, J.C., Roelandts I., Demaiffe D., and Weiss D. (1985) *Contrib. Mineral. Petrol.* 90, 214-225. [3] Duchesne J.C., Wilmart E., Demaiffe D. and Hertogen J. (1989) *Precambrian Res.*, 45, 111-128. [4] Geist D. J., Frost C. D., and Kolker A. (1990) *Amer. Mineral.*, 75, 13-20. [5] Warren P. H. and Wasson J. T. (1979) *Rev. Geophys. Space Phys.* 17, 73-88. [6] Emslie, R.F. (1980) *Geol. Surv. Can. Bull.* 293, 1-136. [7] Duchesne J.C. and Hertogen J. (1988) *C. R. Acad. Sci. Ser. II*, 306, 45-48. [8] Fram M.S. and Longhi J. (1992) *Am. Mineral.*, 77, 605-616.

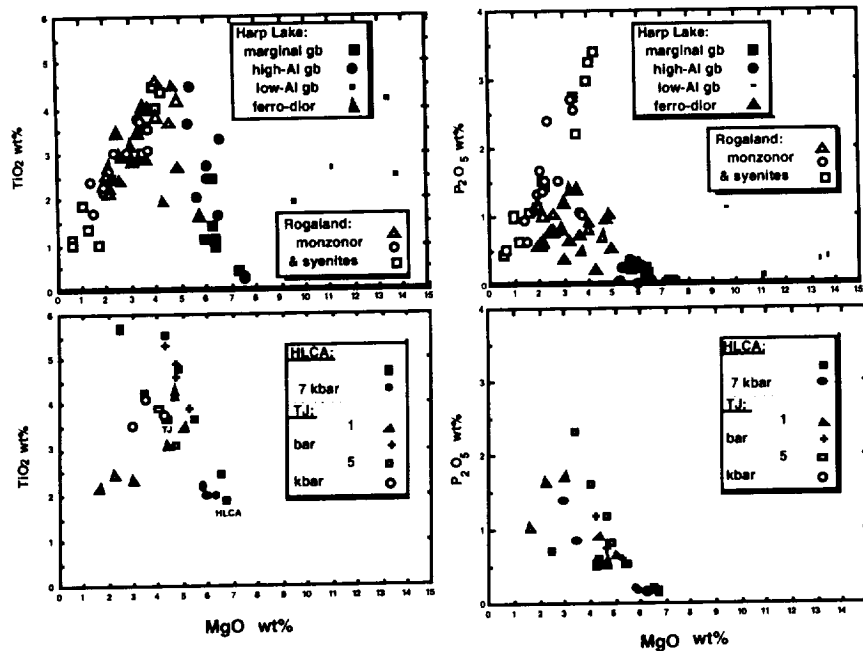


Fig. 1

Fig. 1 Major element variation in gabbros and monzonoritic rocks associated with the Harp Lake (Labrador) [6] and Rogaland (Norway) [3] anorthosites compared with liquid compositions ([8] and this study) obtained from experiments in graphite capsules on natural compositions. Fig. 2 Liquidus equilibria on the plagioclase + ilmenite saturation surface at lower crustal pressures. Liquids shown as filled squares; dashed tie lines connect coexisting pyroxene compositions (small open circles).

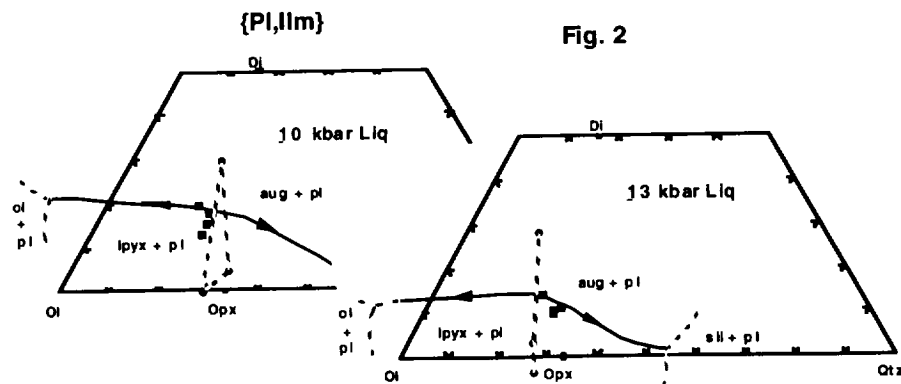


Fig. 2

V32A-8 1330h POSTER

Jotunites from the Rogaland Province (Norway) : constraints from experimental data and the partitioning of Sr (plag/melt) and Cr (opx/melt)

J Vander Auwera (Université de Liège - 4000 Sart Tilman - Belgium)

J Longhi (Lamont-Doherty Earth Observatory, Palisades, NY 10964)

JC Duchesne (Université de Liège - 4000 Sart Tilman - Belgium)

The DS_r (plag/melt) and the DC_r (opx/melt) have been measured with a CAMEBAX electron microprobe in melting experiments performed on the jotunitic border facies of the Bjerkreim-Sokndal lopolith (TJ) (Vander Auwera and Longhi, Terra Abs 1993). There is no significant pressure effect on the DS_r from 1 atm up to 13 kb and depending on the anorthite content, DS_r ranges from 1.7 (An₆₀) to 1.9 (An₄₃). These values are lower than those (2.5 (An₆₀) to 3.6 (An₄₃)) calculated with the regression of Blundy and Wood (GCA, 1991). DC_r is lower than 3 at 1 atm (NNO buffer) and equals to 14 at 10 kb (< MW buffer). This last value is a minimum as DC_r strongly increases with fO_2 (Barnes, GCA 1986).

Melting experiments have been run at 5 kb on the chilled margin and an FTP rock of the Varberg jotunitic dyke (Duchesne et al, CMP 1985). Comparison of phase equilibria in experiments and dyke suggests that the FTP rock is a crystal laden liquid or even a cumulate. A least square regression model corroborates this conclusion. By eliminating these rocks from the Rogaland data set (Duchesne et al, 1985) and using experimental data on TJ, the jotunitic liquid line of descent shows a first increase in FeO_T together with a decrease in SiO₂ followed by a strong decrease in FeO_T and an increase in SiO₂.

Major and minor element compositions suggest a connection between TJ and high-Al gabbros (HAG) through polybaric fractional crystallization coupled with crustal assimilation (Longhi and Vander Auwera, Lun Planet Sci XXIV, 1993). Apparently, this connection is not supported by trace element as some jotunites of Rogaland display no negative Eu anomaly and only a slight depletion in Sr relative to LREE. Nevertheless, calculation of the liquid REE patterns show that when plagioclase crystallizes cotectically with pyroxenes as observed in a high-Al gabbro at 11.5 kb (Fram and Longhi, Am Min 1992), a negative Eu anomaly appears only after 60% crystallization of HAG and is important only after 80% crystallization. Moreover, using the measured DS_r and the same cumulate, the Sr depletion relative to LREE at 60% crystallization is similar to that observed in the least differentiated jotunites of Rogaland. These results give then further support to the connection between high-Al gabbros and jotunites. On the other hand, considering that the DC_r measured at 10 kb is a minimum value, it is possible to crystallize Cr-rich opx from evolved liquids like TJ (Cr ≈ 50 ppm). This is consistent with parent magmas ranging from high-Al gabbros to jotunites in order to produce different massif type anorthosites.

MANTLE-DERIVED PARENT MAGMAS FOR MASSIF ANORTHOSITES??? J. Longhi (Lamont-Doherty Earth Observatory, Palisades, NY 10964, USA) and J. Vander Auwera (LA Géologie, Pétrologie, Géochimie - B20 - Université de Liège, B-4000, Sart Tilman, Belgium)

The Sr, Nd, and Pb isotopic compositions of massif anorthosites suggest an ultimate mantle origin with a variable signature of crustal contamination [e.g. 1]. Recent experimental work [2] has shown that the average high-Al gabbro composition at Harp Lake [3] is multi-saturated (opx+cpx+plag on the liquidus) in the range of 11-12 kbar with opx compositions similar to those of the opx megacrysts and plagioclase similar to the bulk of the plagioclase in the complex. More recent work on a jotunite (Tj) from the Rogaland Province has shown that this rock is close to being a suitable parent for the Bjerkreim-Sokndal (BkSk) layered intrusion [4] — the ideal parent would slightly more magnesian and calcic. Data from this work also show that Tj is multi-saturated with opx+cpx+plag at ~ 13 kbar, and that opx (En₆₇, 600 ppm Cr) and plag (An₄₂) compositions at this pressure are in the range of the more evolved opx megacryst and plagioclase "phenocryst" compositions observed within the massif anorthosites [5]. Thus liquids similar in composition to HLCA and a slightly more primitive Tj may have been residual to the early stages of anorthosite petrogenesis in the lower crust. A constraint for mantle derivation is that anorthosites' parent magma compositions lie along liquid lines descent for primitive basalts. We have shown previously that this is not the case for Tj: Tj is nearly coplanar with its liquidus plagioclase and pyroxene compositions at 13 kbar, implying that Tj lies in or near a thermal divide at lower crustal pressures [4]. Re-examination of the data of [2] shows a similar situation for HLCA at 11.5 kbar. Thus neither composition is likely to be reached by fractionation or fractionation plus assimilation (AFC), because assimilation requires crystallization to provide the heat of melting which will drive the liquid composition away from the thermal divide. At lower pressures the pyx+plag thermal divide disappears, so AFC processes can produce compositions similar to HLCA and Tj, but the range of primitive basalts is highly restricted because another thermal divide, ol+aug+plag, develops as soon as pyx+plag disappears. The coincidence of AFC yielding significant amounts of liquid that both lies in a thermal divide at a higher pressure and is appropriately multi-saturated at the same higher pressure is rendered even less probable by the requirement for AFC to take place in the cooler middle crust.

It thus appears that the lower crustal fusion hypothesis of [6] is most consistent with the data: Large ponded intrusions of basalt provide the heat for an initial stage of melting which extracts a rapakivi granite component from recently accreted [1] lower crust and leaves an anhydrous plagioclase + pyroxene residuum enriched in Sr and Eu relative to Rb and the REE; continued heating produces a second stage of melt that lies close to or within the pyroxene+plagioclase thermal divide and that has at best a small negative, or perhaps even positive, Eu-anomaly. Modest degrees of partial melting produce liquids with the major element composition of high-Al basalt — such liquids are parental to anorthosites with more calcic plagioclase (e.g., Harp Lake [3]); lower degrees of melting produce liquids with higher concentrations of K, Ti, P, and other incompatible elements — such liquids (primitive jotunites) are parental to anorthosites with more sodic plagioclase (e.g., portions of the Rogaland massifs [5]). However, there remains a need for mechanical enrichment of the parental liquids with plagioclase crystals in order to produce anorthositic rocks, because cotectic melts of the lower crust will have Al₂O₃ concentrations much lower than anorthosites. [1] Demaiffe D., Weiss D., Michot J., and Duchesne J.C. (1986) *Chem. Geol.* 57, 167-179. [2] Fram M.S. and Longhi J. (1992) *Am. Mineral.* 77, 605-616. [3] Emslie, R.F. (1980) *Geol. Surv. Can. Bull.* 293, 1-136. [4] Vander Auwera J. and Longhi J. (1994) *Contrib. Mineral. Petrol.*, in press. [5] Duchesne J.C. and Maquil R. (1992) in *The Rogaland Intrusive Massifs*, J.C. Duchesne (ed.), IGCP-290, pp. 7-17. [6] Taylor S. R. and McClennon S. M. (1985) *The Continental Crust*. Blackwell.

PLAGIOCLASE-MELT WETTING ANGLES AND TEXTURES: IMPLICATIONS FOR ANORTHOSITES; J. Longhi¹ and S. R. Jurewicz². ¹Lamont-Doherty Earth Observatory, Palisades, NY USA; ²US Synthetic Corp, 744 South 100 East, Provo, UT 84606 USA.

The rheological properties of crystal-rich magmatic suspensions and mushes play an important role in partial melting, magma transport, and differentiation. Of particular interest to lunar studies is the role that the rheology of plagioclase-melt mixtures plays in the formation of anorthosites [e.g., 1]. Accordingly, we have begun a study of plagioclase-melt wetting angles. Results from a melting experiment on a terrestrial gabbroic-anorthosite show a mean wetting (dihedral) angle of 45° — a result similar to that obtained for alkali feldspar-melt by [2]. However, the distribution of measured wetting angles is non-ideal — reflecting crystalline anisotropy, the development of planar crystalline faces, and heterogeneous melt distribution. These results are qualitatively similar to those obtained for biotite-melt by [3] and suggest: a) that the transition from suspension (liquid rheology) to mush (solid rheology) occurs at lower melt fractions than would be predicted for uniform spheres [2]; and b) that there is a non-zero equilibrium melt fraction that cannot be withdrawn from a plagioclase-rich matrix under hydrostatic stress [3].

Rock powder of anorthositic gabbro 500B from Nain [4] was run in a 1/2 inch piston cylinder apparatus at 1150°C and 10 kbar for 14 days in a graphite capsule according to the procedures of [5]. Measurements of 200 plagioclase-melt wetting angles were made from 2000X backscattered electron microphotographs of the polished surface of the charge. Results are shown in Fig. 1 as percent frequency versus observed wetting angle and yield a median angle of $\sim 45^\circ$. Also shown is the calculated ideal distribution of observed angles expected for randomly oriented 45° crystal-melt junctions intersected by a plane [6]. The observed distribution of wetting angles is much broader than the ideal distribution. Also, melt is distributed non-randomly: in addition to the even-distributed, small (≤ 10 microns) triangular pockets of melt expected for equilibrium, there are large, polycrystalline, melt-free areas as well as local accumulations of melt into pockets, tens of microns in size with numerous, well-faceted bounding crystals. Such textures are different from the uniform distribution of melt pockets bounded by equidimensional olivines with rounded melt interfaces, typically observed in similar experiments on olivine-rich materials [e.g., 7]. Similar disparities observed in experiments on biotite-rich granodioritic materials have been attributed in part to strongly preferred lattice misorientations along grain boundaries [3]. These misorientations produce a non-random distribution of interfacial energies and a dominance of grain boundaries with lower energies. This preference for lower energy grain boundaries will lead to clustering of crystals and crystalline anisotropy will enhance this effect. At the same time crystal-liquid boundaries that are favored energetically will produce faceted crystal faces. The result is the formation of crystal-rich regions with limited ranges of crystalline orientations separated by melt-rich pockets bounded by faceted crystals with range of stable dihedral angles.

There are important implications of these observations. One is the effect on the critical melt fraction below which the viscosity of a crystal-melt suspension increases exponentially with further decreases in melt fraction and becomes a rheological solid (mush) requiring deformation of the crystalline matrix in order to move. The critical melt fraction is a function of contiguity [8] — the fraction of crystalline surface area taken up with crystal-crystal contacts — which is in turn a function of the wetting angle [9]. The higher the contiguity, the higher the critical melt fraction; but the lower the wetting angle, the lower the contiguity. This means that the viscosity of suspensions is not a function of crystallinity alone. [10] showed that planar crystal faces had lower wetting angles than curved faces at the same triple junction and that melt penetrated deeper between crystals bounding a melt pocket if one had a flat face. They inferred higher permeability/porosity and lower viscosities (hence contiguity) for assemblages with planar crystal faces [10]. An apparently contrary conclusion was reached by [3] who observed that the large pockets of melt associated with the development of planar crystal faces (biotite) were separated by dry, highly contiguous, polycrystalline regions, similar to those present (plagioclase) in our experiment. They argued for an overall increase in contiguity and hence viscosity, and concluded that any increase in permeability was only local (leading to the formation of the pockets of melt) [3]. More importantly, they concluded that the polycrystalline regions were impermeable and ultimately isolated the melt pockets so as to stabilize a non-zero equilibrium melt fraction. This melt fraction is not as straightforward to quantify as the equilibrium melt fraction in an ideal system of uniform spheres with constant dihedral angle [2].

The apparent conflict between these conclusions may be resolved by a modification of the model of equilibrium melt fraction for faceted crystals with low dihedral angles: the effect of producing dry, polycrystalline regions separated by large pockets of melt probably isolates the melt thus yielding a low

equilibrium melt fraction as suggested by [2 and 3]; however, once this melt fraction is exceeded and the melt pools interconnected, the large polycrystalline areas may behave as quasi-single crystals with relatively low effective contiguity at very low strain rates. This latter behavior would yield lower viscosity than a uniform crystal-melt assemblage with similar melt fraction. In other words, the controls on bulk physical properties are no longer entirely at the scale of crystal-melt interfaces, but at the scale of the large pools of melt and the polycrystalline aggregates.

The applications to anorthosites are considerable. If textural equilibrium of faceted crystals such as plagioclase leads to the formation of polycrystalline aggregates or clusters that have less extensive external than internal crystal-crystal contacts, then suspensions of faceted, polycrystalline plagioclase may have lower viscosities than equivalent suspensions of plagioclase spheres and perhaps lower viscosities than equivalent suspensions of faceted plagioclase that have not yet reached textural equilibrium. This means that the critical melt fraction for the transition from plagioclase-melt suspensions to mushes may be lower than inferred from uniform sphere models or observations of crystallinity in lavas [e.g., 11], thus facilitating the transport of plagioclase suspensions with less than 50% melt [1]. On another level, because of the non-zero equilibrium melt fraction, the very high modes of plagioclase (up to 99%) in lunar ferroan anorthosites may be impossible to achieve (except on a small scale) without deformation. Thus either a once present, but less durable, mafic constituent of the crust has been rendered cryptic by meteorite bombardment [12], or deformation — possibly in the form of buoyancy-driven, post-accumulation diapirism — has separated plagioclase from trapped liquid yielding ultra-pure anorthosites [1].

REFERENCES

- [1] Longhi J., M.S. Fram, J. Vander Auwera, and J. Monteith (1993) *Am. Mineral.*, 77, 605-616; [2] Jurewicz S. and E.B. Watson (1985) *Geochim. Cosmochim. Acta*, 49, 1109-1122; [3] Laporte D. and E.B. Watson (1995) *Chem. Geol.*, in press; [4] Wiebe R.A (1990) *Am. Mineral.*, 75, 1-12 ; [5] Fram M.S. and Longhi J. (1992) *Am. Mineral.*, 77, 605-614; [6] Jurewicz S.R. and A.J.G. Jurewicz (1986) ; [7] Bulau J.R., H.S. Waff, and J.A. Tyburczy (1979) *J. Geophys. Res.*, 84, 6102-6108; [8] Miller C.F., E.B. Watson, and M.T. Harrison (1988) *Transactions of the Royal Society of Edinburgh: Earth Sciences*, 79, 135-156; [9] German R.M (1984) *Metallurgical Transactions*, 16A, 1247-1252; [10] Waff H.S. and U.F. Faul (1992) *J. Geophys. Res.*, 97, 9003-9014; [11] Marsh B.D. (1981) *Contrib. Mineral. Pet.* 78, 85-98; [12] Korotev R. L. and L.A. Haskin (1988) *Geochim. Cosmochim. Acta*, 52, 1795-1813.

Comparison of Measured and Ideal Distributions

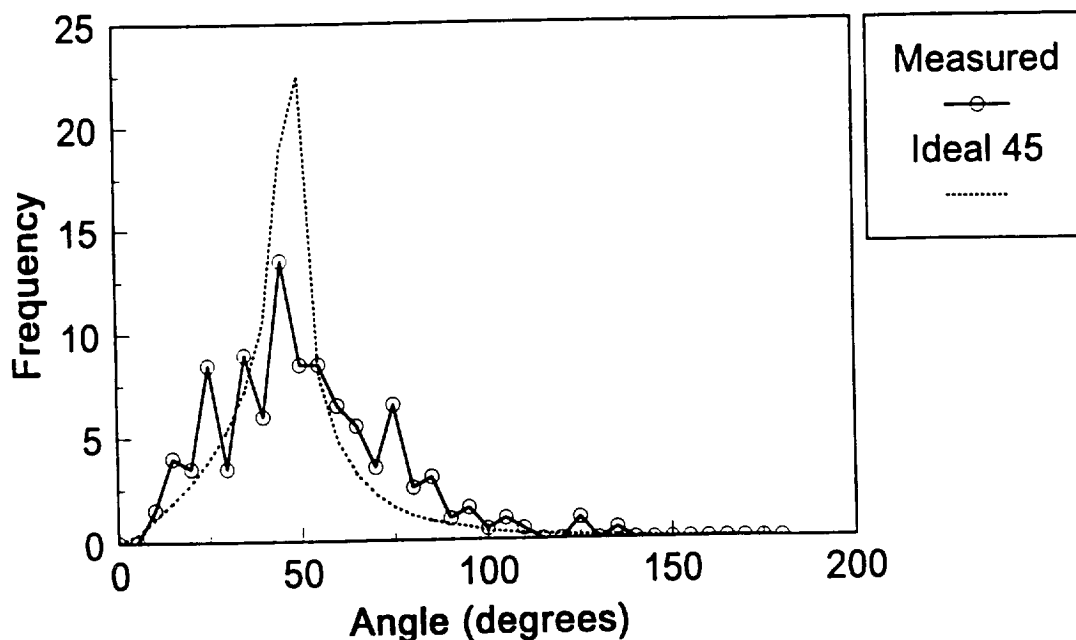


Fig. 1 Plot of percent frequency versus plagioclase-melt wetting angles. Solid lines are results of 200 measurements in a single charge; dashed curve ideal distribution of randomly oriented 45° dihedral angle intersected by a plane [6].

ORIGIN of PROTEROZOIC ANORTHOSITES by FUSION of the LOWER CRUST

J Longhi (Lamont-Doherty Geological Observatory, Palisades, NY 10964; 914-365-8659; longhi@ldeo.columbia.edu)

J Vander Auwera (L.A. Geologie, Petrologie, Geochimie -B20- Universite de Liege, B-4000 Sant Tilman, Belgium)

M S Fram (Dept., of Geology, U. C. Davis, Davis, CA 95616)

We have previously investigated the liquidus phase relations of two synthetic crystal-glass mixtures with broadly high-Al basaltic composition (HLCA, TJ) that had been proposed as parental liquids to Proterozoic (massif) anorthosites (Harp Lake - Labrador; Rogaland - southern Norway). Despite differences in TiO_2 , K_2O , and P_2O_5 that lead to differences in liquidus temperatures, the two have similar phase relations: plagioclase is the liquidus phase at low pressure and in the range of 10-14 kb each becomes multiply saturated with plagioclase, orthopyroxene, and clinopyroxene. Furthermore, at the pressure of multiple saturation not only is the plagioclase in each case in the range of typical plag compositions observed in the respective complexes, but also the liquidus opx are close in composition to the most Al-rich (8-9 wt% Al_2O_3) opx megacrysts found in the respective complexes. However, re-examination of the experimental data shows that near the pressure of multiple saturation both compositions lie in thermal divides formed by the coplanar disposition of coexisting plagioclase, pyroxene, and liquid compositions. A reversal in the direction that residual TJ liquids evolve between 10 (decreasing Qtz component) and 13 kb (increasing Qtz) confirms this observation.

The existence of a pyroxene-plagioclase thermal divide implies that primary mantle melts or their derivatives, saturated with plagioclase, high and low-Ca pyroxene, and olivine and/or spinel must have a lower temperature than the thermal divide for comparable Fe/Mg. Mantle-derived liquids will thus evolve away from the divide. Thus compositions like HLCA and TJ that are multiply saturated at the pressure at which they lie in the pyroxene-plagioclase thermal divide cannot be generated from typical basaltic magmas by fractional crystallization or by AFC. The only alternative is partial melting of a composition already in or near the thermal divide, namely a pyroxene+plagioclase-rich source (mafic granulite) such as is believed to constitute the lower crust.

A lower crustal origin for massif anorthosites is generally consistent with trace element patterns and can satisfy most isotopic constraints if the lower crustal source separated from the mantle no more than 200-400 m.y. before the melting event. Melting of the lower crust still requires large magmatic heat input from the mantle, but phase equilibria constraints exclude significant contribution of mass.

A thermal divide on the plagioclase+pyroxene liquidus surface is stable at modest crustal pressures (3-4 kb) in terrestrial magmas and inhibits silica enrichment in liquids residual to anorthosites [1]. The same divide is predictably stable to lower pressures (1-2 kb) in lunar compositions because of lower alkalis and may play a vital role in explaining the absence of granitoids ("descartesites" = anhydrous trondjemites) residual to the formation of lunar ferroan anorthosites (FAN).

Results of some new modeling of liquids parental to ferroan anorthosites are shown in Figs. 1 and 2. The calculations incorporate new low-pressure experimental data, which show that the algorithm developed by Drake [2] slightly overestimates the Ab content of anorthitic plagioclase — compare open squares (algorithm) with filled squares (experimental plagioclase) in Fig. 1. Dividing the Ab content calculated from eq. 8 of [2] by the term $(1. + (1.-NAB -NOR)*(Fe')^2)$ produces a satisfactory fit. NAB and NOR are the Ab and Or fractions of the normative feldspar; Fe' = molar $FeO/(FeO+MgO)$.

Fig. 1 illustrates the mineral composition paths generated by fractional crystallization of a model FAN parent liquid [3] at 2 pressures, 0 and 3 kb. Although there is little apparent difference in plagioclase composition and Mg' , very different rocks form by accumulation. Ol is present everywhere along the 3 kb track, but is absent where the 0 kb track passes through the field of FAN mineral compositions. More importantly, though, there is a long interval where plagioclase, augite, olivine/pyroxene, and a silica mineral cocrystallize at low-pressure, but not at 3 kb. The calculated fractional crystallization paths of the corresponding liquids are shown in Fig. 2 (filled squares = 0 kb; open circles = 3 kb; the letters *o*, *p*, *i* indicate the first appearances of ol (+plag), pyroxene, and ilmenite, respectively; the last symbol in each set represents 98% crystallization). The 3 kb fractionation path is offset from the 0 kb path because of the pressure-induced shift in liquidus boundaries, especially ol + pyroxene. Note in particular that the liquid where ol, pyroxene, and plagioclase coexist shifts from the Qtz side of the Opx-Pl join at low pressure to the Ol side at 3 kb. In doing so, this pseudo-invariant point changes from peritectic (ol reacts with liquid) to a eutectic and at the same time a coplanarity between liquid and coexisting plagioclase and pyroxene is exposed. At modest pressures this coplanarity is close to the Opx-Pl join, but at mantle pressures, increasing Al-substitution in pyroxene shifts the pyroxene composition toward lower Qtz component and, hence, the coplanarity shifts away from the join. Although this transition is compositionally dependent, it occurs at ~ 1 kb for this parental liquid composition. At 0 kb the silica-bearing cumulates constitute approximately 20 vol% of the sequence; and if efficient separation of mafic and felsic minerals were to have taken place the result would have been an anorthositic rock (An₉₀₋₉₅) with 10-15 % silica mineral ("descartesites"). Conversely, at 3 kb olivine forms only about 10 -15 % of the crystallized mafic component. Thus some apparently ol-free anorthosites might be the result of limited sampling of rocks crystallized from ol-saturated magmas.

The absence of siliceous anorthosites is readily explicable in terms of a well behaved magma ocean (MO): no primary silica is to be expected as long as the floating crust reached a thickness of ~ 20 km before the MO became silica saturated. This stipulation also means, however, that the array of mineral compositions in Fig. 1 has stratigraphic significance with the anorthosites having the minerals with the highest Mg' having formed first and closest to the surface. So far pyroxene exsolution barometry has placed 2 similar ferroan anorthosites at cooling depths of 14 and 21 km [4]. More barometry is needed on samples at both the high- and low- Mg' ends of the FAN array to establish any stratigraphic significance. The presence of olivine-bearing "sodic" ferroan anorthosites [5] is consistent with either a different parent magma or a similar parent magma crystallizing at higher pressure. In either case, a simple MO scenario does not apply, but crystallization at pressures ≥ 1 kb remain essential to avoiding formation of descartesites.

REFERENCES

- [1] Longhi J., Vander Auwera J., and Fram M.S. (1996) EOS, AGU Fall Meeting. [2] Drake M.J. (1976) *Geochim. Cosmochim. Acta*, 40, 457-465. [3] Longhi, J. (1989) *Lunar and Planetary*

Science XX, pp. 584-585. [4] McCallum I.S. and O'Brien H.E. (1996) *Am. Mineral.*, 81, 1166-1175. [5] James, O.B., M. M. Lindstrom, and M. K. Flohr (1988) *Proc. Lunar Planet. Sci. Conf. 19th*, p. 219-243.

Fig. 1 Calculated mineral compositions for 0 and 3 kb fractional crystallization of model FAN parent magma [3]. "ol in" etc. refer to 0 kb track only; silica-bearing cumulates represented by open pattern. 0 kb sequence: ol+plag; pig+plag; aug+pig+plag; sil+aug+pig+plag; ol+sil+aug+plag; ilm+ol+sil+aug+plag (black line). 3 kb sequence: ol+plag;pig+ol+plag;aug+pig+ol+plag; ilm+aug+pig+ol+plag. Also comparison of experimental liquids (filled circles) and plag + ol (filled squares) with plag predicted by eq. 8 of [2] (open squares).

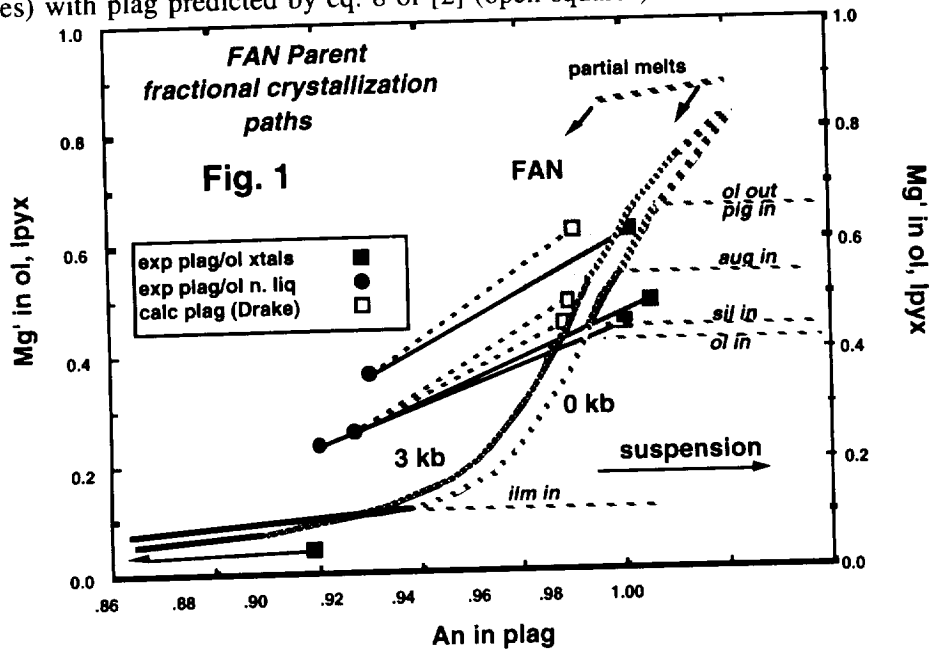


Fig. 2 Calculated liquid compositions for 0 and 3 kb fractional crystallization paths in Fig. 1. Projection from Wo component onto Ol-Pl-Qtz plane. Solid lines are 1 bar liquidus boundaries; heavy broken curves are 3 kb boundaries; both sets of liquidus boundaries appropriate to respective liquids saturated with ol+pig+plag.

